



UNIVERSITÀ DEGLI STUDI DI MILANO

Department of Chemistry

PhD Course in Industrial Chemistry, XXVIII Cycle

Microbial Induced Reinforced Concrete Degradation and Innovative Protection Techniques

Enrico Volpi

Matr. n. R10086

Tutor: Dr. Stefano TRASATTI

Co-tutor: Dr. Pierangela CRISTIANI

Coordinator: Prof. Maddalena PIZZOTTI

2015

Table of contents

Table of contents	I
Acknowledgements	VI
List of Figures	VII
List of Tables	X
List of Abbreviations	XI
Summary	1
1. Introduction	3
1.1 The challenge of a new project	4
1.2 Setup of the concrete laboratory	6
1.2.1 Construction of the accelerated carbonation chamber	8
1.2.2 Construction of the electrochemical probe	9
1.3 Motivation for research	11
1.4 Objective of the thesis	12
1.5 Outline of the thesis	12
2. Literature study	17
2.1 Concrete	18
2.1.1 History of concrete	18
2.1.2 Portland cement	20
2.1.3 Cement hydration	22
2.1.4 Structure of the hydrated cement paste	22
2.2 Durability of concrete structures	24
2.2.1 Acid attack	25
2.2.2 Sulfate attack	26
2.2.3 Alkali-Silica reaction	27
2.2.4 Freezing and thawing	27
2.2.5 Carbonation	27
2.3 Microbial deterioration of RC structures	28
2.3.1 Mechanism	28
2.3.2 Sulfate reducing bacteria	30
2.3.3 Sulfur oxidizing bacteria	31
2.3.4 Chemical, microbiological, and in situ test methods	31

2.3.5 Measures for control	35
2.4 Corrosion of steel in concrete	36
2.4.1 The corrosion process	36
2.4.2 Chloride attack	41
2.4.3 Corrosion monitoring techniques	42
Open circuit potential measurements	42
Concrete resistivity	44
Linear polarization resistance	45
Tafel extrapolation	47
Electrochemical impedance spectroscopy	48
2.4.4 Prevention and remediation	49
References	52

3. Steel passivation in alkaline solutions simulating the concrete environment

3.1 Introduction	58
3.2 Experimental	59
3.2.1 Materials and testing environment	59
3.2.2 Steel metallographic characterization	59
3.2.3 Electrochemical setup	60
3.2.4 Cyclic voltammetry	60
3.2.5 Potentiodynamic polarization, linear polarization resistance and impedance spectroscopy	61
3.3 Results and discussion	61
3.3.1 Steel metallographic characterization	61
3.3.2 Cyclovoltammetric characterization	64
Cyclic voltammetry in 1M NaOH and saturated Ca(OH) ₂	64
Effect of the scanned potential window	66
Effect of variation of the anodic limit	68
Effect of anodic pre-polarization at -0.14 V vs SCE	69
Effect of cathodic pre-polarization at -1.5 V vs SCE	71
Effect of long term cycling	72
3.3.3 Effect of passivation time	73
Anodic polarizations	73
OCP and LPR monitoring	75

EIS measurements	76
3.4 Conclusions	79
References	81
4. Corrosion susceptibility in solutions simulating bacteria metabolites	85
4.1 Introduction	86
4.2 Experimental	87
4.2.1 Materials and testing environment	87
Metallic coupons	87
Reinforced mortar samples	87
4.2.2 Testing and electrochemical monitoring	88
Steel samples in simulated solutions	88
Reinforced mortar samples	89
4.3 Results and discussion	89
4.3.1 Steel samples in model solution	89
Weight loss measurements	89
Open circuit potential monitoring	93
Anodic potentiodynamic polarizations: sulfuric acid	96
Anodic potentiodynamic polarizations: sulfides	99
4.3.2 Reinforced mortar samples	107
Open circuit potential measurements	109
LPR and EIS monitoring	110
4.4 Conclusions	122
References	123
5. Development of “smart” corrosion inhibitors for steel protection from MICC	
5.1 Introduction	128
5.2 Experimental	129
5.2.1 Materials and testing environment	129
5.2.2 Electrochemical measurements	130
5.2.3 Synthesis	130
5.2.4 Characterization	130
5.3 Results and discussion	131
5.3.1 Inhibitor screening	131

5.3.2 Characterization of the hybrid inhibitive systems	141
5.3.3 Steel response in model medium in the presence of MBD-HAP	148
Acidic environment	148
Alkaline environment	157
5.4 Conclusions	163
References	164
6. Preliminary tests of the "Smart" inhibitors in the cementitious matrix	167
6.1 Introduction	168
6.2 Experimental	168
6.2.1 Materials and samples	168
6.2.2 Calorimetric measurements	169
6.2.3 Standard compressive strength tests	170
6.2.4 Conditioning and OCP monitoring	170
6.2.5 ESEM observations	171
6.3 Results and discussion	171
6.3.1 Effects on the cementitious matrix properties	171
6.3.2 Effects on steel rebars embedded in mortar	175
6.4 Conclusions	181
References	183
7. General conclusions and perspectives	185
7.1 Conclusions	186
7.2 Perspectives	189

List of Figures:

- Fig. 1.1:** Concrete lab equipment: mixer devices.
- Fig. 1.2:** Concrete lab equipment: compaction devices.
- Fig. 1.3:** Concrete lab equipment: workability testing devices.
- Fig. 1.4:** Construction phases of the accelerated carbonation chamber.
- Fig. 1.5:** Accelerated carbonation chamber: the control panel.
- Fig. 1.6:** Scheme and picture of the homemade carbonation chamber.
- Fig. 1.7:** Schematic of the probe for electrochemical measurements on reinforced mortar samples.
- Fig. 1.8:** Flow chart of the thesis.
-
- Fig. 2.1:** Pantheon, Rome. (I cen. d.C.)
- Fig. 2.2:** Caracalla baths, Rome. (III cen. d.C.)
- Fig. 2.3:** Eddystone lighthouse.
- Fig. 2.4:** Lambot's reinforced cement boat.
- Fig. 2.5:** Pore size distribution in hydrated cement paste.
- Fig. 2.6:** Relation between the water/cement ratio and the hydration degree at which the capillary pore are blocked
- Fig. 2.7:** Relationship between permeability and w/c ratio for mature cement pastes.
- Fig. 2.8:** Evolution of bacteria population: pH and weight loss over time.
- Fig. 2.9:** Schematic mechanism of MICC in a sewer pipe.
- Fig. 2.10:** Simulating chambers for microbial deterioration testing.
- Fig. 2.11:** Pourbaix diagram for Fe - H₂O systems.
- Fig. 2.12:** Schematic of the corrosion mechanism for steel in concrete.
- Fig. 2.13:** Volumetric expansion of corrosion products formed in concrete.
- Fig. 2.14:** Cracks evolution in corroding reinforced concrete.
- Fig. 2.15:** Fib model for RC structure service life.
- Fig. 2.16:** Schematic of an apparatus for OCP measurement of reinforced concrete.
- Fig. 2.17:** Example of an equipotential contour map.
- Fig. 2.18:** Schematic of a Wenner probe, for concrete resistivity measurements.
- Fig. 2.19:** Schematic of an LPR measurement arrangement.
- Fig. 2.20:** Determination of the corrosion current from a Tafel plot.
- Fig. 2.21:** Nyquist plot of a reinforced concrete sample.
- Fig. 2.22:** Schematic of different concrete surface protection techniques.
-
- Fig. 3.1:** Picture of the B450C steel sample for electrochemical measurements.
- Fig. 3.2:** Macroscopic picture of the B450C steel surface, after 5% Nital etching.
- Fig. 3.3:** Optical microscopy pictures of the B450C steel surface, after 5% Nital etching.
- Fig. 3.4:** Principle of Tempcore process.
- Fig. 3.5:** Localized potentiodynamic curves recorded in sat. Ca(OH)₂ solution.
- Fig. 3.6:** Cyclic voltammetries of B450C steel in NaOH 1M and sat. Ca(OH)₂.
- Fig. 3.7:** Cyclic voltammetries in sat. Ca(OH)₂: different potential scanned ranges.

Fig. 3.8: Cyclic voltammetries in sat. $\text{Ca}(\text{OH})_2$: effect of the variation of the anodic limit.

Fig. 3.9: Cyclic voltammetries in sat. $\text{Ca}(\text{OH})_2$: effect of anodic polarizations.

Fig. 3.10: Cyclic voltammetries in sat. $\text{Ca}(\text{OH})_2$: effect of cathodic polarizations.

Fig. 3.11: Cyclic voltammetries in sat. $\text{Ca}(\text{OH})_2$: effect of long term cycling.

Fig. 3.12: Anodic polarization curves: effect of the aeration.

Fig. 3.13: Anodic polarization curves: effect of pre-passivation.

Fig. 3.14: Steel passivation: corrosion potential and corrosion current density.

Fig. 3.15: Steel passivation: electrochemical impedance spectroscopy.

Fig. 3.16: Best fitting parameters for R1 and CPE1.

Fig. 4.1: Steel sample for weigh loss measurements.

Fig. 4.2: Schematic representation o a reinforced mortar sample.

Fig. 4.3: Gravimetric test in alkaline solution + Na_2S and sulfuric acid.

Fig. 4.4: Surfaces after the in immersion tests in diluted sulfuric acid solutions.

Fig. 4.5: Surfaces after the in immersion test at pH 10.2

Fig. 4.6: Surfaces after the in immersion test at pH 9.2

Fig. 4.7: OCP monitoring of metallic samples in the simulating solutions

Fig. 4.8: OCP fluctuations due to sulfides depletion.

Fig. 4.9: Optical microscopy pictures of the steel surfaces after the OCP monitoring.

Fig. 4.10: Anodic polarizations in 0.5% H_2SO_4 : effect of pre-passivation.

Fig. 4.11: Anodic polarizations in 0.5% H_2SO_4 : response of different steel.

Fig. 4.12: Anodic polarizations in H_2SO_4 : effect of acid concentration.

Fig. 4.13: Optical microscopy pictures of the steel surfaces after anodic polarizations.

Fig. 4.14: Anodic polarizations with sulfides at pH 10.2: effect of sulfides concentration.

Fig. 4.15: Optical microscopy picture after anodic polarization, pH 10.2, Na_2S 50 mM.

Fig. 4.16: Relationship between the inflection points and sulfides concentration.

Fig. 4.17: Anodic polarizations with sulfides at pH 10.2: glassy carbon.

Fig. 4.18: Anodic polarizations with sulfides at pH 10.2: effect of pre-passivation.

Fig. 4.19: Anodic polarizations with sulfides at pH 10.2: effect of aeration.

Fig. 4.20: Anodic polarizations with sulfides at pH 9.2: effect of sulfides concentration

Fig. 4.21: Macroscopic picture of the surface after anodic polarization (pH 9.2) Na_2S 5mM.

Fig. 4.22: Optical microscopy pictures of the surface after anodic polarization (pH 9.2) Na_2S 5mM

Fig. 4.23: Schematic of the iron dissolution process beneath the mackinawite layer.

Fig. 4.24: Phenolphthalein test on two freshly cut cross section mortar prism.

Fig. 4.25: XRD diffractogram of a powder sample after the carbonation treatment.

Fig. 4.26: OCP monitoring of reinforced mortar samples.

Fig. 4.27: Corrosion current densities of reinforced mortar samples.

Fig. 4.28: Typical EIS response of carbonated reinforced mortar sample.

Fig. 4.29: Equivalent electrical circuit used for fitting the experimental EIS data.

Fig. 4.30: Best fitting values of the EIS responses.

- Fig. 4.31:** Comparison of charge transfer resistance values, from LPR and EIS.
- Fig. 4.32:** Pictures of split reinforced mortar samples after a 200 days conditioning
- Fig. 4.33:** Picture of reinforced mortar samples after a 500 days conditioning.
- Fig. 4.34:** XRD pattern of the cementitious matrix at the end of the conditioning period.
- Fig. 4.35:** Pictures of split reinforced mortar samples after a 500 days.

- Fig. 5.1:** Anodic polarizations of B450C carbon steel in a 0.5% H_2SO_4 with MBD.
- Fig. 5.2:** Anodic polarizations of B450C steel in a 0.5% H_2SO_4 with MBD, BZT, CYS.
- Fig. 5.3:** Anodic and cathodic polarization with different inorganic inhibitors.
- Fig. 5.4:** Optical microscopy pictures of surface after the anodic polarizations.
- Fig. 5.5:** OCP evolution for B450C carbon steel in 0.5% H_2SO_4 with of different inhibitors.
- Fig. 5.6:** Optical microscopy pictures of the steel surface OCP monitoring in 0.5% H_2SO_4 .
- Fig. 5.7:** Steel rebars weight loss: effects of different inhibitors concentrations
- Fig. 5.8:** X-ray diffractograms of the unloaded compounds.
- Fig. 5.9:** SEM pictures of the unloaded Vaterite.
- Fig. 5.10:** SEM pictures of the as synthesized hydroxylapatite.
- Fig. 5.11:** Pore size distribution of the HAP powder.
- Fig. 5.12:** pH dependent MBD release from the VAT hybrid.
- Fig. 5.13:** pH dependent MBD release from the HAP hybrid.
- Fig. 5.14:** Mass titration data of HAP in a 0.5 M KNO_3 solution.
- Fig. 5.15:** Anodic and cathodic polarizations with the hybrid inhibitors.
- Fig. 5.16:** LPR of mild steel in 0.5% H_2SO_4 solution: effects of the inhibitors.
- Fig. 5.17:** Nyquist and Bode plots of mild steel in 0.5% H_2SO_4 solution.
- Fig. 5.18:** EIS of mild steel in 0.5% H_2SO_4 solution: HAP and MBD.
- Fig. 5.19:** EIS of mild steel in 0.5% H_2SO_4 solution: MBD-HAB.
- Fig. 5.20:** Equivalent electric circuits used for the fitting of the experimental EIS data.
- Fig. 5.21:** Fitting of EIS spectra.
- Fig. 5.22:** SEM pictures of the surfaces after a four days conditioning in in 0.5% H_2SO_4 .
- Fig. 5.23:** LPR monitoring of mild steel in saturated $\text{Ca}(\text{OH})_2$ solution.
- Fig. 5.24:** Nyquist and Bode plots of mild steel in saturated $\text{Ca}(\text{OH})_2$ solution
- Fig. 5.25:** Fitting of EIS spectra.
- Fig. 5.26:** Voltammetries performed in sat. $\text{Ca}(\text{OH})_2$ with MBD
- Fig. 5.27:** Anodic charges calculated from integration of the voltammetric curves.

- Fig. 6.1:** Schematic and pictures of reinforced mortar cylinders.
- Fig. 6.2:** Pictures of the mortar cubes, before and after the standard compressive tests.
- Fig. 6.3:** Pictures of polished cross-section for ESEM examination.
- Fig. 6.4:** Schematic of the heat evolution during the hydration process of Portland cement.

- Fig. 6.5:** Heat release and heat evolution plots for OPC cement with HAP and MBD-HAP.
- Fig. 6.6:** Heat release and heat evolution plots for OPC cement paste with MBD.
- Fig. 6.7:** Compressive strength of mortar cubes with HAP and MBD-HAP.
- Fig. 6.8:** OCP evolution steel rebars embedded in mortar along the curing period.
- Fig. 6.9:** OCP evolution steel rebars embedded in mortar along the conditioning period
- Fig. 6.10:** Phenolphthalein test performed on the cross-section of two reinforced cylinders.
- Fig. 6.11:** ESEM pictures of the edge area of a cross-section (H_2SO_4).
- Fig. 6.12:** ESEM pictures of a cross-section: bulk area and edge (H_2SO_4).
- Fig. 6.13:** EDX spectra captured on edge and on bulk.
- Fig. 6.14:** ESEM pictures of a cross-section: steel/mortar interface (H_2SO_4).
- Fig. 6.15:** ESEM pictures of a cross-section: edge region (water).
- Fig. 6.16:** ESEM pictures of a cross-section: bulk and steel/mortar interface (water).

List of Tables:

- Table 2.1:** Main components of Portland cement.
- Table 2.2:** Composition limits of Portland cement.
- Table 2.3:** Classification of cement types according to EN 197-1.
- Table 2.4:** Sulfate exposure classes of ACI 318-08.
- Table 2.5:** Thiobacillus strains and their characteristics.
- Table 2.6:** Relationship between OCP and Corrosion risk according to ASTM C876.
- Table 2.7:** Relationship between concrete resistivity and corrosion risk.
- Table 2.8:** Relationship between corrosion current and corrosion of the rebar.
- Table 3.1:** Vickers micro hardness of B450C steel.
- Table 3.2:** Best fitting parameters for the EIS data: steel passivation.
- Table 4.1:** Chemical composition (w%) of B450C mild steel
- Table 4.1:** Relationship between corrosion current density and corrosion risk.
- Table 5.1:** Different organic and inorganic inhibitors used in the preliminary screening.
- Table 5.2:** Vaterite (VAT) and hydroxylapatite (HAP) BET surface area.
- Table 5.3:** Loading capacity of the hybrid systems

List of Abbreviations:

ACI	American Concrete Institute
ASR	Alkali Silica Reaction
BET	Brunauer-Emmett-Teller surface area measurement
BTZ	Benzothiazole
C2S	di-calcium silicate
C3S	tri-calcium silicate
C3A	tri-calcium aluminate
C4AF	tetra-calcium alumino ferrite
CH	calcium hydroxide
CSH	calcium silicate hydrates
CNT	Cerium nitrate
CPE	Constant Phase Element
CYS	Cysteine
CV	Cyclic Voltammetry
DSLR	Digital Single Lens reflex
DSP	Di-sodium phosphate
EIS	Electrochemical Impedance Spectroscopy
ESEM	Environmental scanning electron microscope
HAP	Hydroxylapatite
LPR	Linear Polarization Resistance
MBD	Methylene blue dye
MICC	Microbial Induced Concrete Corrosion
OCP	Open Circuit Potential
OPC	Ordinary Portland Cement
R	Resistance
RC	Reinforced Concrete
R_p	Polarization resistance
SMD	Sodium molibdate
SOB	Sulfur Oxidizing Bacteria
SRB	Sulfate Reducing Bacteria
TSP	Tri-sodium phosphate
XRD	X-ray Diffraction

Acknowledgements

Looking back to the last three years of my PhD research activity I really feel grateful to Dr. Stefano Trasatti and Dr. Pierangela Cristiani, respectively the supervisor and the co-supervisor of the present research project, that allowed me to undertake such an interesting and formative experience.

In particular, I would like to express my deepest appreciation to Dr. Stefano Trasatti for his open-minded view and attitude in the management of the laboratory and the research group. Thanks for having understood and supported my needs and desires of a fully autonomous way of conducting my scientific research.

Also I would like to give my sincerest acknowledgments to Dr. Dessa Koleva, from TU Delft, who gave me the kind opportunity to work in her group for six months, during which I experienced a substantially different approach to the research with respect to the one I was used to live. I learned a lot of things during my very formative stay in the Netherlands.

Undoubtedly a huge thanks goes to Matteo Stefanoni, Andrea Olietti and Cristian Foiadelli that undertook parts of the present work for their thesis researches. It was really a pleasure to share with you ideas, doubts, results, achievements and frustrations...thanks again guys!

I also would like to thanks all the members of the "Corrosion Engineering and Applied Electrochemistry" Laboratory: Edo, Ale, Teo, Monica and Giorgio for being good friends, and all the students that for longer or shorter periods worked in the lab, contributing with their friendliness to the creation of a really nice place where to stay.

Finally, a special thanks to Stefi, whose technical contribution to the present thesis is "limited" to the execution of some BET analysis, but her main provision was that of making these past three years so so pleasant...Thank you!

Summary

Reinforced concrete deterioration due to steel reinforcing bars corrosion is recognized as a serious problem, affecting the durability of various types of civil structures. Many efforts have been dedicated to studying the steel corrosion process induced by chloride penetration, being by far the most frequent cause for reduced durability of reinforced concrete structures. Much less attention has been focused on the microbial degradation of reinforced concrete structures occurring as a consequence of the presence of bacteria involved in the sulfur cycle (Sulfate Reducing Bacteria and Sulphur Oxidizing Bacteria) whose metabolic products react with the cementitious matrix yielding to fast deterioration processes. According to literature, in such field, most of the attentions were focused on concrete deterioration, while if and how bacteria metabolites eventually affect the behaviour of the steel reinforcing bars appears to be still an open issue.

The research project aims at filling up the knowledge gap above mentioned, that is: assessing how risky and aggressive a bacterial environment is, especially focusing on corrosion of steel reinforcing bars. On this purpose, abiotic solutions, simulating bacteria metabolic products were used for all tests. While a second part of the work was devoted to the development of a "smart" inhibitive system able to protect steel rebars from the corrosion induced by biogenic acidity that slowly neutralize cement alkalinity. The prolonged protective effect was meant to be achieved by encapsulating the active substances into pH sensitive microbeads, that would release the inhibitor only when reached by the acidification front, thus preventing a premature leaching of the inhibitor.

As a common practice in concrete science, investigations were started from the easier system of the steel rebars directly immersed into simulating solutions. Thus, a stable passive layer was growth on the steel surfaces by means of a three days immersion into a saturated $\text{Ca}(\text{OH})_2$ solution. Afterwards, samples were moved into sulfides containing alkaline solutions or diluted sulfuric acid, aiming to simulate the metabolic products of SRB and SOB respectively.

The acidic conditioning, into diluted sulfuric acid solutions, easily dissolved the passive layer and caused a fast onset of generalized corrosion, whose extension was found to be dependent on the acid concentration as indicated by both gravimetric and electrochemical tests. Conversely, sulfides were proven to induce localized corrosion, their interactions with the steel surface resulted to be significantly affected by the pH of the environment. Actually, for a prevailing of hydroxyl ions over the sulfides ones the steel surface remained protected by the oxide layer, while at lower pH steel-sulfides interaction were promoted, yielding to a porous, conductive, and thus non protective layer of iron sulfides.

Once clarified the corrosion mechanisms for steel directly immersed in simulating solutions, reinforced mortar samples were cast, cured, carbonated and then conditioned into two different model media: a sulfides containing solution and diluted sulfuric acid solution. The combination of several electrochemical techniques such as OCP, LPR and EIS pointed out the active behavior of the embedded steel rebars. Visual inspection performed at the end of a 500 days conditioning period confirmed that the acidic conditioning yielded to more severe damages.

On the basis of such findings, a "smart" corrosion inhibitor was developed by combining together calcium phosphate and methylene blue dye, being both active compounds in terms of protection of carbon steel from sulfuric acid corrosion. The resulting product was an organic/inorganic hybrid where the organic molecules were entrapped into a porous inorganic matrix, granting their release as a function of a pH drop leading to the dissolution of the latter. Anodic and cathodic potentiodynamic polarizations performed in sulfuric acid solution and in presence of the hybrid inhibitor confirmed that both the anodic and the cathodic processes were hindered as a consequence of the combined effect of methylene blue dye and phosphate ions. The effectiveness of the slow release mechanism was evaluated by means of LPR and EIS monitoring by comparing the responses of the hybrid, its two components singularly used and the free corroding system as a control case. The effect of the organic inhibitor was that of significantly increasing the polarization resistance. Such effect was rapidly lost in the case of methylene blue dye alone, while its slow release, together with the synergic effect of phosphate ions contributed to the prolongation of the protective effect.

Finally the interactions of the hybrid and its components with the cementitious matrix were investigated by means of isothermal calorimetry and standard compressive strength tests. The response of both the hydration rate and the strength evolution were found to be independent from the chemical admixtures.

Once excluded the onset of negative side effects, reinforced mortar samples containing different amount of the unloaded HAP and the hybrid MBD-HAP were cast and exposed to a sulfuric acid environment for about four months. However such a conditioning period proved not to be long enough to induce the corrosion of the steel reinforcing bars.

Chapter 1.

Introduction

1.1 The challenge of a new project

Some time ago, I found a picture on the web, the power of effective visual communication is that, just a quick glance, few seconds, are more than enough to send to the target the desired message, and this was the case of that picture. It showed a steep mountain face covered in ice and snow, just a few black rocks contrasted with the white tone of the picture, such white was also strengthened by a snow storm that was hitting the wall. The feeling was that of freezing and discomfort, no wise man would have desired to be there; but more carefully looking, a colored human shape could be barely noticed in the whiteness of the storm, it was a climber fighting his way up to the summit. Yet the image was strong and impressive, but its sense was underlined by an anonymous quote written overlay. "*Life begins at the end of your comfort zone*" was the text. Certainly as a climber and mountaineer, I was the right target for such a message, and it worked, because it impressed me.

Our present society, but in general all those of the western economies, moved towards a welfare model, where the life quality is mainly based on low fatigue, low suffering, low uncertainties and low doubts. The spread in technological advances led to the idea that the right and the only way to get any desired achievement should always keep us within our comfort zone. Is that true or is just an illusion of the consumerist age we are living?

Coming back to the sentence of the picture, I totally agree with its statement, especially considering that life strictly corresponds with the individual growing process. There is almost nothing to learn or to grow to, while remaining within our "safe" comfort zone. The learning process itself involves the action to make a step from the known ground to the unknown, there is risk in it, of course, and the more you venture out, the greater will be the exposure to failure. We have been taught that failure is a shame, but the only certain failure is standing still and do not trying anything, while the more we risk, and actually fail, the greater our chances of success will be.

In my alpinistic career, I have often had to balance the risk-benefit equation, making my choices outside the comfort zone, and I'm sure that battling the Russian cold and wild winds blowing on Elbrus, or struggling in search of oxygen in the rarefied air of the high altitude of Himalaya and Pamir gave me invaluable chances of growing as person [1].

Up to this point, such words would probably seem a rather unusual introduction to a PhD thesis, what is the sense of all of this? What is worth for life in general, or for sport activities, may also be applicable to other different fields. Why not thinking to science and research as for a learning process? one of the infinite ways we have to generate knowledge and to grow? Accordingly, why remaining confined in a restricted comfort zone?

After the master graduation, and in the two subsequent years during which I worked with a research grant, I got a considerable knowledge in the field of the electrochemical deposition and characterization of conducting polymer used for corrosion protection of light alloys. I had defined a personal comfort zone made with skills, literature studies and experimental practice, where I felt comfortable in. The choice of starting the PhD led to the question of the topic to be investigated in the following three years, the initial natural idea was that of continuing in the same direction going further with different materials and testing techniques.

Until a point, when Dr. Stefano Trasatti, my doctoral supervisor, asked me what was my idea on moving to a completely different field such as the microbial deterioration of reinforced concrete structures. At that moment, I only had a vague idea of what the reinforced concrete was, and nobody else in our research group had any knowledge in that field, so that his proposal seemed unwise far, big and difficult. Wasn't that a good occasion for leaving my scientific comfort zone? Probably yes, it was...that is how I accepted the new challenge. In life, as in sports, as in business, and probably also in science, big challenges generally offer bigger chances to fail, but also bigger chances to learn, and it up to us, as men, as researchers to define what is the acceptable risk level, and how many physical and intellectual resources are we ready to dissipate in the overcoming difficulties.

Any academic research, necessarily starts from a solid foundation of ground knowledge, over which the complexity of a detailed scientific investigation can be built on. In my case such knowledge was not available, so that my first task was to build it. The biggest part of the first year of my PhD was actually spent in literature study, whose results are detailed in the following chapter. Such study resulted to be a multidisciplinary effort due to the variety of the gaps to be filled, ranging from the engineering field of the basics of concrete science, to the biological one in terms of microbially induced corrosion, or the purely electrochemical fields such as learning the principles and the uses of sophisticated measuring techniques such as the electrochemical impedance spectroscopy. The main difficulty of this initial step, and that also persisted in the subsequent years has been the lack of technical mentor. What it is collected in present text, is the result of almost completely autonomous choices, some of them proved to be correct, several others were mistaken, and some of them were certainly due to inexperience. All of them were integral part of the exceptional learning process of the last three years.

1.2 The Concrete Laboratory set-up

Concrete, being a composite material, it is known to have a very complex behaviour as many internal factors such as water/binder ratio, type of cement, type and size of the aggregates, together with many external factors such as temperature, humidity, presence of aggressive species can strongly affect its performance. For this reason a study on the rebar corrosion in concrete can start from the electrochemical testing of mild steel in artificially simulated concrete pore solutions, but then, in order to simulate closer the reality, it is necessary to make tests with steel samples embedded in mortar and concrete. Thanks to the useful indications of my co-tutor, Dr.ssa Pierangela Cristiani from RSE, a private research company, we were able to get all the necessary equipment for mortar and concrete preparation from a decommissioned concrete laboratory. As being unused for several years, equipments were subjected to a complete control of electrical and mechanical parts in order to fully restore their functionality once transferred to our labs. Actually our new concrete laboratory has all the necessary equipment i.e. mixers, vibrating tables, moulds of different sizes, specific for both the production of mortar and concrete samples (fig 1.1-2). Furthermore we dispose of a curing room and a concrete cutting machine. Regarding to the characterization of the mechanical and rheological properties we are actually able to determine the workability of fresh mortar and concrete with two specific equipments, i.e the flow table for mortar, and a Vebe apparatus for concrete, respectively conforming to the standards EN 459-2 and EN12350-3 (Fig. 1.3).

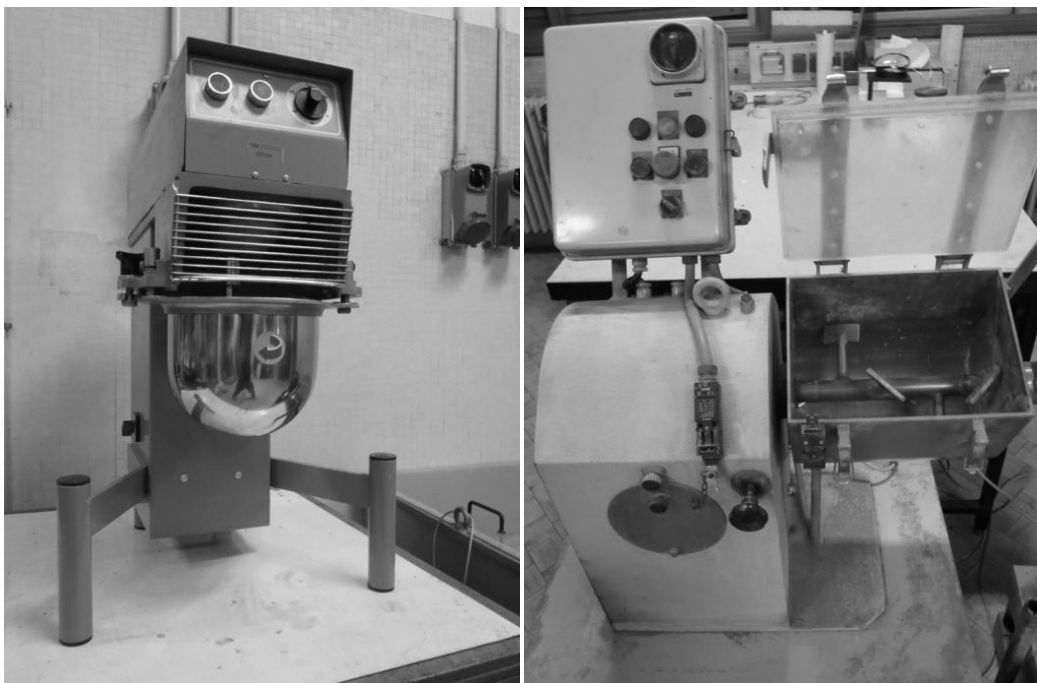


Fig. 1.1: Mixer devices. Left side: 5 Lt capability for mortar. Right side: 10 Lt capability for concrete.

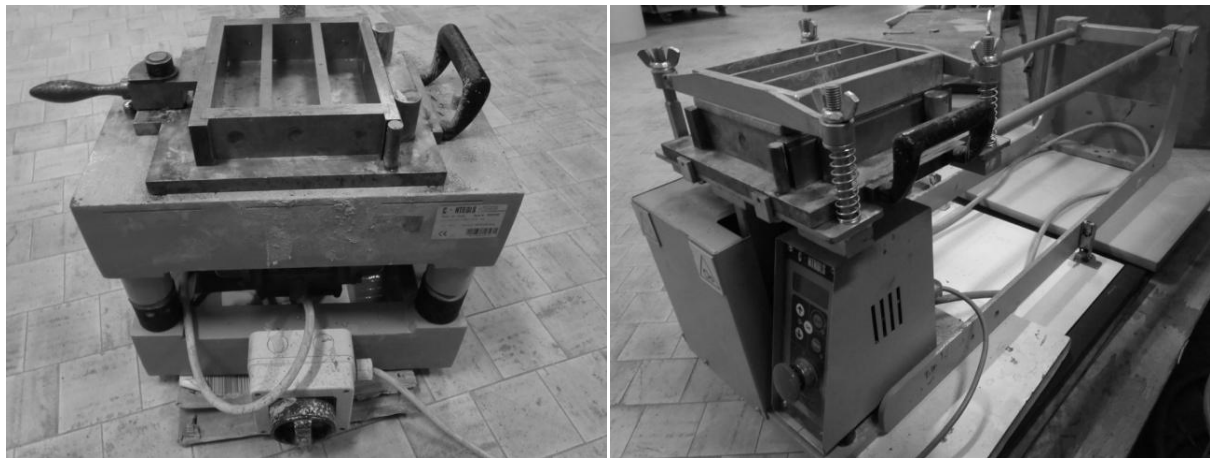


Fig. 1.2: Compaction devices. Left side: vibrating table. Right side: Jolting table.



Fig. 1.3: Workability testing devices. Left side: flow table (mortar). Right side: Vebe apparatus (concrete).

1.2.1 Construction of the accelerated carbonation chamber

Notwithstanding the conspicuous facilities obtained from the dismissed concrete laboratory, still, according to the project plan, there was a lack of a crucial tool. Actually the literature study pointed out that the first step of the microbial deterioration of RC structures was an abiotic neutralization of the concrete natural alkalinity leading from a pH of about 13 to values around 9, thus allowing the growth and the thriving of bacterial colonies. In order to simulate a realistic case, such abiotic pH decrease needed to be re-produced in the lab on the concrete specimens. Atmospheric CO₂ can diffuse through the cement matrix and lowers the concrete pH by reacting with the calcium hydroxide in a process known as carbonation. Such process naturally takes several years to occur and to produce significant changes in the concrete properties because of the very low concentration of CO₂ in the atmosphere (0.04% V/V). The carbonation processes has been thoroughly studied by different groups [2-5] each one having developed an accelerated carbonation chamber with different design, properties and control parameters. From the above cited studies emerged that the carbonation depth was significantly dependent on w/c ratio, temperature, relative humidity, and CO₂ partial pressure. An increased w/c ratio is related to a more porous concrete in which the CO₂ can more easily diffuse and react; its diffusion is hindered in a completely water saturated concrete, while, on the other side, the reaction needs some water molecules to occur, so that the maximum carbonation rate was achieved with a relative humidity value around 60%, furthermore by increasing the temperature and the CO₂ concentration the carbonation rate resulted to be increased. Accelerated carbonation chambers are available on the market, but being their price over 1000 €, such an investment was not justifiable in the framework of my PhD research activity.

An homemade carbonation chamber was built using a HDPE airtight drum, in which a removable structure made of four steel supports and a series of HDPE grids was placed. A mini dehumidifier based on the principle of thermo electric Peltier module was purchased from Cornwall Electronics, together with a thermo-hygrometer that was placed in the inner side of the cap, under a Plexiglass window. A forced air circulation system was studied and realized using four recycled computer fans, thus granting the humidity extraction from the mortar samples as efficient as possible (fig1.4). Both the dehumidifier and the air circulation system could be tuned by a control panel placed on the top of the cap (fig. 1.5). A Teflon flange was specifically designed and produced for airtight CO₂ entrance and exit fluxes. A front and side scheme together with a picture of the completed carbonation chamber are reported in figure 1.6.

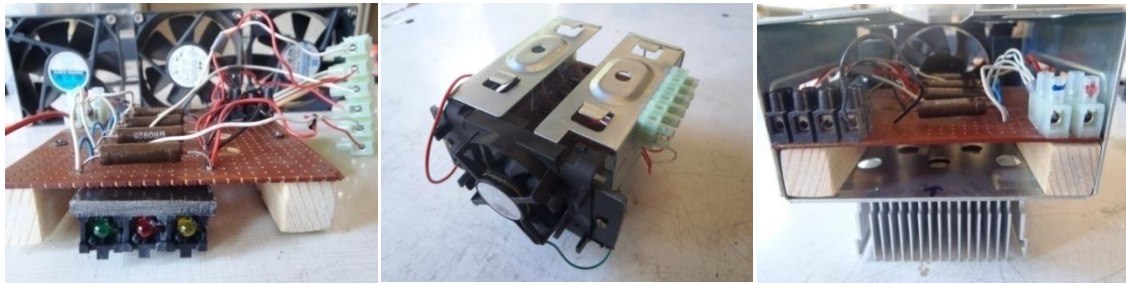


Fig. 1.4: Construction stages of the ventilating system.

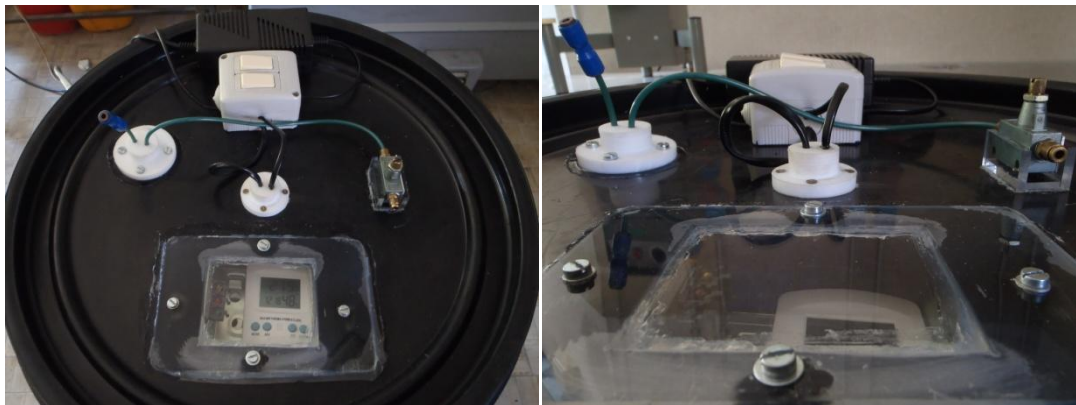


Fig. 1.5: Accelerated carbonation chamber, the control panel.

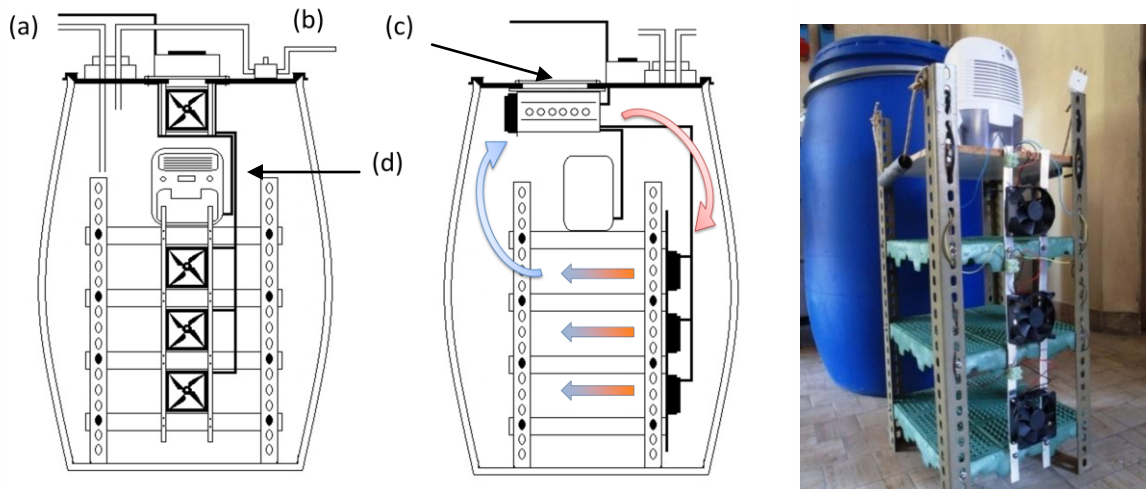


Fig.1.6: Scheme and picture of the homemade carbonation chamber. (a) gas in, (b) gas out, (c) control panel (d) dehumidifier.

1.2.2 Construction of the electrochemical probe

The accelerated carbonation chamber was not the only missing part of the equipment that required a creative effort to be overcome. Actually, once the reinforced mortar samples were cast, cured and carbonated, they were expected to be conditioned for a long time in aggressive solutions, aiming to simulate the deterioration mechanism occurring "on the field". Being all the corrosion processes,

intrinsically related to electron transfer reactions, electrochemical measurements proved to be undoubtedly valuable tools for the investigation of the corrosion mechanism. Most of the electrochemical measurements require a three electrodes arrangement consisting in a working electrode, that is the material to be studied, in the present case the steel reinforcing bar, a reference electrode allowing the potential measurements, and a counter electrode, granting a current flow in between the same and the working.

Generally, all the three electrodes are immersed into the same testing solution, that, being a conductive medium, allows current flows and potential readings. In some cases, the solution conductivity can be enhanced by adding a salt, inert to the system, as supporting electrolyte.

In reinforced concrete samples, the steel rebar is embedded into a porous cementitious matrix. Such pores contain a solution whose volume and composition mainly depend on the concrete type, and the external environment. Concrete cover thickness can be consider as a solid electrolyte, consequently requiring a specifically designed probe, allowing the positioning of the reference and the counter electrode.

Drawing on the device realized by Sathiyanarayanan et al. [6] the electrochemical probe was realized as schematically shown in the picture of fig. 1.7. Two prismatic Plexiglass moulds were assembled and filled with epoxy resin; two titanium square sheets of dimension 4x4 cm, serving as counter-electrodes were placed respectively at the bottom and at the top of the upper and lower part of the probe. The two titanium sheets were electrically connected between each other and with the socket on front panel, electrical connection were realized with a rubber insulated copper wire.

The upper part of the counter electrode was drilled in the centre in order to allow the positioning of the reference electrode, that was connected to and other socket on the probe front panel.

Four stainless steel springs allowed the clamping of the probe on the reinforced mortar prism. The electrical contact between the reference-counter electrode and the mortar surface was granted by a wet sponge.

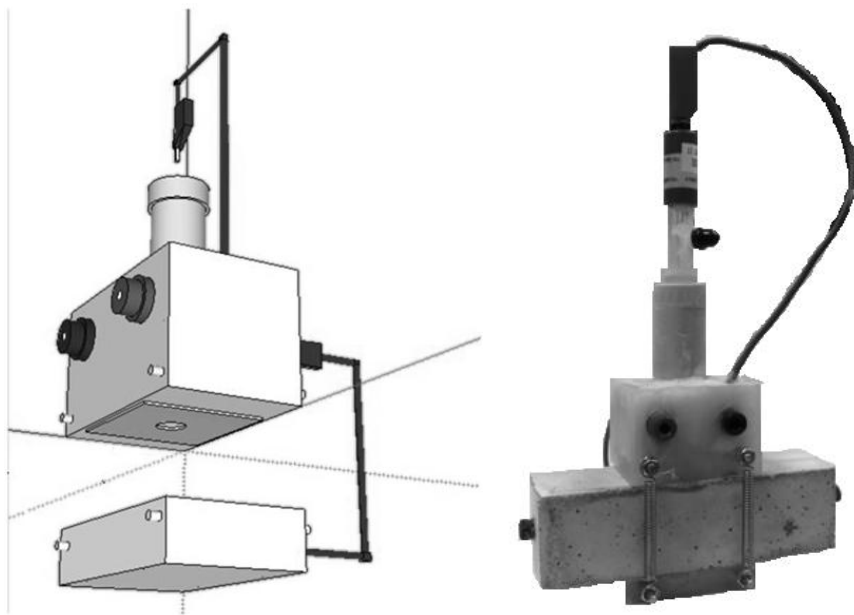


Fig. 1.7: Sketch and picture of the probe designed for electrochemical measurements on prismatic reinforced mortar samples.

1.3 Motivations for research

It is well known that reinforced concrete structures can be subjected to different deterioration mechanisms due to diverse causes: mechanical, physical, structural, chemical, biological and corrosion of the steel rebars. Among these different possibilities, however, the steel corrosion, is by far the most frequently occurring, posing serious issues on the infrastructures service life [7].

Microbially induced concrete corrosion (MICC) has long been recognized, since 1945, when Parker observed the formation of a white, putty-like deteriorated superficial layer on the walls of a concrete sewer [8,9]. Such kind of deterioration can potentially affect all the concrete structures exposed to an aquatic environment, and the risk become increasingly high in the presence of stagnant and/or polluted water, such as in case of sewer networks or wastewater treatment plants. O'Connell et al. [10] stated that in the US alone, the annual investments for wastewater infrastructures are close to \$21 billion, and that annual maintenance cost exceeds \$25 billion [11].

The deleterious effect of microbial environments is recognized to be related to bacteria involved in the sulfur cycle and in particular to their metabolic products: hydrogen sulfides and sulfuric acid. Especially the latter, reacts with portlandite transforming the sound and dense cementitious matrix into a loose and soluble gypsum layer.

Although the microbial deterioration of the cementitious matrix has been thoroughly investigated in several studies, very little is known about [12-16] if and how the same metabolites can in some way affect the integrity of the steel reinforcing bars. Actually, such topic is just barely mentioned in [13,14], while few corrosion studies just used gaseous H₂S [15-19].

1.4 Objectives of the thesis

The research project aims at filling the knowledge gap above mentioned, that is: assessing how risky and aggressive a bacterial environment is, especially focusing on steel reinforcing bar corrosion. Different electrochemical techniques, together with gravimetric measurements and surface analysis were combined in order to get more insight into the corrosion mechanisms.

A second part of the present work was devoted to the development of a "smart" inhibitive system able to provide the maximum efficiency in terms of steel corrosion protection induced by the biogenic acidity. Being the final objective that of increasing the tolerance of mortar / concrete reinforced structures with regard to microbially induced deterioration and increasing their maintenance-free service life. The prolonged protective effect was meant to be achieved by encapsulating the active substances into pH sensitive microbeads, that would release the inhibitor only when reached by the acidification front, thus preventing a premature leaching of the inhibitor.

1.5 Outline of the thesis

The present thesis consists of 7 chapters that are written following the track of the temporal developments of the research activities along the three years of my PhD research. The activities described in chapters 2 to 5 were held in the Corrosion Engineering and Applied Electrochemistry Laboratory at Università degli Studi di Milano; while part of the electrochemical measurements discussed in chapter 5 and the whole experimentation of chapter 6 were performed at the MicroLab of the Civil Engineering and Geosciences department of the Delft University of Technology, The Netherlands.

Fig.1.8 reports a flowchart of the experimental activities highlighting the principal, logical path and collateral branches originated during the course of the work.

Chapter 1 gives a general introduction on how was developed the apparently rash idea of opening a new research line in a completely unknown field, without being able to count on almost any support or pre-existing skill. Furthermore the background, objectives, and an outline on the thesis are provided.

Chapter 2 deals, with a wide literature review, ranging from fundamentals of cement science, to durability issues of reinforced concrete structures, especially focusing on the corrosion of steel rebars and on the microbially induced concrete deterioration.

Chapter 3 investigates the basis for all the subsequent activities, that is the carbon steel passivation mechanism in highly alkaline environments simulating the concrete pore solution. Cyclovoltammetric experiments pointed out the double step mechanism involving the Fe-Fe(II) and Fe(II)-Fe(III) transitions and how their electrochemical responses were affected by different experimental parameters. Emphasis was finally put on the relationship between the passivation time and the growth of a stable, protective oxide film.

Chapter 4 presents the results related to reinforcing steel corrosion exposed to Na_2S and H_2SO_4 solutions, simulating bacteria metabolic products. An initial multivariable study was performed by directly immersing the steel samples in the aggressive solutions, allowing to check the effects of steel pre-passivation, aggressive species concentration, solution aeration and pH. Once clarified the corrosion mechanism in such easier systems the attention was moved to reinforced mortar samples, whose behavior was regularly monitored along a 500 days long period of conditioning into the same simulating solution as above.

Chapter 5 deals with the development of a "smart" corrosion inhibitor aiming to protect the steel reinforcements from the biogenic acid attack. The inhibitive properties of several organic and inorganic compounds were evaluated in an initial screening phase. The most promising compounds were subsequently incorporated into an inorganic, pH sensitive hosting matrix, and their pH controlled released was thoroughly investigated. Finally the protection efficiency of the "smart" inhibitor was evaluated for steel directly immersed into the aggressive solutions.

Chapter 6 discusses some preliminary results concerning the addition of the "smart" inhibitor, previously synthesized, to a cementitious matrix. Attention was initially focused on possible side effects on the cementitious matrix, in terms of hydration rate and compressive strength development. In a second stage, the inhibitor was added to reinforced mortar samples aiming to evaluate its protective efficiency when admixed to a cementitious matrix.

Chapter 7 summarizes the results obtained in this research and gives the conclusions. Some recommendations are given for future research.

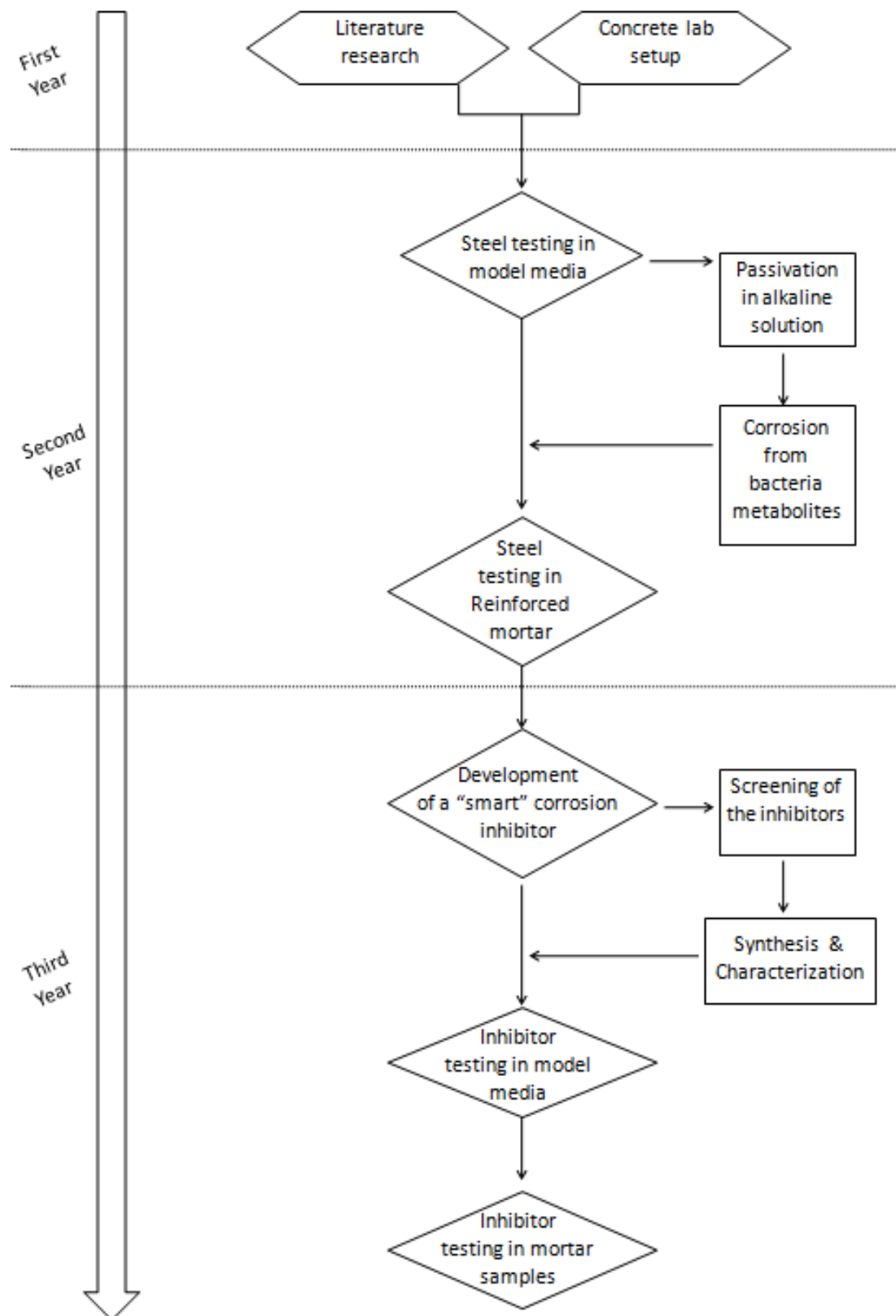


Fig. 1.8: Flow chart of the thesis, showing the distribution of the experimental activities during the three years.

References

- [1] E. Volpi, M. Pietripaoli, Korzhenevskaya, Stile Alpino, No.28 (2015) 56-65.
- [2] G.K. Glass, C.L. Page, N.R. Short, Factors affecting the corrosion rate of steel in carbonated mortars, Vol. 32, No 12 (1991) 1283-1294.
- [3] J. Chi, C. Yang, Effects of carbonation on mechanical properties and durability of concrete using accelerated testing method, J. Marine Sci. and Techn. 10 (2002) 14-20.
- [4] S.K. Roy, K.B. Poh, D. Northwood, Durability of concrete-accelerated carbonation and weathering studies, Building and Environment, Vol. 34, No. 5 (1999) 597-606.
- [5] C. Chang, J. Chen, The experimental investigation of concrete carbonation depth, Cement and Concrete Research 36 (2006) 1760-176.
- [6] S. Sathiyanarayanan, P. Natarajan, K. Saravanan, S. Srinivasan, G. Venkatachari, Corrosion monitoring of steel in concrete by galvanostatic pulse technique, Cement & concrete Composites, 28 (2006) 630-637.
- [7] L. Bertolini, B. Elsener, P. Pedefterri, E. Redaelli, R. Polder, Corrosion of steel in concrete: prevention, diagnosis, repair, John Wiley & Sons, 2013.
- [8] C.D. Parker, The isolation of a species of bacterium associated with the corrosion of concrete exposed to atmospheres containing hydrogen sulfide, Aust. J. Exp. Biol. Med. Sci., 23 (1945) 81-90.
- [9] C.D. Parker, The function of *Thiobacillus concretivorus* (nov. spec.) in the corrosion of concrete exposed to atmospheres containing hydrogen sulfide, Aust. J. Exp. Biol. Med. Sci. 23 (1945) 91-8.
- [10] M. O'Connell, C. McNally, M.G. Richardson, Biochemical attack on concrete in wastewater applications: A state of the art review, Cement & Concrete Composites 32 (2010) 479-485.
- [11] Congressional budget office. future investment in drinking and wastewater infrastructure. ISBN 0160512433, Congressional Budget Office; 2002.
- [12] D. Roberts, D. Nica, G. Zuo, J. Davis, Quantifying microbially induced deterioration of concrete, Int. Biodet. Biodeg. 49 (2002) 227-234.
- [13] N. De Belie, J.J. Lenehan, C.R. Braam, B. Svennerstedt, M. Richardson, B. Sonck, Durability of Building Materials and Components in the Agricultural Environment, Part III: Concrete Structures Journal of Agricultural Engineering Research, Vol. 76, Issue 1(2000) 3-16.

- [14] M.A. El-Reedy, Steel reinforced concrete structures: assessment and repair of corrosion, CRC press, 2008.
- [15] J. Monteny, E. Vincke, A. Beeldens, N. De Belie, L. Taerwe, D. Van Gemert, W. Verstraete, Chemical, microbiological, and in situ test methods for biogenic sulfuric acid corrosion of concrete, Cement and Concrete Research, Vol. 30, Issue 4 (2000) 623-634.
- [16] N. De Belie, J. Monteny, A. Beeldens, E. Vincke, D. Van Gemert, W. Verstraete, Experimental research and prediction of the effect of chemical and biogenic sulfuric acid on different types of commercially produced concrete sewer pipes, Cement and Concrete Research, Vol. 34, Issue 12 (2004) 2223-2236.
- [17] A.F. Idriss, S.C. Negi, J.C. Jofriet, G.L. Hayward, Corrosion of steel reinforcement in mortar specimens exposed to hydrogen sulphide, part 1: impressed voltage and electrochemical potential tests, J. agric. Engng Res., Vol 79, No.2 (2001) 223-230.
- [18] A.F. Idriss, S.C. Negi, J.C. Jofriet, G.L. Hayward, Corrosion of steel reinforcement in mortar specimens exposed to hydrogen sulphide, part 2: diffusion tests, J. agric. Engng Res., Vol 79, No.3 (2001) 341-348.
- [19] V. Assaad Abdelmseeh, J. Jofriet, G. Hayward, Sulphate and sulphide corrosion in livestock buildings, Part II: Reinforcing steel corrosion, Biosystem engineering, 99 (2008) 382-389.

Chapter 2.

Literature study

2.1 Concrete

2.1.1 History of concrete

Concrete is a very ancient construction material, precursor of the currently used cementitious materials that were formerly used by ancient Egyptians and subsequently by Romans. The latter developed what was called "*betonium*" that consisted into a pozzolanic mortar containing crushed stones; such material was initially used only as a filling in between two brick walls. In a following period, crushed stones started to be replaced with broken bricks and tiles resulting in lighter material that was called "*opus caementitium*", furthermore the brick walls were replaced by wood planks [1]. By using such methodology, ancient Romans were able to built impressive structures such as Pantheon (fig.2.1) and Caracalla baths (fig.2.2) that are lasting up to the modern era.



Fig. 2.1: Pantheon, Rome, (I cen. d.C.).



Fig. 2.2: Caracalla baths, Rome, (III cen. d.C.).

However, the pozzolanic cement was still a precursor of the modern cement as it was obtained by simply grinding natural materials, containing silica and alumina from volcanic ashes, found close to Pozzuoli, a small village in the Vesuvio area [2].

The Middle age was characterized by a backward inversion in terms of use and quality of cement, returning to wood and stones as primarily building materials. The

renaissance too, was not a flourishing period for concrete structures, that arose again in XVIII century when John Smeaton used a mixture of pozzolana, limestone and clay in the restoration of the Eddystone lighthouse (1756) shown in fig. 2.3.

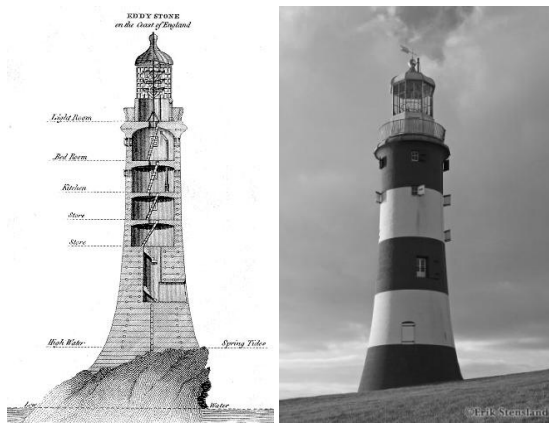


Fig. 2.3: Eddystone lighthouse, in a contemporary engraving (left), and in the actual location in Plymouth (right).

The patent for Portland cement was attributed in 1824 to Joseph Aspdin, who was the first heating a mixture of clay and limestone until the evolution of CO₂, although temperature was not high enough to reach the clinkering. Higher temperature, allowing the material clinkering and the consequent formation of strongly cementitious compounds, were proposed in 1845 by Isaac Johnson.

Three years later, in 1848, in occasion of the universal fair held in Paris, Joseph Lambot presented a boat hull, made with cement paste containing a series of steel elements, this was the first reported application of reinforced cementitious material (fig-2.4).



Fig. 2.4: Lambot's reinforced cement boat (1848).

From these origins to recent years, the use of reinforced concrete spread around the whole world becoming the most used man-made material. Data support the claim that the amount of concrete used for construction worldwide exceeds 12 billion tons annually reaching a volume of about 10 km³ [3]

Multiple are the reasons for such a wide success, undoubtedly one of the most important is the component availability (water, cement and aggregates) both from the geographical point of view and for their very low costs. Secondly, the preparation procedure is extremely straightforward, just consisting in mixing the components in suitable ratios.

Furthermore, reinforced concrete, combining the compressive strength of the cementitious material with the steel tensile strength proved to be an extremely durable material able to withstand heavy loads and demanding environmental conditions.

2.1.2 Portland cement

Portland cement is made from a mixture of calcareous material such as limestone with silica and alumina deriving from clay or shale. The productive process consists in finely grinding the raw materials and then mixing them in the appropriate proportion; the mix is subsequently burned in large rotary kilns reaching temperatures above 1450°C. At such high temperatures the mineral materials partially melt and sinter resulting in the formation of a spherically shaped product (3 to 25 mm in diameter) known as clinker. Once cooled down, the clinker is grinded again, mixed with a certain amount of gypsum and commercialized as Portland cement [2].

During the time spent into the kiln, the raw materials react with each others, yielding more complex products and reach a chemical equilibrium. Such equilibrium is not maintained during the subsequent cooling step, so that the resulting product has both crystalline and amorphous phases, whose ratio strictly depends on the cooling rate.

Table 2.1 reports a list of the major components of Portland cement. However, in addition to such components also minor compounds such as MgO, TiO₂, Mn₂O₃, K₂O and Na₂O are formed, accounting for a few per cent of the mass of cement. The two latter compounds above listed, notwithstanding their low concentration can in some case react with aggregates in concrete, leading to detrimental effect known as alkali-silica reaction (ASR) [2].

Table 2.1: Main components of Portland cement.

Name of compound	Oxide composition	Abbreviated name
Tricalcium silicate	3CaO.SiO ₂	C ₃ S
Dicalcium silicate	2CaO.SiO ₂	C ₂ S
Tricalcium aluminate	3CaO.Al ₂ O ₃	C ₃ A
Tetracalcium aluminoferrite	4CaO.Al ₂ O ₃ .Fe ₂ O ₃	C ₄ AF

Table 2.2: Composition limit of Portland cement.

Oxide	Content %wt
CaO	60-67
SiO ₂	17-25
Al ₂ O ₃	3-8
Fe ₂ O ₃	0.5-6.0
MgO	0.5-4.0
Alkalies	0.3-1.2
SO ₃	2.0-305

According to the norm EN 197-1 [4] five main cement classes are available in Europe, each one divided in sub-categories as a function of the type and the amount of supplementary materials added to the clinker. The resulting 27 cement types are summarized in table 2.3.

Table 2.3: Classification of cement types according to EN 197-1 [4].

Main types	Notation of the 27 products (types of common cement)		Composition (percentage by mass ^a)										Minor additional constituents	
			Main constituents											
			Clinker	Blast-furnace slag	Silica fume	Pozzolana		Fly ash		Burnt shale	Limestone			
			K	S	D ^b	P	Q	V	W	T	L	LL		
CEM I	Portland cement	CEM I	95-100	—	—	—	—	—	—	—	—	—	0-5	
	Portland-slag cement	CEM II/A-S	80-94	6-20	—	—	—	—	—	—	—	—	0-5	
		CEM II/B-S	65-79	21-35	—	—	—	—	—	—	—	—	0-5	
	Portland-silica fume cement	CEM II/A-D	90-94	—	6-10	—	—	—	—	—	—	—	0-5	
		CEM II/A-P	80-94	—	—	6-20	—	—	—	—	—	—	0-5	
	Portland-pozzolana cement	CEM II/B-P	65-79	—	—	21-35	—	—	—	—	—	—	0-5	
		CEM II/A-Q	80-94	—	—	—	6-20	—	—	—	—	—	0-5	
		CEM II/B-Q	65-79	—	—	—	21-35	—	—	—	—	—	0-5	
		CEM II/A-V	80-94	—	—	—	—	6-20	—	—	—	—	0-5	
CEM II	Portland-fly ash cement	CEM II/B-V	65-79	—	—	—	—	21-35	—	—	—	—	0-5	
		CEM II/A-W	80-94	—	—	—	—	—	6-20	—	—	—	0-5	
		CEM II/B-W	65-79	—	—	—	—	—	21-35	—	—	—	0-5	
		CEM II/A-T	80-94	—	—	—	—	—	—	6-20	—	—	0-5	
	Portland-burnt shale cement	CEM II/B-T	65-79	—	—	—	—	—	—	21-35	—	—	0-5	
		CEM II/A-L	80-94	—	—	—	—	—	—	—	6-20	—	0-5	
	Portland-limestone cement	CEM II/B-L	65-79	—	—	—	—	—	—	—	21-35	—	0-5	
		CEM II/A-LL	80-94	—	—	—	—	—	—	—	—	6-20	0-5	
		CEM II/B-LL	65-79	—	—	—	—	—	—	—	—	21-35	0-5	
		CEM II/A-M	80-94	<----- 6-20 ----->									0-5	
		CEM II/B-M	65-79	<----- 21-35 ----->									0-5	
CEM III	Blastfurnace cement	CEM III/A	35-64	36-65	—	—	—	—	—	—	—	—	0-5	
		CEM III/B	20-34	66-80	—	—	—	—	—	—	—	—	0-5	
		CEM III/C	5-19	81-95	—	—	—	—	—	—	—	—	0-5	
CEM IV	Pozzolanic cement ^c	CEM IV/A	65-89	—	<----- 11-35 ----->				—	—	—	—	0-5	
		CEM IV/B	45-64	—	<----- 36-55 ----->				—	—	—	—	0-5	
CEM V	Composite cement ^c	CEM V/A	40-64	18-30	—	<----- 18-30 ----->		—	—	—	—	—	0-5	
		CEM V/B	20-38	31-50	—	<----- 31-50 ----->		—	—	—	—	—	0-5	

a The values in the table refer to the sum of the main and minor additional constituents.
 b The proportion of silica fume is limited to 10 %.
 c In Portland-composite cements CEM III/A-M and CEM II/B-M, in pozzolanic cements CEM IV/A and CEM IV/B and in composite cements CEM V/A and CEM V/B the main constituents other than clinker shall be declared by designation of the cement (for example see clause 8).

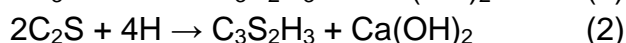
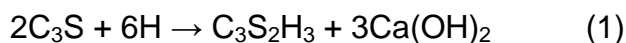
2.1.3 Cement Hydration

By simply mixing the cement powder with water a fluid paste is initially obtained, that undergoes to a slow stiffening process yielding to a solid mass, the hydrated cement paste. It has to be mentioned that the hydration process is a general term which includes the different interactions occurring between cement grains and water molecules, involving either the water molecule addition and hydrolysis reactions.

It can be easily imagined that the hydration process does not proceed at a constant rate, but significantly slow over time due to diffusion limitations occurring as a consequence of the stiffening paste, so that even after a long period, still remain an appreciable amount of unreacted cement.

It is well known that products of cement hydration are chemically equivalent to hydration products of the single components under similar condition, thus in order to get more insight into the cement hydration, tricalcium silicate hydrate (C_3SH), dicalcium silicate hydrate (C_2SH) and tricalcium alluminate hydrate (C_3AH) can be individually discussed. Tetracalcium aluminoferrite is believed to be hydrated as tricalcium alluminate hydrate and an amorphous phase such as $CaO.Fe_2O_{3(aq)}$.

The hydration of the two calcium silicates occurs at different rate being faster for C_3S and slower for C_2S but leads to the same products indicated as calcium silicate hydrates (CSH). Calcium silicates are the responsible for cement paste alkalinity as their hydration reaction produces portlandite ($Ca(OH)_2$) as shown in reaction 1,2 where H stands for H_2O .



The reaction of pure C_3A is extremely fast and leads to an immediate stiffening of the paste known as flash-set; the gypsum addition to the clinker limits such reaction as the two components react together yielding insoluble calcium sulfoaluminate ($3CaO.Al_2O_3.3CaSO_4.32H_2O$) [2]. The C_3A hydration reaction can be expressed as in (3):



C_3A do not contribute to the strength of cement paste, and in addition it can cause some issue because of its immediate stiffening, the main motivation for its presence in the clinker is that it reduces the clinkering temperature facilitating the lime and silica combination. A further positive aspect of C_3A is its ability of binding chlorides.

2.1.4 Structure of the hydrated cement paste

Contrarily to what could be expected, most of the mechanical properties of hardened cement paste, depend more on the physical structure of the hydrated

cement paste rather than on its chemical composition; thus, understanding the development of cement microstructure during the hydration process plays a key role in the study of the transport properties of the hardened paste.

At any stage of hydration, the hardened paste consist of poorly crystalline hydrates of the various cement components, $\text{Ca}(\text{OH})_2$ crystals, unreacted cement grains and the residue of the water filled spaces in the fresh paste [2]. These latter are known as capillary pores and are characterized by dimensions in the micron range (fig.2.5). Capillary pores are not the only porosity form in hardened cement past, actually most of the hydrated product are colloidal, thus characterized by a high surface area due to interstitial voids, such pores are known as gel pores and have a nominal diameter around 3 nm. Furthermore, an erroneous compaction of the fresh mixture, or the addition of air entrapping agents can induce the presence of bigger air voids as indicated in fig. 2.5.

Gel pores and capillary pores are generally filled with an interstitial solution, whose composition is mainly dependent on the cement type. Such pore solution results to be extremely alkaline, having a pH values of 13 of higher, because of the dissolved $\text{Ca}(\text{OH})_2$, furthermore it generally contains also Na^+ , K^+ and Ca^+

Taking into consideration that the pores relevant to permeability are those with a diameter of at least 120-160 nm, capillary pores constitute the preferential pathways for ion diffusion so that they are considered as the main factor affecting the cement paste permeability and its susceptibility to freeze-thaw damaging. Such kind of porosity evolves with the cement hydration being initially higher and decreasing as water reacts with unhydrated cement grains. However it has been demonstrated that for a water/cement ratio higher than 0.38 there will be some volume of capillary pores left, even after the hydration process has been completed [2].

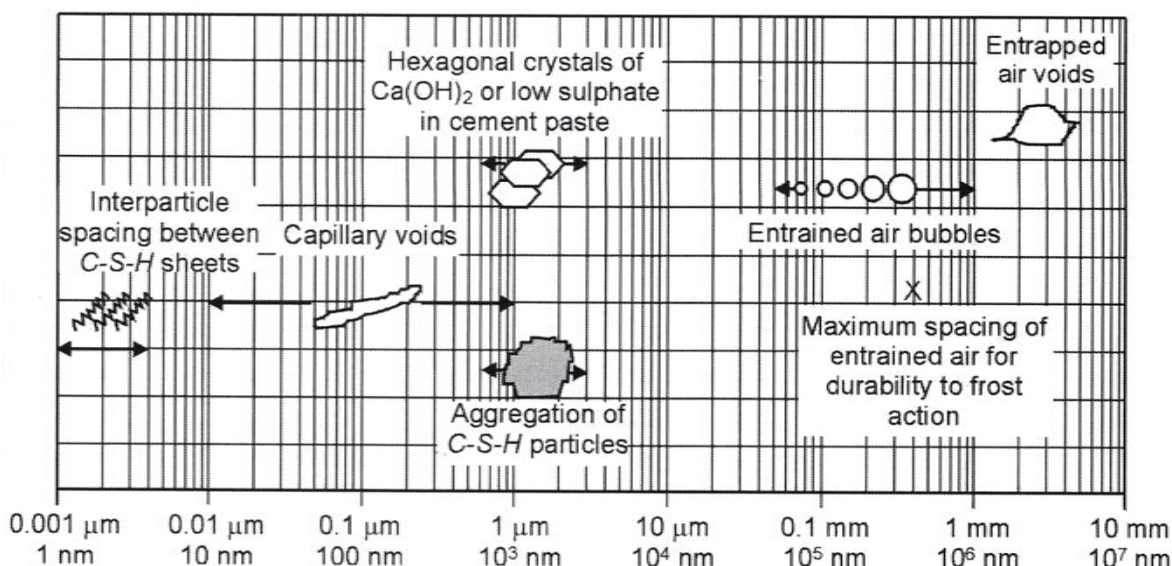


Fig.2.5: Pore size distribution in hydrated cement paste [5].

Capillary pores, allow ions migration, unless they constitute an interconnected network; as the hydration process advance, the solid content of the paste increase and part of the original pores are blocked. Figure 2.6 shows the relation between the water/cement ratio and the hydration degree at which the capillary pore are blocked, it clearly points out that for w/c ratio above 0.7 even the complete hydration would not produce enough gel to block all the pores [2].

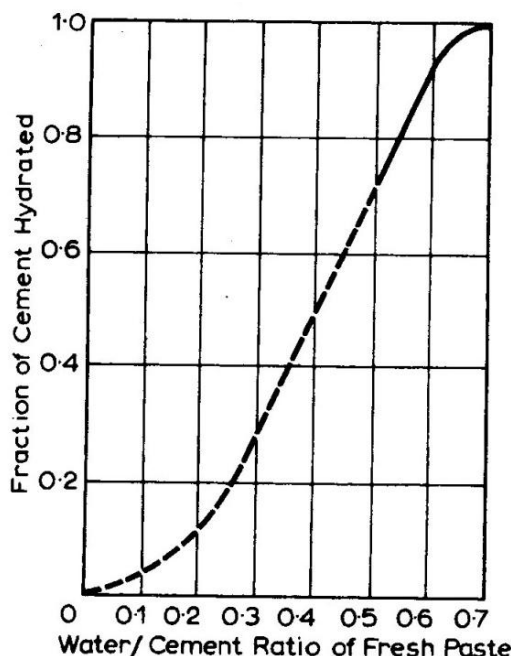


Fig. 2.6: Relation between the water/cement ratio and the hydration degree at which the capillary pore are blocked [6].

2.2 Durability of concrete structures

Durability of concrete may be defined as the ability of concrete to resist weathering action, chemical attack, and abrasion while maintaining its desired engineering properties. Different concrete structures require different degrees of durability, depending on the exposure environment and desired properties. For example, concrete exposed to tidal seawater will have different requirements than an indoor concrete floor.

There are several factors that can affect the concrete durability, the main important are:

Cement content: Mix must be designed to ensure cohesion and prevent segregation and bleeding. An appropriate balance between the water/cement ratio has to be found. Lowering the water content, leads to a reduced workability and could induce an inadequate compaction. Conversely, if water is added to improve workability, water/cement ratio increases, resulting in highly permeable material.

Compaction: An inadequate compaction generally leads to heterogeneous distribution of concrete elements, thus introducing defects in the structure.

Curing: It is very important to permit proper strength development by keeping the freshly cast concrete within certain ranges of temperature and humidity.

Cover: In order to protect steel rebars from corrosion the concrete cover thickness should respect the limits set in codes

Permeability: It is considered the most important factor for durability. It can be noticed that higher permeability is usually caused by higher porosity .Therefore, a proper curing, sufficient cement, proper compaction and suitable concrete cover can provide a low permeability concrete. Fig.2.7 shows the relation between permeability and w/c ratio for mature cement.

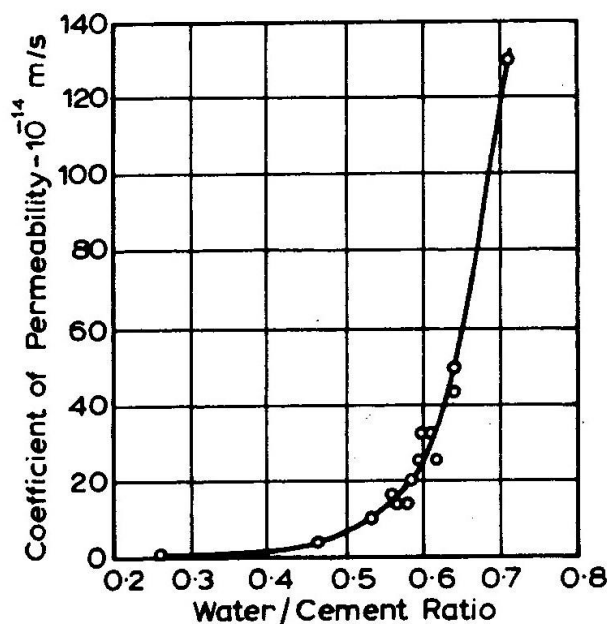


Fig. 2.7: Relationship between permeability and w/C ratio for mature cement pastes. [7].

2.2.1 Acid attack

Concrete is generally well resistant to chemical attack, however some acid compounds, both inorganic (nitric, phosphoric, sulfuric, hydrochloric etc.) and organic (acetic, citric, formic, lactic etc.) can cause serious durability issues.

Actually, concrete made of Portland cement is not resistant to strong acids, as they react with cement hydration products yielding to compounds characterized by either an increased solubility or lower mechanical properties.

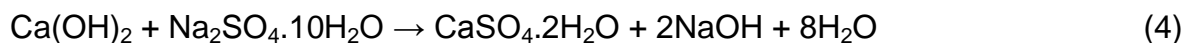
Among the cement hydration products, portlandite is certainly the most vulnerable to an acid attack, however calcium silicates hydrate can also be attacked. According to the literature [8], the limit safe pH should be around 6.5, and the attack becomes extremely severe for pH values lower than 4.5.

In case of acid attack the deterioration rate does not proceed linearly with time, but it is roughly proportional to its square root, being initially higher and slowing over time. The main motivation of such behavior is that the $\text{Ca}(\text{OH})_2$ dissolution leaves a gradually thickening surface layer of insoluble products that hinder the further penetration of the aggressive solution. Furthermore, the rate of attack decrease when, because of the fully deteriorated superficial cementitious layer, the aggregates become exposed thus decreasing the vulnerable surface [2]

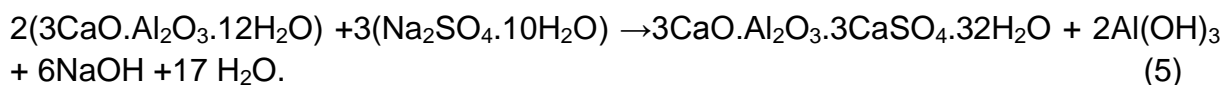
2.2.2 Sulfate attack

Soils and ground waters can be considered as fairly saline environments, among all the possible dissolved salts, sulfates are known to exert a disrupting effect on concrete structures. Actually, sulfates can react with the cement paste yielding to expansive products and thus originating cracking and spalling phenomena [9].

The reaction of sulfates with hardened cement paste proceeds by means of a double step: initially $\text{Ca}(\text{OH})_2$ is converted into gypsum according to reaction (4).



Calcium sulfate can attack the tricalcium aluminate hydrates forming a calcium sulfoaluminate known as ettringite as in reaction (5).



According to ACI 318-08 [10] five classes of risk are defined as a function of the sulfates concentration either in water or in soil (table 2.4)

Table 2.4: Sulfate exposure classes of ACI 318-08 [10].

Exposure	Concentration of water soluble sulfates	
	<i>In soil</i> (wt%)	<i>In water</i> (ppm)
Mild	<0.1	<150
Moderate	0.1 to 0.2	150 to 1500
Severe	0.2 to 2.0	1500 to 10 000
Very severe	>2.0	>10 000

2.2.3 Alkali-Silica reaction

As above mentioned in section 2.1.2 in the present chapter, Portland cement contains small amounts of alkalis, i.e. Na₂O and K₂O that once hydrated become NaOH and KOH contributing to the high alkalinity of the concrete pore solution. Such compounds can react with certain type of siliceous aggregates resulting in a hygroscopic gel made of alkali and calcium silicates. Upon water absorption, such gel expands leading to extended concrete cracking [11].

The more disordered and amorphous is the structure of the siliceous aggregates, the higher will be their reactivity with cement alkalis. So that highly crystalline quartz is scarcely reactive, conversely, the amorphous opal results to be highly reactive.

2.2.4 Freezing and thawing

When the external temperature drops below 0°C, the concrete pore solution can freeze, consequently increasing its volume up to 9%; obviously the resulting pressures, and in particular their repetitiveness due to daily temperature fluctuations, can produce damages in concrete structures, generally in the form of extensive cracking.

Freezing is a gradual process, because of three main reasons: (i) the rate of heat transfer through concrete is quite low, (ii) salts of the concrete pore solution migrate, and concentrate into the unfrozen solution thus lowering the freezing temperature, (iii) the freezing point depends on the size of the pore, decreasing with their size. According to these statements, the freezing starts from largest pores and gradually extends to the smaller ones. However it is important to notice that only capillary pores are involved in such a deterioration mechanism, as gel pore are so small that their water freeze only if temperature drop below -78°C [12]. On the other side, bigger pores such as those due to air entrapping agents, are generally filled with air, and consequently do not contribute to the deterioration mechanism.

2.2.5 Carbonation

CO₂ is naturally part of the atmosphere, in concentrations ranging from 0.04% to 0.2% in rural and highly anthropic area respectively. Being an acidic gas, tends to react with hydrated cement paste neutralizing its alkalinity in a process that is known as carbonation, (reaction 6).



With respect to durability, the effect of carbonation is that of significantly decrease the pH of the pore solution up to values around 8. Carbonation itself, does not damage concrete, conversely the CaCO₃ precipitation contributes in reducing the

porosity. Durability issues arise when the carbonation front reaches the steel interface, as at such pH the protective oxide layer is dissolved the steel starts corroding.

Carbonation occurs progressively from the outside, the propagation rate slows over time because CO₂ diffusion is hindered by the outer carbonated layer [13]; the rate determining factors are:

Relative humidity: gaseous CO₂ cannot react with solid hydrated products, so that for RH lower than 40% carbonation is negligible; on the other hand, the CO₂ diffusion in water filled pores is four order of magnitude lower than the in empty ones. Both these features concurs in determining a RH range of 50 - 70% where carbonation rate are the highest.

CO₂ concentration: higher CO₂ concentrations result in increased carbonation rate.

Temperature: increasing temperatures lead to higher carbonation rates.

Concrete alkalinity: Different cement types, especially in terms of clinker / supplementary materials ratio, result in a different portlandite content of the hydrated paste, so that blended cement producing a lower amount of Ca(OH)₂ are more prone to carbonation.

Water / cement ratio: being the carbonation process related to a diffusion mechanism, the lower concrete porosity due to a lower w/c ratio contributes in slowing the process.

2.3 Microbial deterioration of RC structures

2.3.1 Mechanism

Although attracting less attention than the deterioration mechanisms above discussed, the microbially induced concrete corrosion (MICC) can significantly decrease the service life of several reinforced concrete structures. Most of the studies dealing with such topic are focused on concrete pipes in sewer network, this is because several conditions such as the high organic carbon content of sewer water, generally slow flows, and the coexisting of aerobic/anaerobic regions result in a favorable environment for the growth of bacteria colonies [14,15]. According to a recent (2005) U.S. survey, performed by the Environmental Protection Agency (EPA) the US would need an investment of \$ 390 billion along 20 years, to repair, replace and build wastewater infrastructures.

However, concrete deterioration attributed to microbial activities has been observed in several other concrete structures provided that they are partially immersed in

steady water, examples are: wastewater treatment plants [16], swimming pools [17], cooling towers [18], bridge piers[19] animal housing facilities [20-22].

According to [23] the microbial deterioration of concrete sewer pipes occurs in three well temporally defined stages whose schematic is shown in figure 2.8.

Initially, sound concrete is characterized by an extremely alkaline pH, and microorganism capable of converting hydrogen sulfide to sulfuric acid cannot grow at such elevated pH. However, as detailed in section 2.2.5, the concrete surface does not remain basic through its whole life, as the joint effect of atmospheric CO₂ together with the biogenic H₂S can induce an pH decrease up to values around 8. Biogenic H₂S arises from sulfate reducing bacteria (SRB) metabolism that anaerobically converts sulfates into sulfides, whose chemical equilibrium transform into the poorly soluble H₂S that consequently leaves the solution and accumulates into the pipe headspace. Poor ventilation of these areas leads to an H₂S enrichment and consequently to its dissolution into the thin moisture film present on the concrete walls above the water level where it is oxidized to elemental sulfur by the atmospheric oxygen. Once the pH on the concrete surface is reduced to about 9, and provided that enough nutrients, moisture, and oxygen are available, some sulfur oxidizing bacteria can proliferate. Such kind of bacteria can be classified as neutrophilic (NSOB) or acidophilic (ASOB) according their pH range for growth. Neutrophilic bacteria produce some acidic products and convert sulfides into elemental sulfur and polythionic acid, thus initiating a microbial succession. Around pH 4 or 5, acidophilic bacteria begin to colonize the concrete surface, and oxidizing sulfur to sulfuric acid, their growth is accompanied by a drastic pH decrease that can reach values as low as 0.5. During this last stage the biogenic sulfuric acid reacts with the cementitious material according to mechanisms of acid and sulfate attacks described in sections 2.2.1 and 2.2.2 leading to expansive products such as gypsum and ettringite.

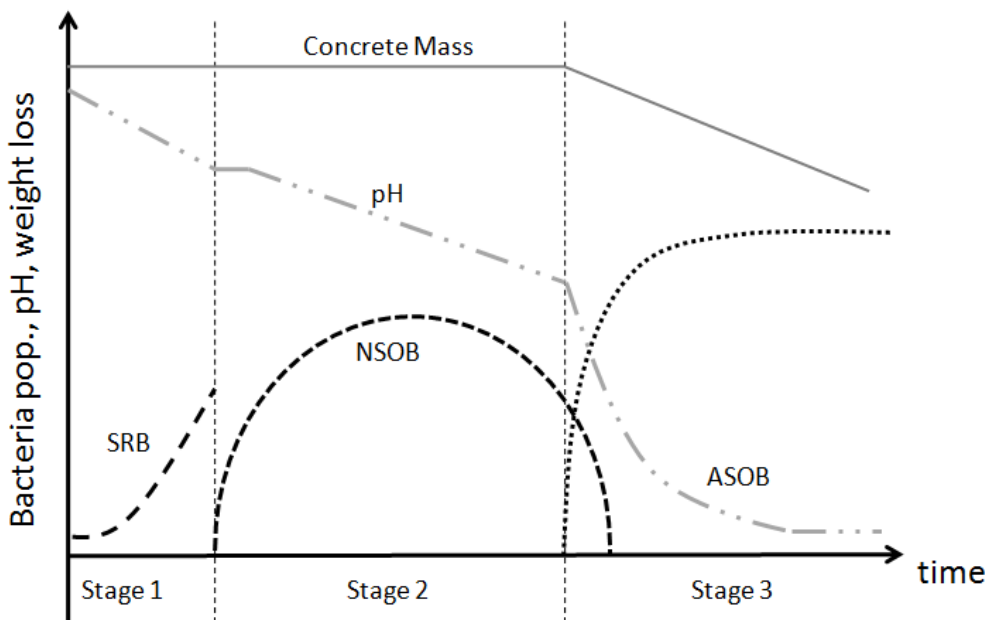


Fig. 2.8: Evolution of bacteria population, pH and weight loss over time.

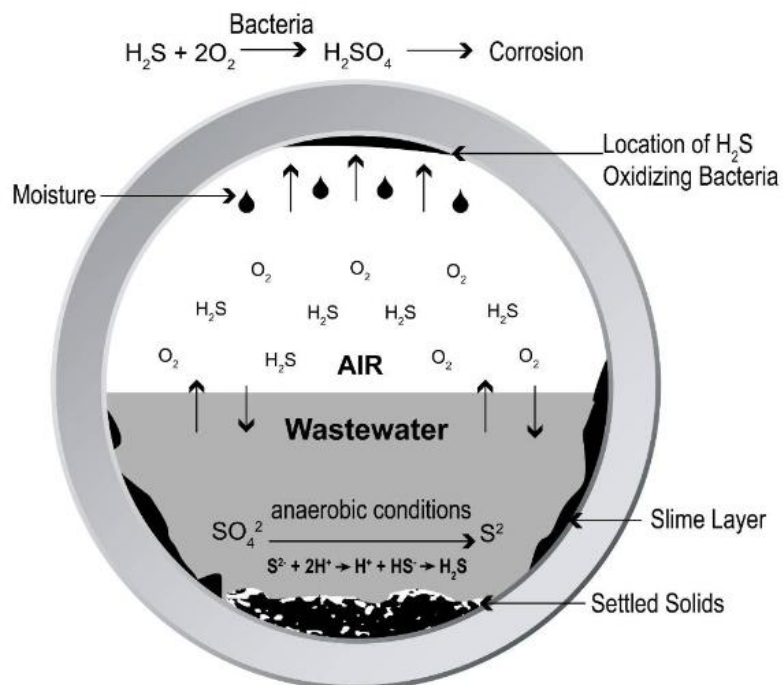


Fig.2.9: Schematic mechanism of microbially induced concrete corrosion in a sewer pipe.

2.3.2 Sulfate reducing bacteria

Sulfate-reducing bacteria (SRB) are those bacteria that can obtain energy by oxidizing organic compounds or molecular hydrogen while reducing sulfate to sulfide. The group of sulfate reducing bacteria is very wide and heterogeneous in

terms of substrate utilization, they can be classified into two different metabolic groups: species that only partially oxidize their substrate up to acetate, and those able to completely oxidize the substrate up to carbon dioxide. *Desulfovibrio* species, one of the most common and active in sewers, belongs to the former group [24]. SRB can proliferate only in anoxic environment, condition that is generally found within the slime layer below the water level, furthermore slow flow and long retention time gives more time to aerobic bacteria to consume all available dissolved oxygen in water thus contributing to the creation of anaerobic conditions.

2.3.3 Sulfur oxidizing bacteria

Conversely to SRB, sulfur oxidizing bacteria are aerobic microorganisms, and they can colonize the concrete surface once its pH is decreased below 9. Five species of *Thiobacillus* are known to be involved in the microbial deterioration of concrete, not all thriving in the same environmental conditions. Table 2.5 reports the five *Thiobacillus* strains, together with their ideal pH ranges and metabolic substrates and products. As can be easily deducted from the pH ranges, the first four strains belong to the neutrophilic class, while the latter to the acidophilic one.

Table 2.5: *Thiobacillus* strains and their characteristics [23].

Species	pH for growth	Substrates	Products
<i>T. thioparus</i>	4.5 - 10	Thiosulfate / H ₂ S	Polythionic acids / Sulfur
<i>T. novellus</i>	5 - 9.2	Thiosulfate	Sulfur
<i>T. neapolitanus</i>	4 - 9	Thiosulfate / H ₂ S / S	Polythionic acids / H ₂ SO ₄
<i>T. intermedius</i>	1.9 - 9	Thiosulfate	Polythionic acids / H ₂ SO ₄
<i>T. thiooxidans</i>	0.5 - 4	Thiosulfate / S	Sulfur / H ₂ SO ₄

2.3.4 Chemical, microbiological, and in situ test methods

Notwithstanding the numerous and detailed investigations performed in the last decades on the microbially induced concrete corrosion, a literature review highlights that still there is a lack of accepted and standardized method. Extremely different methods has been used by different groups producing results whose comparison is undoubtedly rather questionable. Researches performed on concrete biogenic deterioration can be roughly divided into three different classes on the basis of the rationale behind the testing method: chemical simulation tests, microbiological simulation tests, and in situ tests [25]. The former deal with samples immersion into abiotic solutions, such as diluted sulfuric acid, simulating bacteria metabolites; one step further, aiming to get closer to real systems is that of performing the deterioration tests in simulating chambers inoculated with the desired selection of bacteria strains. Finally in situ investigations consist in directly exposing concrete samples in specific areas where microbially induced corrosion naturally occurs.

Chemical tests

Because of their ease of setting, and getting reproducible experimental conditions, most of the studies dealing with microbial concrete deterioration are just abiotic, chemical tests. Within such category, two more classes can be individuated: (i) realistic concentration experiments that are generally based on long term monitoring or (ii) accelerated tests where the degradation rate can be increased by means of higher concentration of the aggressive medium, higher temperature or larger contact surfaces [25].

Both the approaches have advantages and drawbacks, so that the choice of one over the other should be carefully evaluated on the basis of the research objectives.

Present service life expectations for modern reinforced concrete structures generally lie in the range between 50 - 100 years, this immediately points out the main drawback of close-to-reality investigations. No measurements can be reasonably carried out for such a long period, thus only the very first stages of the deterioration can be investigated, while long terms considerations can only arise from extrapolation of the initial data. This implicate the risk of not considering certain deterioration mechanisms not noticeable during the monitoring period and gaining importance in a later period [25]. As an example, Romben [26] stated that in the case of sulfuric acid attack of concrete, as it involves a complex series of different processes, extrapolation procedures do not allow to obtain reliable results.

The above discussed limitation, can be overcome, by accelerated degradation tests, in which the entire life of a specific sample can be simulated until its failure, by increasing the aggressive species concentrations or the area/volume ratio, raising temperature, or using wetting and drying cycles [25]. On the other hand, such approach could modify the mechanisms of the attack, thus giving misleading results if the aim is that of precisely predicting the behavior in the field. On this purpose, Cohen et al. [27] found that in the case of sulfate attack the mechanism significantly change as a function of sulfates concentration.

Furthermore it seems important to mention that cementitious samples for laboratory studies can be produced as cement paste (cement/water), mortar (cement/water/sand) or concrete (cement/water/sand/concrete), but results obtained on one of these types cannot be easily extrapolated to the remaining ones because of the substantial microstructural differences arising from the presence of interfacial transition zones between aggregates and cement paste.

Microbiological tests

As can be easily deducted from what above discussed, the microbiologically induced concrete deterioration is an extremely complex process, where fine cement chemistry merges with microbial activities, both of them being significantly affected by external, environmental conditions such as temperature, nutrients availability, water flow rate etc. From this point of view, purely chemical simulation of bacteria metabolites, is an extremely simplified system where most of such important variables are not taken into account.

For this purpose researchers tried to simulate the microbial degradation mechanism as it happens in situ, by means of on purpose designed simulation chambers like those depicted in fig.2.10.

Fig.2.10(a) shows the simulation chamber developed by Sand et al. [28]. According to the authors such system was able to accelerate about eight times the rate of the processes occurring in situ. Concrete blocks were partially immersed in water lying on the bottom of the chamber and maintained at controlled temperature (30°C) and humidity (100%). Thiobacilli were separately growth in an external fermentor feed with sulfur and thiosulfate. The obtained microbial culture was periodically sprayed over the concrete samples. Such chamber was successfully used for investigating how different *Thiobacillus* strains and sulfur sources affect the concrete deterioration.

Hormann et al. [29] developed a similar chamber (fig. 2.10(b)) in which mortar cubes were periodically flooded for 5 min followed by 1 hour interruption with a *Thiobacilli* culture. Weight loss measurements detected different values for the different cement types after just one month of accelerated test.

Mori et al. [30] aiming to investigate the effect of nutrients on concrete corrosion, used a chamber with a very high H₂S concentration in which their mortar samples were partially immersed into three different solutions: water, a special culture medium and sewage. Test specimens were inoculated with *T. Thiooxidans* every two weeks and the corrosion rate was estimated by measuring the cross section reduction of the mortar prisms (fig. 2.10(c)).

Finally Vinkle et al. [31-33] developed an accelerated test method for the evaluation of biogenic sulfuric acid corrosion of concrete, aiming to investigate the responses of different concrete mixtures. The above cited method consists in a four step procedure according to which the mortar sample are initially exposed to H₂S (step 1) followed by an incubation period in a biological sulfur suspension containing bacteria (step 2); then, corrosion products removal because of sewage flow is simulated by rinsing the samples with water (step 3) and a final drying concludes a deteriorating cycle (step 4). The duration of single cycle is 17 days (3 + 10 + 2 + 2) and they can be repetitively performed one after each other.

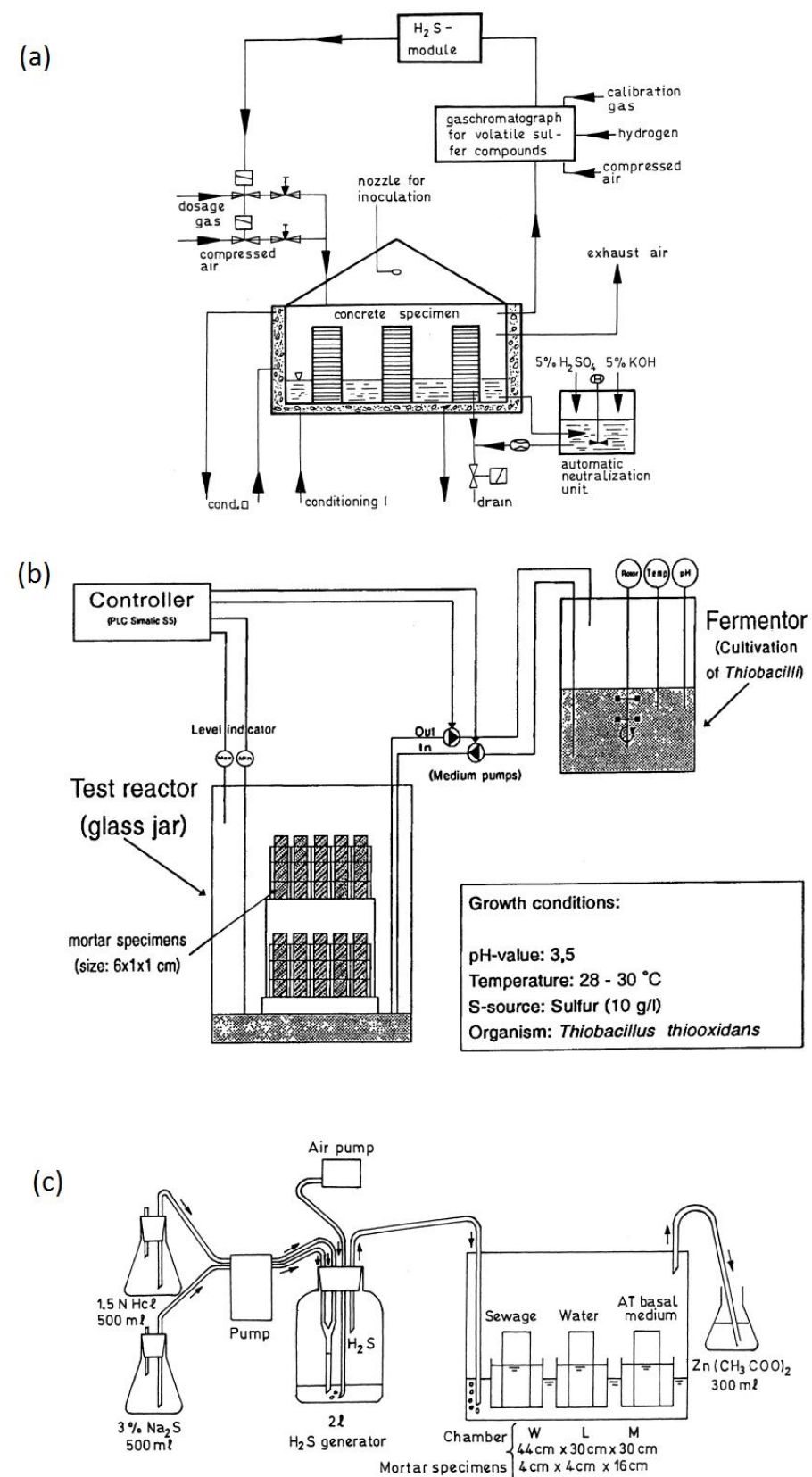


Fig. 2.10: Simulating chambers for microbial deterioration testing.

In situ tests

Notwithstanding the above described efforts of realistically simulating the sewer environment, reproducing all the natural conditions is still an hard task, so that the only way to study the real processes taking into account all factors and interaction is the in situ exposure test [25]. According to this method, series of samples are placed in sewer pipes where the microbial deterioration was found to occur and monitored over long period of time. As an example, a series of in situ measurement were performed in the Netherlands [34,35] where concrete samples made with different mixes were exposed for 35 months in 10 different locations and mass loss, neutralization depth, porosity and flexural strength were regularly monitored.

2.3.5 Measures for control

As thoroughly discussed in the previous paragraphs, microbially induced concrete corrosion is due to a double step process in which SRB and SOB are involved. Accordingly the measures of control, acting either on the first or on the second step can be potentially effective in the overall inhibition of the deterioration process.

Focusing on the H₂S production step, the conventional treatment method involves the addition of some chemicals in the flowing waste water to control the sulfide concentration. Chemicals used for such purpose are ferric or ferrous chloride, ferric nitrate and hydrogen peroxide [36]. The mechanism by which such chemicals control the sulfide emission is chemical oxidation or precipitation. Sulfides can also be successfully oxidized by treatment with ozone. Alternatively, as SRB proliferate in anoxic environment, air injection is an effective method to control the H₂S concentration [37].

Prevention strategies, aiming to protect concrete from the biogenic sulfuric acid attack can be divided into two main approaches the first one based on modifying the cement mixture while the second one on using acid resistant coating and lining.

As it has been clearly demonstrated that conventional cement type does not offer a suitable resistance to acidic conditions that can be found in sewer networks, several attempts have been performed to modify the cementitious matrix aiming to guarantee a longer durability. Schmidt et al. [38] found significantly better performance of high alumina cement. Alternatively, blending some polymers was found to led to a denser cementitious matrix characterized by small discontinuous pores, both these features hindering the sulfuric acid diffusion [39].

Concerning the coating approach, several alternatives have been tested such as those based on bituminous material, polyurethane and epoxy resins, polymer

modified mortar lining have also been successfully used for corrosion protection against biogenic sulfuric acid attack.

Biocides substances, such as quaternary ammonium compounds, were found to have biocidal properties against sulfur oxidizing bacteria, however their use, and of any other biocidal agent, should be considered with exceptional care, as they could also have important and undesired effect on the downstream biological processes [36].

2.4 Corrosion of steel in concrete

Up to this point, several deterioration mechanisms have been presented, affecting the durability of reinforced concrete structures, all of them dealing with chemical reactions occurring between the hydrated cement products and external aggressive agents such as acids, sulfates, CO_2 etc. However, reinforced concrete is a composite material, whose performance, arises from the combination of the cementitious matrix with steel reinforcing bars, and in certain conditions, that will be thoroughly discussed in the following paragraphs, the reinforcements itself can suffer from severe deterioration thus undermining the structural integrity, and leading, in extreme cases, to its collapse.

According to literature [40], corrosion of reinforcements is the predominant factor causing widespread premature deterioration of concrete constructions worldwide, especially for structures located in the coastal marine environment. This results in an enormous economic loss due to maintenance and repair costs. A report by the United States Secretary Transportation stated that rebars corrosion is a multibillion dollar problem and that the annual expenditure for repair and rehabilitation exceeds fifty per cent of the total construction costs [41]

2.4.1 The corrosion process

The success of reinforced concrete as a building material probably comes from the mutual advantages resulting from the combination of steel and concrete, the former providing tensile strength to the structure, while sound concrete is characterized by several features such as high alkalinity, high electrical resistivity, and mass transport limitations that protect steel from corrosion.

As already discussed in the previous paragraphs, the cement hydration leads to the formation of a porous cementitious matrix whose pores are filled with an extremely alkaline solution due to the presence of $\text{Ca}(\text{OH})_2$, NaOH and KOH resulting from the hydration of C_3S , Na_2O and K_2O respectively. Such an alkaline environment, characterized by pH values around 13 is the main responsible for the formation of an ultrathin oxide layer on the steel rebar surface. The Pourbaix diagram reported in fig.

2.11 shows the correlation between the half cell potential and the environment pH in determining the thermodynamic stability of iron products. The lower region of the diagram, where potential are below -0.5 V vs. NHE, defines the immunity area in which corrosion does not occur. At higher potential values, the left portion (low pH) of the diagram delineates the termodynamical stability of iron ions thus indicating the occurrence of corrosion process. At higher pH, such as those of sound concrete, the steel surface is covered by protective iron oxides that prevent corrosion (passivation region).

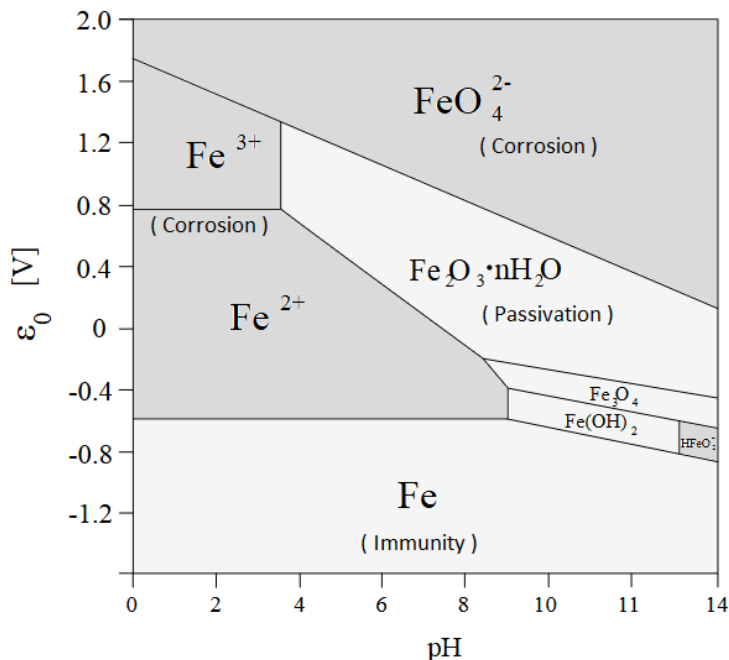


Fig.2.11: Pourbaix diagram for Fe - H₂O systems.

Another important factor that contributes to the corrosion protection of steel rebars embedded into a concrete matrix is its high electrical resistivity. The conduction in concrete is principally through the motion of ions such as Na⁺, K⁺, Ca²⁺, OH⁻ and SO₄²⁻ in the pore solution. A typical values of electrical resistivity of pore solution is about 25-35 Ωcm [42]. However, in a well designed and properly cured concrete the amount of interconnected pores should be very low. Furthermore it has to be considered that conventional aggregates, are relatively good insulator having electrical resistivity in the order of 10⁵ -10¹⁴ Ωcm while typical values for the cement paste ranges from kΩcm to MΩcm according to the moisture content [43]. Considering the overall system the global low electrical conductivity certainly contributes in hindering the corrosion processes.

Finally, it is important to mention that the reinforcing steel corrosion is determined by mass transport process: oxygen diffusion, neutralization front (CO₂ and other acids)

and aggressive ions diffusion. A good quality concrete provides an efficient physical barrier, preventing the penetration of such aggressive species.

Notwithstanding the above discussed protecting features, it is well known that concrete does not maintain all its initial properties over time, but that certain external environmental factors can lead to substantial modifications, undermining the oxide layer stability and consequently initiating the rebar corrosion process. There are three main motivations for the reinforcing steel transition from the passive state to the active-corroding one:

(1) *Carbonation*: as previously discussed, the carbonation procedure leads to the neutralization of the concrete alkalinity, and when its front reaches the steel-concrete interface, the protective oxide layer becomes instable and the underlying steel suffers from generalized corrosion.

(2) *Chlorides*: Aggressive species, such as chloride can easily penetrate and diffuse through the concrete matrix, if their concentration at the steel/concrete interface reach a certain threshold value (0.4 - 1 wt% respect to cement weight) the passive film is locally damaged thus resulting in pitting corrosion.

(3) *Stray currents*: in the case of buried structures and in presence of external currents interfering with reinforcing bars, where electrons leave the reinforcement to close their circuit corrosion occurs.

The loss of passivation is not the unique required condition for the onset of the corrosion process, but necessarily has to be accompanied by two others, namely the oxygen and the moisture presence [44]. Once all the three conditions are verified, corrosion inevitably starts.

A corroding system requires the presence of four elements, an anodic area, where oxidation reaction occurs, a cathodic area, where electrochemical reduction reaction occurs, an electrical conductor, and an electrolyte. In the case of reinforcing bars embedded into a cementitious matrix, both the anodic and the cathodic area are placed on the rebar that itself constitutes the electrical conductor, while the pore solution is the electrolyte. The steel rebar corrosion mechanism is shown in the schematic of fig.2.12.

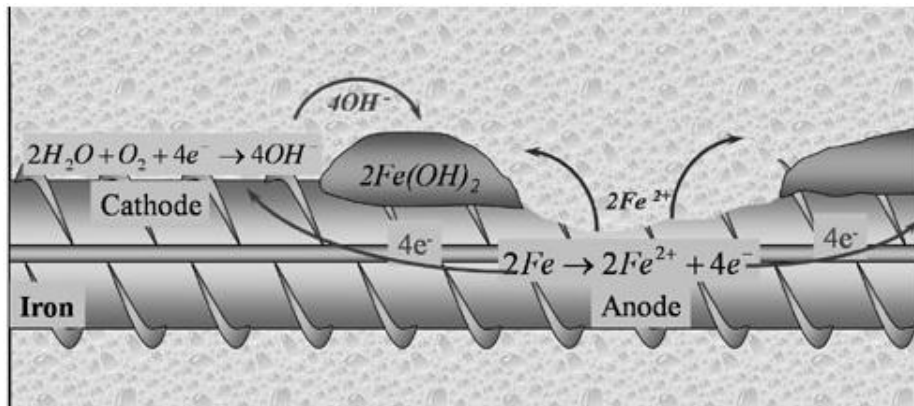
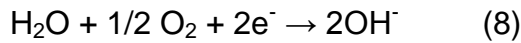


Fig. 2.12: Schematic of the corrosion mechanism for steel in concrete.

Anodic areas, corresponding with the damage in the passive layer, are the sites where the iron oxidation occurs according to reaction (7).



The resulting electrons flow through the reinforcing bar to cathodic sites where they combine with water and oxygen giving rise to reduction reaction as in (8)



Subsequently, ions produced in anodic and cathodic zones recombine originating iron(II)hydroxide which further evolve in several other different mixed Fe(II) and Fe(III) oxides / hydroxides.

Together with the loss of ions, resulting in a reduction of the rebar cross-section, eventually leading to a decrease of its technological properties, there is also an other deleterious effect arising from the steel corrosion process. As clearly shown in fig. 2.13, iron hydroxides imply a significant volumetric increase of a factor ranging from three to four [45].

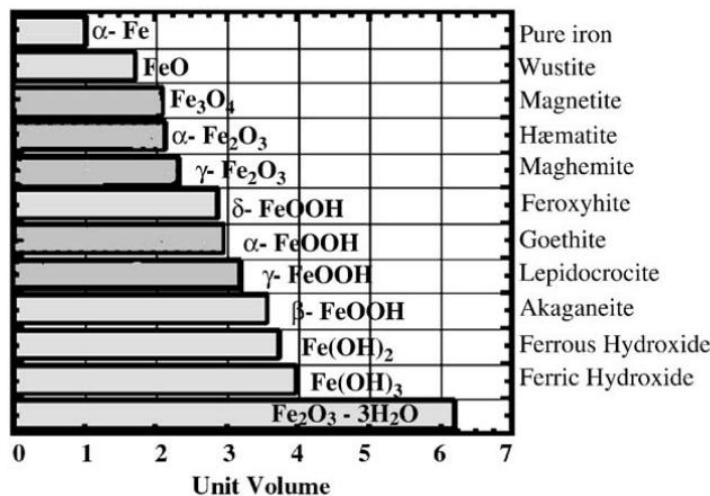


Fig. 2.13: Volumetric expansion of corrosion product formed in concrete [45].

As a consequence, the accumulation of corrosion products at the steel concrete interface generates some pressures into the bulk of the cementitious matrix, and once passed the threshold values originate cracks and eventually the spalling of the concrete cover (Fig. 2.14)

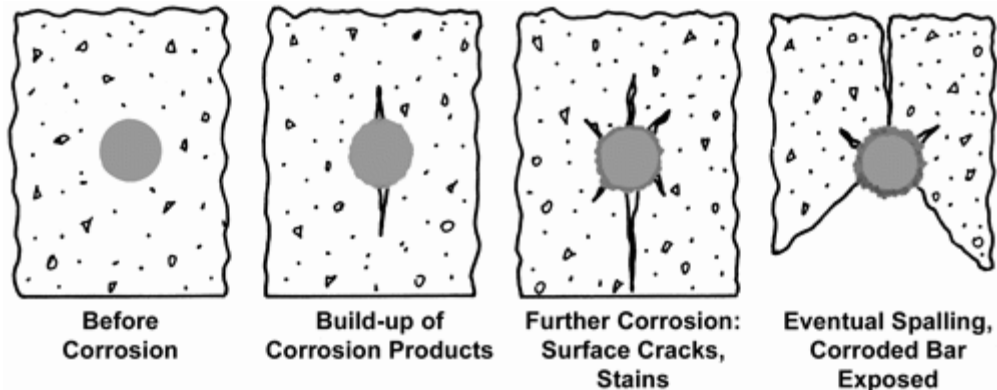


Fig. 2.14: Cracks evolution in corroding reinforced concrete.

It is worth underlining that the above described cracks formation mechanism, or the reinforcing steel exposure due to spalling phenomena significantly contribute to accelerate the aggressive species and O₂ diffusion into the concrete matrix, thus leading an increase of the corrosion rate. Such self accelerated deterioration mechanism is also shown in the *fib* model for service life modeling of reinforcement corrosion [46].

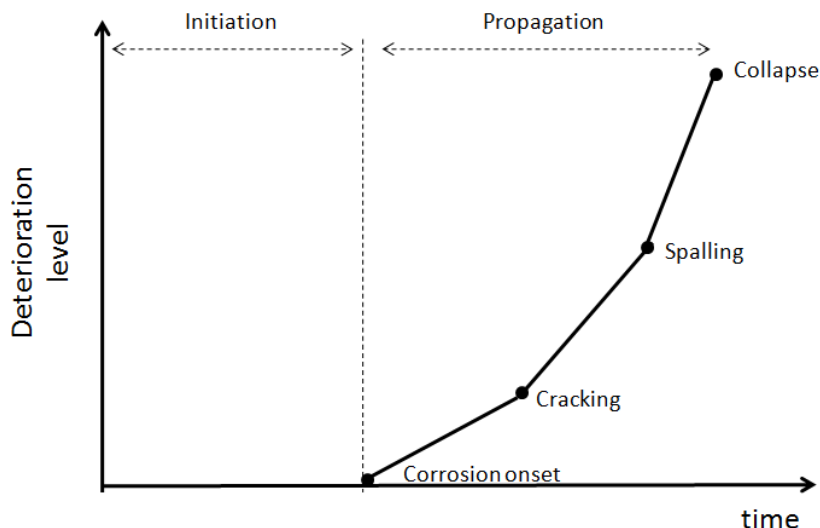


Fig. 2.15: *Fib* model for RC structure service life.

2.4.2 Chloride attack

Among the causes leading to the reinforcements corrosion, chloride attack is by far the more frequently occurring, so that a huge number of studies has been focused on such topic [47-49].

The chlorides sources, can be distinguished into two main classes, whether they are introduced as contaminants or additives in the fresh mixture, or if they propagate because of a concentration gradient between concrete and the outer environment. The former class generally induces a very fast degradation that starts occurring immediately after casting, while in second case longer times are required for the chlorides diffusion through a mature concrete matrix (initiation time) [40].

Internal chloride contamination can occur as consequence of the use of seawater in the concrete mix, or because of chloride containing aggregates or calcium chloride addition aiming to accelerated the setting time. Nowadays, in the developed countries such chlorides contamination can be easily avoided, however in countries where the knowledge of durability issues is not yet diffused or common, this kind of engineering negligence still causes considerable damages.

However, the most frequent causes of chloride induced corrosion of reinforced concrete structures are those resulting from a "post-setting" exposure such as in the case of seawater or chloride-bearing air in marine area, or the action of deicing salts in winter times. In this latter cases initiation phase is much more longer than the case of the internal contamination, as chlorides diffusion in a wet or highly moist concrete is a rather slow process, being the diffusion coefficient in the order of $10^{-12} \text{ m}^2/\text{s}$ [50].

Once chlorides reach the steel-concrete interface in a sufficient concentration known as chloride threshold or critical chloride concentration, the passive layer is destroyed and corrosion initiates. It is well known that the passive film breakdown occurs in correspondence with metallographic defects that transform into corroding anodic zones, while the remaining oxide layer acts as cathodic region [51]. As a consequence, the cathodic/anodic area ratio is generally very high, resulting in a stimulation of the corrosion intensity. Furthermore, inside the pit, a series of reactions involving chlorides and ferric ions occur, leading to the formation of hydrochloric acid, which by locally increasing the acidity contribute to the self-accelerating mechanisms of pitting corrosion.



2.4.3 Corrosion monitoring techniques

There are several electrochemical techniques that can be profitably used in the assessment of rebar corrosion in reinforced concrete structures; their widespread success comes from the fact that generally, they are rapid, non destructive, and easy to perform. However, electrochemical measurements performed on reinforced concrete, whether real structures or lab samples, are far more complicate than common measurements involving a liquid electrolyte. The main reason for that are[52]:

Non destructiveness: the chosen technique should preserve the integrity and consequently the bonding of the steel/concrete interface.

Microenvironment variability: measurements can be significantly altered by local variation of microenvironmental conditions such as pH, chloride content, moisture content, etc.

Concrete resistivity: the high resistivity of the concrete cover requires an appropriate correction in order to filter such resistive response and allowing to detect only that of the steel/concrete interface.

Mass transport: steel corrosion is decisively influenced by the transport mechanisms of reactants and products within the pore structure of concrete.

Undefined testing area: in concrete it's always difficult to precisely determine the polarized area of the rebar during the electrochemical measurement.

Notwithstanding the above mentioned problematics, electrochemical techniques still remains a valuable tools, especially if performed and interpreted by a skilful operator.

Below, follows a list and details of the most commonly used electrochemical techniques for corrosion investigation in concrete:

Open Circuit Potential Measurements:

OCP measurement is certainly the easier and most widespread technique. It is based on the fact that where corrosion occurs, ions migrate through the concrete cover generating an electrical field that can be detected as a potential variation with respect to a reference electrode [44].

Set up is extremely straightforward, and consists in creating an electrical connection with the steel rebar and attaching it to the positive terminal of a high impedance voltmeter ($>10M\Omega$), while the negative terminal is connected to a reference electrode that is moved on the concrete surface. A wet sponge may be placed between the reference tip and the concrete surface in order to enhance conductivity (fig. 2.16). It is important to highlight that OCP measurements do not give any information about

corrosion rate, but only allow to determine the likelihood of corrosion activity, indicated by lower potentials.

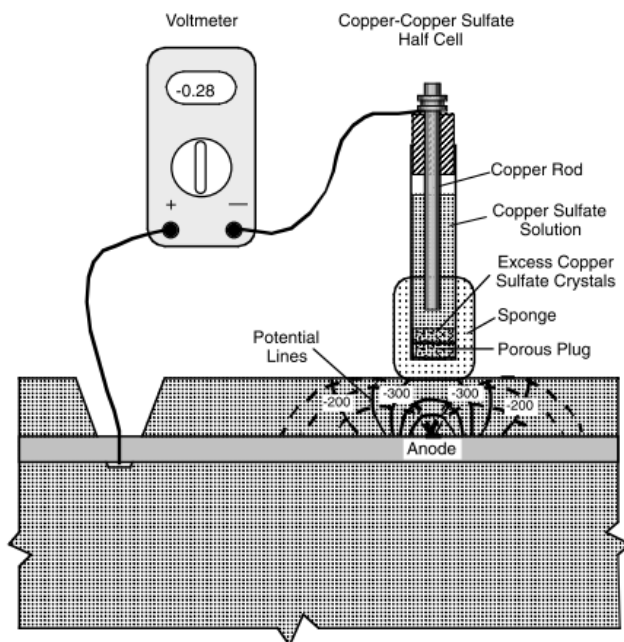


Fig. 2.16: Schematic of an apparatus for OCP measurement of reinforced concrete [44].

Data collected from OCP measurement can be visualized in equipotential contour map, as shown in fig. 2.17, that can give a quite precise indication of the locations where corrosion is more likely to occur.

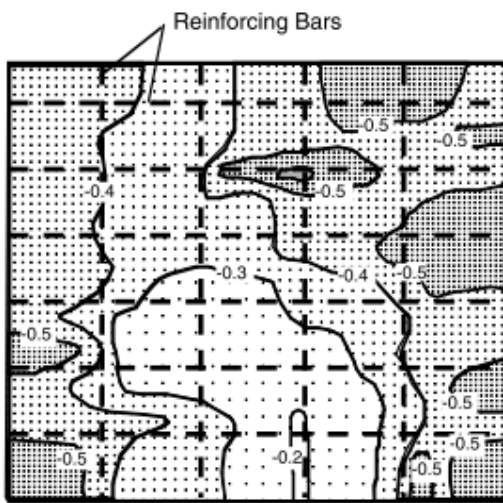


Fig. 2.17: Example of an equipotential contour map [44].

ASTM C876 [53] defines the threshold values for potential readings and divides them into four categories of corrosion risk (Table 2.6).

Table 2.6: Relationship between OCP and Corrosion risk according to ASTM C876.

Open circuit potential values		
[mV vs SCE]	[mV vs CSE]	Corrosion Risk
< -426	< -500	Severe risk
-426 to -276	-500 to -350	High risk
-276 to -126	-350 to -200	Intermediate risk
> -126	> -200	Low risk

The main advantage of OCP monitoring is the ease of performance and the fast acquisition rate, that easily allow to determine the potentially corroding location even on wide surface. However it is generally accepted that OCP measurement alone is not sufficient for corrosion assessment, thus it should be coupled with other methods such as chloride content, carbonation depth etc. [54] Furthermore, it is important to notice that such technique has some limitations: it does not give reliable results if there is any kind of coating on the concrete surface or on the steel surface, if concrete is saturated with water, or if the carbonation front reached the depth of the reinforcement [44].

Concrete resistivity

The measurement of concrete resistivity is another cheap, easy and fast technique that can be used in order to estimate the likelihood of corrosion in reinforced concrete structures.

Once corrosion is initiated, electrons flow into the steel rebar from anodic to cathodic areas, correspondingly, ions moves into the cementitious matrix, so that it has been demonstrated that the electrical resistivity of concrete is inversely proportional to the corrosion rate [55].

Concrete resistivity is generally measured with the Wenner probe that consists in four, equally spaced electrodes, that are placed on the concrete surface; the external pins are connected to a source of AC current, while the resulting potential between the two inner pins is read through a voltmeter (Fig. 2.18).

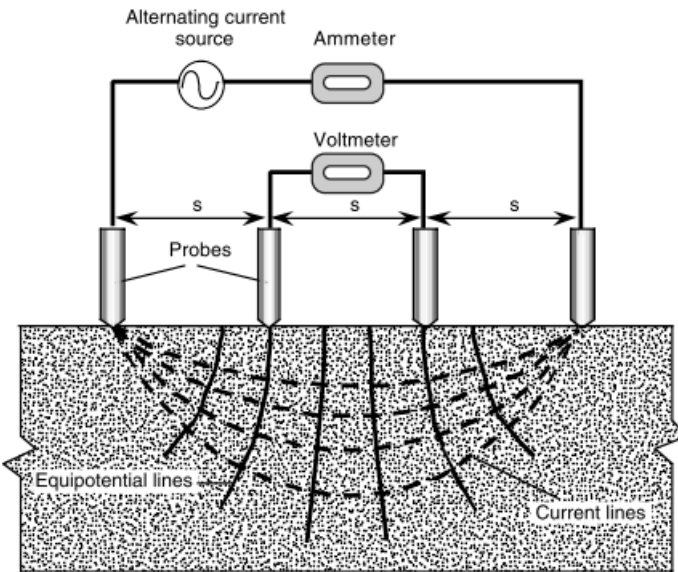


Fig. 2.18: Schematic of a Wenner probe, for concrete resistivity measurements [44].

The resistivity can be calculated through the equation 11:

$$\rho = \frac{2 \pi s V}{I} \quad (11)$$

Where s stands for the distance between the pins, I is the applied current and V the measured potential.

Differently from OCP measurements, there is no ASTM method for concrete resistivity, however there exist commonly accepted values correlating the experimental values with the corrosion risk (Table 2.7)

Table 2.7: Relationship between concrete resistivity and corrosion risk [56].

<i>Resistivity (kΩ cm)</i>	<i>Corrosion risk</i>
> 20	Low
10 to 20	Moderate
5 to 10	High
< 5	Very high

Linear Polarization Resistance (LPR)

Both the above presented techniques, although having important advantages in terms of ease of application and acquisition rate, suffer from a main drawback, as they do not give any information on the actual corrosion rate. Such value, can be instead determined through the linear polarization resistance method.

Linear polarization resistance measurements consist in performing a potentiodynamic polarization at very slow scan rate, generally 0.1667 mV/s, over a small potential range centered around the OCP. In such a small interval the measured current density varies linearly with the scanned potential.

According to the Ohm law, the polarization resistance R_p is defined as the slope of the potential/current density plot (Eq.12).

$$R_p = \frac{\Delta E}{\Delta i} \quad (12)$$

Stern and Geary established the relationship between the polarization resistance and the corrosion current density (eq. 13), where B is a coefficient expressed as in eq.14 containing the values of both the anodic and cathodic Tafel slopes, b_a and b_c respectively.

$$i_{cor} = \frac{B}{R_p} \quad (13)$$

$$B = \frac{b_a b_c}{2.303 (b_a + b_c)} \quad (14)$$

Calculation of the Tafel slopes, in order to determine the value of the B coefficient, would result in complex and time consuming procedure, thus it is commonly assumed to use the value of 26 mV for actively corroding steel, and 52 mV if the rebar is still in its passive state [57].

Differently from OCP, LPR measurements require a three electrodes arrangement: the examined steel rebar is the working electrode and its potential is varied with respect to a reference electrode, while the corrosion current flows and is measured between the working and a counter electrode that is placed on the concrete surface (fig. 2.19)

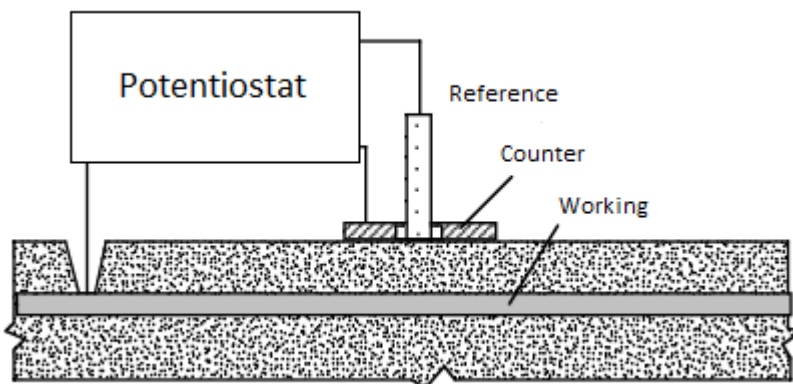


Fig. 2.19: Schematic of an LPR measurement arrangement [44].

The main issue, with the above presented setup, is that it is nearly impossible to determine the polarized area of the steel rebar, as the unconfined current flow can spread laterally with respect to the counter electrode, and an inaccurate knowledge of the polarized area can lead to significant errors in the calculation of the corrosion current density. Such issue is not a big deal on the lab scale where the active area of the working electrode can be defined during the sample preparation, but certainly it is for on-site measurements. In this latter cases, it is common practice to use more sophisticated probes, characterized by a secondary counter electrode, known as guard ring, that provides a confinement to the electrical field between the steel rebar and the original counter electrode [54].

The calculated corrosion current densities can be compared with the threshold values reported in table 2.8 in order to determine the state of the rebar.

Table 2.8: Relationship between corrosion current and corrosion of the rebar [57].

<i>Corrosion current density (μAcm^{-2})</i>	<i>Condition of the rebar</i>
< 0.1	Passive condition
0.1 to 0.5	Low corrosion rate
0.5 to 1	Moderate corrosion rate
> 1	High corrosion rate

Whether on lab sample or on-site, LPR measurement must be consider with care if the concrete surface is cracked, is the steel is galvanized, and if the rebar is cathodically protected or there is the possibility of stray current.

Tafel extrapolation

The Tafel extrapolation method is another way to determine the instantaneous corrosion rate, the principles of the measurement are very similar to those of LPR except for the fact that the scanned potential range is significantly wider (hundreds of mV instead of about a dozen). Because of this wider potential range, the steel/concrete interface can be damaged, especially during the anodic scan, thus such method finds more applications on a lab scale than on real reinforced concrete structure.

As clearly shown in fig. 2.20 the corrosion current density is calculated by extrapolation of current curves from either the anodic or the cathodic Tafel region to the open circuit potential [52]

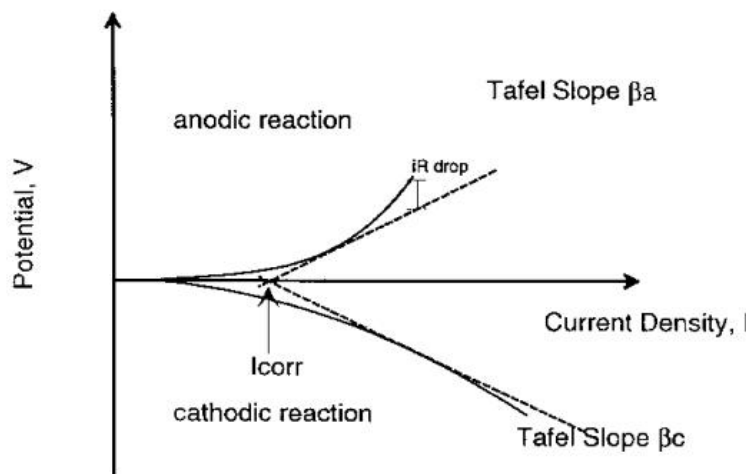


Fig. 2.20: Determination of the corrosion current from a Tafel plot [52].

Electrochemical impedance spectroscopy (EIS)

Electrochemical impedance spectroscopy is an extremely powerful technique, widely used in the characterization of the electrical properties of materials and their interfaces. Differently from LPR and Tafel extrapolation, that are steady-state technique in which measurements are performed in equilibrium condition, EIS method is transient technique. During an EIS measurement a small, sinusoidal potential perturbation is applied to the system, by varying its frequency, while the resulting current oscillation are recorded.

The experimental setup, is similar to that of LPR and Tafel extrapolation, apart a frequency response analyzer is required coupled with the potentiostat. Because of its expensive and not portable equipment, together with the long times required for a spectra acquisition, EIS measurements are more frequently performed in lab studies than on the field.

The main advantage of EIS with respect to the other techniques is the possibility of collecting information not only on the steel/concrete interface but also on the bulk cementitious matrix.

According to Crentsil et al. [58] the Nyquist plot for reinforced concrete samples shows three partial semicircles, the one at the higher frequencies being correlated with concrete matrix, that of intermediate frequencies corresponding to an interfacial film, while at the lower frequencies the response of the steel interface is detected (fig. 2.21). From the fitting of this low frequencies semicircle with a suitable electric equivalent circuit values such as those of R_p can be calculated.

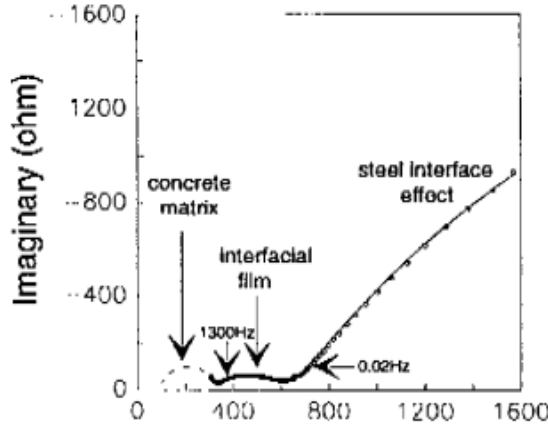


Fig. 2.21: Nyquist plot of a reinforced concrete sample [58].

2.4.4 Prevention and remediation

In reinforced concrete structures, the steel rebars are deeply embedded into the cementitious matrix that provides a physical barrier against the penetration of aggressive species, moreover it guarantees the growth and the stability of a protective passive layer at the steel concrete interface. Both these features points out that a good quality concrete can be considered the primary protection method; for certain specific cases, where particularly aggressive conditions can be expected some supplementary protection methods can be planned.

Taking into consideration that preventing corrosion in a reinforced concrete structure is certainly easier and less expensive than repairing it, a good quality control in design and construction is certainly the most important prerogative for an extended service life, additional protecting methods can be divided into four different classes [40]:

- Acting on the steel corrosion resistance
- Applying external membranes to the concrete surface
- Using cathodic protection
- Modifying the mix design, by adding corrosion inhibitors

Focusing on the steel rebars, their corrosion resistance properties can be enhanced by the application of coating that can be either organic such as epoxy resins or metallic as in the case of the galvanizing procedure. Alternatively, for application in extremely aggressive environment, higher quality steel such as stainless steels can be used instead of the ordinary carbon steel.

Epoxy coated steel proved to give positive results especially in the case of seawater exposure [40], however, their use has two important drawbacks, as it makes

corrosion monitoring through OCP and LPR methods quite inaccurate and the steel-concrete bonding strength results to be significantly decreased.

The galvanizing procedure of carbon steel is a well established method for increasing its corrosion resistance; focusing of reinforced concrete applications galvanized bars are effectively used in structure exposed to carbonation [40]. The zinc layer deposited over the steel surfaced is characterized by a less noble potential than steel, so that at the occurrence of a corrosion process, the zinc behave as a sacrificial layer, granting the restoration of the passive film.

Eventually, austenitic and austenoferritic (duplex) stainless steels offer a good combination of corrosion resistance and mechanical properties. With slight fluctuations, depending on the Ni and Mo content, their cost is 4 - 9 times higher than that of common carbon steel, however it has been estimated that their use would cut the maintenance costs of about 50%, granting service life as long as 120 years in coastal areas [59]

Except for the cases where chlorides are inadvertently admixed to fresh concrete, the aggressive species, whether CO_2 or chlorides, penetrate into the concrete matrix from the outside. Consequently, enhancing the barrier properties of the concrete cover by means of a protective coating or a membrane could increase the structure service life. There exist two commonly used method for the protection of concrete surfaces: spraying or painting a protective film and using bituminous sheets based on rubber, plastic or textile [40].

Sealers and membranes can be classified into several types according to their insulating mechanism (fig. 2.22).

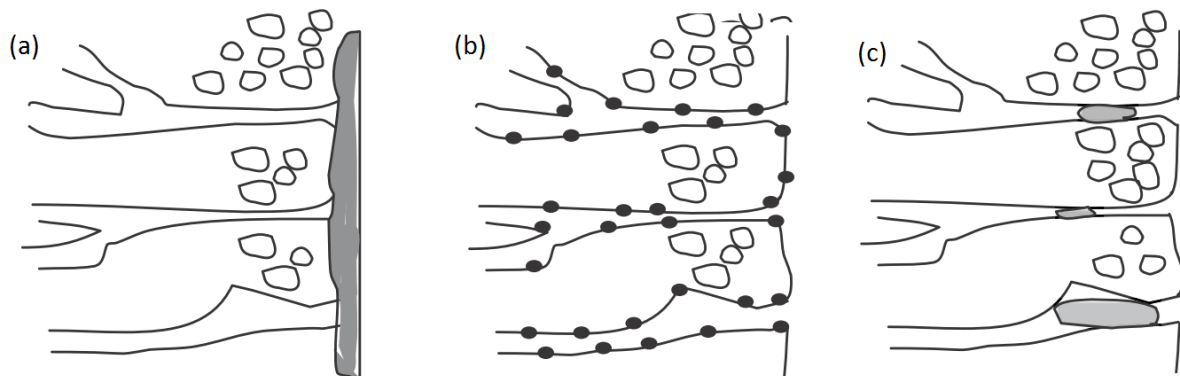


Fig. 2.22: Schematic of different concrete surface protection techniques [40].

Coating: consist in a continuous film applied on the concrete surface and characterized by a thickness in the range of 100-300 μm (Fig. 2.22(a)).

Pore lining: the surface of the pores is lined with material that reduce the surface energy to make the concrete water repellent. (Fig. 2.22(b)).

Pore blocking: the treatment penetrate into the pore and reacts with the cement compounds resulting in insoluble products that occlude the pores (Fig. 2.22(c)).

Cathodic protection is a very effective method for corrosion protection, but its complexity and costs limits the applications to special structures. The principle of cathodic protection is that of modifying the electrochemical system so that the steel reinforcing bars behave as cathodes, thus avoiding corrosion risk. Such objective can be accomplished in two different ways: by connecting the steel rebar to a less noble sacrificial electrode serving as anode, or by supplying the electrons to the rebar from an external electrical power source.

Finally over years, a huge number of compounds have been added to the concrete mix aiming to inhibit the corrosion of the steel reinforcing bars, a detailed literature review of most commonly used corrosion inhibitors for reinforced concrete application can be found in the introduction of chapter 5 in the present thesis.

References

- [1] M. Hassoun, A. Al-Manasser, Structural Concrete, 4th edition, John Wiley & Sons, 2008.
- [2] A.M Neville, Properties of Concrete, 5th edition, Pearson, 2013.
- [3] P. Jahren, T. Sui, Concrete and Sustainability, CRC press, Taylor & Francis, 2013.
- [4] EN 197-1, Cement, part 1: composition, specifications and conformity criteria for common cements, 2000.
- [5] P.K. Mehta, P.J. Monteiro, Concrete microstructure, properties and materials, McGraw-Hill, 2006.
- [6] T.C.Powers, L.E Copeland, H.M. Mann, Capillary continuity or discontinuity in cement pastes, J. Port. Cem. Assoc. Research and Development Laboratories, Vol.1, No.2 (1959) 38-48.
- [7] T.C.Powers, L.E Copeland, J.C. Hayes, H.M. Mann, Permeability of Portland cement paste, J. Amer. Concr. Inst., 51 (1954) 285-298.
- [8] L. Romben, Aspect of testing methods for acid attack on concrete, CBI Research (1978).
- [9] P.K. Mehta, Mechanism of sulfate attack on portland cement concrete-Another look, Cement and Concrete Research, Vol. 13, No. 3 (1983) 401–406.
- [10] ACI318-08, Building Code Requirements for Structural Concrete and Commentary, American Concrete Institute (2008).
- [11] R.N. Swamy, The alkali silica reaction in concrete, Taylor & Francis (2003).
- [12] T.C. Powers, Resistance to weathering - freezing and thawing, ASTM Sp. Tech. Publ. No.169 (1956) 182-187.
- [13] V.G. Papadakis, C.G. Vayenas, M. Fardis, Fundamental Modeling and Experimental Investigation of Concrete Carbonation, Materials Journal, Vol. 88, No. 4 (1991) 363-373.
- [14] M. Guadalupe, D. Gutierrez-Padilla, A. Bilefeldt, S. Ovtchinnikov, M. Hernandez, J. Silverstein, Biogenic sulfuric acid attack on different types of commercialy produced concrete sewer pipes, Cement and Concrete Research, 40 (2010) 293-301.
- [15] H. Satoh, M. Odagiri, T. Ito, S. Okabe, Microbial community structures and in situ sulfate reducing and sulfur oxidizing avtivities in biofilms developed on

- mortar specimens in a corroded sewer system, *Water Research* 43 (2009) 4729-4739.
- [16] J.A Redner, E.J. Esfandi, R.P. Hsi, Evaluation of protective coatings for concrete exposed to sulfide generation in wastewater treatment facilities, *Journal of Protective Coatings and Linings*, 8 (1991) 48–58.
- [17] S. Chandra, L. Berntsson, Deterioration of concrete in swimming pools in the south of Sweden, *ACI Materials Journal* (1988) 485-489.
- [18] T.V. Zherebyateva, E.V. Lebedeva, G.I. Karavaiko, Microbiological corrosion of concrete structures of hydraulic facilities, *Geomicrobiology Journal*, 9 (1991) 119–127.
- [19] S. Wei, M. Sanchez, D. Trejo, C. Gillis, Microbial mediated deterioration of reinforced concrete structures, *International Biodeterioration & Biodegradation* 64 (2010) 748-754.
- [20] V. Abdelmseeh, J. Jofriet, G. Hayward, Sulphate and sulphide corrosion in livestock buildings, Part I: concrete deterioration, *Biosystem Engineering*, 99 (2008) 372-381.
- [21] V. Abdelmseeh, J. Jofriet, G. Hayward, Sulphate and sulphide corrosion in livestock buildings, Part II: reinforcing steel corrosion, *Biosystem Engineering*, 99 (2008) 382-389.
- [22] N. De Belie, J.J. Lenehan, C.R. Braam, B. Svennerstedt, M. Richardson, B. Sonck, Durability of Building Materials and Components in the Agricultural Environment, Part III: Concrete Structures *Journal of Agricultural Engineering Research*, 76 (2000) 3-16.
- [23] D.J. Roberts, D. Nica, G.Zuo, J.L. Davis, Quantifying microbially induced deterioration of concrete: initial studies, *International Biodeterioration & Biodegradation* 49 (2002) 227-234.
- [24] M. O'Connel, C. McNally, M.G. Richardson, Biochemical attack on concrete in waste water application, *Cement and Concrete Composites*, 32 (2010) 479-485.
- [25] J. Monteney, E. Vinkle, A. Beeldens, N. De Belie, L. Taerwe, D. van Gemert, W. Verstraete, Chemical, microbiological, and is situ test methods for biogenic sulfuric acid corrosion of concrete, *Cement and Concrete Research*, 30 (2000) 623-634.
- [26] L. Romben, Aspects on testing methods for acid attack on concrete, *CBI Forsk* 78 (1) (1978) 1-61.
- [27] M.D. Cohen, B. Mather, Sulfate attack on concrete-research needs, *ACI Mater J.* 88 (1) (1991) 62-69.

- [28] W. Sand, E. Bock, D.C. White, Biostest system for rapid evaluation of concrete resistance to sulfur-oxidizing bacteria, Mater Perform 26 (3)(1987) 14-17.
- [29] K. Hormann, F. Hofmann, M. Schmidt, Stability of concrete against biogenic sulfuric acid corrosion, a new method for determination, Proceedings of the 10th International Congress on the Chemistry of Cement, Gothenburg, June 2-6, 1997.
- [30] T. Mori, T. Nonaka, K. Tazaki, M. Koga, Y. Hikosaka, S. Noda, Interactions of nutrients, moisture and pH on microbial corrosion of concrete sewer pipes, Water. Res. 26 (1) (1992) 29-37.
- [31] E. Vinkle, S. Verstichel, J. Monteney, W. Verstraete, A new test procedure for biogenic sulfuric acid corrosion of concrete, Biodegradation 10 (1999) 421-428.
- [32] J. Monteney, N. De Belie, E. Vinkle, W. Verstraete, L. Taerwe, Chemical, microbiological tests to simulate sulfuric acid corrosion of polymer modified concrete, Cement and Concrete Research, 31 (2001) 1359-1365.
- [33] E. Vinkle, E. Van Wanseele, J. Monteney, A. Beeldens, N. De Belie, L. Taerwe, D. van Gemert, W. Verstraete, Influence of polymer addition on biogenic sulfuric acid attack of concrete, International Biodeterioration & Biodegradation 49 (2002) 283-292.
- [34] J.M. Pluym-Berkhout, J. Mijsbergen, R.B. Polder, Rioleringen (II), biogene zwavelzuuraantasting, Cement 9 (1989) 16-20.
- [35] A.C.A. van Mechelen, R.B. Polder, Rioleringen (XI), biogene zwavelzuuraantasting, verslag van een vervolgonderzoek in Rotterdam, Cement 2 (1991) 26-30.
- [36] R. Sydney, E. Esfandi, S. Surapaneni, Control concrete sewer corrosion via the crown spray process, Water Environ. Res. Vol 68, No.3 (1996) 338-347.
- [37] T. Ochi, M. Kitagawa, S. Tanaka, Controlling sulfide generation in force mains by air injection, Wat.Sci.Technol. 37 (1998) 87-95.
- [38] M. Schmidt, K. Hormann, F. Hofmann, E. Wagner, Beton mit erhöhtem widerstand gegen saure und biogene schwefelsaurekorrosion, Concrete Precasting Plany Technol., 4 (1997) 64-70.
- [39] F. Shaker, A. El-Dieb, M. Reda, Durability of styrene-butadiene latex modified concrete, Cem. Concrete Res. Vol. 27, No.5 (1997) 711-720.
- [40] M. El-Reedy, Steel reinforced concrete structures, assessment and repair of corrosion, CRC press, 2008.

- [41] J. Flis, A. Sehgal, D. Li, Y. Kho, S. Sabotl, H. Pickering, P. Cady, Condition evaluation of concrete bridges relative to reinforcement corrosion, National Research Council, Washington DC., 1992
- [42] N. Buenfeld, J. Newman, The permeability of concrete in a marine environment, Magazine of Concrete Research 36 (1984) 67-80.
- [43] H. Whittington, J. McCarter, M. Forde, the conduction of electricity through concrete, Magazine of Concrete Research 33 (1984) 48-60.
- [44] V.M. Malhotra, N. J. Carino, Handbook on Nondestructive Testing of Concrete, Second Edition CRC Press 2003.
- [45] J. Shahzma, C. M. Hansson, Chloride-induced corrosion products of steel in cracked-concrete subjected to different loading conditions, Cement and Concrete Research, Vol. 39, No. 2 (2009) 116-125.
- [46] fib. Model code for service life design. Technical Report 34, FIB, April 2006.
- [47] X. Shi, N. Xie, K. Fortune, J. Gong, Durability of steel reinforced concrete in chloride environments: An overview, Construction and Building Materials, 30 (2012) 125-138.
- [48] U. Angst, B. Elsener, C. Larsen, Ø. Vennesland, Critical chloride content in reinforced concrete: A review, Cement and Concrete Research, Vol.39, Issue 12 (2009) 1122-1138.
- [49] A. Suryavanshi, J. Scantlebury, S. Lyon, Corrosion of reinforcement steel embedded in high water-cement ratio concrete contaminated with chloride, Cement and Concrete Composites, 20 (1998) 263-381.
- [50] C. Page, N. Page, A. El-Tarras, Diffusion of chloride ions in hardened cement paste, Cement and Concrete Research, 11 (1981) 395-406.
- [51] B. Lin, Ronggang Hu, Chenqing Ye, Yan Li, Changjian Lin, A study on the initiation of pitting corrosion in carbon steel in chloride-containing media using scanning electrochemical probes, Electrochimica Acta, Vol. 55, No. 22, (2010) 6542-6545.
- [52] V.S. Ramachandran, J.J. Beaudoin, Handbook of analytical techniques in concrete science and technology, William Andrew Publishing.
- [53] ASTM C876 (1999) Standard test method for half cell potentials of uncoated reinforcing steel in concrete.
- [54] H. Song, V. Saraswathy, Corrosion monitoring of reinforced concrete structures: A review, internation Journal of Electrochemical Science, 2 (2007) 1-28.

- [55] S. Feliu, J.A. Gonzalez, S. Feliu, Jr., C. Andrade, Relationship between conductivity of concrete and corrosion of reinforcing bars, *Brit. Corr. J.* 24 (1989) 195-198.
- [56] Bungey, J.H., *Testing of Concrete in Structures*, 2nd ed., Chapman & Hall, New York, 1989.
- [57] C. Andrade, C. Alonso, Test method for on-site corrosion rate measurement of steel reinforcement in concrete by means of the polarization resistance method, RILEM Recommendation, *Materials and Structures*, 37 (2004) 623 - 643.
- [58] K. Sagoe-Crentsil; F. P. Glasser; J. T. S. Irvine, Electrochemical characteristics of reinforced concrete corrosion as determined by impedance spectroscopy, *British Corrosion Journal* Vol 27, No 2 (1992) 113-118.
- [59] S. Cramer, B. Covino, S. Bullard, G. Holcomb, J. russel, F. Nelson, H. laylor, S. Soltesz, Corrosion prevention and remediation strategies for reinforced concrete coastal bridges, *Cement and concrete composites*, 24 (2002) 101-117.

Chapter 3:

Steel passivation in alkaline solutions simulating the concrete environment

The majority of the studies on corrosion mechanism and protection of reinforcing steel bars are performed in alkaline solutions simulating the concrete environment, thus avoiding the complications related to the preparation of representative reinforced concrete samples. In this work the electrochemical behavior of B450C mild steel was studied in saturated Ca(OH)₂ solution by cyclic voltammetry. Comparison with the electrochemical response in 1 M NaOH was also carried out, being such electrolyte the most commonly used for iron passivation studies. Results confirm the coexistence of two main processes, one leading to Fe(OH)₂ and the following (reversible) to Fe(III) oxo-hydroxides. The latter appears more relevant to the growth of a protective layer and in turn strictly connected to the operative condition of the cyclic voltammetry. The influence that time has on the passive film growth was then investigated by means of anodic polarization and electrochemical impedance spectroscopy. All the results indicated that at least three days of immersion in Ca(OH)₂ are required to guarantee the stabilization of the electrochemical response, thus leading to a protection similar to that observed with reinforced concrete.

Reprinted from Journal of Electroanalytical Chemistry, 736, E. Volpi, A. Olietti, M. Stefanoni, S. P. Trasatti, Electrochemical characterization of mild steel in alkaline solutions simulating concrete environment, 38–46, 2015, with permission from Elsevier

3.1 Introduction

Since the 80's, when the engineers community became conscious that reinforced concrete structures could suffer from severe forms of degradation, leading to extremely high maintenance and repair costs [1-3], lot of attentions were focused on detailed studies aiming to get more insight into the deterioration mechanisms.

The long time necessary for chloride penetration, or for complete carbonation of the concrete cover, together with complications related to the production of representative reinforced mortar samples, can be avoided by using alkaline solutions simulating the concrete environment. Sound concrete is generally simulated with alkaline solutions such as aqueous NaOH, KOH or Ca(OH)₂ [4-6]. Among the various possibilities, saturated Ca(OH)₂ seems to be the most used solution for such a purpose [4-10]. Different quantities of chlorides can be added to such solutions to study the onset of a localized attack, while a carbonated environment is usually simulated using a sodium carbonate/bicarbonate buffer of pH around 10 [4,5].

The most studied passive Fe/electrolyte systems are Fe in borate buffer (pH 8.4) [11-13], and in 1 M NaOH or KOH [14-19]. In the open literature referring to concrete simulation, there appears to be lack of in-depth electrochemical characterization of steel in saturated Ca(OH)₂ solution, which prompted us to systematically investigate the electrochemical behavior of mild steel in such solution.

With respect to the passive behavior of iron in alkaline solutions, results are sometimes controversial, and the nature of the passivating layer is not unambiguously established. However, it is well accepted that anodic oxidation of iron in alkaline solution implies at least two steps. First, iron is converted to Fe(OH)₂ and then, different oxy-hydroxy Fe(III) species are formed. More recent works have investigated the structure of the oxide film, pointing out the presence of a denser inner layer formed by mixed iron oxides like magnetite (Fe₃O₄), overlapped by an outer hydrous (FeOOH) gelatinous layer, which confers passivity to the metallic substrate [20,21].

According to [22], electrochemical steady state measurements on iron in alkaline media are relatively difficult and scarcely reproducible. In the present work, a non-steady-state technique such as cyclic voltammetry was used to characterize the behavior of B450C mild steel immersed into a saturated Ca(OH)₂ solution.

As steel bars are embedded in concrete to produce reinforced samples, a curing time (generally 28 days) is needed for complete hydration of the cement. This implies that the steel surface remains in contact with an alkaline environment for a long time, which allows the growth of a protective layer. Accordingly, in the present work we decided to investigate the influence of the passivation time on the electrochemical response of metallic samples immersed in the alkaline solution. In the open literature there is no consensus on the time necessary to obtain the growth of a representative

oxide layer, so much that different authors use times ranging from half an hour to several days [4,5,7,23]. The stabilization of the electrochemical response, being related to the growth of a stable and protective oxide layer, was investigated by means of open circuit potential monitoring, linear polarization resistance, potentiodynamic anodic polarization and electrochemical impedance spectroscopy.

3.2 Experimental

3.2.1 Materials and testing environment

Tests were carried out with 8 mm diameter B450C mild steel reinforcing bars with chemical composition: C 0.22%, Cr 0.13%, Ni 0.15%, Mn 0.78%, Mo 0.03%, N 0.007%, Si 0.24%, Cu 0.56%, S 0.039%, P 0.013%. Bars were purchased from Feralpi Group (Lonato, Brescia, Italy).

Small specimens were produced by cutting samples of 15 mm length that were subsequently embedded into a thermoplastic resin leaving a 0.6 cm^2 cross-section as exposed area. Before embedding, specimens were softly brushed to remove the abundant rust deposits. Electrical connection was realized with a 3 mm diameter AISI 304 threaded rod by drilling a hole at the opposite end of the specimen (fig.3.1). Before electrochemical testing, the metallic surface was polished with emery paper from 320 to 1200 grit and ultrasonically degreased in hexane for 10 min.

Test solutions were prepared using NaOH pellets and Ca(OH)₂, purchased from Sigma-Aldrich as ACS reagent grade. Saturated Ca(OH)₂ solution (pH 12.6) was filtered prior to use.

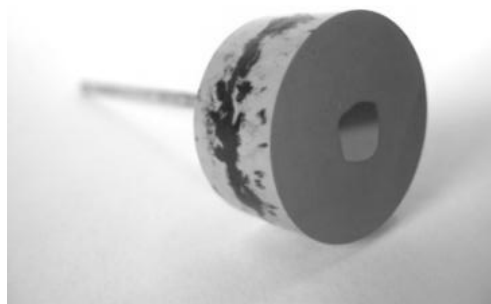


Fig.3.1: Picture of the B450C steel sample for electrochemical measurements.

3.2.2 Steel metallographic characterization

B450C steel samples, prepared as above described, were metallographically characterized after an accurate polishing up to 0.25 μm diamond paste and a steel

surface etching with 5% Nital reagent [24]. Pictures were taken by means of a Nikon Eclipse metallographic optical microscope.

The Vickers micro-hardness was measured on different spots on the cross section of the steel rebar with a Leitz Wetzlar indenter, and the given results are an average of at least 10 measurements.

Localized anodic potentiodynamic polarizations were performed using a specifically designed electrochemical cell, measuring on a 0.01 cm^2 area. The electrolyte, sat. Ca(OH)_2 solution, was recirculated in the cell by means of a peristaltic pump, in order to avoid the clogging of the active area due to the presence of eventual corrosion products.

3.2.3 Electrochemical setup

All electrochemical measurements were performed using a conventional three electrode cell (electrolyte volume: 300 ml), in which the active steel surface acted as working electrode, a Pt wire as counter electrode, and a saturated calomel electrode (SCE) was used as reference electrode. Specimens were mounted into the cell with the working surface facing downwards, thus keeping the electrical connection above the electrolyte level.

Each experiment was repeated at least three times, using a new polished surface each time, to check the reproducibility and reliability of the results. Measurements were carried out at $23 \pm 2^\circ\text{C}$.

3.2.4 Cyclic voltammetry (CV)

The electrochemical characterization of the growing oxide layer was carried out by cyclic voltammetry at 100 mV/s. Prior to each testing, the electrolyte was deaerated for 30 minutes by nitrogen bubbling, and a potentiostatic cathodic pretreatment at -1.5 V vs. SCE was carried out for 10 minutes to guarantee uniform surface conditions with reduction of the surface oxides in the hydrogen evolution region [14-17]. The CV was started in the anodic direction from the potential of the cathodic pretreatment .

The electrochemical response to multiple triangular potential waves (CV) was checked over diverse potential windows, the larger being the one including oxygen and hydrogen evolution at the anodic and cathodic limits, respectively.

Correlations between different current peaks were investigated with a systematic variation of the anodic limit ($E_{\lambda a}$). Three cycles were completed before regenerating the surface with 10 min cathodic polarization at -1.5 V vs. SCE, switching then to a more anodic limit. The anodic limits ranged from -1.2 to 0.8 V vs. SCE [15].

The effect of the oxide film ageing was studied through a set of 1 to 20 minutes anodic potentiostatic polarization inserted every three voltammetric cycles. Conversely, cathodic potentiostatic polarizations were introduced every three cycles aiming to investigate the response of the passive film to a reductive process.

3.2.5 Potentiodynamic polarization (PD), linear polarization resistance (LPR) and impedance spectroscopy (EIS)

How the passivation time affects the electrochemical response of mild steel was studied by immersing several specimens in saturated $\text{Ca}(\text{OH})_2$ for different times. The resulting electrochemical behaviour was investigated by OCP and LPR monitoring (measurements performed every 20 minutes for the first day, and every hour in the following days), and by means of anodic potentiodynamic polarization and electrochemical impedance spectroscopy (measurements performed 0, 4, 24, 48, 72 and 96 hours of immersion). Cyclic anodic potential sweeps were performed at the scan rate of 0.1667 mV/s. The same value was used for linear polarizations while corrosion currents were calculated using the Stern-Geary equation: $i_{\text{corr}} = B/LPR$, being parameter B a function of the Tafel slopes. In the present work, the B values used for calculations were those suggested by Andrade et al. [27], i.e. 26 mV (active behavior) was used for the Tafel parameter in the first 6 hours, switched to 52 mV (passive behavior) for all successive measurements. The above described experiments were performed with a PAR 273A potentiostat.

The EIS measurements were obtained with a Gamry potentiostat at the open circuit potential resulting from a five minutes equilibration time in the testing media. The frequency range was 10^5 to 4×10^{-3} Hz, with a logarithmic sweeping frequency of 10 points per decade. The modulation amplitude of potential was 10 mV (rms).

3.3 Results and discussion

3.3.1 Steel metallographic characterization

The macroscopic picture of the steel surface after the 5% Nital etching, reported in fig. 3.2, immediately pointed out a differentiation between the core of the steel cross section and the external section.

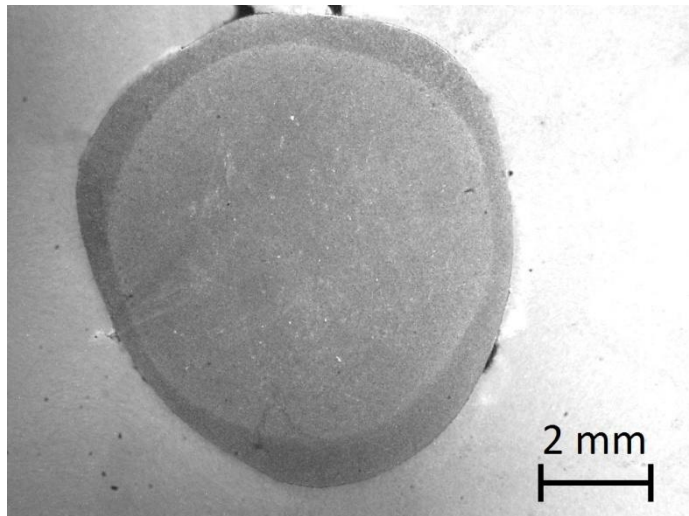


Fig. 3.2: Macroscopic picture of the B450C steel surface, after 5% Nital etching.

Further observations, performed with the optical microscopy, showed the presence of two significantly different microstructures (fig. 3.3). The core region (fig.3.3(a)) exhibited a crystalline structure where the grain boundaries were clearly detectable. From the morphological point of view, the coexistence of dark and bright areas was attributed to ferrite/perlite phases. On the superficial section a less clear structure was observed, where however it was still possible to detect the grain boundaries.

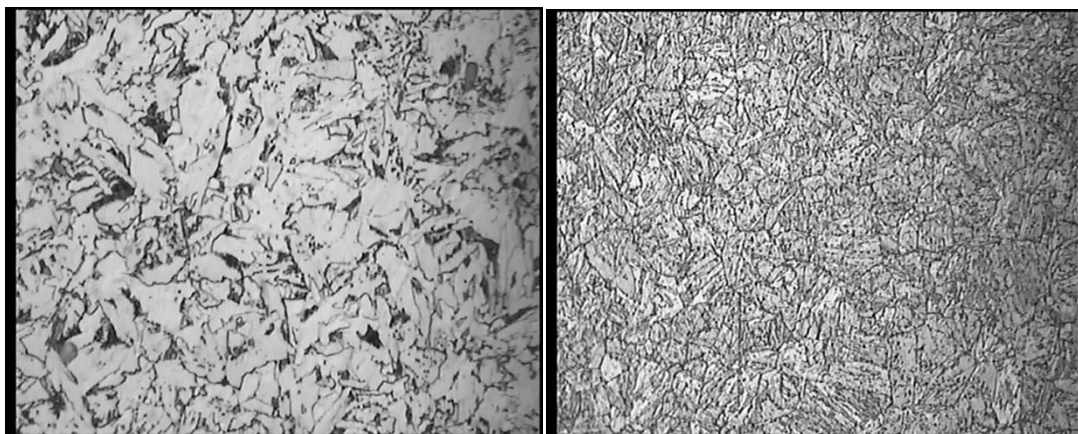


Fig. 3.3: Optical microscopy pictures of the B450C steel surface, after 5% Nital etching (magnification: 500X). (a) core, (b) surface.

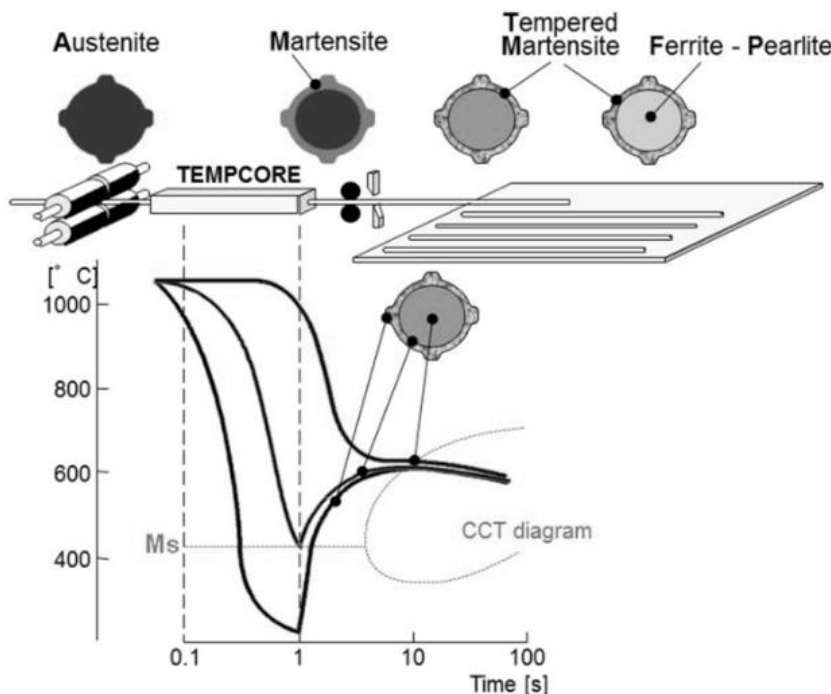
The different morphology was reflected in a different penetration of the pyramidal indenter, values for the Vickers microhardness are shown in table 1

Table 3.1: Vickers micro hardness.

Region	Micro hardness	σ
Core	209.4 HV	4.3
Surface	302.1 HV	4.5

The above presented differences in terms of hardness and microstructures come from a particular process used for the production of the steel reinforcing bars known as Tempcore® process.

Such process, whose schematic is reported in fig. 3.4, consists of an in-line thermal treatment leading to the formation of tempered shell and resulting in an increase of the steel mechanical properties allowing to obtain high strength weldable rebars with low carbon and low manganese contents [25].


Fig. 3.4: Principle of Tempcore process.

The rebar leaving the last stand of the hot rolling mill passes through a special water cooling section whose cooling efficiency is such that a surface layer of the bar is quenched into martensite, the core remaining austenitic. The quenching treatment is stopped when a determined thickness of martensite has been formed. When the rebar leaves the intense cooling section, the temperature gradient established in its cross section causes heat to release from the centre to the surface. This increasing of the surface layer temperature results in the self-tempering of the martensite.

Finally, during the slow cooling of the rebar on the cooling bed, the austenitic core transforms into ferrite and perlite or into bainite, ferrite and perlite[26].

The coexistence of a double structure on the cross section of the steel rebar, could lead to some concerns, as the two phases could behave differently from the electrochemical point of view, while the instrument would only record an average response. For such a motivation, a series of localized anodic potentiodynamic curves were recorded on both the core and the external ring of the steel cross section.

Two representative curves are reported in fig. 3.5, where it can be clearly noticed that although a small difference was detected in terms of current densities, being that of the external layer slightly higher than that of core, the overall responses were however rather similar. Furthermore an estimation of the surface area ratio between the core and the external ring led to a value of 0.2, thus allowing to consider the differences in terms of electrochemical responses absolutely negligible.

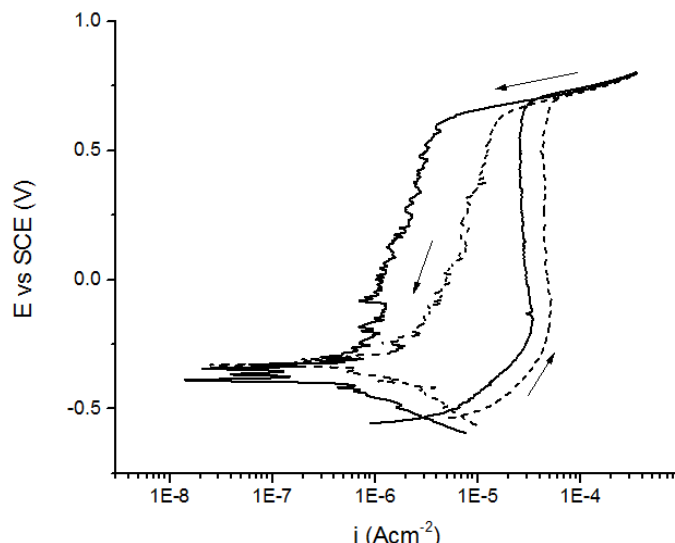


Fig. 3.5: Localized potentiodynamic curves recorded in sat. $\text{Ca}(\text{OH})_2$ solution, $v = 1\text{mV/s}$. (—) external shell, (—) bulk.

3.3.2 Cyclovoltammetric characterization

Cyclic voltammetry in 1M NaOH and saturated $\text{Ca}(\text{OH})_2$

The cyclovoltammetric response to a ten cycles perturbation performed in 1M NaOH at a scan rate of 100 mV/s is reported in Figure 3.6(a).

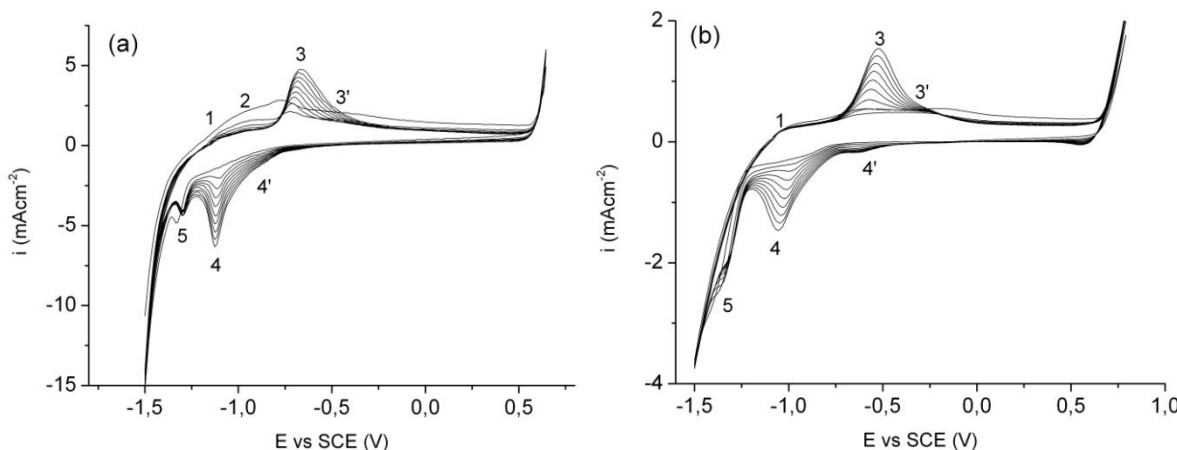


Fig.3.6: Cyclic voltammetries (ten cycles) of B459C mild steel performed at 100 mV/s in deaerated solutions: (a) NaOH 1M pH: 13 (b) saturated Ca(OH)₂ pH12.6.

In agreement with literature, the E/I plot exhibits a complex contour which changes with cycling. Starting from the positive forward scan, two small, stable anodic peaks (1 and 2) were detected at -1.1 V and -0.95 V, respectively. Peak 3 (-0.7 V) was characterized by higher currents and a continuous increase in height with cycling. A further interesting feature of peak 3 is its asymmetric shape, being characterized by the presence of a shoulder on the more positive potential side that is commonly referred to as peak 3'. Such shoulder was followed by a wide capacitive region, which extended for about 0.9 V, and ended with a sudden current increase related to oxygen evolution. The negative going potential scan was characterized by two cathodic current peaks, 4 and 5, located at -1.15 and -1.3 V, respectively. Similarly to peak 3, also peak 4 exhibited an asymmetric shape, and its shoulder located on the positive side was defined as peak 4'. The negative going potential scan ended with a significant cathodic current increase attributed to hydrogen evolution. Although mechanism and kinetics of oxide layer formation are still not fully understood, there are no doubts that the metallic surface undergoes at least two successive electrochemical processes during the polarization, the first being related to $\text{Fe}(0) \leftrightarrow \text{Fe}(\text{II})$, attributed to peaks 1,2 and 5, while the next process, involving $\text{Fe}(\text{II}) \leftrightarrow \text{Fe}(\text{III})$, is believed to be related to peaks 3, 3', 4 and 4' [6,14,15].

The E/I plot for a 10 cycles voltammetric experiment performed in saturated Ca(OH)₂ solution is reported in Figure 3.6(b). Like in 1M NaOH, the main features of the voltammogram are the presence of the two asymmetric peaks 3 and 4, whose intensity increases with cycling, together with that of their corresponding shoulders 3' and 4'. The capacitive zone extends from -0.2V to 0.65V, while oxygen and hydrogen evolve at the anodic and cathodic limits of the scanned potential range, respectively. What differentiates the two voltammograms in Figure 3.6 is the fact that in saturated Ca(OH)₂ peaks 1 and 2 are harder to detect if compared with the case of NaOH. In particular, peak 2 disappears in the calcium containing solution. Some differences are also detected in the shape of peak 5, being sharp and stable in NaOH, while broader and subjected to anodic shift with cycling in saturated Ca(OH)₂. By

comparing the current densities of peak 3 and 4 in the two different solutions, it can be noticed that current peaks recorded in NaOH are significantly higher, by a factor of 3, than those in Ca(OH)₂. Such difference may be explained considering the inhibitive properties of Ca(OH)₂ solution [16], according to which preferential adsorption of Ca²⁺ ions at the outer plane of the inner oxide film should decrease the strength of the electric field assisting the displacement of iron ions from the substrate to the outer layer region, thus enhancing passivation during potential cycling. Another study [28] confirms that adsorbed cations such as Ca²⁺, Mg²⁺ and Ba²⁺ can accelerate accumulation of passivating oxides.

Effect of the scanned potential window

Repetitive cycling was performed over different potential windows to better understand the electrochemical behavior of mild steel in saturated Ca(OH)₂ solution, and aiming to investigate how the different peaks are intercorrelated; results are shown in Figure 3.7. By setting the limiting anodic value ($E_{\lambda a}$) at -0.14 V, thus excluding capacitive and oxygen evolution regions, the voltammogram presents the same features as the one performed in the extended potential range: two anodic peaks 1 and 3, and two cathodic peaks 4 and 5 (Figure 3.7(a)). The only remarkable difference is that the growth of peaks 3 and 4 is clearly inhibited, and the resulting currents are significantly lower (for example 0.6 mA/cm² against 1.5 mA/cm² for peak 3 at the 10th cycle). The drastic decrease registered in the current densities by changing the anodic limit from 0.8 V to -0.14 V may be attributed to exclusion of the oxygen evolution region, such phenomenon playing a major role in the formation of a porous outer layer. By excluding oxygen evolution, a more compact oxide layer is expected, characterized by increased barrier effect hindering the reduction/oxidation mechanism and giving rise to the signals of Figure 3.7(a). By further decreasing the width of the scanned potential window to -0.8 V, thus also excluding the region of peaks 3 and 3', the resulting cyclovoltammogram changes dramatically with respect to the previous cases. As clearly shown in figure 3.7(b), the exclusion of peak 3 results in the absence of peak 4, which indicates interconnection between the two signals. According to the literature [6,14,15], the peaks are related to oxidation and reduction of the redox couple Fe(II) - Fe(III), respectively. Differently from expectations based on the literature for NaOH solutions [15], also peak 5 disappears in the cyclovoltammograms of Figure 3.7(b), which points out that a necessary condition for its occurrence is the preceding oxidation-reduction process related to peak 3 and 4. Motivation for such behavior may be attributed to the different nature and structure of the oxide film, more compact and insulating in the inner layer, more porous and less dense in the outer layer .

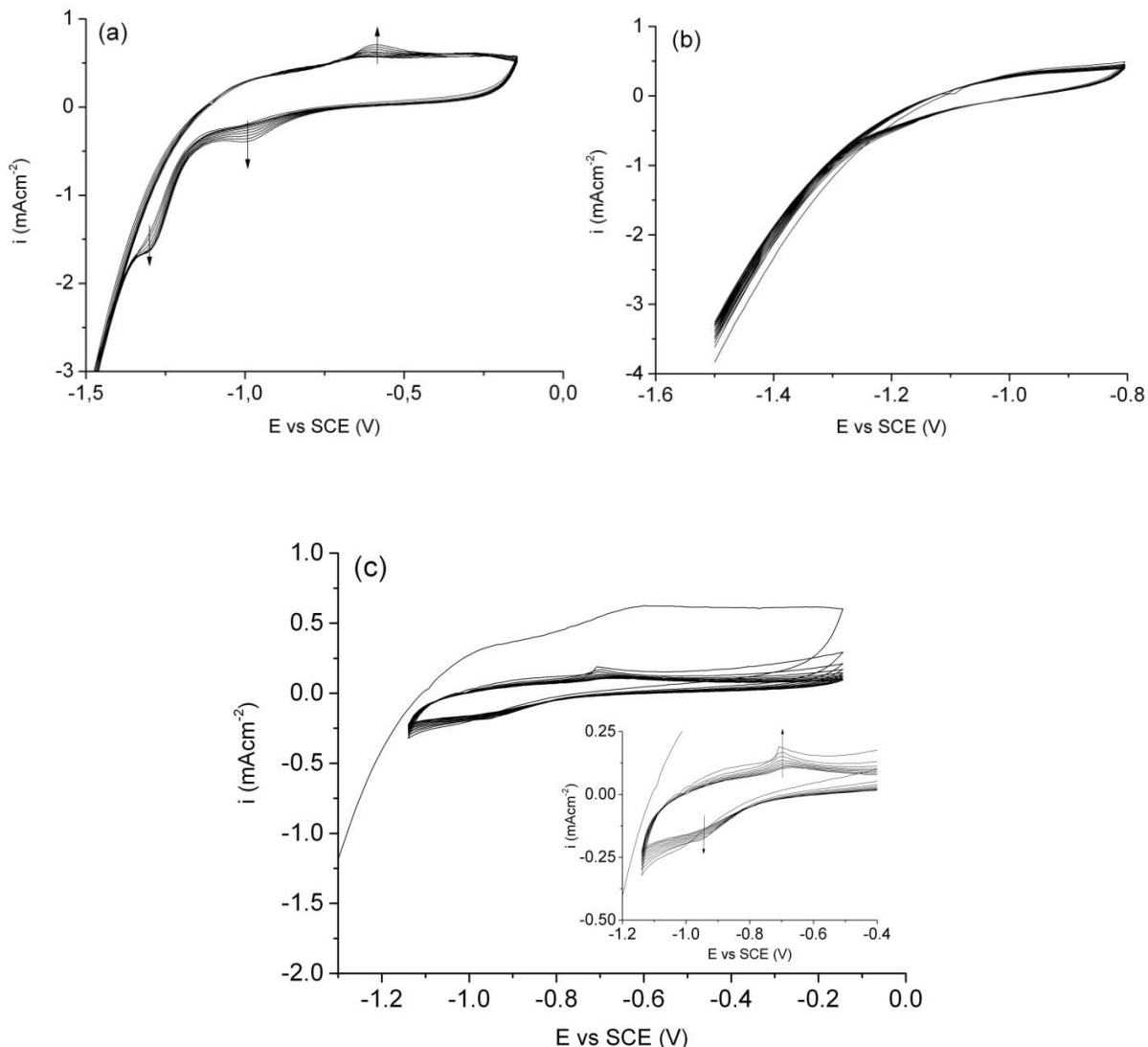


Fig. 3.7: Cyclic voltammetries of steel B450C (ten cycles) performed in saturated $\text{Ca}(\text{OH})_2$ at 100 mV/s using different potential scanned ranges: (a) from -1.5 V to -0.14 V (b) from -1.5 V to -0.8 V (c) from -1.14 V to -0.14 V.

In the voltammogram reported in Figure 3.7(c), after a cathodic potentiostatic polarization at -1.5 V the potential was scanned anodically till to -0.14 V, thus including peaks 3 and 4, then reversed till -1.14 V, keeping these last two values as the limits for the following 9 cycles. As expected, the first cycle of Figure 3.7(c) overlapped with the first one of Figure 3.7(a), while significant differences emerged in the subsequent cycles. By setting -1.14 V as cathodic limit, the region of peak 5 and that of hydrogen evolution are excluded from the voltammogram, which avoids significant reduction of the oxide film generated during the anodic scan. Although not causing a complete reduction, otherwise all voltammograms should overlap with the first cycle, keeping the specimen at a more cathodic potential than -1.14 V resulted in partial reduction of the anodically formed oxide layer, i.e., partial regeneration of the surface allowing continuous increase of current in the subsequent cycles. The inset

of Figure 3.7(c) clearly shows that avoiding such reduction contributes to the rapid growth of a protective layer as indicated by the much lower current recorded for peaks 3 and 4 with respect to Figure 3.7(a).

Effect of the variation of the anodic limit ($E_{\lambda a}$)

E/I curves were recorded by gradually increasing $E_{\lambda a}$ aiming to confirm the interconnection of the voltammetric signals and to investigate the genesis of different current peaks.

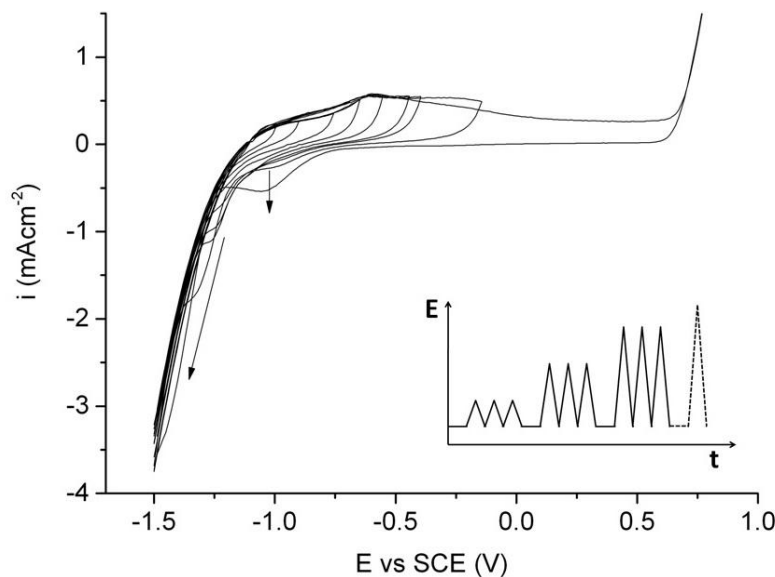


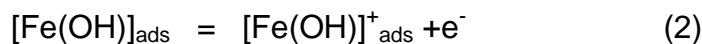
Fig. 3.8: Effect of the variation of the anodic limit, thirds voltammetric cycles recorded after each anodic limit increase ($v = 100$ mV/s).

The results of Figure 3.8 clearly highlight that peak 4 begins to be detected only from the 5th curve ($E_{\lambda a} = -0.65$ V) where at the end of the positive going scan the current increases slightly due to the emerging peak 3. In the subsequent cycles, the height of peak 4 increases slightly, with an abrupt enhancement of the signal as oxygen evolution is generated as for the case of the 10th curve ($E_{\lambda a} = 0.8$ V), confirming the coupling of peaks 3 and 4, and the connection of the latter with O_2 evolution. As for peak 5, it starts to appear with the 5th curve, in agreement with the above discussed requirement of the presence of a porous oxide layer originated from peak 3. Furthermore, by increasing the anodic limit, peak 5 potential shifted cathodically, indicating that an increased overpotential is required to reduce Fe(II) to Fe(0) as the anodic layer becomes thicker.

The above results highlight the presence of anodic and cathodic complementary processes that involve different conjugated redox couples: current peak 3 is clearly related to current peak 4, while the behavior of peak 5 appears to differ from that

reported by other authors [15], being related to some extent to the presence of peaks 3 and 4

According to the literature [6,15,16,21,29] in alkaline solution the stable product that firstly forms in the potential range of peak 1 is Fe(OH)_2 , via reactions 1 to 3 reported below. Such compound is electro-oxidized to magnetite (Fe_3O_4) in the potential range of peak 3 (reaction 4). Products formed in this ways are subsequently subjected to chemical reactions or structural rearrangements related to ageing processes that lead to further modifications of the oxide layer (reactions 5, 6). The final structure of the oxide layer is commonly considered as to be constituted by a compact inner layer of magnetite and a less dense, gelatinous layer composed of hydrated products such as goethite (α - FeOOH), lepidocrocite (γ - FeOOH) and akaganite (β - FeOOH). The double layer nature of the oxide film was confirmed by the presence of the shoulders 3' and 4' that according to [6] are related to redox phenomena occurring in the inner layer, while the most prominent peaks 3 and 4 are related to those occurring in the porous outer layer.



Effect of anodic prepolarizations at -0.14V vs SCE

As a further step to the investigation of how the electrochemical response of the passivating system changes as a function of time, a series of anodic potentiostatic polarizations at $E_{\lambda a}$: -0.14 V were introduced in the voltammetric experiments (inset Fig. 3.9(c)). Presumably, the effect of the anodic polarization at $E_{\lambda a}$ should be equivalent to the ageing of the electrochemically formed oxide layer [30,31].

The first and the third voltammograms recorded after 1 and 20 minutes of anodic potentiostatic polarization at -0.14 V vs SCE are reported in Figure 3.9(a) and 3.9(b), respectively, while the full series of the first voltammogramms preceded by polarizations ranging from 1 to 20 min are shown in Figure 3.9(c).

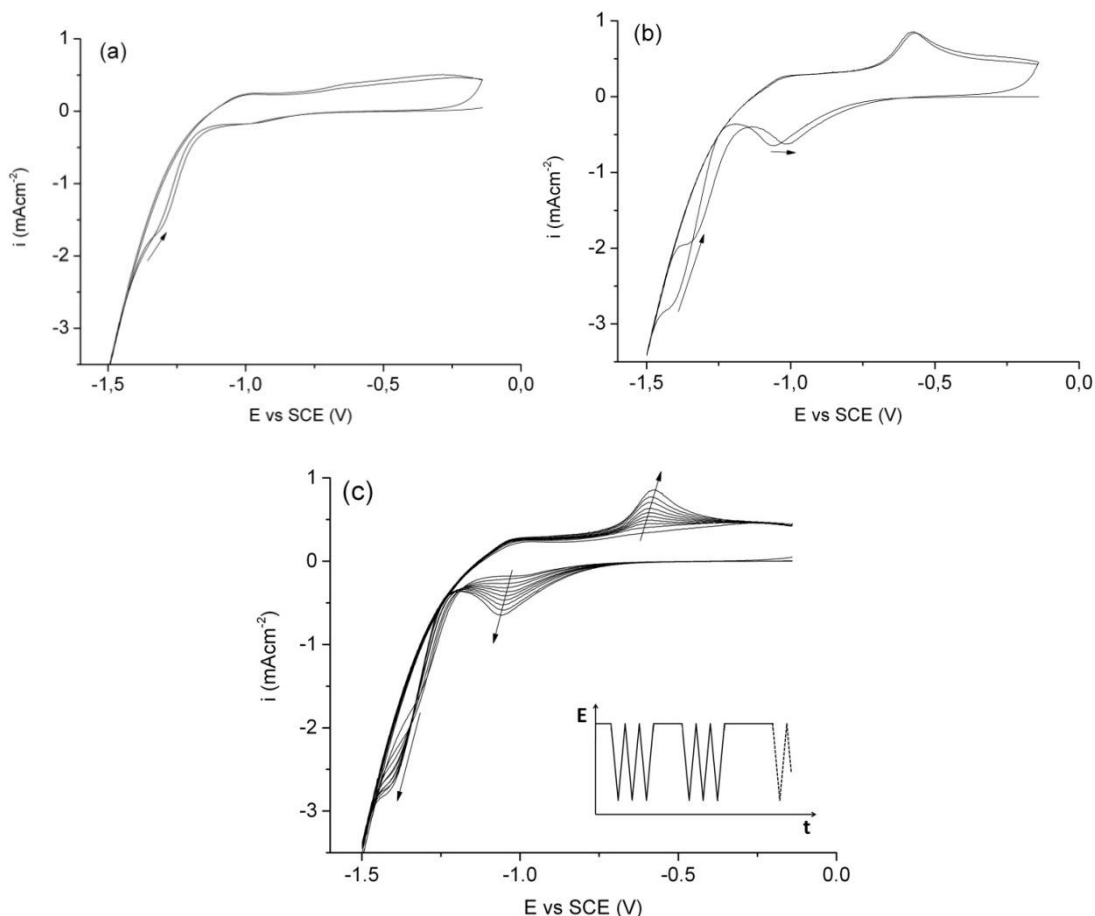


Fig. 3.9: Effect of anodic polarizations at the $E_{\lambda,a}$ of $-0.14V$ vs SCE ($v = 100$ mV/s), (a) first and third cycle after a 1 min polarization, (b) first and third cycle after 20 min polarization, (c) full view of the first cycles after anodic polarizations ranging from 5 to 20 minutes.

Scrutiny of the changes between the first and the third cycle following each polarization revealed a trend in current density and peak position related to the polarization duration (fig.3.9(a,b)). The anodic polarization affects the cathodic branch of the voltammogram: as indicated by arrows, both reduction peaks 4 and 5 appear at more cathodic potential in the first cycle with respect to the third one, being such shift more marked by increasing the duration of the anodic polarization. Considering current density, although no changes were detected for peak 4, significant increment of peak 5 was observed by increasing the polarization time from 1 to 20 min (Figures 3.9(a,b,c)). Expected effect of the anodic polarization is that of stimulating the growth of the oxide film, higher film thickness may justify an increase of the overpotential required for the reduction processes reflected in the cathodic shift of the peak potentials for the first cycles following polarization. With further cycling, going through the hydrogen evolution region towards the anodic direction, the effect of the anodic polarization turns out mitigated, as indicated by reduction processes occurring at less cathodic potentials with respect to the first cycle. According to [15], the height of current peak 5 diminishes as the number of potential scans increases, a more remarkable phenomenon as $E_{\lambda,a}$ increases. This behavior is attributed to the existence of non-equilibrium states of both reactants and products participating in

the reaction. The explanation could fit the present case if the anodic pre-polarization had an effect on the film growth comparable to that of an extensive cycling of the system. The whole series of the cyclic voltammograms reported in Figure 3.9(c) presents similar features to those discussed for the ten successive cycles recorded in the same scanned potential range, and reported in Figure 3.7(a). The only remarkable difference results to be an overall decrease in the current density attributed to the increased thickness of the oxide layer caused by anodic polarization.

Effect of cathodic pre-polarizations at -1.5V vs SCE

With the aim to check the effect of potentiostatic polarizations on the electrochemical behavior of the oxide film, an opposite experiment was designed, a cathodic potentiostatic polarization in the hydrogen evolution region was inserted every three voltammetric cycles. The results are shown in Figure 3.10. Differently from the previous case, no significant differences were recorded between the first and the third cycle of each set, except for the already discussed current increment of peaks 3 and 4. The effect of a cathodic potentiostatic polarization is thought to be that of reducing the oxide layer formed during the previous anodic scan. As a consequence, the fact that cyclicvoltammograms from subsequent sets did not overlap, as indicated by arrows, pointing out a continuous increase in peak 3 and 4, may be considered as a demonstration of the partial irreversibility of the processes occurring on the metallic surface.

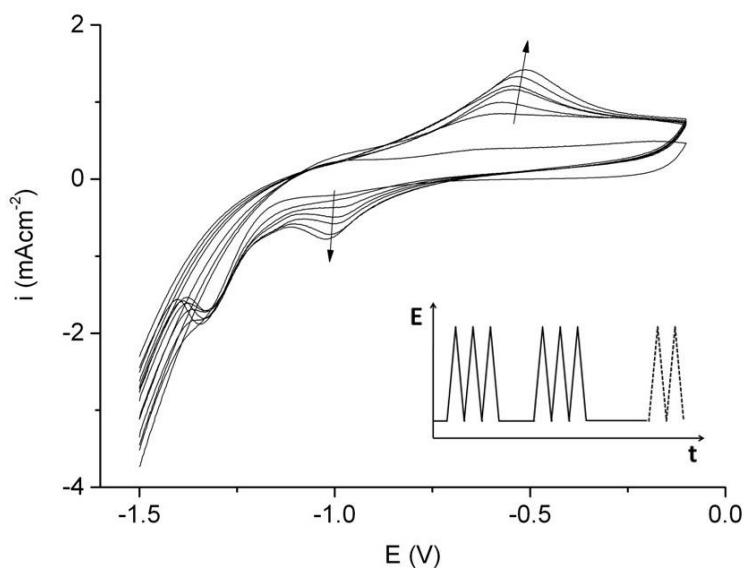


Fig 3.10: Effect of cathodic polarizations at the $E_{\lambda c}$ of -1.5 V vs SCE ($v = 100$ mV/s), full view of the first cycles after polarizations ranging from 1 to 20 minutes.

Although incomplete, the reduction of the oxide layer causes a decrease of its barrier properties, as demonstrated by significantly higher currents than in the cases

discussed previously. The current of peaks 3 and 4 is modified during cycling as already mentioned, indicating accumulation of anodically formed oxide layer. By comparing Figure 3.10 with the cyclicvoltammogram of Figure 3.9(c), it appears evident that potentiostatic polarizations affects the features of the current peaks related to the Fe/Fe(II) transition, being peak 1 and peak 5 more stable and defined in case of anodic and cathodic pre-polarization, respectively.

Effect of long term cycling

As a further step toward the understanding of how the presence of a passive film affects the electrochemical response of the system, the effect of the oxide layer thickness was studied by applying a perturbation consisting of thirty cycles. In addition to just polished surfaces, the experiment was also performed on an already existing passive layer grown during three days of immersion in saturated Ca(OH)₂.

Figure 3.11(a) shows the E/I contour plot of the thirty cycles for a polished sample. Coherently with the results of [15], the current of peak 1 results stable throughout the experiment, while the correlated peak 5 undergoes anodic shift in the first ten cycles and stabilizes in the successive ones. Conversely, peaks 3 and 4 do not show sign of stabilization, and their height continues to increase with cycling. Together with current density increase, significant shift of the peak potential in the anodic and cathodic direction was detected for peaks 3 and 4, respectively. The shift, which represents the increasing overpotential needed to oxidize and reduce the oxide layer at each successive cycle, clearly indicates the protective nature of the oxide that hinders charge transfer during potential scan.

Similarly to what already discussed in the case of anodic pre-polarizations as the oxide layer is artificially created, the presence of the naturally grown oxide layer causes significant decrease in current (not shown).

By converting E/I plots into time/current plots and by numerically integrating the anodic branches, the charge involved in the oxidation process of each cycle was determined (Figure 3.11(b)).

The anodic charge significantly increases along the thirty cycle experiment, clearly indicating the accumulation of the anodically formed surface layer during cycling. The accumulated charge was principally related to the pair of peaks 3, 3' and 4,4' thus confirming the major role that the corresponding reactions play in the passivation process [16]. As expected, the accumulated charge calculated in the case of a passivated sample resulted significantly lower than that of the case of a polished surface.

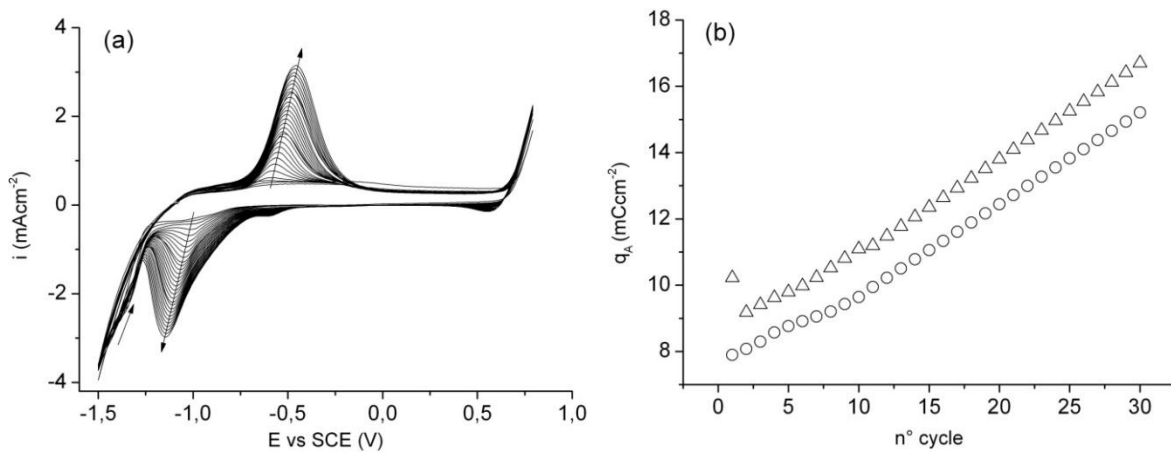


Fig.3.11: Effect of long term cycling, (a) thirty cycles performed on a polished surface at 100 mV/s, (b) comparison of the accumulated anodic charge during cycling between a polished surface (Δ) and naturally passivated sample obtained by three days immersion in saturated Ca(OH)_2 (\circ).

3.3.3 Effect of passivation time

Anodic polarization

Anodic polarization is commonly used to study the corrosion mechanism of alloys in a given environment. Generally, a polarization curve recorded in the absence of aggressive species can be considered as a reference. For this reason, anodic polarizations were performed with the aim to investigate the effect of different experimental conditions. Figure 3.12 shows a comparison among anodic polarizations of freshly polished specimens in deaerated saturated Ca(OH)_2 with a preceding 10 min cathodic potentiostatic polarization at -1.5 V vs SCE, in the same deaerated solution but without cathodization and in a naturally aerated solution. As expected, higher corrosion potentials and lower current were obtained going from completely reduced surface to one covered by a very thin oxide layer formed during the time elapsed between the polishing and the beginning of the experiment. Although less marked than cathodization, also the presence of oxygen in solution appears to affect the electrochemical response of the system by facilitating the growth of the protective layer as indicated by slightly lower currents. All curves show typical features of passive systems, i.e., low current in the potential range from the open circuit potential to the oxygen evolution potential at which an abrupt current increase is observed. The main effect of cathodization is that of revealing a marked current peak at -0.7 V vs SCE, followed by a less defined signal occurring at the more anodic potential of -0.4 V. These values are hardly comparable with current peaks obtained from voltammetric experiments, since anodic polarization, using a very slow scan rate, is a quasi-stationary technique. Conversely, cyclic voltammetry is a non-stationary experiment.

According to the literature [32], the marked current peak obtained at -0.7 V vs. SCE with previously cathodized specimens can be assigned to Fe(II)-Fe(III) oxidation; while at lower potentials the Fe(0)-Fe(II) couple may be partially masked by the open circuit potential anodically shifted during the time required for recording the cathodic branch of the curve. Joiret et al. [32] performed voltammetric experiments at much slower scan rates ($v = 0.5$ mV/s) than those commonly reported in the literature [15]. The authors detected additional peaks at more anodic potentials than that related to the Fe(II)-Fe(III) transition. Such peaks were attributed to the formation of different Fe^{3+} species from magnetite. Similarly, in the present case, both the curves performed in a deaerated solution showed a small and broad signal at about -0.3 V vs. SCE. Such peaks could be attributed to the process related to reactions 5 and 6 (see above). The polarization performed in a naturally aerated solution showed only a straight passive current without any other particular feature. Such behavior can be attributed to the response of the oxide layer grown during the 15' of equilibration before the anodic potential scan. This implies that after the relatively short time of equilibration the potential attained a value high enough to allow the occurrence of reactions 5 and 6.

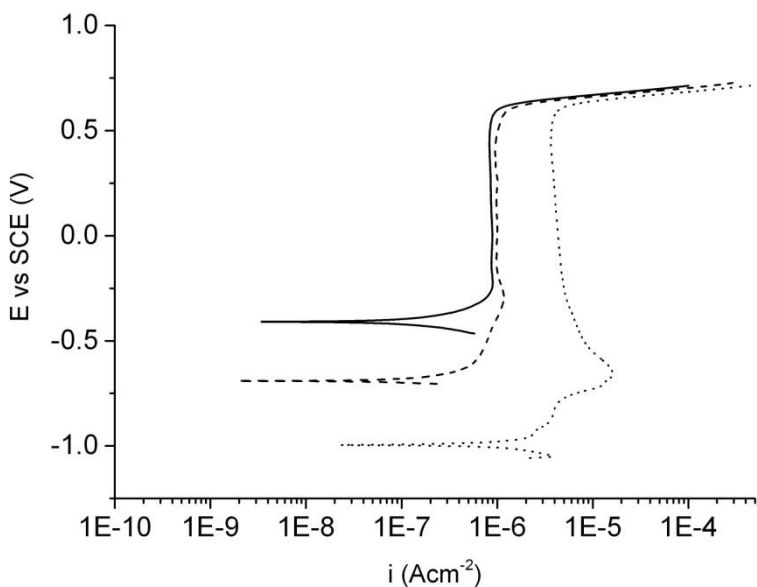


Fig. 3.12: Anodic polarization curves performed in saturated $\text{Ca}(\text{OH})_2$ at 0.1667 mV/s (.....) deaerated solution and sample cathodically pretreated, (--) deaerated solution, (—) naturally aerated solution.

The effect of a naturally grown oxide film on the electrochemical response to anodic polarization is shown in Figure 3.13. As expected, longer immersion times lead to higher corrosion potentials, thus highlighting the protective nature of the oxide film. Such increased protection can be attributed to the conjugated effects of increasing thickness with time and its ageing leading to enrichment in less conductive Fe(III) oxides (reactions 5 and 6).

It has been demonstrated that the composition of the passive layer depends on potential, being significantly different between naturally grown and anodically stimulated oxide films [21,29]. Accordingly, the main effect of increasing anodic potential is to cause dehydratation of the oxide film. As a consequence, modification of the structure and of the properties of the oxide layer can be expected during the run of an anodic polarization, in which the potential is scanned up to the limit of the water stability domain (0.7 V vs. SCE).

For just polished specimens, the growth of the oxide layer was immediately under control of the anodically scanned potential. Conversely, in all other cases, naturally grown layers responded to the changes induced by anodic polarization by hindering charge transfer. As clearly indicated by the lower current, increasing resistance to the electrochemically induced modifications of the oxide layer was offered by longer passivated samples.

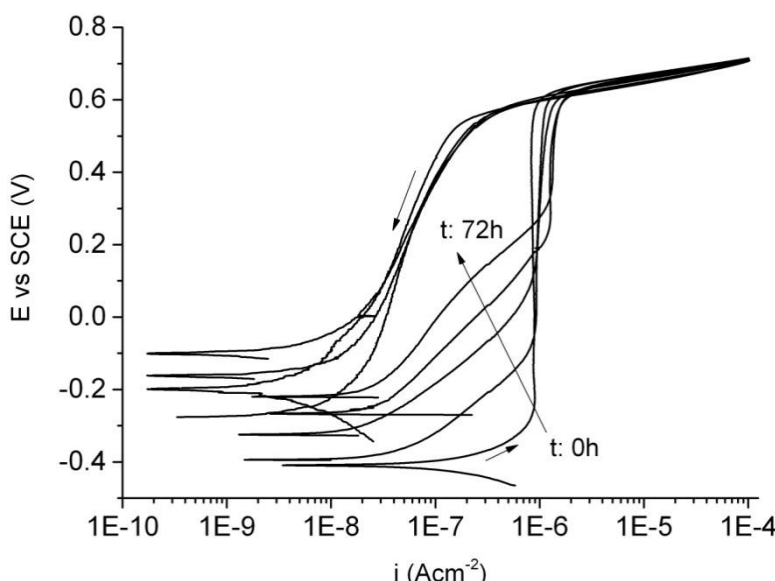


Fig. 3.13: Anodic polarization curves performed in naturally aerated, saturated $\text{Ca}(\text{OH})_2$ solution ($v = 0.1667 \text{ mV/s}$). Sample were prepassivated in the same solution for different time ranging from 10 minutes to 3 days.

OCP monitoring and linear polarization resistance

The trend of the corrosion potentials (E_{corr}) of four different specimens during six days is reported in Figure 3.14(a). All samples exhibit reproducible behavior, characterized by a starting potential of about -400 mV (vs. SCE) that rapidly increases during the first 6 hours of immersion, which indicates spontaneous growth of a protective oxide layer on the polished metal surface. The potential increase continues for two more days, after which the average value of E_{corr} of all samples was around -220 mV. In the successive four days, the E_{corr} grows very slowly reaching a final value of ca. -180 mV.

Similarly to E_{corr} monitoring, also the specimens subjected to LPR measurements (Figure 3.14(b)) show good reproducibility and coherence with those reported by other authors [5, 23]. The initial corrosion currents were of the order of $0.5 \mu\text{Acm}^{-2}$ falling in the range of moderate to high corrosion range, but after the first day all samples exhibited i_{corr} of $0.1 \mu\text{Acm}^{-2}$ or lower, being thus classifiable in passive state. Likewise the case of E_{corr} monitoring, also i_{corr} values showed stabilization of the electrochemical response after the third day of immersion in the alkaline solution.

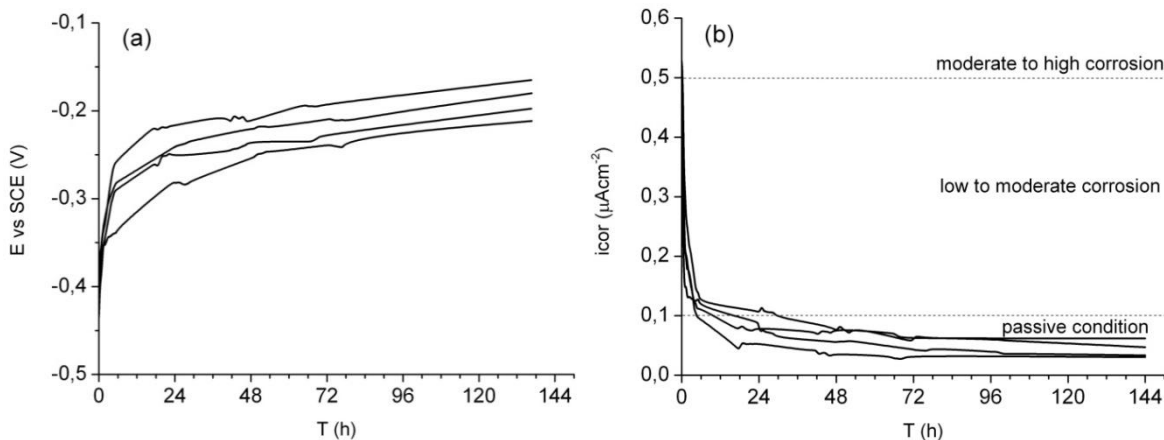


Fig. 3.14: Corrosion potential (a) and corrosion current (b) monitoring along six days of immersion of a polished surface of B450C steel, in a saturated $\text{Ca}(\text{OH})_2$ solution (pH 12.6).

EIS measurements

Further confirmation of the results discussed above comes from EIS measurements, whose Nyquist plots are reported in Figure 3.15 together with the two equivalent electric circuits used for fitting experimental data. Once again, major differences in the electrochemical response were detected during the first hours of immersion. The Nyquist plot of the polished surface (t_0) resulted to be an almost perfect semicircle. While the overall resistance of the system increased over time, the semicircle became increasingly wider and less defined.

Except for the case of the measurement performed on the just immersed specimens, the presence of two time constants was observed for all other impedance spectra. In the former case, EIS data were fitted using an equivalent electric circuit constituted by solution resistance (R_s) followed by a parallel RC circuit (Figure 3.15(a)). In all other cases, a circuit with two hierarchical parallel RC loop in series with the electrolyte resistance was used for the fitting (Fig. 3.15(b)) [21,29,32-34].

The non-ideality of the metallic surface, clearly indicated by the depression of the semicircles, was considered by substituting pure capacitances with constant phase

elements (CPE), so that the impedance $Z(\omega)$, at the angular frequency ω , was given by equations 9 and 10 for the circuits of Fig. 3.15(a) and 3.15(b), respectively.

$$Z(\omega) = R_s + \frac{R_1}{1+(j\omega R_1 C_1)^{\alpha_1}} \quad (9)$$

$$Z(\omega) = R_s + \frac{R_1}{\frac{1}{1+(Z_2(\omega)/R_1)} + (j\omega R_1 C_1)^{\alpha_1}} \quad (10)$$

$$\text{being } Z_2(\omega) = \frac{R_2}{1+(j\omega R_2 C_2)^{\alpha_2}}$$

α_1 and α_2 are the parameters that tunes the properties of the CPE, having the value of 1 for an ideal capacitor and 0.5 for a Warburg component; intermediate values are generally attributed to inhomogeneities due to the roughness of the metallic surface [35].

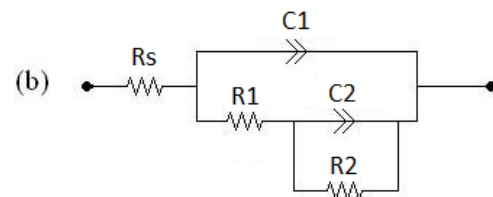
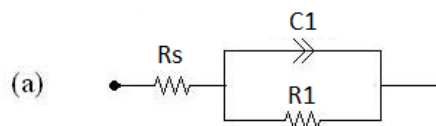
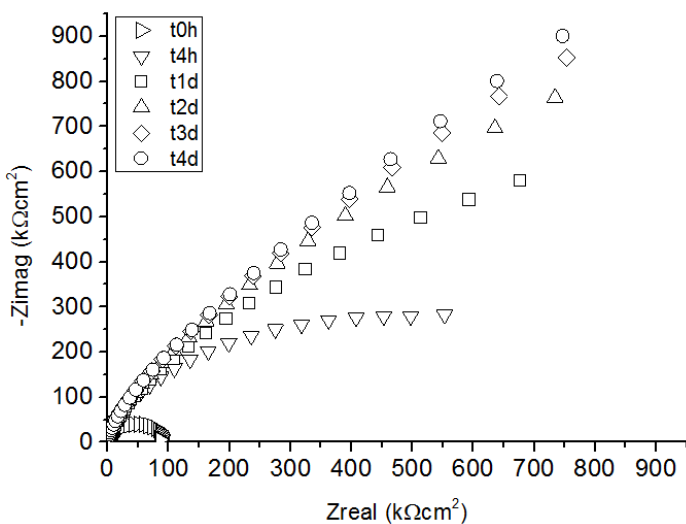


Fig.3.15: EIS Nyquist plots, registered at different time, of B450C steel immersed in a saturated $\text{Ca}(\text{OH})_2$ solution (pH 12.6). On the right: equivalent circuits used for fitting the impedance data, circuit (a) used for the just immersed sample, circuit (b) is used for all the other times.

According to the literature [21,32-34], R_s is generally attributed to the electrolyte resistance, while the high frequency time constant R_1CPE_1 is associated with the charge transfer resistance and double layer capacitance at the metal/electrolyte interface. The low frequency time constant R_2CPE_2 is attributed to redox processes occurring in the passive film. Values of such parameters are reported in Table 2, as calculated from fitting of the experimental data.

Table 3.2: Best fitting parameters for the EIS data.

time	R_s Ωcm^2	R_1 $k\Omega cm^2$	R_2 $k\Omega cm^2$	CPE_1 $\mu F s^{(1-\alpha)} cm^{-2}$	α_1	CPE_2 $\mu F s^{(1-\alpha)} cm^{-2}$	α_2
t=0	44.9	34.5	/	49.4	0.9	/	/
t=4h	44.4	52.0	381.2	27.2	0.9	14.7	0.4
t=1d	46.1	53.4	1196.4	24.3	0.9	14.3	0.5
t=2d	50.4	64.9	1832.8	23.1	0.9	14.3	0.5
t=3d	51.7	64.5	3177.8	22.1	0.9	13.5	0.5
t=4d	53.5	68.1	4580.5	21.7	0.9	13.8	0.5

It is important to stress that the values of α_1 , all around 0.9, confirm the capacitive nature of CPE_1 . On the contrary, the values for the parameter α_2 are all close to 0.5, which makes interpretation of CPE_2 as a capacitance questionable. The α_2 values might be indeed related to a Warburg element indicating diffusion control through the oxide layer at the lower frequencies [29].

As expected, during the experimentation, the solution resistance showed some increase that may be attributed to carbonation of the solution, transforming the soluble $Ca(OH)_2$ into the insoluble $CaCO_3$, thus reducing the available amount of charge carrying species.

The evolution of charge transfer resistance (R_1) and double layer pseudocapacitance (CPE_1) are reported in Figure 3.16. R_1 increased according to an exponential trend, while CPE_1 decreased with a similar exponential decay, and settled at $22 \mu F s^{(1-\alpha)} cm^{-2}$, a typical value for passive steel, presumably indicating coverage of the whole surface by iron oxides [36]. Coherently with the literature [33] such trend turned out to be similar to that of the corrosion potential of Figure 3.14(a) reaching the steady state after about three days of immersion.

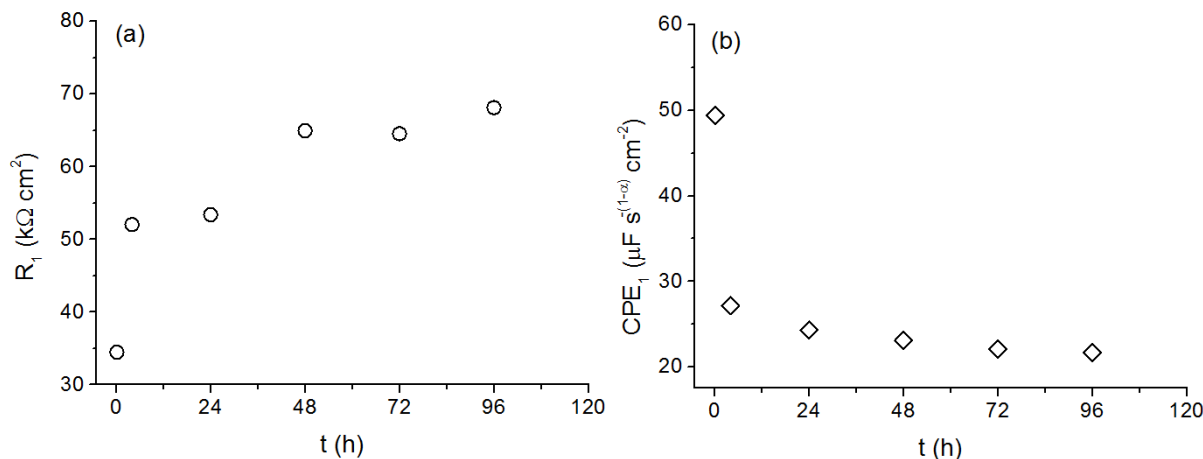


Fig 3.16: Representation of the R_1 and CPE_1 values, calculated from the fitting of experimental data, as a function of the immersion time.

The redox process occurring in the oxide layer, i.e., magnetite oxidation to Fe(III) oxo-hydroxides, as indicated by equations 7 and 8, has been associated with the RC loop observed at lower frequencies [37]. As above mentioned, such values should be considered with care because of the not completely capacitive nature of the element CPE_2 . However, differently from the literature [21,33], in the present case the plot of R_2 and CPE_2 as a function of the immersion time follows a linear instead of an exponential trend, likewise the case of R_1CPE_1 . Such differences could be attributed to the different electrolyte used in the cited studies. However, the increasing trend of R_2 and the decreasing one of CPE_2 , both concurred in indicating the significant co-participation of the gelatinous FeOOH outer layer to the passivation of the metallic surface.

3.4 Conclusions

Cyclic voltammetry proved to be a valid tool for investigating the electrochemical process occurring on a mild steel surface immersed in an alkaline solution, allowing an easy detection of the double steps, involving Fe(II) and Fe(III) transformations, leading to the formation of a protective oxide layer. The electrochemical response of the mild steel, evaluated in saturated $\text{Ca}(\text{OH})_2$ solution, aiming to simulate the interstitial concrete pore solution, resulted to be comparable with those reported in the literature, about iron passivity in the more alkaline solution of NaOH and KOH, the main difference being a significant decrease in current densities for the Ca^{2+} containing solution. As reported in literature [16,28] metallic cations such as those of Ca, Mg, and Ba can accelerate the passivation process. By changing experimental parameters, such as the scanned potential windows or the preconditioning of the metallic surface, significant variations were detected, especially in the position and intensity of the current peaks related to the Fe(II) / Fe(III) transition, being such reaction the most relevant in the protective layer growing

process as indicated by the continuous increase of the current of the correlated peaks with cycling.

Anodic polarization performed at different passivation times indicated that a naturally grown oxide layer significantly affects the electrochemical response of the metal surface by hindering the charge transfer mechanism, which results in lower current as the thickness of the oxide layer increases.

The stabilization of the electrochemical response of the oxide film, being attributed to the growth of a passive layer that, in term of thickness, structure and protective performance, may be comparable to that forming naturally as steel is embedded in concrete, was monitored with time. Three days of immersion in a saturated $\text{Ca}(\text{OH})_2$ solution turned out to be the minimum time required for a realistic simulation of a stable passive film.

References

- [1] American concrete institute. Committee 222, Corrosion of metal in concrete 81 (1985) 3-32.
- [2] J.P. Broomfield, Corrosion of steel in concrete: understanding, investigation and repair, Architecture price book, London 2007.
- [3] M. El-Reedy, Steel reinforced concrete structure, assessment and repair of corrosion, CRC press 2008.
- [4] B. Huet, V. L'Hostis, F. Miserque, H. Idrissi, Electrochemical behavior of mild steel in concrete: influence of pH and carbonate content of concrete pore solution, *Electrochim. Acta* 51 (2005) 172-180.
- [5] M. Moreno, W. Morris, M.G. Alvarez, G.S. Duffo, Corrosion of reinforcing steel in simulated concrete pore solutions, effect of carbonation and chloride content, *Corrosion Science* 46 (2004) 2681-2699.
- [6] J.T. Hinatsu, W.F Graydon, F.R Foulkes, Voltammetric behavior of iron in cement. Development of a standard procedure for measuring voltammograms, *J.App. Electrochem.* 19 (1988) 868-876.
- [7] M. Saremi, E. Mahallati, A study of chloride-induced depassivation of mild steel in simulated concrete pore solution, *Cement and Concrete research* 32 (2002) 1915-1921.
- [8] S. Alvarez, A. Bautista, F. Velasco, Corrosion behavior of corrugated lean duplex stainless steels in simulated concrete pore solutions, *Corrosion Science* 53 (2011) 1784-1755.
- [9] H. Yu, K. Chiang, L. Yang, Threshold chloride level and characteristics of reinforcement corrosion initiation in simulated concrete pore solutions, *Constr. Build. Mat.* 26 (2012) 723-729.
- [10] L. Veleva, M. Aviles, D. Wipf, Voltammetry and surface analysis of AISI 316 stainless steel in chloride containing simulated concrete pore environment, *J. Electroanal. Chem.* 578 (2005) 45-53.
- [11] I.V. Sieber, H. Hildebrand, S. Virtanen, P. Schmuki, Investigations on the passivity of iron in borate and phosphate buffers, pH 8.4, *Corrosion Science* 48 (2006) 3472-3488.
- [12] I. Diez-Perez, F. Sanz, P. Gorostiza, Electronic barriers in the iron oxide film govern its passivity and redox behavior: Effect of electrode potential and solution pH, *Corrosion Science* 48 (2006) 1595-1602.

- [13] P. Meisterjahn, J.W. Schultze, B. Siemensmeyer, U. Stimming, M.H. Dean, Electron transfer reactions on passive iron electrodes, *Chemical Physics*, 141, Issue 1 (1990) 131-141.
- [14] D. Geana, A. El Miligy, W. Lorenz, Electrochemical behavior of iron in alkaline sulphate solutions, *J. Appl. Electrochem.* 4 (1974) 337-345.
- [15] R. Schrebler Guzman, J. Vilche, A. Arvia, The potentiodynamic behavior of iron in alkaline solutions, *Electrochim. Acta* 24 (1978) 395-403.
- [16] O. Albani, J. Zerbino, J. Vilche, J. Arvia, A comparative electrochemical and ellipsometric study of iron electrodes in different alkaline electrolytes, *Electrochim. Acta* 31 n°11 (1986) 1403-1411.
- [17] R. Schrebler Guzman, J. Vilche, A. Arvia, The voltammetric detection of intermediate electrochemical processes related to iron in alkaline aqueous solutions, *J. Appl. Electrochem.* 11 (1981) 551-562.
- [18] L. Ojefors, SEM studies of discharge products from alkaline iron electrodes, *J. Electrochem. Soc.* 123 N° 11 (1976) 1691-1695.
- [19] G. Kalaignan, V. Muralidharan, K. Vasu, Triangular potential sweep voltammetric study of porous iron electrodes in alkali solutions, *J. Appl. Electrochem.* 17 (1987) 1083-1092.
- [20] M. Sanchez - Moreno, H. Takenouti, J.J. Garcia-Jareno, F. Vicente, C. Alonso, A theoretical approach of impedance spectroscopy during the passivation of steel in alkaline media, *Electrochim. Acta* 54 (2009) 7222-7226.
- [21] L. Freire, X.R. Novoa, M.F. Montemor, M. Carmezim, Study of passive film formed on mild steel in alkaline media by the application of anodic potentials, *Mat.Chem.Phys.* 114 (2009) 962-972.
- [22] C.M. Shepherd, S. Schuldiner, Potentiostatic Current-Potential Measurements on Iron and Platinum Electrodes in High-Purity Closed Alkaline Systems *J. Electrochem. Soc.* 1968 115(11): 1124-1130.
- [23] A. Poursaei, C. Hansson, Reinforcing steel passivation in mortar and pore solution, *Cement and Concrete Research* 37 (2007) 1127-1133.
- [24] G.F. Vander Voort, *Metallography, Principles and Practice*, ASM International, 1984.
- [25] P. Simon, M. Economopoulos, P. Nilles, Tempcore, an economical process for the production of high quality rebars; *MPT*, No. 3 (1984) 80-93.
- [26] J.F. NovilleTEMPCORE®, the most convenient process to produce low cost high strength rebars from 8 to 75 mm, *ESTAD 2015*, Dusseldorf.

- [27] C. Andrade, C. Alonso, Corrosion rate monitoring in the laboratory and on site, *Const. Build. Mat.* 10 No5 (1996) 315-328.
- [28] S. Volosova, Z. Iofa, T. Stepina, Russ, Effect of direction of grain on magnetic properties of silicon sheet steel, *J. Electrochem.* 13 (1977) 393-396.
- [29] M. Sanchez, J. Gregori, M. Alonso, J. Garcia-Jareno, F. Vicente, Anodic growth of passive layer on steel rebars in alkaline medium simulating the concrete pores, *Electrochim. Acta*, 52 (2006) 47-53.
- [30] A.J Calandra, N.R. De Tacconi, A.J. Arvia, Ageing and dissolution processes affecting the electroreduction of monomolecular oxide films formed on platinum electrodes in molten sodium bisulphate-potassium bisulphate melts, *J. Electroanal. Chem.* 49 (1974) 145-148.
- [31] C.M. Ferro, A.J Calandra, A.J. Arvia, The formation and dissolution of an electrochemical oxide film of up to a monolayer thickness on gold, *J. Electroanal. Chem.* 50 (1974) 403-407.
- [32] S. Joiret, M. Keddam, X.R. Novoa, M.C. Perez, C.M. Rangel, H. Takenouti, Use of EIS, ring disk electrode, EQCM and Raman spectroscopy to study the film of oxides formed on iron in 1M NaOH, *Cem. Concr. Comp.* 24 (2002) 7-15.
- [33] M. Sanchez, J. Gregori, M. Alonso, J. Garcia-Jareno, H. Takenouti, F. Vicente, Electrochemical impedance spectroscopy for studying passive layer on steel rebars immersed in alkaline solution simulating concrete pores, *Electrochim. Acta*, 52 (2007) 7634-7641.
- [34] C. Andrade, M. Keddam, X.R. Novoa, M.C. Perez, C.M. Rangel, H. Takenouti, Electrochemical behavior of steel rebars in concrete: influence of environmental factors and cement chemistry, *Electrochim. Acta*, 46 (2001) 3905-3912.
- [35] U. Retter, A. Widman, K. Siegler, H. Kahlert, On the impedance of potassium nickel(II) hexacyanoferrate(II) composite electrodes - the generalization of the Randles model referring to inhomogeneous electrode materials, *J. Electroanal. Chem.* 546 (2003) 87-96.
- [36] G. Glass, C. Page, N. Short, J. Zhang, The analysis of potentiostatic transients applied to the corrosion of steel in concrete, *Corr. Sci.* N°9 39 (1997) 1657-663.
- [37] C. Andrade, P. Merino, X. Novoa, M. Perez, L. Soler, Passivation of reinforcing steel in concrete, *Mater.Sci. Forum* 891 (1995) 192-194.

Chapter 4:

Reinforcing bars

corrosion in solutions

simulating

bacteria metabolites

Microbial induced deterioration of reinforced concrete structures is generally attributed to bacteria involved into the sulfur cycle, that is Sulfate Reducing Bacteria and Sulfur Oxidizing Bacteria. The aim of the present work is to investigate the effects of solutions simulating their metabolic products on the corrosion of steel reinforcing bars. A simplified system was initially studied, consisting in metallic samples passivated in an alkaline medium and subsequently immersed in solutions containing Na_2S and H_2SO_4 aiming to simulate the bacteria metabolites. Afterwards, carbonated reinforced mortar samples were produced and tested in similar solutions aiming to mimic a system more closer to the reality. Corrosion monitoring was performed through several electrochemical measurements such as corrosion potential monitoring, linear polarization resistance, electrochemical impedance spectroscopy and anodic polarizations.

4.1 Introduction

Reinforced concrete deterioration due to corrosion of steel bars is recognized as a serious problem, affecting the durability of several type of civil structures. Many efforts have been dedicated to study the depassivation induced by chloride penetration[1-3], being by far the most frequent cause of the steel corrosion in reinforced concrete structures exposed to marine environment or in contact with deicing salts. Much less attentions have been focused on the microbial degradation of reinforced concrete structures although being a serious issue strongly affecting the service life of sewer pipes, waste water treatment plants, animal housing and manure storage structures. As already detailed in Chapter 2, section 2.3, the microbial deterioration of reinforced concrete structures is commonly attributed to bacteria involved in the sulfur cycle, in particular Sulfate Reducing Bacteria (SRB) and Sulfur Oxidizing Bacteria (SOB), being respectively H_2S and H_2SO_4 their metabolic products [4,5].

Clear evidences of the detrimental effects of the SOB activity on the cementitious matrix were thoroughly demonstrated by De Belie et al. [6 - 9], while how the bacteria metabolites affect the behaviour of the steel reinforcing bars (rebars) seems to be a neglected issue; just a few papers mentioned it [10,11], and to the author knowledge no detailed studies were performed on such topic.

For this reason, the aim of the present study is to simulate the metabolic products of SRB and SOB using respectively solutions of Na_2S and H_2SO_4 and to investigate how they interact with mild steel used for reinforced concrete structures.

The preparation of representative reinforced mortar samples is very complex and time consuming, which does not allow multivariable study. For this reason, the initial use of simulated concrete pore solution turns out to be the most convenient option. Once understood the deterioration mechanism in such simplified systems, the investigation was extended to steel bars embedded in carbonated mortar.

H_2S induced steel corrosion, has been thoroughly investigated [12-16] as an extremely dangerous deterioration source in steel pipes for the oil and gas industry. In such case, it is very often associated with CO_2 or in acidic environments. Much less literature seems to be available on sulfide induced corrosion of mild steel occurring at alkaline pH; early in the 80's Shoesmith et al. [17,18] and Salvarezza et al.[19,20] published some researches on the growth/precipitation mechanisms of iron sulphides and the resulting onset of localized corrosion. However the above cited literature was only performed at extremely alkaline pH such as 12-14, while no information were found about lower pH such as those of carbonated concrete.

4.2 Experimental

4.2.1 Materials and testing environment

All the chemical reagents used for the preparation of simulating solutions were purchased from Sigma-Aldrich as ACS reagent grade. A saturated Ca(OH)₂ solution (pH12.6), filtered prior use, was used for the prepassivation of steel samples, while sodium carbonate- bicarbonate buffer allowed to simulate two different carbonation degrees, at pH 9.2 and 10.2 (as a function of their molar ratio). Sulfides were introduced at different concentrations as Na₂S 9H₂O. Diluted H₂SO₄ solutions were used as model media, aiming to simulate the concrete acidification due to SOB metabolites.

Metallic coupons

Steel samples for electrochemical measurements were prepared from B450C reinforcing bars (composition in table 4.1) according to the procedures already described in Chapter 3 section 3.2.1.

Table 4.1: Chemical composition (w%) of B450C mild steel.

STEEL	C	Cr	Ni	Mn	Mo	N	Si	Cu	S	P
B450C	0.22	0.13	0.15	0.78	0.03	0.007	0.24	0.56	0.039	0.013

Additionally, specific samples for weight loss measurements were produced by cutting specimen of 45mm length; the two extremities were then protected with Novolac epoxy coating leaving an exposed length of 30mm. A Teflon loop was added at one extremity as hanging support (Fig. 4.1)



Fig.4.1: Steel sample for weigh loss measurements.

Reinforced mortar samples

Reinforced mortar prisms of dimensions 40x40x140 mm were produced according to the Norm EN196-1 with a water/binder ratio of 0.5 and using limestone

cement type CEM II - B -LL 32.5 (Colacem, Caravate (VA) Italy). Each sample had an embedded steel reinforcing bar whose length was 155mm and having both the extremities protected with epoxy resin and thermal shrinkable sheaths, as to leave an exposed length of 110mm. 24 hours after casting, samples were demoulded and cured for 28 days at 30°C and 95% relative humidity. Square faces of the prism were covered with epoxy resin thus leaving only the transversal direction for penetration of liquids and gases (Fig. 4.2). The complete carbonation of the mortar samples was achieved by keeping them for one month in a carbonation chamber saturated with CO₂ and with a controlled humidity set to the value of 60%. The electrical connection was realized by longitudinally drilling a hole into one extremity of the bar and by soldering a copper wire in it; the electrical junction was then protected with an epoxy coating.

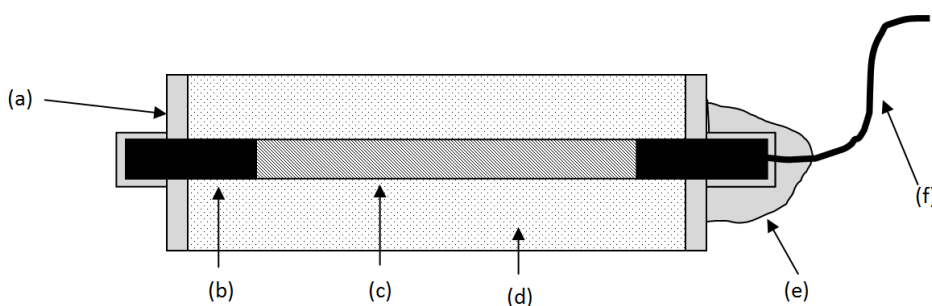


Fig. 4.2: Schematic representation o a reinforced mortar sample: (a) epoxy coating, (b) insulating sheath, (c) exposed length, (d) mortar paste, (e) epoxy protection of the electric connection, (f) copper wire.

4.2.2 Testing and electrochemical monitoring

Steel samples in simulated solutions

Immersion tests were performed according to the recommendation of ASTM G31-72 standard, by completely immersing the steel samples into 200 ml of the testing solutions for 10 days at 30°C. Samples were tested into solutions simulating two different carbonation degrees with Na₂S ranging from 0 to 10mM, and in diluted sulfuric acid solutions (from 0.01% to 5%). After the conditioning period, pictures of the surfaces were shot with a Nikon D5000 DSLR camera. Corrosion products were subsequently removed using a di-ammoniumcitrate solution as in ASTM G1-03, and further images were taken by means of a microscope (Wide Heerbrugg M 400). Weight loss, reported as a percentage of initial weight, were averaged among 3 replicates per each exposure condition.

Metallic samples, after three day of passivation in Ca(OH)₂ sat were transferred into the testing solutions containing different concentration of aggressive species. The corrosion susceptibility was investigated by performing long term Open Circuit

Potential measurements (OCP) as well as cyclic anodic polarizations ($v = 0.1667$ mV/s). All the electrochemical measurements were performed using a standard three electrode configuration cell, in which the active steel surface acted as working electrode, a Pt wire as a counter electrode, and a saturated calomel electrode (SCE) was used as a reference electrode. Several repetitions of each experiments were done in order to check the reproducibility of the results.

Reinforced mortar samples

Reinforced mortar samples were placed into three different plastic vessel (five replicates per vessels) and partially immersed into three different solutions: carbonate/bicarbonate buffer (pH 9.2) as reference system, carbonate/bicarbonate buffer containing 2mM of Na_2S , and diluted sulfuric acid (1%). The solutions were weekly refreshed. The corrosion monitoring was performed by measuring the OCP (daily), the linear polarization resistance (weekly), and by recording EIS spectra (every two weeks). Polarization resistances were determined from the slopes calculated in a small interval around the corrosion potential of anodic linear polarizations. The ohmic drop, occurring through the mortar cover thickness, was automatically calculated and subtracted from the measured values by the potentiostat through the current interrupt method. The corrosion currents were calculated using the Stern-Geary equation (Tafel parameter: 26 mV/dec). EIS measurements were obtained with a Gamry potentiostat between the frequency range of 10^6 and 2×10^{-3} Hz, taking ten point per decade. The modulation amplitude of potential was 10mV rms. A specific probe described in Chapter 1, section 1.2.2, was ad hoc designed and developed in order to perform the above described electrochemical monitoring.

At the end of the conditioning period cementitious matrix samples were collected by grinding the superficial layer of the mortar prism and characterized by means of XRD. X-Ray powder diffraction (XRPD) patterns were recorded on a Philips PW3020 powder diffractometer, by using the $\text{Cu-K}\alpha$ radiation ($\lambda = 1.54056\text{\AA}$) in a 2θ range from 10 to 80° (0.02° steps, 1s counting).

4.3 Results and Discussion

4.3.1 Steel samples in model solution

Weight loss measurements

A preliminary, although extremely effective screening, in order to assess the aggressiveness of testing solutions on B450C mild steel was performed by means of immersion tests. Results are reported in fig. 4.3. At a first glance, it is immediately noticeable that the aggressiveness of the acidic environment is much more higher with respect to that of sulfides in an alkaline medium, being characterized by a weight

loss of about thirty times higher. Furthermore, as expected, in sulfuric acid solutions the weight loss increased by increasing the concentration of the aggressive species. Such a trend was also confirmed by the pictures shown in fig. 4.4

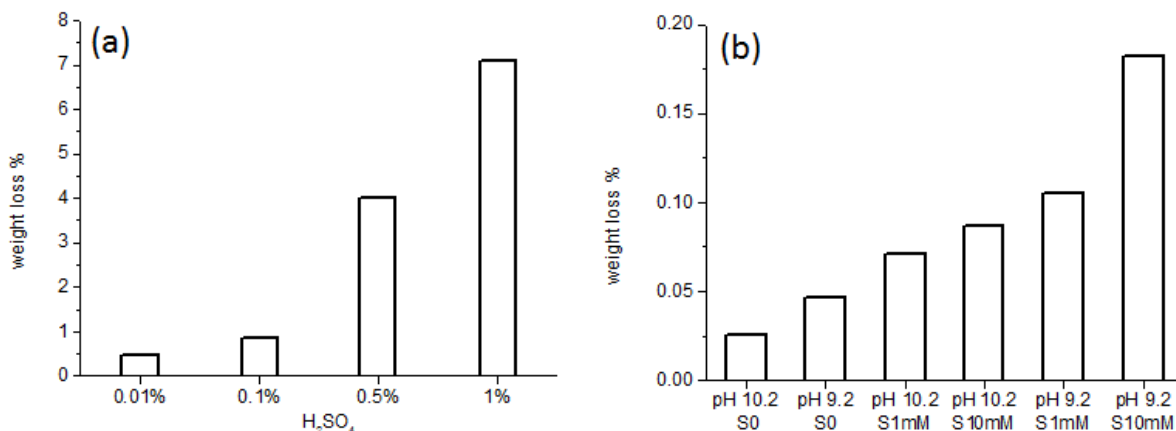


Fig. 4.3: Average weight loss from immersion test. (a) diluted sulfuric acid with concentration ranging from 0.01% to 1%. (b) Carbonate/ bicarbonate buffers (pH 10.2 and 9.2) with Na_2S concentration ranging from 0 to 10 mM.

It is well known that sulfuric acid leads to the generalized corrosion of mild steel, the extent of the damage being proportional to the concentration of the aggressive species. Actually, in the case of the two lower concentrations (Fig. 4.4(a,b)) steel surfaces resulted to be covered by reddish corrosion products, being such a layer thicker and denser for H_2SO_4 0.1% than 0.01%. Upon removal of the corrosion products according to ASTM G1-03, the surface exposed to the lower concentration, although corroded, still showed an homogeneous pattern, while in the case of 0.1% concentration , spots can be easily observed where the corrosion attack led to more deep defects.

Less differences were detected in the case of the higher sulfuric acid concentration (Fig. 4.4(c,d)): for such samples the conditioning environment resulted to be so aggressive that the corrosion products layer was easily dissolved leaving exposed a significantly damaged surface.

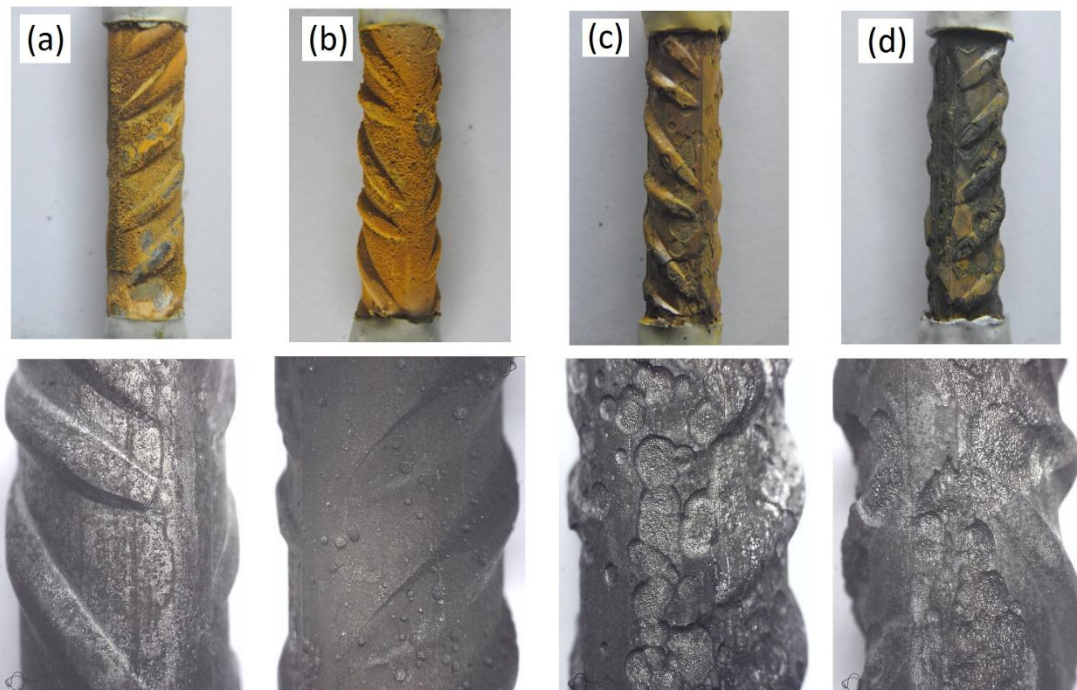


Fig.4.4: Pictures of the metallic surfaces after the in immersion test in diluted sulfuric acid solutions at different concentrations. (a) 0.01% (b) 0.1% (c) 0.5% (d) 1%.

The weigh loss of steel samples conditioned in the carbonate/bicarbonate buffer, in the presence of sulfides (Fig.4.3(b)) also showed a certain trend in the values, pointing out that both the solution pH and the sulfides concentration seems to play a role in determining the weight loss. The lower weight loss was registered in the more alkaline solution without sulfides. At pH 10.2 steel should be still in a passive state thus justifying the low weight loss. Lowering the pH to the value of 9.2, thus approaching the active behavior of steel, a slightly higher weight loss was measured. Increasingly higher deteriorations were afterwards detected for both the more and to the less alkaline solutions by adding sulfides, in the latter case being however the weight loss more significant. Such a behavior could be related to the more efficient protection offered by the oxide layer at the more alkaline pH.

Pictures of the steel surfaces after the conditioning in carbonate-bicarbonate solutions are reported in fig. 4.5 and fig. 4.6 for pH 9.2 and 10.2, respectively. In such cases the after-cleaning microscope images (bottom rows) did not have magnification enough to appreciate significant differences. However, for both the pH an increase in the surface roughness due to the sulfide induced corrosion was detected passing from the almost unaffected control cases to those with Na_2S 10mM.

The pre-cleaning pictures (upper rows) showed clean, as immersed steel surface for both the pH in the absence of sulfides. Hardly detectable deposits of corrosion

products were obtained with 1mM sulfide solution at pH 10.2, while the same concentration in the less alkaline pH led to a clearly visible thin layer of yellowish corrosion products. Finally, by increasing ten times the sulfides concentrations a black deposits was observed on the steel surfaces for both the pH.

In the case of the more alkaline pH (fig.4.5(c)) the black deposit was thin and blister-like, while a thicker, with powdery consistency layer, was obtained in the case of the less alkaline pH.

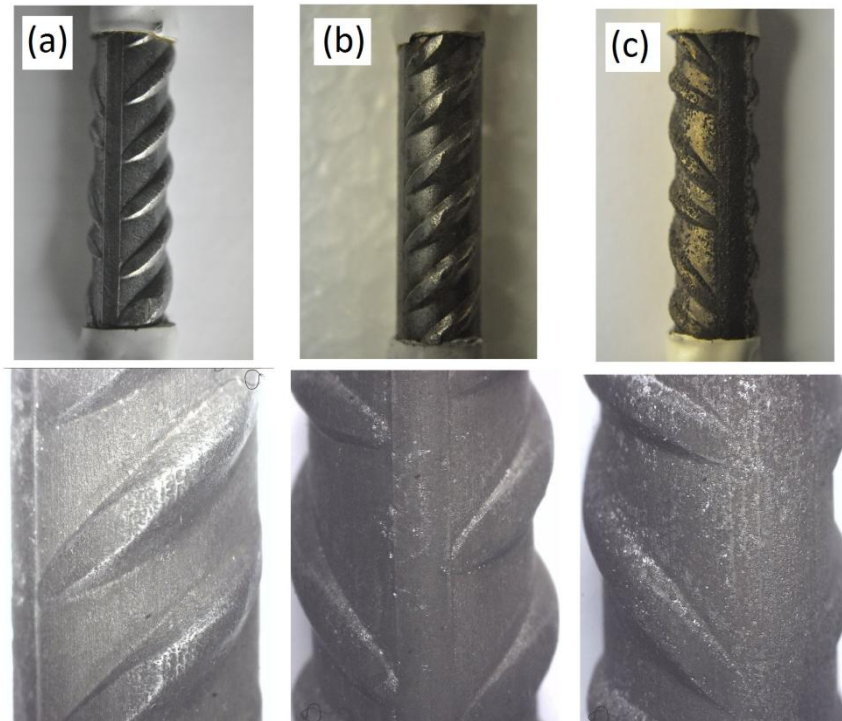


Fig. 4.5: Pictures of the metallic surfaces after the in immersion test in the carbonate bicarbonate buffer solution (pH 10.2) with different sulfides concentrations. (a) no sulfides (b) 1mM (c) 10mM.

The above presented results pointed out that sulfides are potentially aggressive species for mild steel, even in an alkaline environment, being the damage extent directly correlated with the solution pH, that is: a more alkaline environment, leading to a more stable a superficial oxide layer, results in reduced interactions between steel and sulfides. On the contrary, a less alkaline pH of the environment leads to an increased damage, clearly indicated by higher weight loss and visual observations.

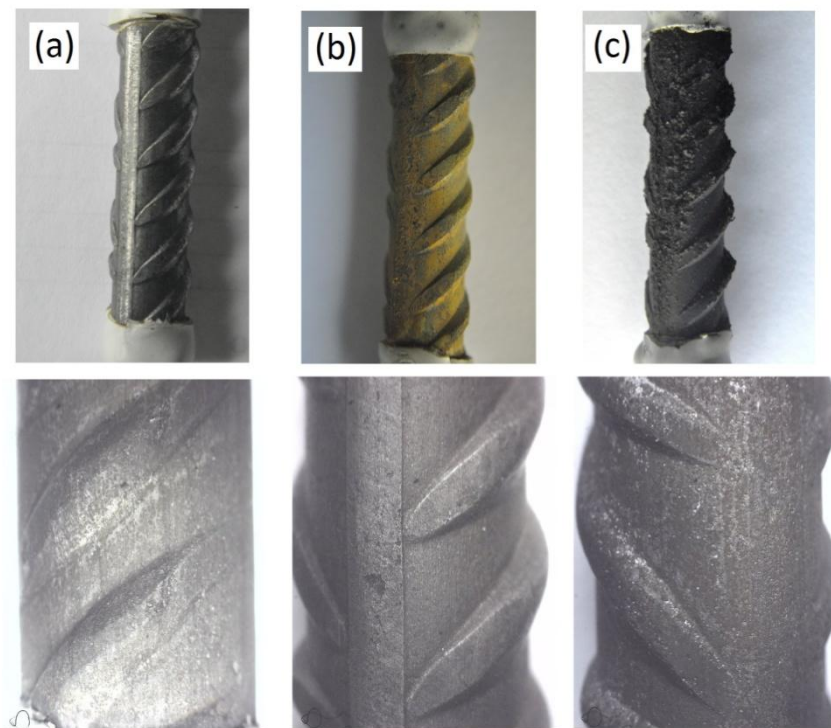


Fig. 4.6: Pictures of the metallic surfaces after the in immersion test in the carbonate bicarbonate buffer solution (pH 9.2) with different sulfides concentrations. (a) no sulfides (b) 1mM (c) 10mM.

Open circuit potential monitoring

From the electrochemical point of view the easier parameter to study in order to investigate how the surrounding environment affects the behavior of a steel sample is to monitor its open circuit potential.

After three days of prepassivation in saturated $\text{Ca}(\text{OH})_2$, according to the findings of Chapter 3, the steel samples were removed from the passivating media and conditioned for 4 days into the following solutions:

- Sodium carbonate/bicarbonate buffer pH 9.2, without sulfides
- Sodium carbonate/bicarbonate buffer pH 9.2, containing Na_2S 2 mM,
- Diluted H_2SO_4 solution at 1% wt.

Such solutions where chosen on the basis of the weight loss measurements above discussed, aiming to check the steel electrochemical response when exposed to severe aggression from the environment. Averaged values, resulting from the six replicates per each exposure condition, are reported in fig.4.7.

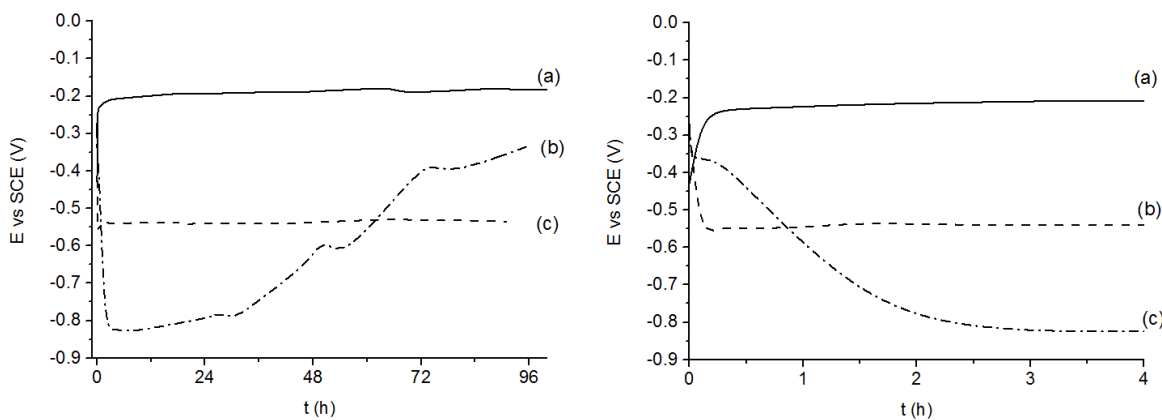


Fig. 4.7: Averaged open circuit potential monitoring of metallic samples immersed in (a) carbonate/bicarbonate buffer (pH 9.2) (b) carbonate/bicarbonate buffer and Na₂S 2mM (c) diluted sulfuric acid 1%. On the right side: details of the first hour of immersion.

All the initial values (≈ -0.350 V vs SCE) corresponded to the last measurement performed during the pre-passivation step; after moving the samples into the aggressive solutions, the OCP fast evolved and reached a constant value at the latest, for the sulphide containing solution, within 3 hours.

Steel samples conditioned in the carbonate/bicarbonate buffer, without sulfides, showed a clearly passive behavior: the potential increased as a consequence of the lower pH than the one of the passivating solution, and being the steel surface already coated by an oxide layer, the steady state was reached after 15 min only.

The steel response, when exposed to the sulfuric acid solution, was very fast as well, but differently from the previous case the corrosion potential dropped immediately to an active value (-0.550 V vs SCE) and maintained it till the end of the experiment thus confirming the uneffective protection of the passive layer when exposed to such an aggressive environment.

Finally, steel samples immersed in the sulfides containing solution exhibited an initial, dramatic drop of the corrosion potential, reaching extremely negative values, even lower than in the sulfuric acid case, and getting to stable state after 3 hours.

Such a drop in the E_{cor} values was attributed to the strongly reducing nature of sulfides ions that did not allow the growth of a passivating oxide film, and thus leading to corrosion processes in which the formation of a non protective iron sulfide deposit took place.

After some time (≈ 36 hours) the corrosion potential started to rise. This was likely due to the equilibrium reactions bringing from S²⁻ to H₂S that is volatile and leaves the solution thus mitigating the reducing environment generated by the sulfides. Actually, studies of sulfide thermodynamic equilibria, performed by Sun and al.[21] pointed out the natural tendency of aqueous sulfides to be transformed into gaseous H₂S.

In order to get a further confirmation that the pH rise was due to a sulfide depletion, after one week, when the OCP had almost reached its initial values, new sulfides were added to the solution. The resulting OCP fluctuation, reported in fig.4.8, confirmed that the potential drop was undoubtedly due to the sulfide availability within the testing media.

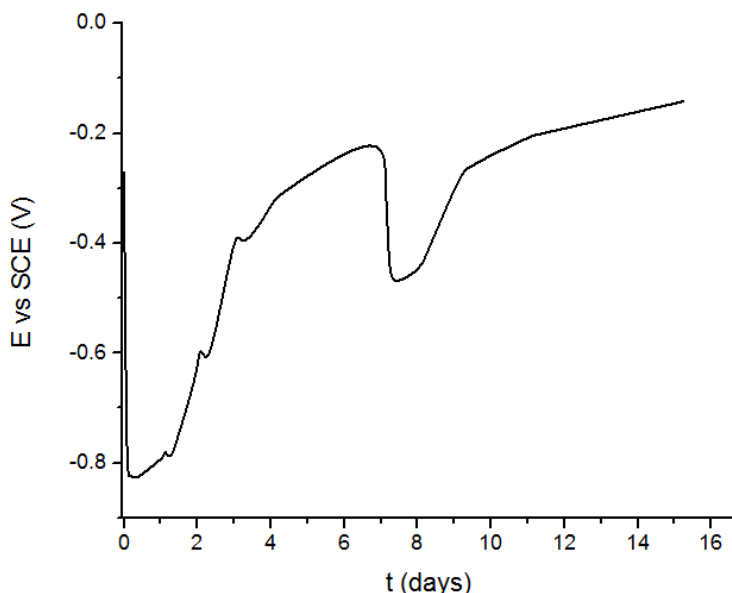


Fig. 4.8: OCP fluctuation for steel sample immersed into a carbonate/bicarbonate buffer (pH 9.2) sulfides were added to the solution on day 0 and day 7.

Discussions on the OCP monitoring results were confirmed by the observation of the steel surfaces at the end of the 4 days monitoring period by means of the optical microscopy; whose pictures are shown in fig.4.9.

The passive potential values of the carbonate/bicarbonate buffer was reflected in the absolutely smooth and unaffected surface of fig. 4.9(a), while sulfides led to the precipitation of a dense layer of corrosion products (fig. 4.9(b)). Heavy deterioration was finally observed for the steel immersed into the sulfuric acid solution(fig. 4.9(c)).

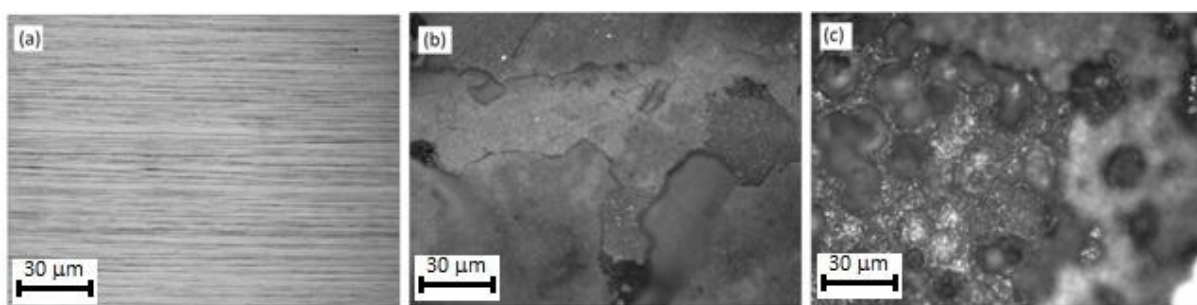


Fig. 4.9: Optical microscopy pictures of the steel surfaces after the 4 days of OCP monitoring. (a) carbonate/bicarbonate buffer (pH 9.2), (b) carbonate/bicarbonate buffer (pH 9.2) with sulfides 2mM, (c) H_2SO_4 1%.

Anodic potentiodynamic polarizations: sulfuric acid

As the OCP measurements for steel in the sulfuric acid solution showed an almost immediate drop to characteristic values of an active behavior, cyclic anodic potentiodynamic polarizations were performed on both the pre-passivated and the as polished steel surface in order to check eventual effects of the passive layer.

The resulting curves, reported in figure 4.10, being almost overlapped, confirmed that the oxide layer, grown during the passivation step, was easily dissolved during the 20 min of equilibration that precedes the polarization experiment. As expected, the steel response is that of an active material, that is undergoing to a corrosion process. By scanning the potential towards more anodic values, a continuous increase in current densities was obtained reflecting the steel dissolution in the aggressive media. Between potential values of -0.5V and -0.4V vs. SCE, the anodic curve raised as for a protective effect resulting from a corrosion product layer. However above such value the current density increased again until 0.01Acm^{-2} that was set as limiting current. Upon inversion of the potential scan, higher current densities with respect to the forward scans were recorded, producing an hysteresis: such behavior is typical of heavily corroded systems, and indicates that the steel is not able to recover the damage caused by the anodic scan.

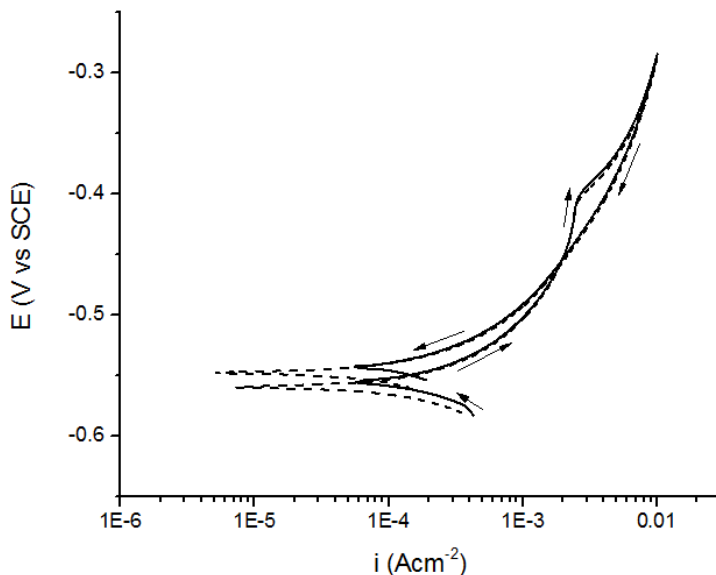


Fig. 4.10: Cyclic anodic potentiodynamic polarizations performed on B450C steel in 0.5% H_2SO_4 at a scan rate of 0.1667 mV/s. (—) Sample pre-passivated for 3 days in sat. $\text{Ca}(\text{OH})_2$. (—) Just polished steel surface.

In order to get more insight on the change in current density detected at -0.4V vs. SCE, the electrochemical response of an anodic potentiodynamic polarization for steel B450C was compared to that of FeB500HKN (Dutch steel for RC application).

As can be clearly observed from fig. 4.11, where the two curves are compared, although starting from the same corrosion potential the FeB500HKN steel showed a

continuous increase in the current density. The increased corrosion resistance of the B450C steel as compared to FeB500HKN, could be therefore attributed to some alloying elements such as Cr, Ni, Mo, that being present only in the former material, although in the very small percentages (0.13, 0.15 and 0.03, respectively) could contribute to the formation of a slightly protective corrosion products layer. The value of -0.4 V sc SCE could represent a breakdown potential for such partially protective layer, accordingly, more anodic potentials led to currents again close to that of FeB500HKN.

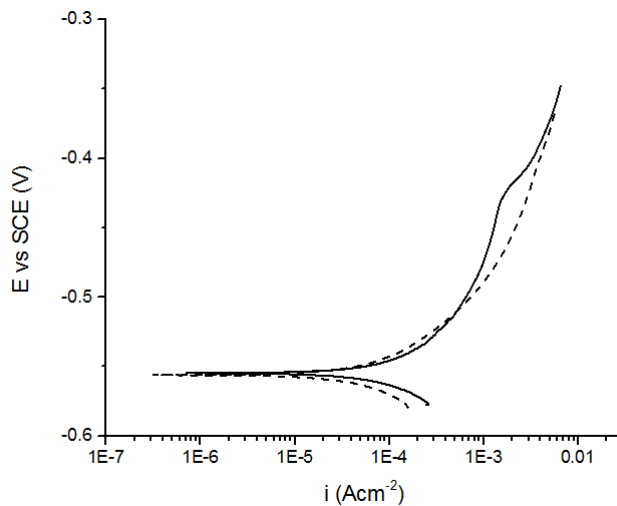


Fig. 4.11: Anodic potentiodynamic polarizations performed on B450C steel (—) and FeB500HKN steel (---) in 0.5% H_2SO_4 at a scan rate of 0.1667 mV/s.

A series of anodic polarizations were subsequently performed on B450 steel in H_2SO_4 solutions at different concentrations, ranging from 0.01% to 1%, with the aim to check the variations in the steel response as a function of the surrounding environment (Fig. 4.12)

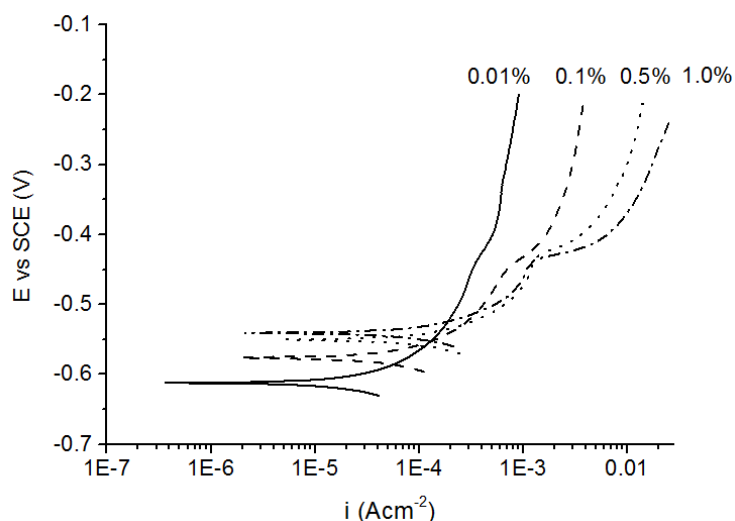


Fig. 4.12: Anodic potentiodynamic polarizations performed on B450C steel in H_2SO_4 at different concentrations ($v = 0.1667 \text{ mV/s}$).

As expected, and in fully agreement with weight loss measurements, the increase of the acid concentrations led to significantly higher current densities indicating a more intense steel dissolution. Furthermore it seems important to underline that all curves were characterized by an accelerated dissolution above -0.4 V SCE; the occurrence of such breakdown at the same potential in all the different cases confirmed its attribution to the formation of corrosion products becoming thermodynamically unstable above a certain potential value.

Optical microscopy pictures of the steel surfaces, were shot after the anodic polarizations and are reported in fig. 4.13. All the steel samples exhibited heavily deteriorated surfaces, the extent of the damage was found to be dependent on the sulfuric acid concentration.

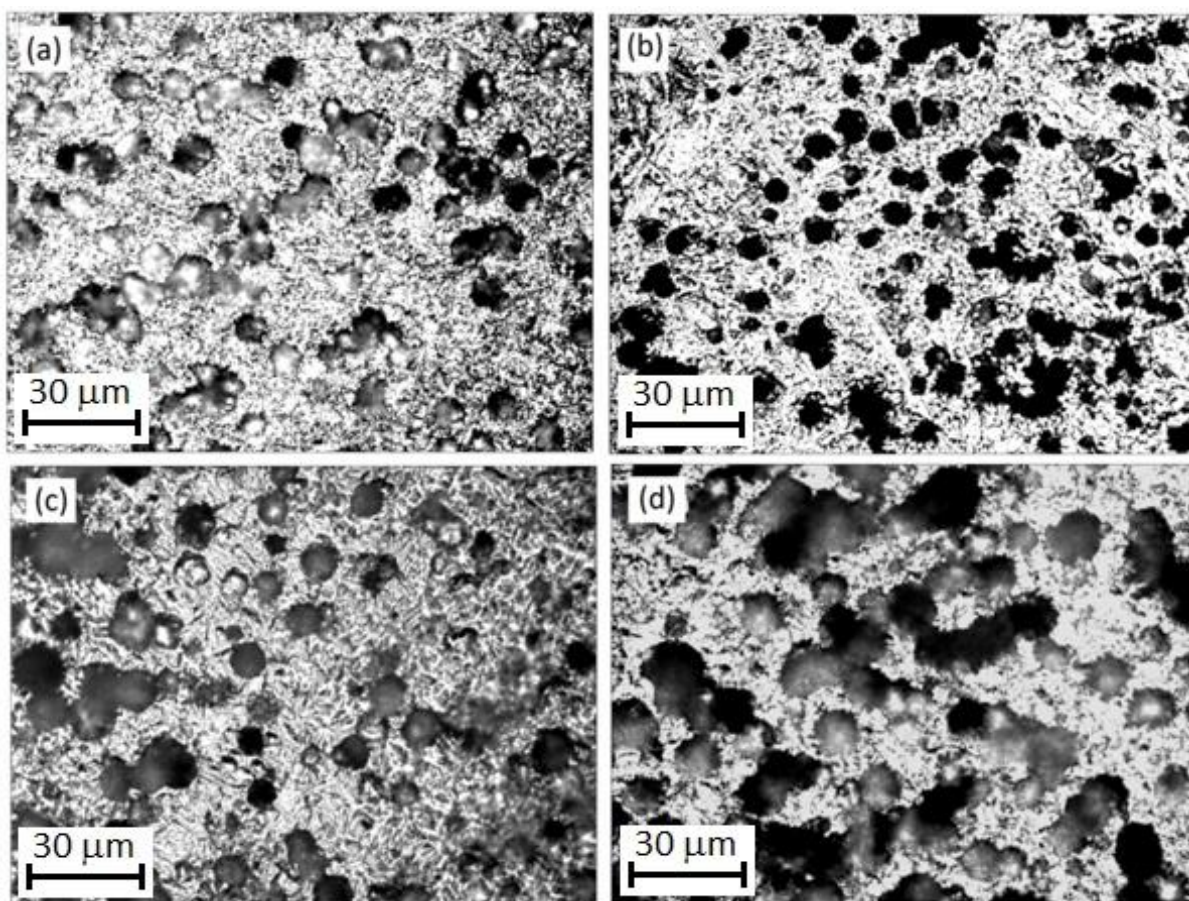


Fig. 4.13: Optical microscopy pictures of the steel surfaces after anodic polarizations. Magnification: 500X. (a) H_2SO_4 0.01% , (b) H_2SO_4 0.1%, (c) H_2SO_4 0.5%, (c) H_2SO_4 1%.

Anodic potentiodynamic polarizations: sulfides

The effects of sulfate reducing bacteria (SRB) metabolic products were investigated by means of cyclic anodic polarizations in sulfide containing carbonate/bicarbonate solutions (pH 10.2) and carried out on three days pre-passivated samples. The curves, reported in fig. 4.14, were characterized by the presence of a double inflection in the forward scan and by a single inflection in the backward direction, corresponding, in terms of potential, to the second one of the forward scan. Furthermore, it's important to notice that in all cases the current densities recorded in the forward direction were higher with respect to those of the backward scan.

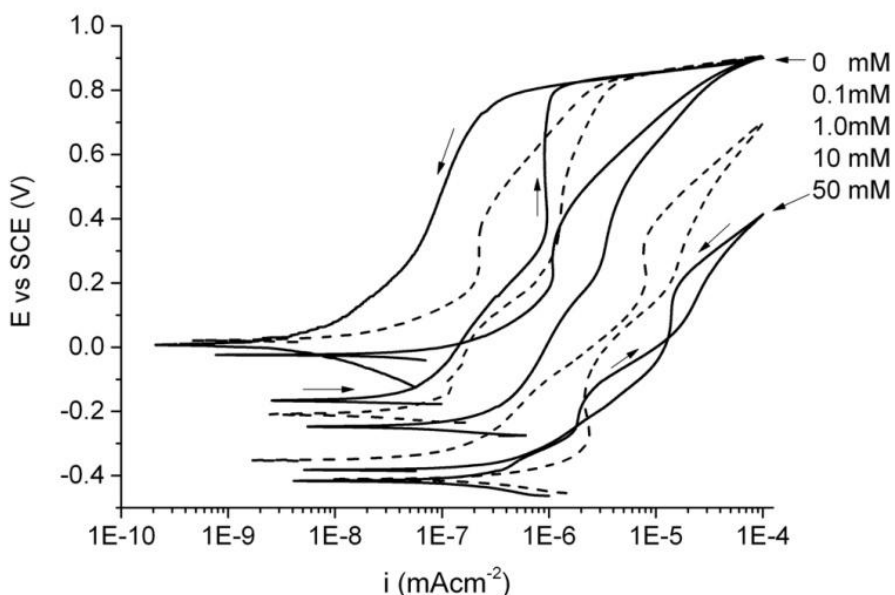


Fig. 4.14: Anodic polarizations of prepassivated samples in carbonate/bicarbonate (pH 10.2) buffer containing different sulfides concentrations.

The effect of the increasing sulfide concentration was to lower the corrosion potential and to cause an overall current increase; both these features are generally attributed to the onset of a corrosion phenomenon, but in the present case, as confirmed by optical microscopy analysis, the surfaces subjected to the anodic polarization did not show any sign of corrosion activity neither at the highest sulfide concentration of 50 mM (Fig.4.15). Moreover, this is coherent with the lower currents recorded during the backward scan. Actually, the breakdown of the passive layer should be indicated by the presence of an hysteresis once the current is reversed.

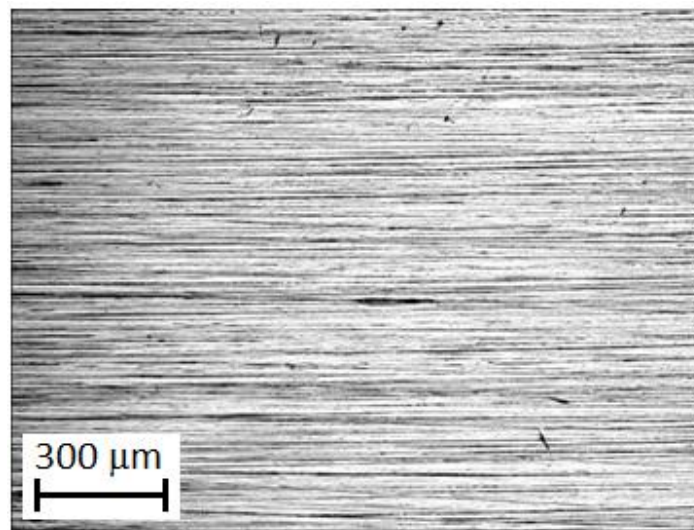


Fig. 4.15: Optical microscopy picture of the steel surface after anodic polarization in carbonate/bicarbonate (pH 10.2) containing Na_2S 50 mM. Magnification 50 X.

It was therefore supposed that such electrochemical response was not related to an interaction between steel and sulfides, leading a deterioration process, but to oxidation reactions to higher valence sulfur compounds. Literature seems to be rather controversial on this theme: Bolmer assigned the current increase to sulfide oxidation yielding to free sulfur or soluble polysulfide [22], Tromans attributed it to the electro-oxidation leading to tiosulfates [23]; conversely, Salvarezza et al. observed the breakdown of the passive layer and pits formation [20]. In the present case, supporting the hypothesis of sulfide electro-oxidations, the inflection potentials resulted to be correlated to the sulfide concentrations by a semilogarithmic function, similar to a Nernst-type relationship Fig(4.16).

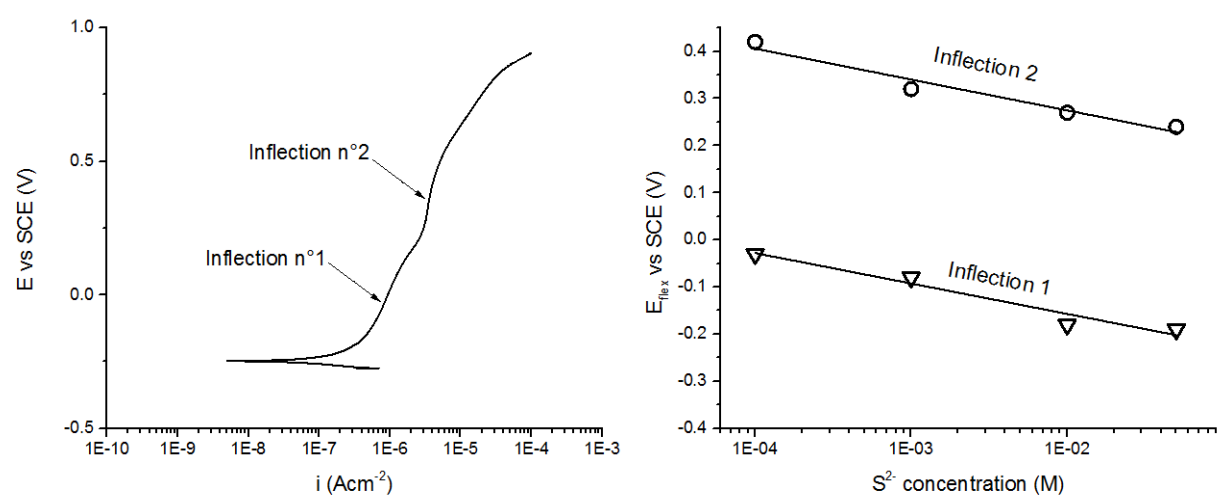


Fig. 4.16: Semilogarithmic relationship between the inflection points of the polarization curves and sulfides concentration.

Aiming to further confirm the above presented assumptions, a series of cyclic anodic polarizations were performed in the same alkaline, sulfide containing solution, but using an inert glassy carbon electrode instead of the active steel surface. Results are depicted in fig. 4.17.

As expected, without sulfides, the electrochemical response was that of a capacitive system, exhibiting low and almost constant current density until the oxygen evolution region, where a marked current increase was detected. The addition of 1 mM Na₂S, similarly to the steel case, led to a decrease of the starting potential and to an increase in current density. Furthermore, the double inflection points were detected in the forward scan, thus confirming the hypothesis of their attribution to sulfide oxidative reactions, instead of steel-sulfide interactions.

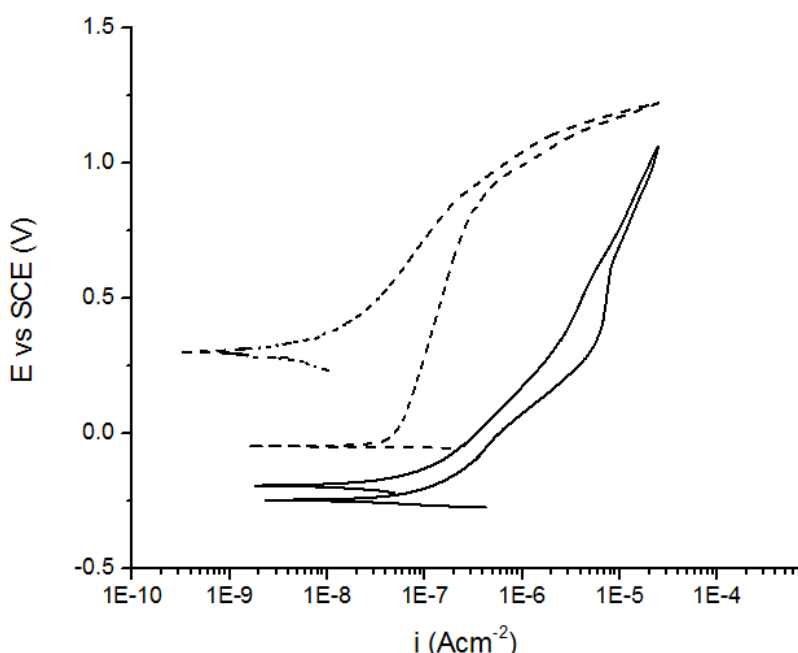


Fig. 4.17: Anodic potentiodynamic polarizations of a glassy carbon electrode in the carbonate/bicarbonate buffer (pH 10.2). (—) control case. (—) 1mM Na₂S.

Although the literature about the steel-sulfide interaction in alkaline environments is neither abundant nor focused on the concrete field [17-20], there is clear evidence of a competitive adsorption among S²⁻ and OH⁻. In the present case, steel-sulfide interactions are probably hindered by the pre-existing oxide layer growth during the pre-passivation stage.

Aiming to stimulate the onset of corrosion processes, the system was subsequently unbalanced toward the steel-sulfide interactions, by singularly acting on three different parameters:

- The pre-existing oxide layer growth during the pre-passivation stage.

- De-aerating the testing solution, thus reducing its oxidizing power.
- Testing the steel in a less alkaline environment

A comparison of the potentiodynamic curves obtained for the pre-passivated steel surface and the as polished sample is reported in fig. 4.18. Slightly lower corrosion potential and higher current density were obtained for the non-passivated steel surface, indicating a less hindered charge transfer in the absence of the stable oxide layer. However, similarly to the previous case, visual and microscopic observation of the steel surface did not show any corrosion attack.

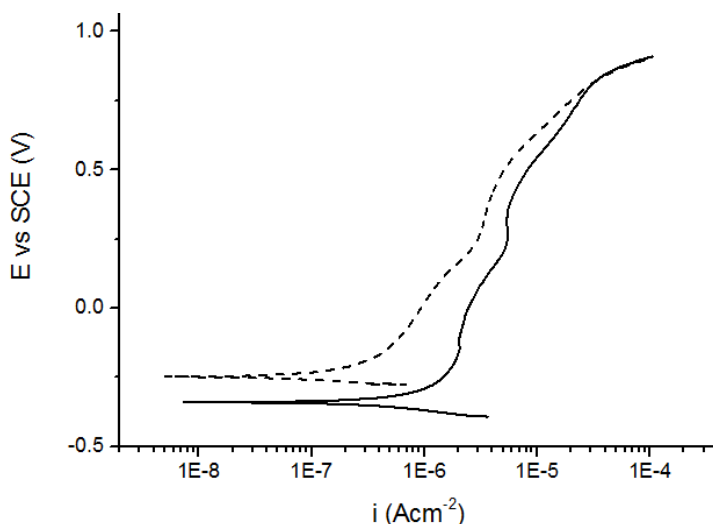


Fig. 4.18: Anodic potentiodynamic polarizations of B450C steel in the carbonate/bicarbonate buffer (pH 10.2) with 1mM Na_2S . (—) Pre-passivated surface (—) Just polished surface.

It is very well known that the oxygen presence plays a crucial role in the growth of the oxide layer on the steel surface, thus a solution deaeration by means of a 20 minutes N_2 bubbling prior testing, could stimulate the sulfides attack. The resulting curves at different sulfide concentrations, are reported in fig. 4.19. No significant differences from those in aerated solution were noticed but a little decrease in the open circuit potentials due to the reduced oxygen content.

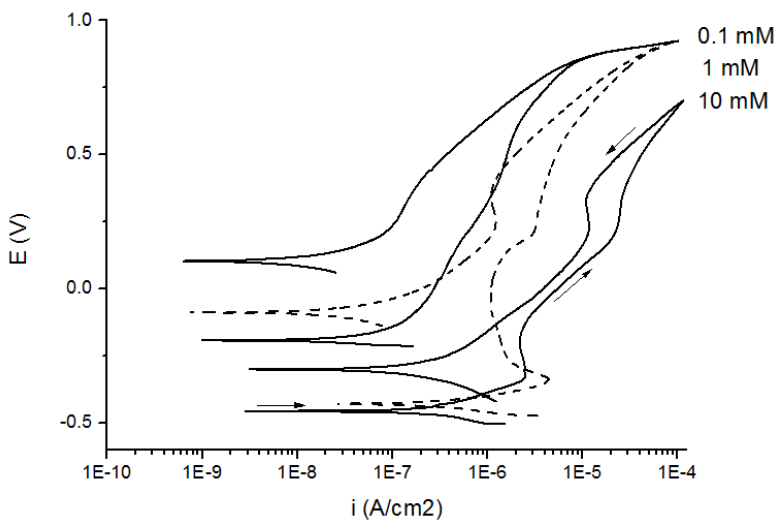


Fig. 4.19: Anodic potentiodynamic polarizations of B450C steel in the deaerated carbonate/bicarbonate buffer (pH 10.2).

When the carbonation front passes through the concrete cover thickness and reaches the steel concrete interface, the pH in such interfacial region can be lowered from 14 of sound concrete to values around 9.

In order to simulate a fully carbonated concrete, the carbonate/bicarbonate ratio of buffer solution was modified up to obtaining a pH 9.2 medium.

Potentiodynamic polarizations registered at the less alkaline pH (Fig. 4.20) showed a behavior similar to that above described when very low amounts of sulfides were added ($< 1\text{mM}$). For higher sulfide concentrations the plots drastically changed: corrosion potentials were lowered of about 500 mV and current densities were from two to three orders of magnitude higher. In these latter cases, the responses resulted to be rather complex being characterized by an initial marked current peak, followed by a series of other peaks and a significant current decrement before the scansion inversion. The irregular current fluctuations in the potential range between -0.7 and 0 V vs. SCE could be attributed to the continuous formation and breakdown of a scarcely protective corrosion product layer.

At the end of the polarization measurements, the surface treated with 0.5 mM sulfides did not show any deterioration, while in all the remaining cases specimens exhibited a black loose corrosion product layer, probably mackinawite, which was easily removed just by rinsing the electrode surface with distilled water and wiping it with a soft tissue.

After such soft cleaning, macroscopic observation of the steel sample pointed out a deteriorated surface characterized by blister-like isolated spots (fig.4.21). Such blister-like morphology of the sulfide attack has already been reported in literature by Sherar et al. and Salvarezza et al. [20, 24]

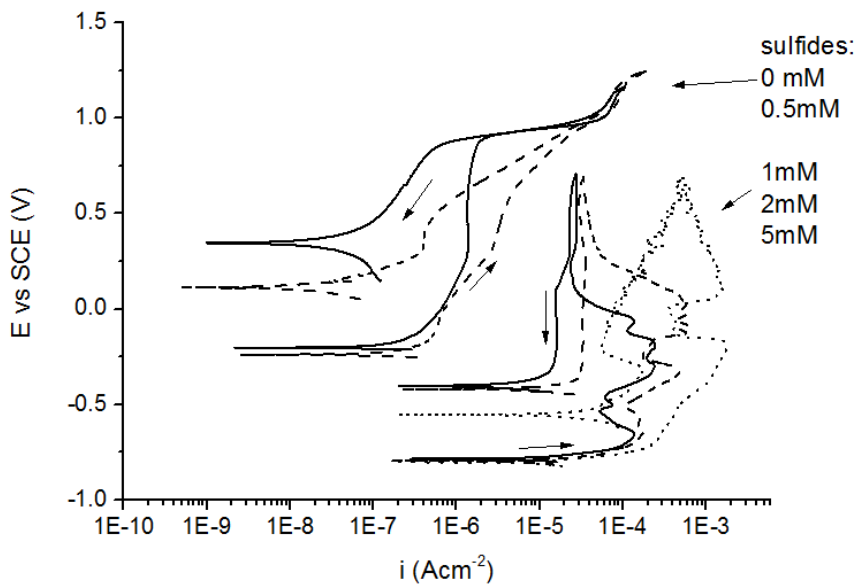


Fig. 4.20: Anodic polarizations of prepassivated samples in carbonate/bicarbonate (pH 9.2) buffer containing different sulfides concentrations.

A more in-depth observation of the same steel surface was performed by means of the optical microscopy, whose pictures are shown in fig. 4.22. The lower magnification picture showed an irregular surface characterized by different morphologies: an homogeneously gray area where the detectability of the polishing lines indicated a minor deterioration, and outward this region a more irregular surface. Several pits, whose details are shown in fig. 4.22(b) were found, spread on the overall surface.

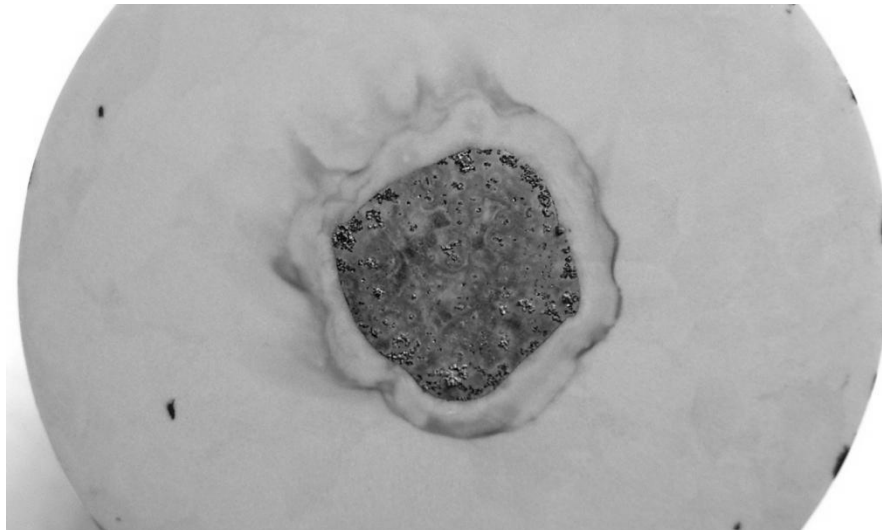


Fig. 4.21: Macroscopic picture of the steel surface after anodic polarization of a prepassivated samples in carbonate/bicarbonate (pH 9.2) Na_2S 5mM.

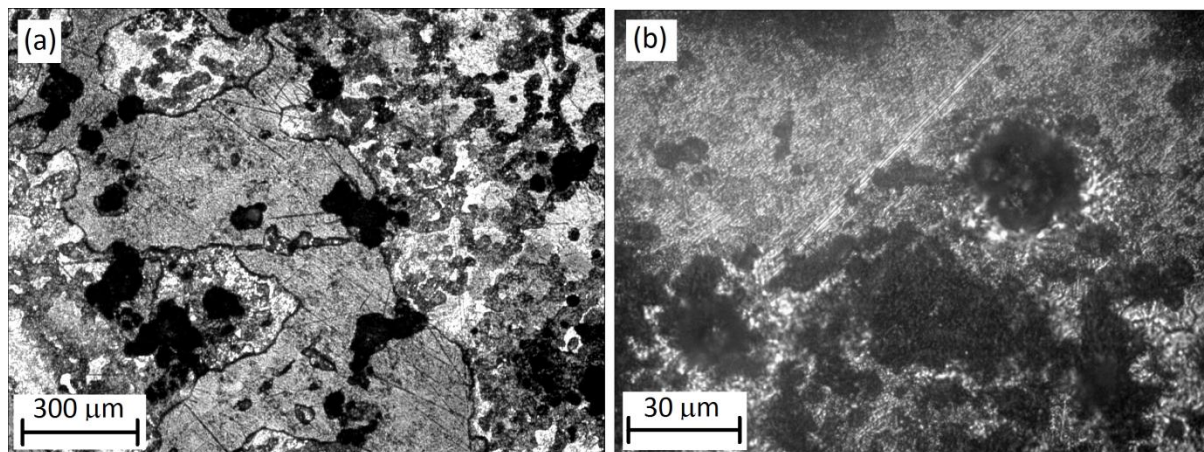
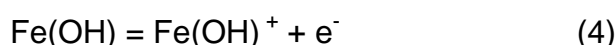
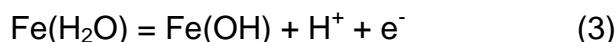
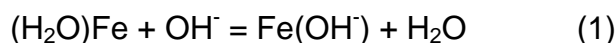


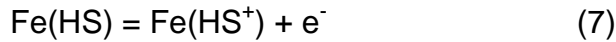
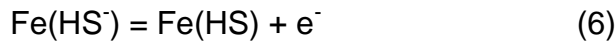
Fig. 4.22: Optical microscopy pictures of the steel surface after anodic polarization of a prepassivated samples in carbonate/bicarbonate (pH 9.2) Na₂S 5mM. (a) magnification 50X, (b) magnification 500X.

Considering all the above discussed measurements and observations, seems evident that sulfides are a potentially aggressive species with regard to B450C rebars. However, their interactions with the steel surface are strictly connected to the environment conditions, especially to the electrolyte pH. This fits very well with the findings of Salvarezza et al., [20] who postulated a competitive adsorption of HS⁻ and OH⁻ on the steel surface yielding to sulfide and oxide species, respectively.

Such a competitive adsorption can be written as in the reaction 1 and 2, where brackets indicate adsorbed species.

Reactions from 3 to 5 have already been thoroughly discussed in the previous chapter, being related to the formation of the oxide passive layer, while reactions 6 - 8 describe the steel-sulfide interaction, leading to mackinawite (FeS) and to the onset of corrosion processes. According to the authors, reactions 3 - 5 prevail over 6 - 8 when the degree of surface coverage by OH⁻ is higher than that of HS⁻ ions. Conversely, the mackinawite formation, prevails at lower pH values. This would explain the difference between pictures 4.15 and 4.22, taken after anodic polarizations in a sulfide containing solution of pH 10.2 and 9.2, respectively: the former showing an unaffected surface and the latter a heavily corroded sample.





The blister-like corrosion morphology was explained by Sherar et al. [24], who proposed a mechanism reported in the schematic of fig 4.23, according to which corrosion rapidly proceeds underneath a loosely adherent mackinawite layer. This is possible because of the very high porosity of the mackinawite layer; furthermore such iron sulfide is known to be a good electrical conductor thus the iron dissolution reaction is likely to be supported by oxygen reduction occurring on the outside shell of the blister. As depicted on the right side of the sketch, mackinawite conversion to sulfur and iron oxide is also possible, but its rate is significantly lower if compared with the corrosion process beneath the film.

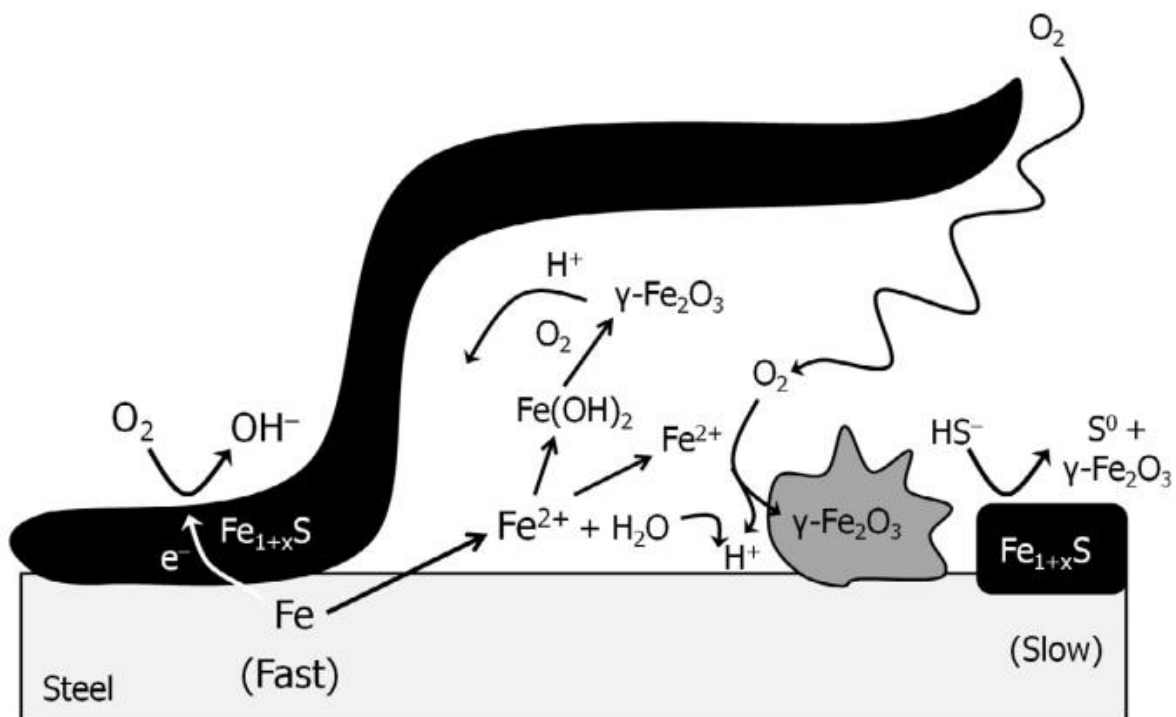


Fig. 4.23: schematic of the iron dissolution process occurring beneath the mackinawite film [24].

4.3.2 Reinforced mortar samples

Once got a better understanding of the corrosion mechanism and morphology occurring for steel in model media, the attention was moved towards more complex, but closer to the reality, systems such as reinforced mortar samples.

As previously discussed in detail in Chapter 2, Section 2.3.1, the extremely alkaline environment naturally granted by sound concrete does not allow bacteria colonization. Actually, a necessary prerequisite for the occurrence of concrete microbial induced deterioration is an initial abiotic pH decrease (from pH 13 to pH 9), mainly due to atmospheric CO₂.

Accordingly, reinforced mortar samples were produced as described in 4.2.1 and were submitted to an accelerated carbonation procedure, into an on-purpose designed carbonation chamber (see Section 1.2.1).

There exist several methods for the determination of the carbonation degree of RC structures, the easier, faster and more commonly used is the phenolphthalein test, according to which a transversal section of the sample is cut and sprayed with an alcoholic solution of phenolphthalein. A violet turning of the surface indicates superficial pH above 10, while an uncoloured response, attributed to lower pH, indicates carbonation.

An unreinforced mortar prism, cast on-purpose, was cut before the accelerated carbonation, and the phenolphthalein sprayed surface resulted, as expected, to be completely violet because of the alkaline pH (fig.4.24(a)). After one month in the carbonation chamber a new cross section was cut, but conversely to the previous case, no turning in color was detected, thus indicating the full carbonation of the mortar sample (fig. 4.24 (b)).

In order to confirm the complete carbonation of the mortar prism, a small amount of powder was taken away from the core of the cross section (dashed circle in fig 4.24(b)) by means of mechanical abrasion: the resulting XRD is reported in fig.4.25.

The diffractogram exhibited sharp and well defined peaks, and they were attributed to quartz, dolomite, and calcite by comparison with XRD pattern database. The first two are typical components of the limestone cement, while calcite is the resulting product of the carbonation process. Furthermore, portlandite (Ca(OH)₂) should have peaks at 18° and 34°, and their absence, meaning that was completely converted into calcite, confirmed the fully carbonation of the sample.

According to literature dealing with accelerated carbonation test [25-28], a penetration rate of the carbonation front of 2 cm/month resulted to be rather higher than the average. However, it has to be said that most the cited studies, being interested in the carbonation mechanism, used a lower CO₂ concentration than in the present case, where the objective was only to get a complete carbonation as fast as possible. Furthermore, samples of the present study were cast with CEM II / B- LL,

thus containing a 20 - 35 % of inert limestone (see table 2.3), and consequently having a significantly lower amount of initial portlandite with respect to an ordinary Portland cement.

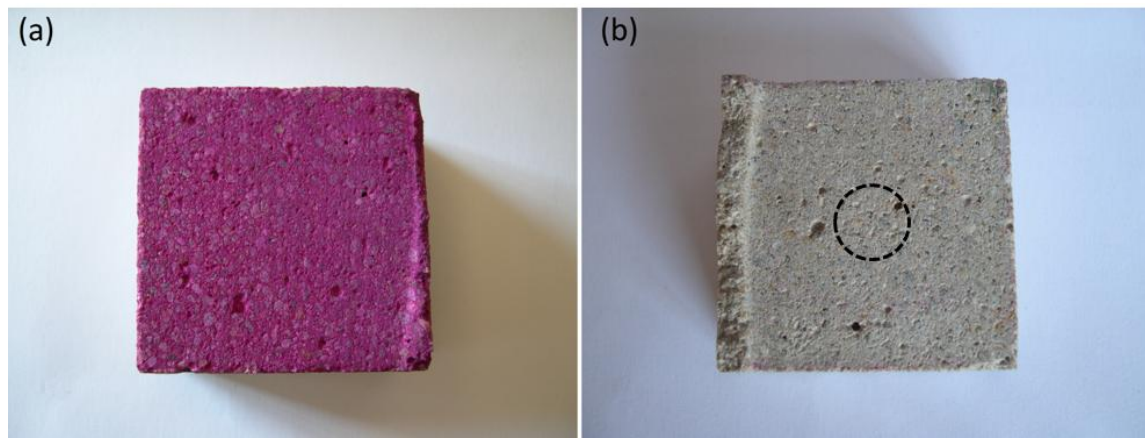


Fig. 4.24: Phenolphthalein test on two freshly cut cross section of a not reinforced mortar prism. (a) before accelerated carbonation, (b) after 1 month in the carbonation chamber. The dashed circle represents the subsequently abraded area for XRD measurement.

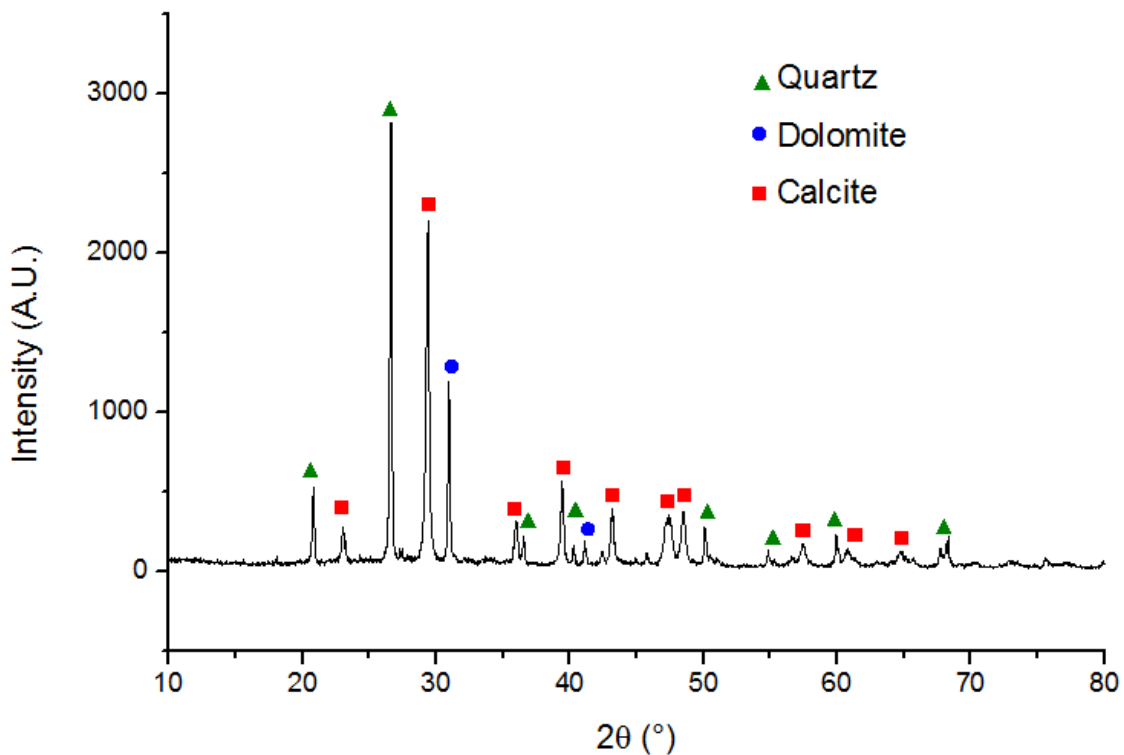


Fig. 4.25: XRD diffractogram of a powder sample mechanically abraded from the core of the mortar prism after one month of accelerated carbonation treatment.

OCP measurements

Daily OCP measurements of reinforced mortar samples, partially submersed in the three testing environment (Carbonate-bicarbonate solution, carbonate-bicarbonate solution with 2 mM Na₂S and 0.5% H₂SO₄), are shown in fig. 4.26. Every point results from the average of the 5 replicates per each conditioning environment, although a rather good homogeneity in the measurements was obtained within the replicates; the OCP responses exhibited a certain fluctuation in the order of ± 15 mV between consecutive measurements. The magnitude of such fluctuations does not cause any concern and can be easily attributed to the natural heterogeneity of cementitious materials.

However, despite the OCP fluctuations, in all cases the corrosion potentials exhibited similar trends, starting from values of about -0.580 V, significantly decreasing in the first twenty days, and maintaining the slightly decreasing trend up to the end of the conditioning period on the hundredth day.

According to the ASTM C876, corrosion potential lower than -0.426 V vs. SCE indicates severe risk of corrosion. However the same standard warns about the reliability of OCP measurements performed on fully water saturated concrete. It seems thus important to underline that such negative values, although being partially justified by the carbonation that is certainly responsible for the transition to the active behaviour, could also be related to an oxygen depletion due to the immersed condition of the samples. .

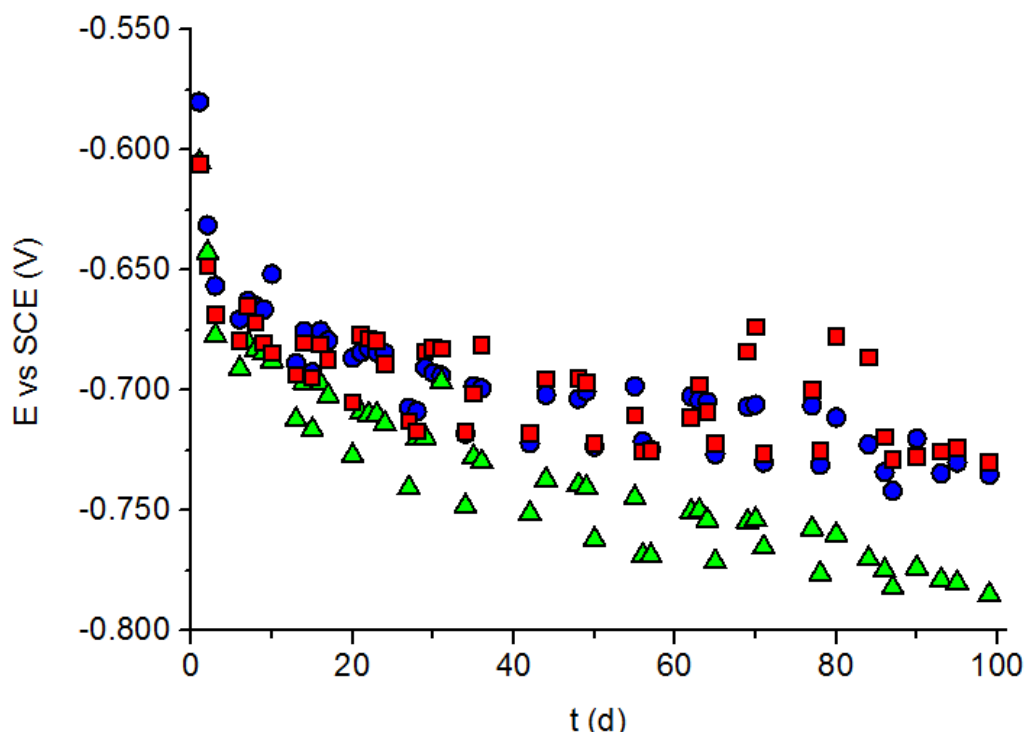


Fig. 4.26: OCP monitoring of reinforced mortar samples. (●) Na₂CO₃ / NaHCO₃ pH 9.2. (▲) Na₂CO₃ / NaHCO₃ pH 9 + Na₂S 2 mM. (■) 1% H₂SO₄.

By comparing the results among the different solutions, samples in the sulfide containing vessel resulted to have a significantly lower corrosion potential: this is coherent with the lower OCP previously measured for steel in the sulfide solution (Section 4.3.1 in the present chapter) and was attributed to the strong reducing power of sulfides.

As already explained in Chapter 2, Section 2.3.2, OCP measurements only give an indication of the probability of corrosion activity, but they cannot be correlated with its rate. Thus the above presented readings confirmed the steel activity in all the three cases, but did not allow any differentiation between the different cases.

LPR and EIS monitoring

It is well known that OCP measurements alone are not considered enough to assess the state of a reinforced concrete structure, so they need to be integrated with other measurement such as LPR.

The averaged values for the corrosion current densities, calculated from the linear polarization measurements, are shown in fig. 4.27, while accepted threshold values and their corresponding corrosion risk are reported in table 4.1 [29,30].

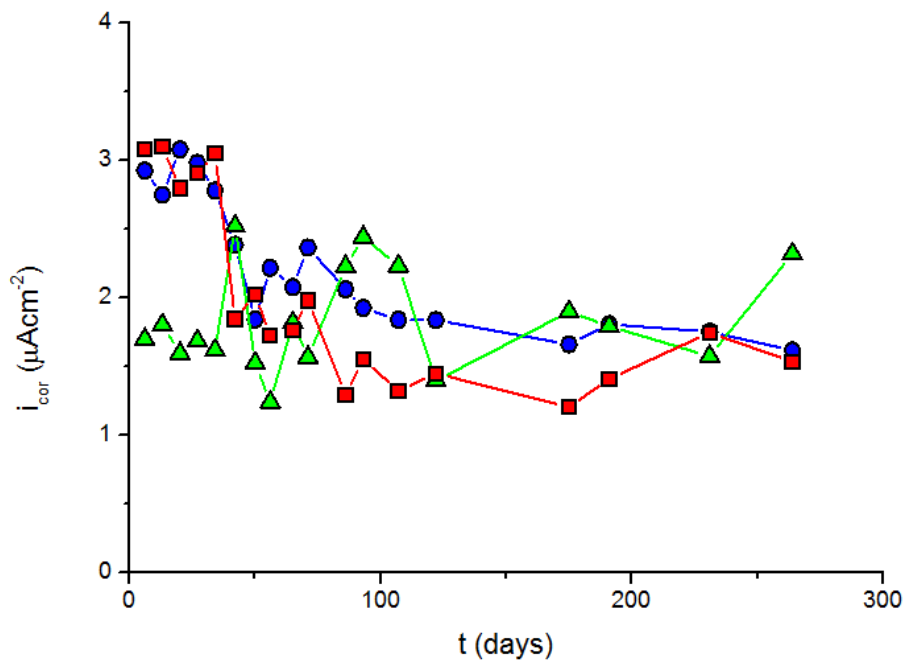


Fig. 4.27: Corrosion current densities of reinforced mortar samples calculated from LPR measurements. (●) $\text{Na}_2\text{CO}_3 / \text{NaHCO}_3$ pH 9, (▲) $\text{Na}_2\text{CO}_3 / \text{NaHCO}_3$ pH 9 + Na_2S 2 mM, (■) H_2SO_4 .

Table 4.1: Relationship between corrosion current density and corrosion risk.

Corrosion Current Density, µA/cm ²	Corrosion Risk
<0.1	Negligible
0.1 to 0.5	Low
0.5 to 1	Moderate
>1	High

According to the threshold values, all the three different cases, having corrosion currents higher than $1 \mu\text{Acm}^{-2}$ resulted to fall into the higher corrosion risk category. The case of the reference solution at pH 9 without sulfides, and that of the diluted sulfuric acid solution, showed higher initial current densities, for the first conditioning month, if compared to the case of the sulfide containing solution. However, after the first month of immersion, all the samples attained an almost stable corrosion current density of value around $1.5 \mu\text{Acm}^{-2}$.

Similarly to OCP monitoring, LPR measurements confirmed the active, corroding state of the steel rebars embedded into the carbonated mortar prisms, but did not detect any significant difference between the diverse conditioning environments.

Additional measurements were performed by means of electrochemical impedance spectroscopy, being such technique a powerful method widely used for characterizing complex electrochemical process occurring in inhomogeneous or multiphase materials. Although not yet extremely diffused as a monitoring technique "on the field", because of its inherent complexity and relatively long acquisition time, EIS has been widely used for laboratory evaluation of corrosion process in steel-concrete systems [31-40]. Consequently, a huge number of equivalent electric circuits have been proposed for the interpretation of EIS data, some of them significantly differ between each others.

The typical EIS response of a carbonated reinforced mortar sample conditioned into the diluted sulfuric acid solution is shown in fig. 4.28. The two other different conditioning media (alkaline solution with/without sulfides) gave similar patterns.

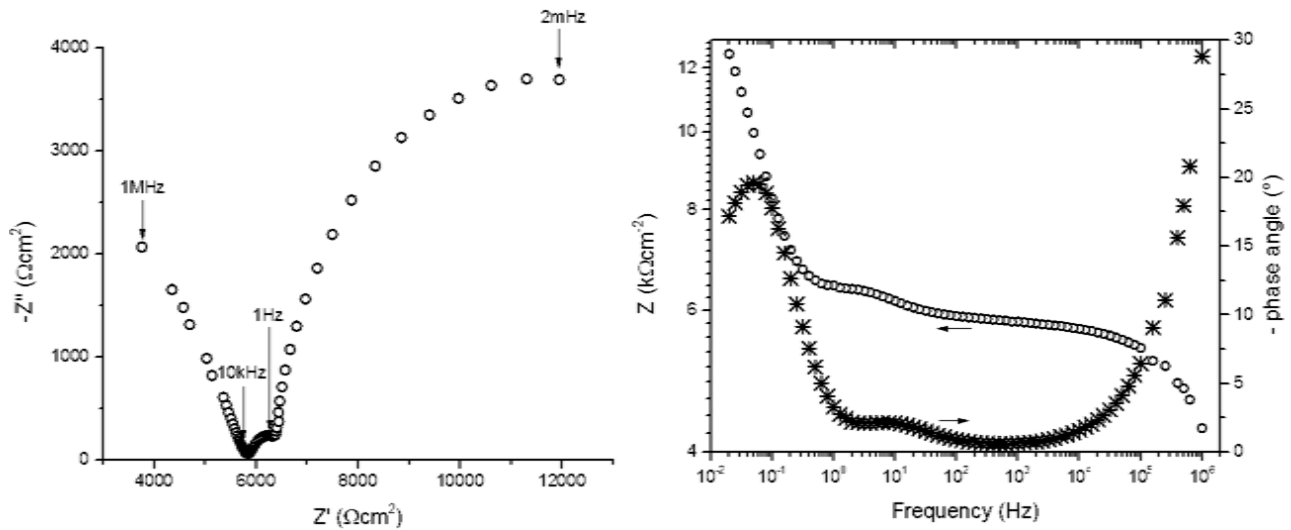


Fig. 4.28: Typical EIS response of carbonated reinforced mortar sample. (a) Nyquist plot, (b) Bode plot.

The Nyquist plot clearly pointed out the presence of three well defined partial semicircles. In agreement with such observation, the optimized electrical equivalent circuit used for the fitting of experimental data resulted to be a three time constants circuit, composed by three hierarchically distributed RC circuits (fig. 4.29). As a common practice with such measurements, pure capacitances were substituted with constant phase elements (CPE) accounting for the irregular distribution of the applied potential due to material heterogeneity, steel surface roughness, etc.

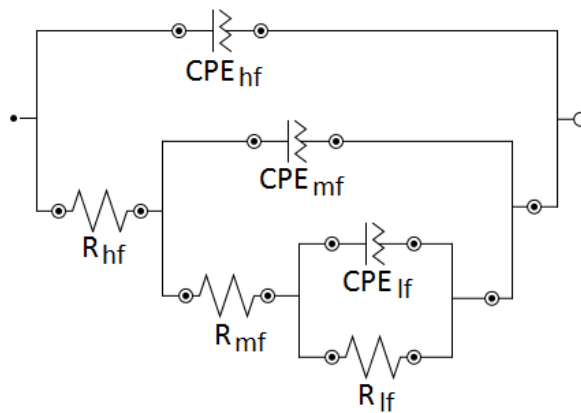


Fig. 4.29: Equivalent electrical circuit used for fitting the experimental EIS data of carbonated reinforced mortar samples.

A similar circuit was proposed by Dhouibi et al. [39] and subsequently successfully used by Criado et al. [40] who investigated the EIS response of fully carbonated reinforced mortar samples cast with different cement types and different organic corrosion inhibitors. According to [40], the high frequency time constant, covering the frequencies range from 1MHz to 10 / 1 kHz as a function of the cement type, corresponds to the bulk mortar cover response. The intermediate frequency time constant, extending from 10/1 kHz to 10/1 Hz is attributed to the characteristics of the

transition zone, where both the cement microstructure and its composition differ from the bulk region. Microstructural deviations consist in a higher porosity of the transition zone and in a higher content of calcium hydroxide while, at the same time, lower amounts of anhydrous cement and calcium silicate hydrate were detected if compared with the bulk cement paste [41]. From the composition point of view, differences rise from the reaction of cement components with the steel, leading to the formation of hydrated calcium ferrite, $4\text{CaO} \cdot \text{Fe}_2\text{O}_3 \cdot 13\text{H}_2\text{O}$ [41].

Finally, the impedance response collected at the lower frequencies can be attributed to the mortar/steel interface, being composed of a resistance and a CPE element, accounting respectively for the charge transfer resistance and the double layer capacitance. The frequency values displayed in the Nyquist plot of fig. 4.28, corresponding to starting and ending points of three capacitive arcs, seemed to fit very well with the above described frequency ranges. Furthermore, values obtained from the fitting of the experimental EIS data resulted to be comparable with those published on [40], both this features confirming the reliability of the below discussed results.

Fig. 4.30 shows the best fitting values calculated from the experimental data using the equivalent circuit of fig. 4.29; results were averaged among the 5 replicates per each conditioning environment.

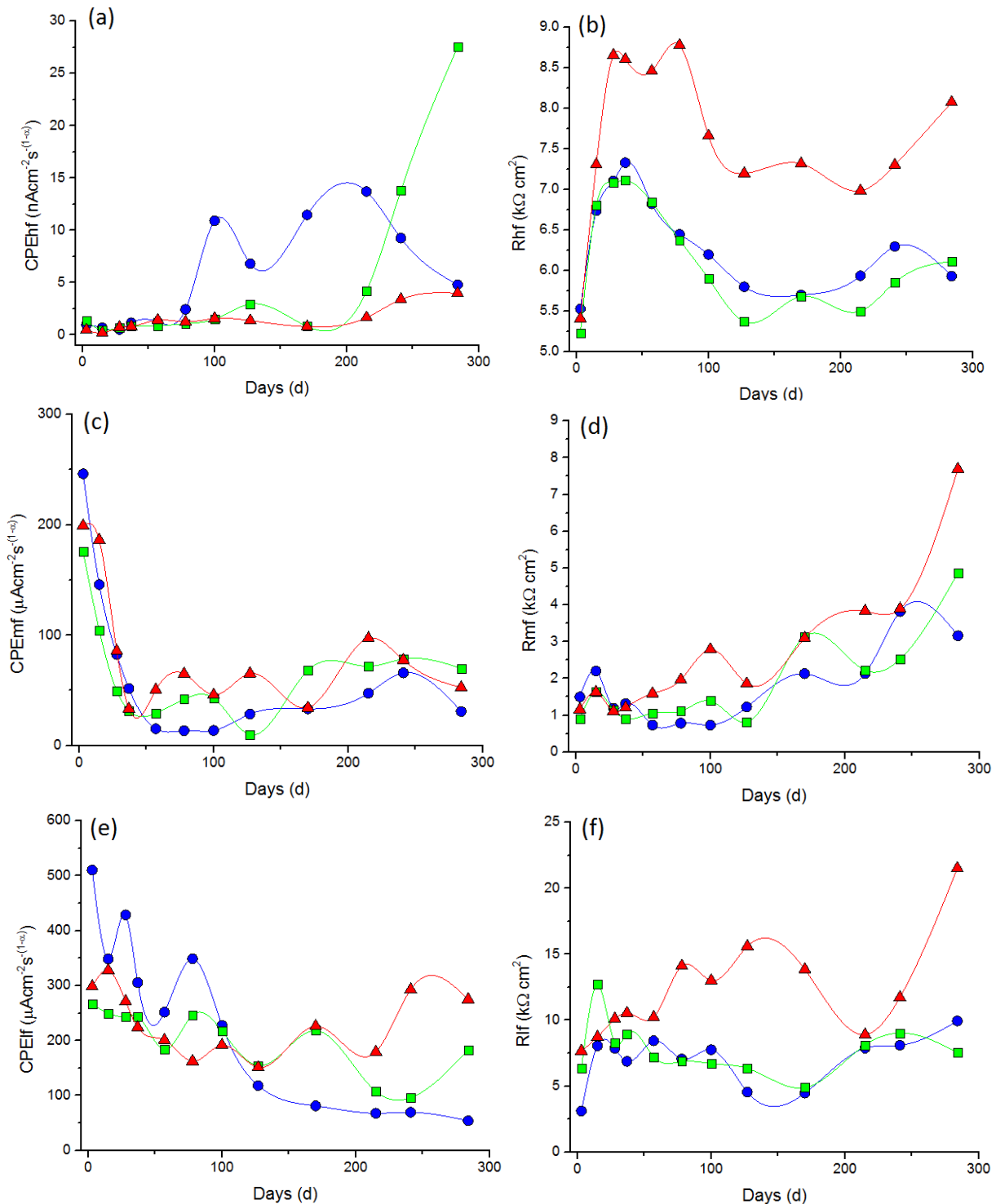


Fig. 4.30: Best fitting values of the EIS responses for: (●) $\text{Na}_2\text{CO}_3 / \text{NaHCO}_3$ pH 9, (■) $\text{Na}_2\text{CO}_3 / \text{NaHCO}_3$ pH 9 + Na_2S 2 mM, (▲) H_2SO_4 .

Focusing on the higher frequencies responses, the pseudocapacitance values resulted to be in the order of nano Farad, and this was coherent with data available in literature [40]. However, they did not exhibit a clear trend. Conversely, resistances attributed to the bulk cement matrix depicted similar trends, being characterized by a significant increase during the first conditioning months, followed by a slight decrease leading to a subsequent stabilization that persisted up to the end on the monitoring

period. The initial increase in the bulk matrix resistance could be attributed to a residue of the mortar curing process stimulated by the saturated condition, thus leading to a decrease of concrete porosity and a consequent increase in its resistivity [40]. According to [42], a concrete resistivity decrease was reported to occur after 100 days of ageing in corroding samples as a consequence of volume expanding corrosion products at the steel/mortar interface, leading to cracks that can propagate up to 2000 µm into the bulk mortar, thus resulting in a sharp drop of the resistance. It is worth to remind that in the present case, as confirmed by OCP and LPR measurements, all the samples were in an active, corroding state because of the accelerated carbonation treatment, thus, according to the above cited study, this could justify the decreasing values of the mortar bulk resistance. Finally, in fig. 4.30(b) it can be clearly seen that conditioning in the diluted sulfuric acid solution led to consistently higher resistances. Such response could be justified referring to the concrete-sulfuric acid reactions, elsewhere described (Chapter 2, Section 2.2.1), according to which gypsum and secondary ettringite are formed. Both these products are known to have significantly bigger volumes than the initial reagents, thus leading to an obstruction of the mortar pores, and a consequent higher resistance.

The intermediate frequency responses exhibited similar trends and values among the different conditioning environments for both the pseudocapacitances and the resistances (fig. 4.30(c,d)). Values of the former were characterized by a significant decrease occurring in the first conditioning month followed by a stabilization lasting until the end of the monitoring period. The resistances, attributed to the corrosion products layers displayed a continuous slight increase over time, being that of the sulfuric acid case always slightly higher than the remaining cases. Generally speaking, a capacitance decrease, together with a resistance increase are attributed to a dense layer formation. In the present case, such a behaviour could be attributed to the growth of corrosion product layer as a consequence of the steel activity due to carbonation, the acidic environment may also lead to a thicker layer.

Finally, also in the low frequency time constant (fig.4.30(e,f)), pseudocapacitance and resistance values resulted to be rather equivalent among the different conditioning environments, being characterized by a slight decrease over time of the former, and an almost stable response of the latter. Such parameters, corresponding to the double layer capacitance and the charge transfer resistance, should be precise indicators of the corrosion processes, and once again, similarly to the LPR measurements, no significant differences were detected as a consequence of the conditioning media.

Taking into consideration that LPR measurements give the overall resistance of the system, but once detracted the cementitious bulk matrix resistance, the remaining value should be that of the charge transfer resistance. Consequently, as an internal check, aiming to confirm the reliability of the above discussed results, fig. 4.31 shows a comparison of the charge transfer resistances as calculated from LPR and EIS measurements.

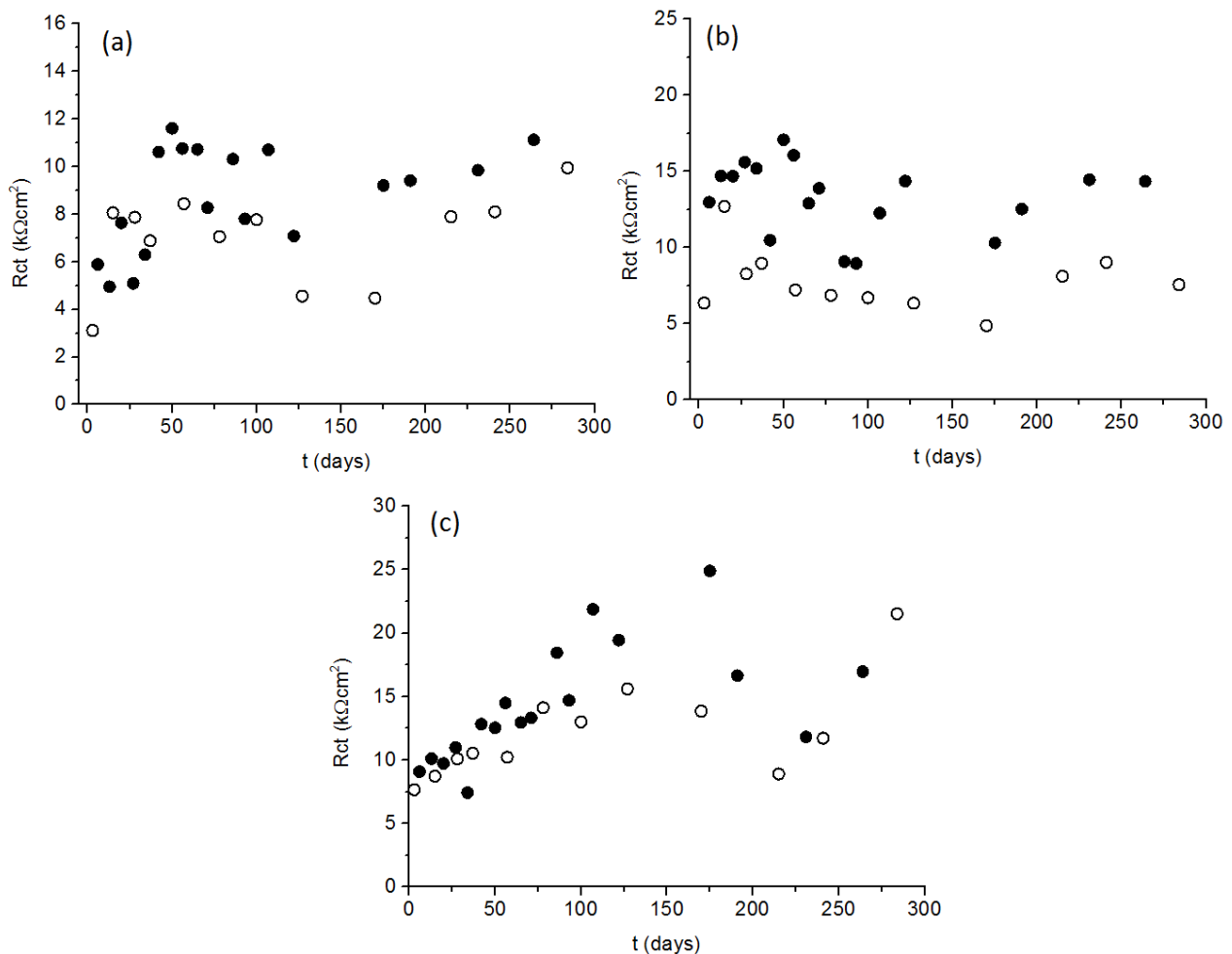


Fig. 4.31: Comparison of charge transfer resistance values, as calculate from LPR (●) and EIS (○) for the different conditioning media: (a) $\text{Na}_2\text{CO}_3 / \text{NaHCO}_3$ pH 9, (b) $\text{Na}_2\text{CO}_3 / \text{NaHCO}_3$ pH 9 + $2\text{ mM Na}_2\text{S}$, (c) 0.5% H_2SO_4 .

In all the three cases, R_{ct} values from LPR measurements resulted to be slightly higher than those calculated from impedance spectra. Such discrepancy could be attributed to a non complete ohmic drop compensation, resulting from the an instrumental limitation. However, although not overlapping, results from the two different techniques resulted to have extremely similar trends, thus confirming their reliability. Such confirmation, together with the relatively stable responses as depicted in fig.4.31, finally allowed to state that the above discussed monitoring did not detect significant differences in the electrochemical responses of steel rebars embedded into carbonated mortar and conditioned into different solutions. All the techniques (OCP, LPR, EIS) pointed out an active corroding/behaviour due to the mortar carbonation, while apparently, the aggressive species simulating the bacteria metabolites did not significantly affect the corrosion rate.

After 200 days of conditioning, one sample per each of the three media was chosen to be split allowing a visual observation of the embedded steel rebar. Pictures are reported in figure 4.32.

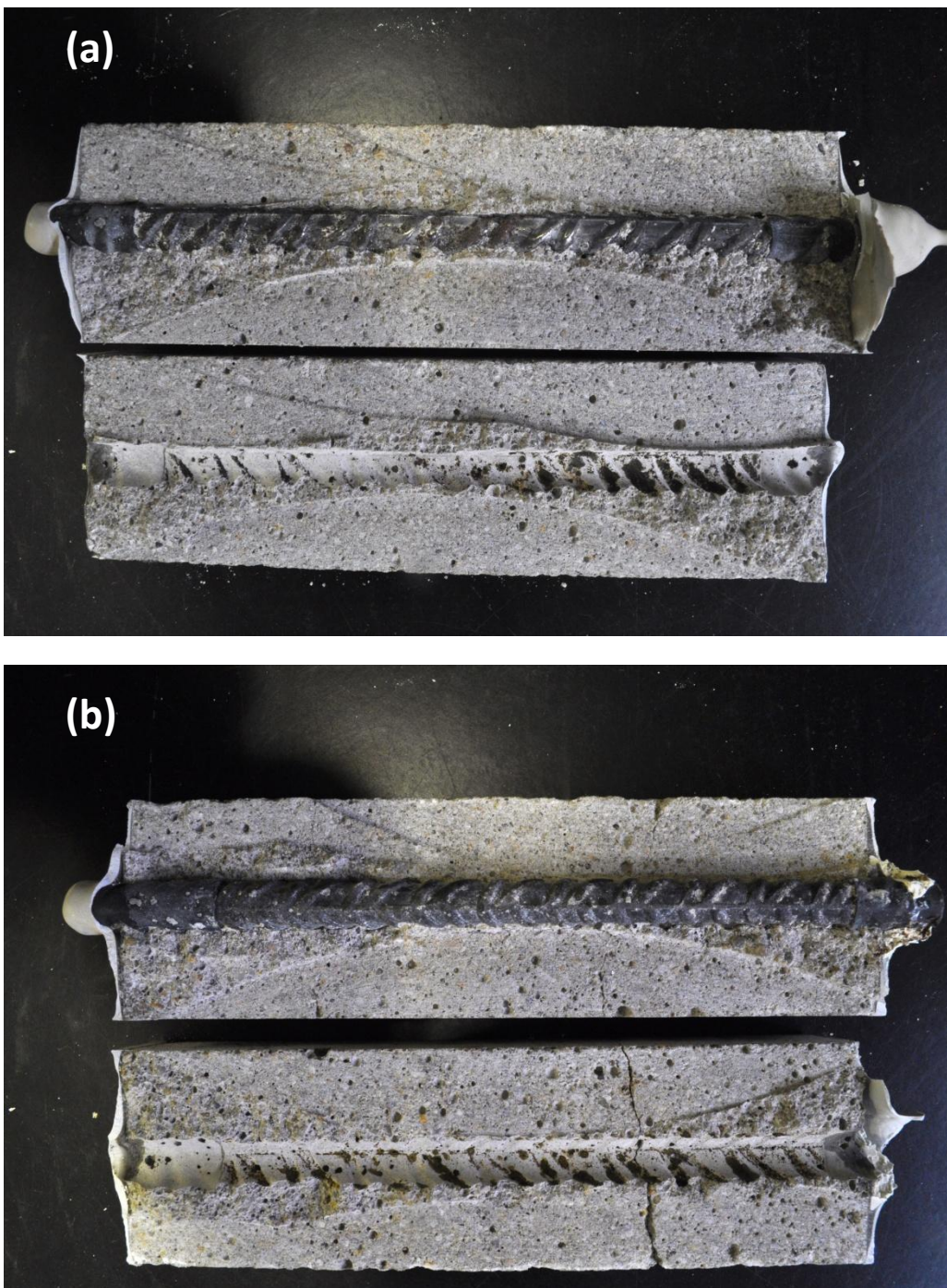




Fig. 4.32: Pictures of split reinforced mortar samples after a 200 days conditioning in three different solutions : (a) $\text{Na}_2\text{CO}_3 / \text{NaHCO}_3$ pH 9, (b) $\text{Na}_2\text{CO}_3 / \text{NaHCO}_3$ pH 9 + Na_2S 2 mM, (c) 0.5% H_2SO_4 .

Such pictures, showing the overall appearance of split samples do not allow to evaluate the steel corrosion by looking at the rebar surface, as an higher magnification would be required. However the dark corrosion products clearly visible on the other part of the sample could be considered as a good indicator of the damage entity. Barely noticeable differences were observed within the two alkaline solutions with and without sulfides, being in agreement with the similarities recorded by the electrochemical monitoring. Conversely, when the reinforced mortar samples were conditioned into the diluted sulfuric acid solution a much more extended corrosion product layer grew at the steel-mortar interface (fig.4.32(c)). Such phenomenon was however barely recognised by the different electrochemical techniques used for corrosion monitoring. Just the intermediate frequencies response of impedance spectra pointed out slightly higher values of the corrosion product layer resistance in the case of the acidic conditioning, thus confirming the visual observations above discussed.

The electrochemical monitoring was stopped after 300 days, because of the stabilization of the electrochemical responses. However reinforced mortar samples were left partially immersed into the three conditioning solution for additional seven months. The experiment was thus concluded after an immersion time of 500 days by splitting the remaining samples for further visual observations.

It is worth showing the appearance of the reinforced mortar samples at the end of the 500 days conditioning period; a picture is shown in fig. 4.33. Both samples, conditioned in the alkaline solutions, with or without sulfides, maintained their initial

shape; conversely, the acidic solution led to a dramatic deterioration of the cementitious matrix. As thoroughly explained in Chapter 2, Section 2.3.1, sulfuric acid easily reacts with portlandite and calcite leading to gypsum formation. Gypsum forms a loose and incoherent superficial layer, where both the internal stresses due to its expanding volume, and its higher solubility with respect to the initial reagents concur in its dissolution and detachment.



Fig. 4.33: Picture of reinforced mortar samples after a 500 days conditioning in three different solutions.

The gypsum presence, in the sulfuric acid conditioned samples, was confirmed by means of XRD diffractograms reported in fig.4.34. The X-ray diffractograms for mortar samples conditioned in the alkaline solutions, with and without sulfides (fig. 4.34(a,b)), resulted to be equivalent to that recorded at the beginning of the monitoring period assessing the carbonation state (fig. 4.25), thus indicating that the ten-months immersion did not cause any significant change in crystalline phases of the cement matrix. As expected, and as highlighted by arrows in figure 4.34, the sample from the acidic conditioning exhibited the XRD signals attributed to gypsum.

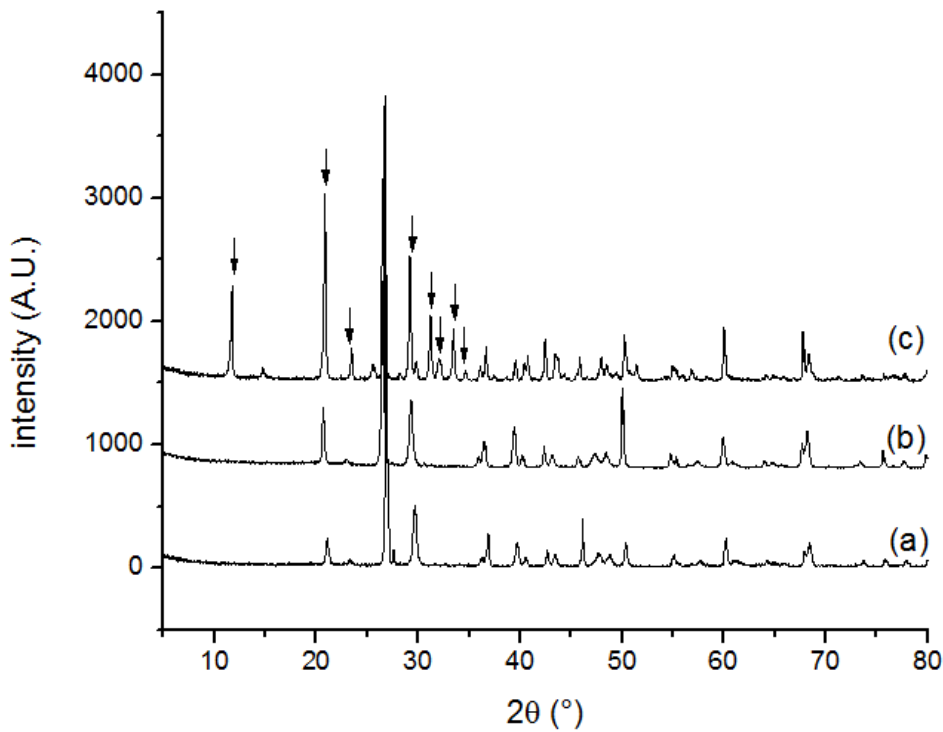


Fig. 4.34: XRD pattern of the cementitious matrix grinded from the reinforced mortar samples at the end of the conditioning period. (a) Na_2CO_3 / NaHCO_3 pH 9, (b) Na_2CO_3 / NaHCO_3 pH 9 + Na_2S 2 mM, (c) 0.5% H_2SO_4 .

Samples shown in fig. 4.33 were successively split and the resulting pictures are reported in fig. 4.35. The massive changes in the external appearance of fig. 4.30, as a consequence of the further 300-days conditioning, were not directly reflected in the deterioration of the embedded rebar. Actually, pictures of fig. 4.35 (500 days), did not depict a significantly different situation from that reported in fig. 4.29 (200 days); minor rust deposits were observed in the case of both the alkaline solutions, while a major presence of corrosion products was detected for the sulfuric acid case.

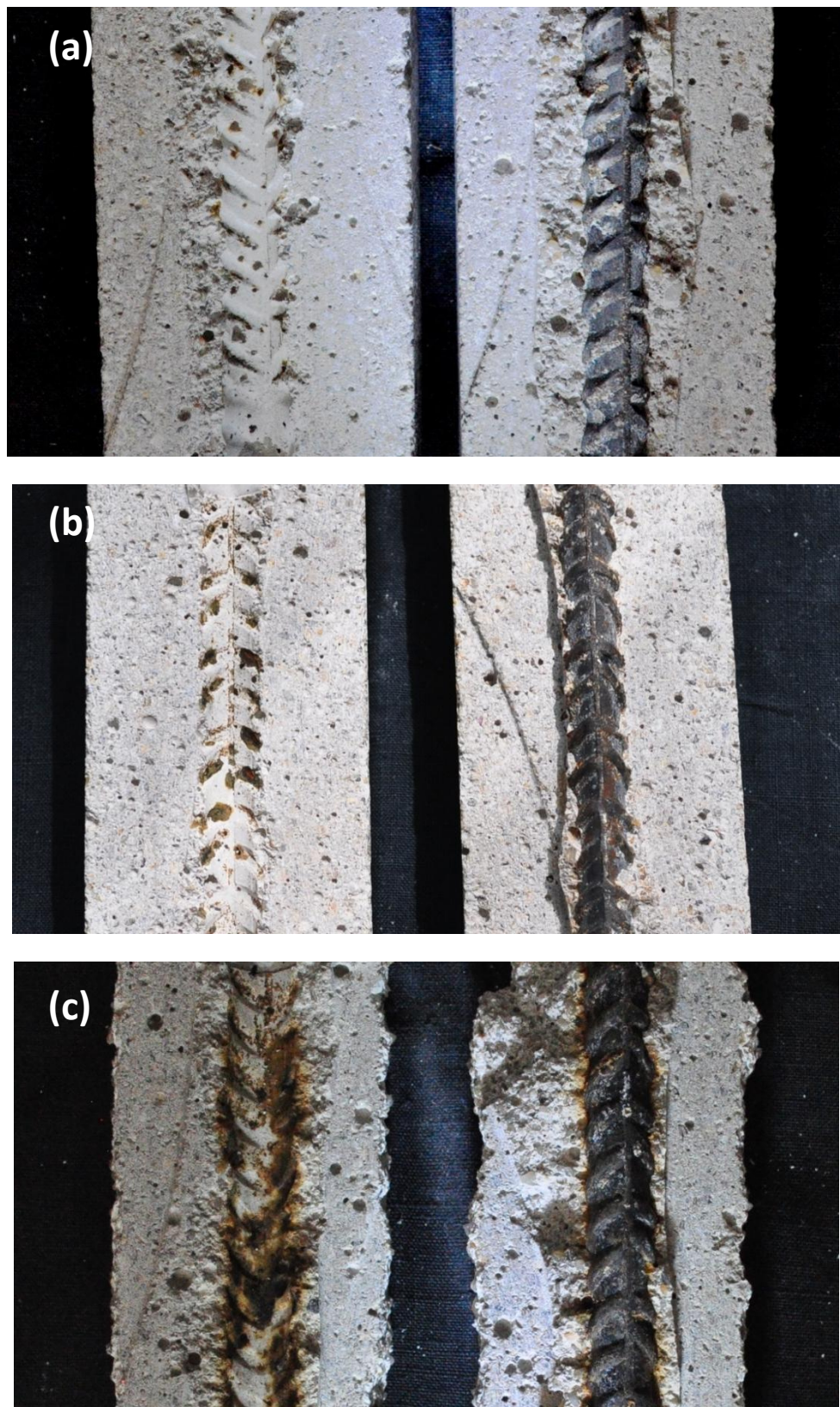


Fig. 4.35: Pictures of split reinforced mortar samples after a 500 days conditioning in three different solutions : (a) Na_2CO_3 / NaHCO_3 pH 9, (b) Na_2CO_3 / NaHCO_3 pH 9 + Na_2S 2 mM, (c) 0.5% H_2SO_4 .

4.4 Conclusions

Aiming to systematically investigate how abiotic solutions, simulating certain bacteria metabolites, affect the integrity of steel reinforcing bars an experimental plan was designed, starting from the easier system where the steel samples were directly immersed into the aggressive solutions, and ending with a 300-days electrochemical monitoring of reinforced mortar samples conditioned into different media simulating bacteria metabolites.

Being well known that bacteria mostly involved in the deterioration mechanism of reinforced concrete structures are those related to the sulfur cycle, Na_2S in slightly alkaline solution and diluted H_2SO_4 were used for the simulation of SRB and SOB metabolic products.

As expected, in case of steel directly immersed into the diluted sulfuric acid solution, both the gravimetric and the electrochemical monitoring pointed out the onset of a corrosion process, consisting in a fast dissolution of the protective oxide layer and a subsequent attack to the underneath steel surface. The attack morphology resulted to be of a generalized type. A more complicated behavior, was instead obtained with sulfide additions to alkaline solutions simulating a carbonated concrete. In order to get more insight into the deterioration mechanism, a multivariable study was required, where different parameters such as sulfide concentration, steel pre-passivation, electrolyte oxygenation and pH were singularly modified. Sulfides resulted to be a potentially aggressive species, their interactions with the steel surface being essentially dependent on the environment pH. At the more alkaline pH, the protective effect of the oxide layer prevails on the sulfide adsorption, but lowering the pH, the equilibrium was unbalanced toward the steel-sulfide interaction leading to a loose iron-sulfide film (mackinawite) and localized corrosion processes.

The electrochemical testing of reinforced mortar samples resulted to be much more complicated and time consuming as compared with the above discussed case, as the mortar cover thickness protected the steel by providing a physical barrier against all the aggressive species. The accelerated carbonation partially neutralized the cement alkalinity, leading to the rebar transition from the passive state to the active.

However, in the present saturated conditions, once the corrosion process was initiated by carbonation induced pH drop, the employed electrochemical techniques were not able to detect significant accelerations in the corrosion process as a function of the external aggressive environment. Nevertheless, the splitting of reinforced mortar samples pointed out a major formation of corrosion products in case of the acidic conditioning, thus highlighting that the external environment, simulating the biogenic acidity, can affect the steel corrosion process.

References

- [1] X. Shi, N. Xie, K. Fortune, J. Gong, Durability of steel reinforced concrete in chloride environments: An overview, *Construction and Building Materials*, 30 (2012) 125-138.
- [2] U. Angst, B. Elsener, C. Larsen, Ø. Vennesland, Critical chloride content in reinforced concrete - A review, *Cement and Concrete Research*, Vol.39, Issue 12 (2009) 1122-1138.
- [3] A. Suryavanshi, J. Scantlebury, S. Lyon, Corrosion of reinforcement steel embedded in high water-cement ratio concrete contaminated with chloride, *Cement and Concrete Composites*, 20 (1998) 263-381.
- [4] D. Roberts, D. Nica, G. Zuo, J. Davis; Quantifying microbially induced deterioration of concrete, *Int. Biodet. Biodeg.* 49 (2002) 227-234.
- [5] M. O'Connel, C. McNally, M.G. Richardson, Biochemical attack on concrete in waste water application, *Cement and Concrete Composites*, 32 (2010) 479-485.
- [6] N. De Belie, J.J. Lenehan, C.R. Braam, B. Svennerstedt, M. Richardson, B. Sonck, Durability of Building Materials and Components in the Agricultural Environment, Part III: Concrete Structures *Journal of Agricultural Engineering Research*, Vol. 76, Issue 1(2000) 3-16.
- [7] J. Monteny, E. Vincke, A. Beeldens, N. De Belie, L. Taerwe, D. Van Gemert, W. Verstraete, Chemical, microbiological, and in situ test methods for biogenic sulfuric acid corrosion of concrete, *Cement and Concrete Research*, Vol. 30, Issue 4 (2000) 623-634.
- [8] N. De Belie, J. Monteny, A. Beeldens, E. Vincke, D. Van Gemert, W. Verstraete, Experimental research and prediction of the effect of chemical and biogenic sulfuric acid on different types of commercially produced concrete sewer pipes, *Cement and Concrete Research*, Vol. 34, Issue 12 (2004) 2223-2236.
- [9] S. Wei, M. Sanchez, D.Trejo, C. Gillis, Microbial mediated deterioration of reinforced concrete structures, *International Biodeterioration & Biodegradation*, 64 (2010) 748-754
- [10] V.A. Abdelmseeh, J. Jofriet, G. Hayward, Sulphate and sulphide corrosion in livestock buildings, Part II: Reinforcing steel corrosion, *Biosystem engineering*, 99 (2008) 382-289.
- [11] A. Idriss, S.C. Negi, J. Jofriet, G. Hayward, Corrosion of steel reinforcement in mortar specimens exposed to hydrogen sulphide, Part I: impressed voltage and electrochemical potential tests, *J. Agric. Engng. Res.* 79 (2001) 223-230.
- [12] W. Sun and S. Nesic, A mechanistic model of H₂S corrosion of mild steel, NACE corrosion 2007, paper n°07655.

- [13] F.H. Meyer, O.L. Riggs, R.L. McGlasson, J.D. Sudbury, Corrosion Products of Mild Steel In Hydrogen Sulfide Environments. *Corrosion*: February 1958, Vol. 14, No. 2, pp. 69-75.
- [14] C Ren, D Liu, Z Bai, T Li, Corrosion behavior of oil tube steel in simulant solution with hydrogen sulfide and carbon dioxide, *Materials chemistry and physics*, Volume 93, Issues 2–3, (2005) 305-309.
- [15] Scott P. Ewing, Electrochemical Studies of the Hydrogen Sulfide Corrosion Mechanism. *Corrosion*: November 1955, Vol. 11, No. 11, pp. 51-55.
- [16] Y.Chi, S. Nesic, S. Ling, Effect of H₂S on the CO₂ corrosion of carbon steel in acidic solutions *Electrochimica Acta*, Volume 56, Issue 4 (2011) 1752-1760.
- [17] D.W. Shoesmith, M. Bailey, B. Ikeda, Electrochemical formation of Mackinawite in alkaline sulphide solutions, *Electrochimica Acta*, Vol.23 (1978) 1329-1339.
- [18] D.W. Shoesmith, P. Taylor, M. Bailey, B. Ikeda, Electrochemical behavior of iron in alkaline sulphide solutions, *Electrochimica Acta*, vol. 23, no. 9 (1978) 903-916.
- [19] R.C. Salvarezza, H. Videla, J. Arvia, A comparative pitting corrosion study of mild steel in different alkaline solutions containing salts with sulphur containing anions, *Corrosion Science*, Vol 24, n°9 (1984) 751-767.
- [20] R.C. Salvarezza, H. Videla, J. Arvia, The electrodissolution and passivation of mild steel in alkline sulphide solutions, *Corrosion Science*, Vol 22, n°9 (1982) 815-829.
- [21] W. Sun, S. Nesic, D. Young, Equilibrium expression related to the solubility of sour corrosion product mackinawite, *Ind. Eng. Chem. Res.* 47 (2008) 1738-1742.
- [22] P.W. Bolmer, Polarization of Iron in H₂S-NaHS Buffers, *Corrosion*, Vol. 21, No. 3: (1965) 69-75.
- [23] D. Tromans, Anodic Polarization Behavior of Mild Steel in Hot Alkaline Sulfide Solutions, *J. Electrochem. Soc.* vol. 127, No. 6 (1980) 1253-1256.
- [24] B. Sherar, P. Keech, D. Shoesmith, The effect of anaerobic corrosion on anaerobically formed sulfide layer on carbon steel in ditute near neutral pH saline solutions, *Corrosion Science*, 77 (2013) 257-264.
- [25] M. O'Connel, C. McNally, M. Richardson, Cement and Concrete Composites 32 (2010) 479-485.
- [26] S. Wey, C. Gillis, D. Trejo, Microbial mediated deterioration of reinforced concrete structures, *Int. Biodegradation & Biodegradation* 64 (2010) 748-754.
- [27] C. Chang, J. Chen, The experimental investigation of concrete carbonation depth, *Cement and Concrete Research* 36 (2006) 1760-1776.

- [28] J. Chi, C.Yang; *J. Marine Sci. and Techn.* 10 (2002) 14-20.
- [29] C. Andrade, C. Alonso, Corrosion rate monitoring in the laboratory and on-site, *Constr. Build.Mater.*, Vol.10, No 5 (1996) 315-328.
- [30] S. Feliú, J.A. González, C. Andrade, Electrochemical methods for on-site determinations of corrosion rates of rebars, in *Techniques to Assess the Corrosion Activity of Steel Reinforced Concrete Structures*, ASTM STP 1276, N.S. Berke, E. Escalante, C. Nmai, D. Whiting, Eds., ASTM, West Conshohocken, PA, 1996, 107.
- [31] P. Gu, P. Xie, J.J. Beaudoin, Some Applications of AC Impedance Spectroscopy in Cement Research, *Cem. Concr. Aggregates*, 17(2) (1995) 113-118.
- [32] P. Gu, Z. Xu, P. Xie, J.J. Beaudoin, Application of A.C. Impedance Techniques in Studies of Porous Cementitious Materials. (I):Influence of Solid Phase and Pore Solution on High Frequency Resistance, *Cem. Concr. Res.*, 23(3) (1993) 531-40.
- [33] P. Gu, P. Xie, Y. Fu, J.J. Beaudoin, A.C. Impedance Phenomena in Hydrating Cement Systems: Frequency Dispersion Angle and Pore Size Distribution, *Cem. Concr. Res.* 24(1) (1994), 86-88.
- [34] D.D. MacDonald, M.C.H. Mckubre, U.Macdonald, Theoretical Assessment of AC Impedance Spectroscopy for Detecting Corrosion of Rebar in Reinforced Concrete, *Corrosion*, Vol. 44, No. 1 (1988) 2-7
- [35] M.F. Montemor, A.M.P. Simoes, M.G.S. Ferreira, Chloride-induced corrosion on reinforcing steel: from the fundamentals to the monitoring techniques, *Cement & Concrete Composites* 25 (2003) 491-502.
- [36] S.C. Kranc, A.A. Sagues, Polarization current distribution and electrochemical impedance response of reinforced concrete when using guard ring electrodes, *Electrochim. Acta* 38 (1993) 2055-2061.
- [37] G. Trabanelli, C. Monticelli, V. Grassi, A. Frignani, Electrochemical study on inhibitors of rebar corrosion in carbonated concrete, *Cement and Concrete Research*, 35 (2005) 1804-1813.
- [38] L.Dhouibi, E. Triki, A. Raharinaivo, The application of electrochemical impedance spectroscopy to determine the long term effectiveness of corrosion inhibitors for steel in concrete, *Cement & Concrete Composites*, 24 (2002) 35-43.
- [39] L. Dhoubi, E. Triki, J. Grandet, A. Raharinaivo, Comparing the steel concrete interface state and its electrochemical impedance, *Cement and Concrete Research*, Vol. 26, No. 2 (1996) 253-266.

- [40] M. Criado, C. Monticelli, S. Fajardo, D. Gelli, V. Grassi, J.M. Bastidas, Organic corrosion inhibitor mixtures for reinforcing steel embedded in carbonated alkali-activated fly ash mortar, *Construction and Building Material*, 35 (2012) 30-37.
- [41] A.T. Horne, I.G. Richardson, R.M.D. Brydson, Quantitative analysis of the microstructure of interfaces in steel reinforced concrete, *Cement and Concrete Research* 37 (2007) 1613-1623.
- [42] D.A. Koleva, K. van Breugel, J.H.W. de Wit, E. van Westing, O. Copuroglu, L. Veleva, A.L.A. Fraaij, Correlation of microstructure, electrical properties and electrochemical phenomena in reinforced mortar. Breakdown to multi-phase interface structures. Part I: Microstructural observations and electrical properties, *Materials Characterization*, 59 (2008) 290-300.

Chapter 5.

Development of “smart”

corrosion inhibitors

for steel protection

from MICC

Among a series of different organic / inorganic compounds, known for their inhibitive properties, methylene blue dye and tri-sodium-phosphate resulted to be the most promising candidates for steel protection in a diluted sulfuric acid solution. Two different inorganic reservoirs, constituted of Vaterite (VAT) and Hydroxyapatite (HAP), impregnated with methylene blue dye, were successfully synthesized. The novel hybrid systems were characterized by means of SEM, XRD, BET, and the dye release mechanism was thoroughly investigated. The HAP based hybrid resulted to have a significantly higher storage capacity if compared to the VAT based system, therefore was chosen for further electrochemical experimentation.

The electrochemical response of steel specimens in simulated environments, with loaded and empty HAP host, was monitored by means of Linear Polarization Resistance (LPR) and Electrochemical Impedance Spectroscopy (EIS). Results confirm the inhibitive properties of the chosen compounds in acidic medium, pointing out a synergic effect resulting from the release of the organic compound and the dissolution of the inorganic matrix.

5.1 Introduction

There are several different methods that are widely used in the prevention of rebar corrosion of reinforced concrete structures, ranging from the use of blended cement to external concrete coating, from using corrosion resistant steel, to applying a cathodic protection system etc. The corrosion inhibitor addition is also a very useful and well established technique having several advantages over the others in terms of costs and ease of application. According to the Standard ISO 8044 - 1989 a corrosion inhibitor is defined as "*A chemical substance that decrease the corrosion rate when present in the corrosion system at a suitable concentration, without significantly changing the concentration of any other corrosion agent.*"

Corrosion inhibitors for reinforced concrete structures can be applied either by addition to the fresh mixture or on the hardened concrete surface, being the so called penetrating inhibitors. Furthermore, corrosion inhibitors can be classified according to their protection mechanism: film forming agents, locally pH buffering or competitive migration and adsorption with regards to the aggressive species [1]

The first corrosion inhibitor for RC structures was commercialized around 1970 and was constituted by nitrite-based compounds. Nitrite is a passivating inhibitor, that competes with chloride ions for the ferrous ions, promoting the formation of a stable passive layer. Unfortunately nitrites have some important drawbacks such those due to their high toxicity and mechanical loss. For such reasons in the last decades many researchers focused their attentions to new, efficient and environmentally friendly alternatives. Inorganic compounds such as molibdate, borates and sodium phosphate, and organic substances such as amines, alkanolamines, aliphatic carboxylic acid and saturated fatty acids were thoroughly tested [2]. Several reviews, investigating and trying to compare the protection efficiency of a wide range of different compounds are available in the open literature [3,4]. However, it is worth mentioning that most of the available papers deals with chloride induced corrosion; much less studies were performed on corrosion induced by neutralization of concrete alkalinity due to carbonation [5] or acid rains [6,7]; none studied a prevention system for microbial induced acidification.

Being the objective of the present chapter the development of a "smart" corrosion inhibitor, efficient in the corrosion prevention for structures exposed to biogenic acidity, several different substances were tested for such a purpose. Starting from those well known and experimented for concrete applications such as sodium phosphate salts [8], moving to those tested for acid rain acidification such as sodium molibdate [6,7] and ending with some organic compounds like cysteine [9] and methylene blue dye [10,11] that had never been tested for concrete applications.

That of organic molecules, for corrosion inhibition purposes, is a continuously expanding field of interest, being very strong, especially in recent years, the search

for a more efficient protection. It's well known that organic inhibitors act by adsorption, and protect the metal surface by film formation [12]. In general, the most effective and efficient compounds are those having π bonds in their structure and/or bearing heteroatoms with high electron density such as nitrogen, sulphur and oxygen [13]. This is because, taking into consideration that the steel-inhibitor interaction occurs through iron vacant 'd' orbitals, the higher the electron density on the organic compound, the stronger the co-ordination bond with steel will be [14].

One of the main problem to be faced when dealing with corrosion inhibitors, either in concrete or in any other application such as epoxy or sol-gel coatings, is how to avoid a premature leaching of the active substances with the consequent loss of their effectiveness. Storing the inhibitors inside nano/micro reservoirs can overcome the above mentioned limitation [15]. The main feature requested for a material to be considered of interest as a possible reservoir is a high porosity or a hollow structure allowing the storage of the active substances. Furthermore, reservoirs, to be efficient should fulfill a number of other requirements such as chemical and mechanical stability, compatibility with the surrounding environment, ability to sense the corrosion onset and ability to release the inhibitor on demand [15].

Polymeric nanovesicles filled with an alkalizing agent were successfully tested for concrete applications [16]. Layered double hydroxides and hollow cerium molibdate nanocontainers filled with mercaptobenzothiazole, were studied by Montemor et al. [17] and the same authors published also on vaterite and hydroxyapatite microbeads, loaded with different organic and inorganic inhibitors and dispersed into an epoxy coating [15,18].

The rationale behind the present work is based on the synergism between the inhibitive properties of phosphate and methylene blue dye in a single product, thus realizing an hybrid organic/inorganic inhibitor. Furthermore, the immobilization of MBD in a phosphate based matrix, that can dissolve at a given acidic pH, could result in a valid and superior alternative to overcome issues due the premature depletion of the inhibitor.

5.2 Experimental

5.2.1 Materials and testing environment

All the compounds, tested for their potential inhibitive properties, that is methylene blue dye (MBD), benzothiazole (BTZ), cysteine (CYS), sodium molibdate (SMD), cerium nitrate (CNT), di-sodium phosphate (DSP) and tri-sodium phosphate (TSP) were purchased from Sigma-Aldrich as ACS reagent grade.

A saturated $\text{Ca}(\text{OH})_2$ and diluted 0.5% H_2SO_4 solutions were used as model media, aiming to simulated the alkalinity of sound concrete and its acidification due to bacteria metabolites. Steel samples for electrochemical and weight loss

measurements were prepared according to the procedures, described in Chapters 3 and 4, Sections 3.2.1 and 4.2.1, respectively.

5.2.2 Electrochemical measurements

Experiments in simulated solutions were carried out at room temperature in a glass electrochemical cell with the classical three-electrodes setup: the carbon steel was the working electrode, a platinum wire served as a counter electrode and a saturated calomel electrode (SCE) was used as a reference electrode. Anodic and cathodic potentiodynamic polarizations with a scan rate of 0.5 mV/s were performed in order to assess the corrosion protection performance of the inhibitors. Moreover, 4-days monitoring tests were carried out by means of LPR and Electrochemical Impedance Spectroscopy (EIS) measurements. Linear polarization resistance measurements were carried out at a scan rate of 0.1667 mV/s in an interval of \pm 15 mV vs. OCP. EIS was performed in the frequency range from 50kHz to 10mHz by superimposing an AC excitation perturbation amplitude of 10 mV (rms).

5.2.3 Synthesis

Similar procedures were used for the two synthesis of the VAT and HAP based hybrid inhibitors [19]. A 0.2 M Na_2CO_3 solution for the former or a 0.2 M Na_3PO_4 in the case of the latter, were thermostated at 37°C in a glass reactor together with MBD 0.03 M. An equal volume of a 0.3 M CaCl_2 solution was added drop-wise through a dropping funnel mounted over the reactor. The only difference between the two synthesis was that vaterite, being thermodynamically unstable, required L-aspartic acid (1mg/mL) as organic template admixed to the CaCl_2 solution. During the addition of CaCl_2 and for the subsequent 30 minutes, the system was maintained under agitation with a magnetic stirrer. The obtained precipitate was repetitively rinsed and centrifuged with distilled water in order to remove reaction by-products. Ethanol was used for the last washing; the solid product was then left drying overnight and finally ground in an agate mortar.

5.2.4 Characterization

X-Ray powder diffraction (XRPD) patterns of the as synthesized powder were recorded on a Philips PW3020 powder diffractometer, by using the Cu-K α radiation ($\lambda = 1.54056\text{\AA}$) in a 2θ range from 10 to 80° (0.02° steps, 1s counting). The Brunauer-Emmett-Teller (BET) specific surface area was obtained from the N_2 adsorption/desorption isotherms at 77 K using a Micromeritics Tristar 2 apparatus. Before measurements, sample powders were heat-treated at 150°C for 4 h under a N_2 flow to remove adsorbed and undesired species from the sample surface. In order to investigate the MBD release mechanism, six different solutions with pH ranging from 12.6 to 1.5 were prepared by neutralizing a saturated $\text{Ca}(\text{OH})_2$ solution with 1%

H_2SO_4 . A defined amount of inhibitor (10 mg) was left under agitation overnight in 10 mL of such solutions; the MBD concentration was then determined through spectrophotometric measurements. The point of zero charge (PZC) was measured by means of the mass titration method, according to which different amounts of the inorganic host (0 - 1.5 g) were immersed into 10mL of 0.5 M KNO_3 solution and the resulting pH was measured after 24 hour of agitation. The morphological appearance of the as synthesized inhibitors was observed with a 1430 LEO scanning electron microscope (SEM) working at a chamber pressure of 8×10^{-6} Torr and 20 keV of accelerating voltage. In TU Delft, the effects of the hybrid inhibitor, and those of its components singularly considered, on the corrosion morphology of steel in H_2SO_4 were evaluated by means of an environmental scanning electron microscopy (ESEM) Philips XL30.

5.3 Results and discussion

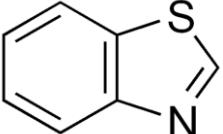
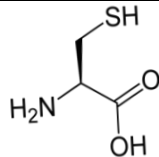
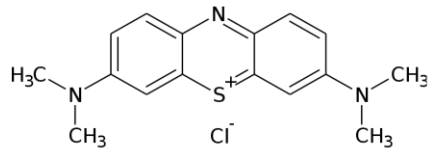
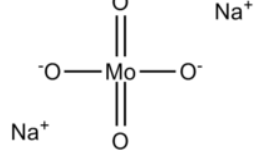
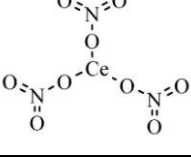
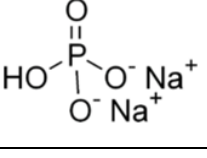
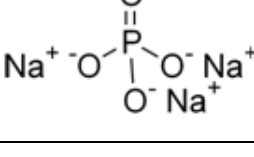
5.3.1. Inhibitors screening

Different compounds, both organic and inorganic, which have been reported in the literature as potential inhibitors for mild steel, were evaluated by means of anodic and cathodic polarizations in 0.5 % H_2SO_4 solution in which the metallic sample was directly immersed (Table 5.1).

Among the organic compounds, Benzothiazole and its derivatives are well known for being efficient corrosion inhibitors [12,20,21], while Cysteine was recently investigated as an environmentally friendly inhibitor for steel and copper [9,22]; finally, some recent journal papers indicated that methylene blue dye can protect a mild steel surface from the aggressiveness of sulfuric acid solutions [10,11]. Furthermore, bearing in mind that the final objective would be the development of a "smart" inhibitor against the microbial induced corrosion, MBD has two important advantages that is worth to mention: (i) being a dye, the release from a matrix can be easily investigated by means of Vis-spectroscopy, (ii) MBD is also known for its antiseptic properties, being used as antibacterial agent in different medical devices [23,24] and therapies.

Concerning the inorganic inhibitors involved in the preliminary screening, sodium molibdate and the two different sodium phosphates are typical corrosion inhibitors used in reinforced concrete structure in order to prevent the rebar corrosion [6,8]. However, as most of the studies on rebar corrosion available in the open literature deals with the chloride ingress, the efficiency of such classical inhibitors towards a different kind of corrosive attack still needs to be verified. Cerium nitrate comes from a completely different field. According to Srihinova et al. [18], CNT offers a good compatibility with vaterite microbeads, and results in a significant corrosion protection, in that case evaluated on the aluminum alloy AA2024.

Table 5.1: Different organic and inorganic inhibitors used in the preliminary screening.

Compound	Structure	Reference
Benzothiazole (BTZ)		[12, 20, 21]
Cysteine (CYS)		[9,22]
Methylene blue dye (MBD)		[10,11]
Sodium Molibdate (SMD)		[6,7]
Cerium Nitrate (CNT)		[18]
Di-sodium phosphate (DSP)		[8]
Tri-sodium phosphate (TSP)		[8]

Anodic potentiodynamic polarizations, performed into a diluted sulfuric acid solution containing different amount of MBD (from 0.01 mM to 5 mM) are reported in Fig. 5.1.

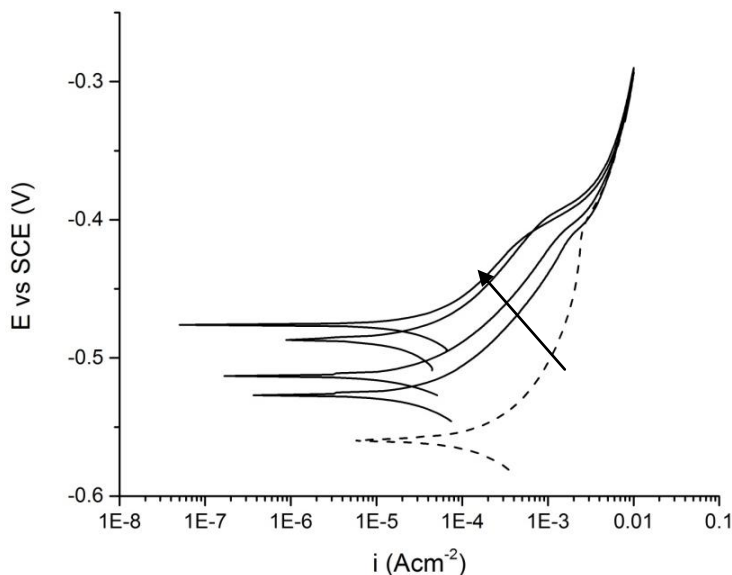


Fig. 5.1: Anodic potentiodynamic polarizations of B450C carbon steel in a 0.5% diluted solution of sulfuric acid containing different amounts of MBD. The dashed line is the control case i.e. no inhibitor.

Taking into consideration that the dashed line represents the already discussed control case, that is the steel response in 0.5% H₂SO₄ without any kind of corrosion inhibitor (see Chapter 4 Section 4.3.1), it is clearly noticeable that the MBD presence leads to a significant ennobling of the corrosion potential and to a decrease of the corrosion current density, being both these trends dependent on the MBD concentration. According to Oguzie et al. [10] MBD is adsorbed on the steel surface and the organic layer formed in such way can provide a certain corrosion protection from the aggressive acidic environment. The above presented results confirm that MBD is able to inhibit the anodic process; no effects were instead detected on the cathodic process, being the cathodic potentiodynamic curves (not reported) almost overlapped to that of the control case.

In agreement with the above cited literature, also the two other organic compounds included into the preliminary screening, that is benzothiazole (BZT) and cysteine (CYS), resulted to be able to inhibit the anodic process. As a direct comparison of their responses ,fig. 5.2 shows the three anodic polarization curves for MBD, BZT and CYS at the concentration of 1 mM.

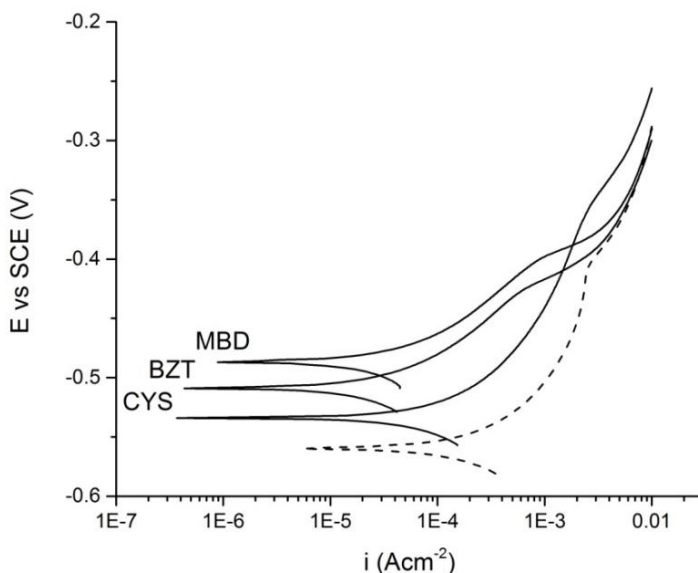
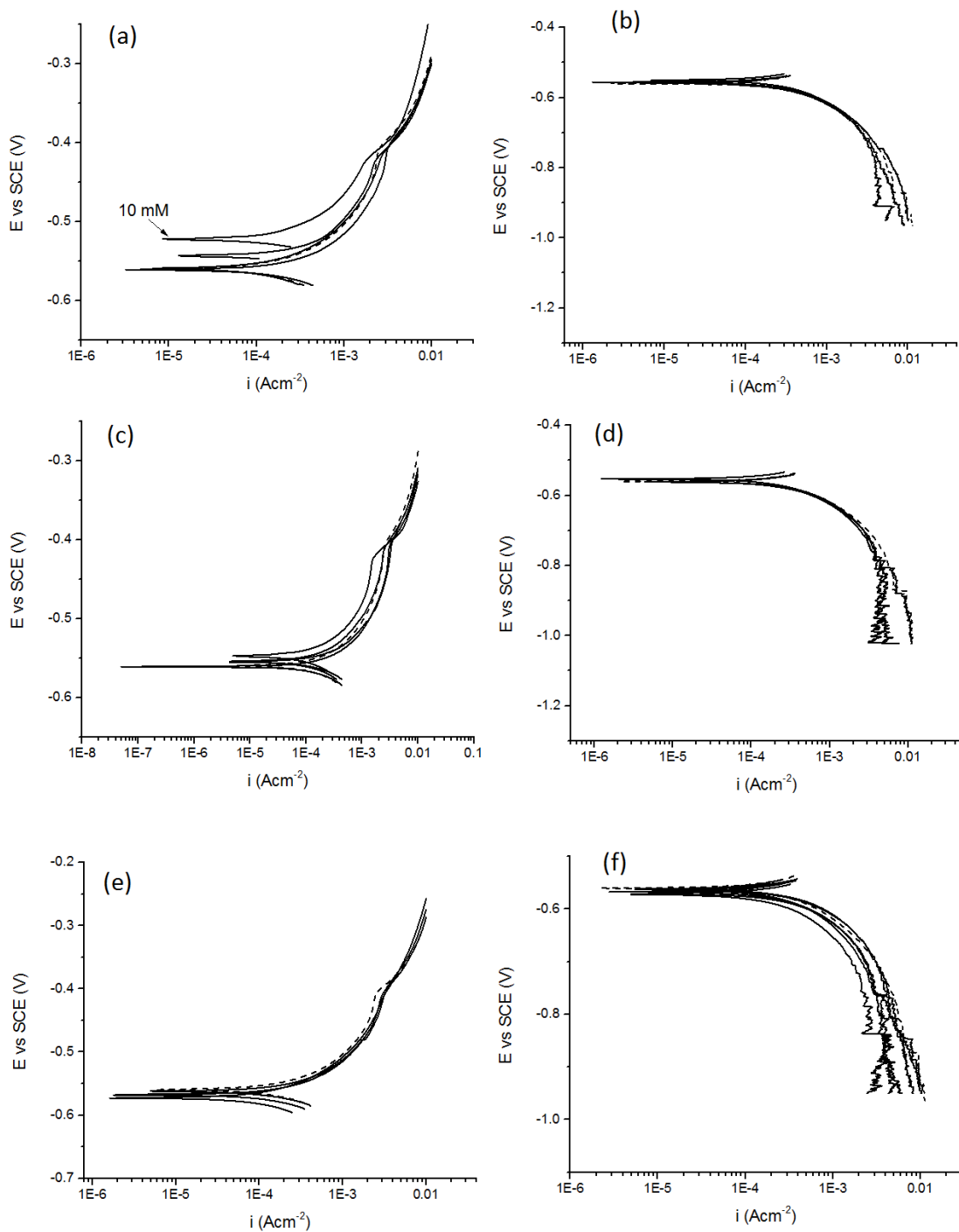


Fig. 5.2: Anodic potentiodynamic polarization of B450C carbon steel in a 0.5% diluted solution with methylene blue dye, benzothiazole and cysteine 1mM. The dashed line is the control case.

The most significant increase in terms of corrosion potential was obtained in the case of MBD. Furthermore, MBD resulted to guarantee the lower current density until a potential of about -0.400 V vs. SCE. For such reasons, and taking into consideration the two previously discussed MBD advantages over the other organic inhibitors, the former was chosen for further experimentation concerning its impregnation into an inorganic hosting matrix.

Anodic and cathodic potentiodynamic polarizations, performed in the presence of different concentrations of the inorganic inhibitors are reported in Fig. 5.3. In the case of sodium molibdate (Fig. 5.3(a,b)) no effects were detected on the cathodic process, while a slight inhibition of the anodic one was recorded only at the higher concentration, that is 10 mM. As can be easily observed from Fig. 5.3(c,d), the presence of cerium nitrate did not affect neither the anodic nor the cathodic process, thus proving to be completely ineffective in terms of corrosion protection of steel in diluted sulfuric acid solutions. Similarly to the previous case, also di-sodium phosphate, although indicated in literature as effective against chloride induced corrosion, did not show any protective effect in the strongly acidic environment of the present measurements. Among the inorganic corrosion inhibitors, the most interesting case was undoubtedly that of tri-sodium phosphate; similarly to the above discussed case of DSP, the presence of TSP had no effects on the anodic curves, but it significantly affected the cathodic ones, leading to a decrease in the current density of more than one order of magnitude with respect to the control case. Although different types of phosphate salts have been extensively used for corrosion inhibition in RC structures, the protection mechanism is still not fully understood. It is believed that the salt hydrolyzes in aqueous media and then phosphate ions react either with metal ions resulting from the onset of a corrosive process [1], or with other

ions such as Ca^{2+} [8,25], in both case a protective film precipitating on the steel surface. In fully agreement with the experimental evidences, such layer is claimed to be effective by limiting the access of dissolved oxygen to the metal surface [26].



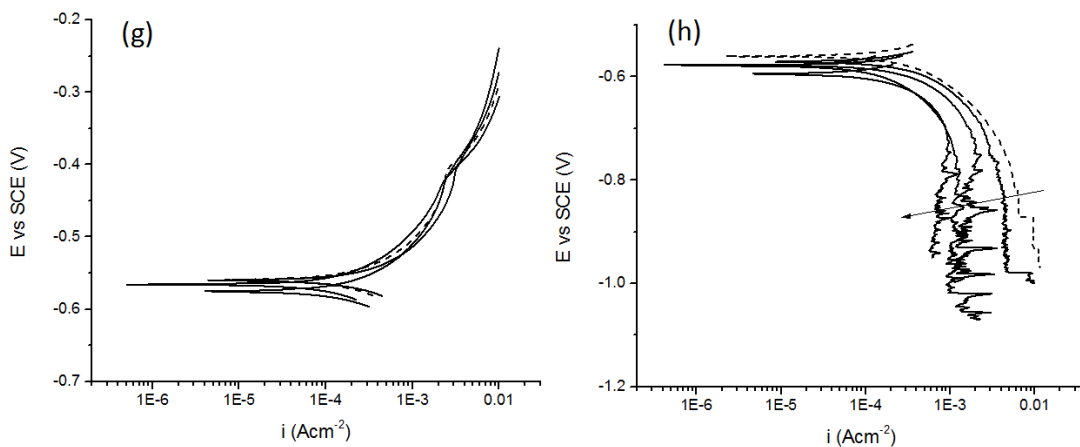


Fig. 5.3: Anodic and cathodic potentiodynamic polarization of B450C carbon steel in a 0.5% diluted solution with different amount of inorganic inhibitors (solid lines). The dashed line is the control case, without any addition. (a,b) SMD, (c,d) CNT, (e,f) DSP, (g,h) TSP.

After the anodic polarizations, the steel surfaces were observed at the optical microscopy aiming to investigate how the different inhibitors affected the corrosion morphologies. Fig.5.4 shows the appearance of the steel surfaces of the relevant tests above presented (inhibitors concentration 1 mM), at two different magnifications: 50X and 500X.

As expected, and as previously described in Chapter 4, Section 4.3.1, the control case (Fig.5.3 (a,b)) was characterized by a very rough surface, due to the generalized corrosion attack induced by the sulfuric acid solution. However, some spots are also clearly visible at higher magnification where a localized attack occurred.

The presence of 1mM MBD significantly affected the surface morphology. Fig. 5.3(c) shows an higher level of heterogeneity, if compared to the previous case. Large areas of the surface, characterized by a brighter colour, presented a smooth surface where the polishing lines were still detectable, but darker areas, probably due to the presence of corrosion products, were also observed. The higher magnification picture of Fig. 5.3 (d) confirmed the presence of a barely attacked surface together with some deep and well defined pits.

Pictures after the anodic polarizations in the presence of SMD and TSP (Fig 5.3 (e-h)) resulted to be rather similar to each other and not extremely different from those of the control case. Such similarities are in agreement with the electrochemical measurements of Fig. 5.3, where it is clearly shown that for the concentration of 1mM the curves for both SMD and TRP overlapped that of the control case.

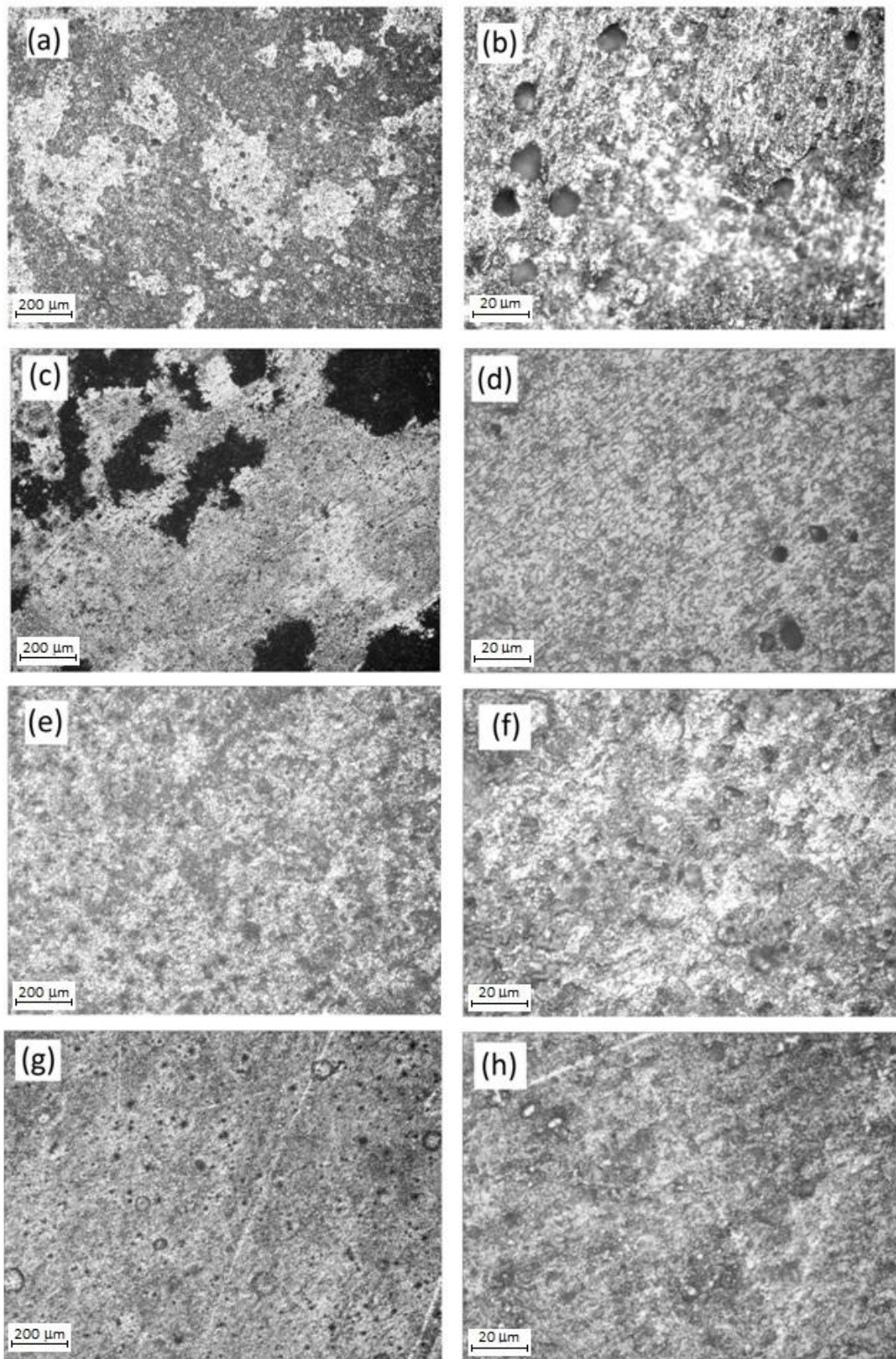


Fig. 5.4: Optical microscopy pictures of the steel surface after the anodic polarizations in 0.5% H_2SO_4 . Left row: magnification 50X, right row: magnification 500X. (a,b) control case, (c,d) MBD 1mM, (e,f) SMD 1mM, (g,h) TSP 1mM.

Open circuit potentials of steel samples exposed to both the inhibited and non-inhibited sulfuric acid solutions are reported in Fig. 5.5. The inhibitor concentration was 1mM except for the case of SMD, according to which anodic polarizations showed an inhibitive effect only at the higher concentration; thus the 10 mM experiment was added to the series.

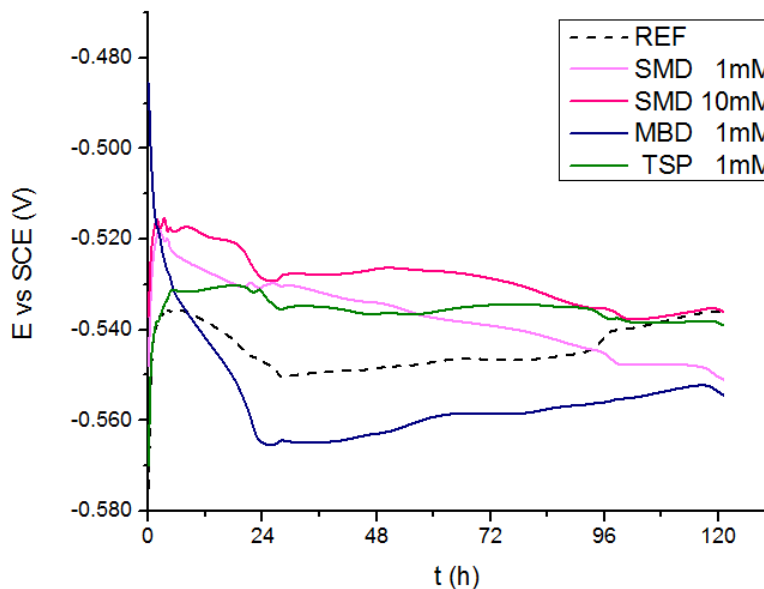


Fig. 5.5: Five days monitoring of the OCP evolution for B450C carbon steel in 0.5% H_2SO_4 and in presence of different corrosion inhibitors.

In all cases, except for that of MBD, corrosion potentials started from very negative values, around -0.570 V vs. SCE, and had a fast increase during the first minutes of immersion. Such an increase could be attributed to the formation of some corrosion products on the freshly polished surface of the steel samples. After the initial rise, the OCP remained rather stable especially in the control case and in the TSP case, being the corrosion potential of the latter slightly more anodic than that of the former. Steel samples immersed in the SMD containing solution exhibited instead a slow and regular decrease overtime. The higher concentration of 10 mM led to an almost negligible increase of the OCP with respect to the case of the lower (1mM) concentration. Coherently with the results from the anodic polarizations, the MBD presence led to a subitaneous ennobling of the OCP, but it drastically decreased in the subsequent hours getting stable after a one day immersion at a more negative value as compared to that of the control case.

Fig.5.6 shows pictures from the optical microscopy as performed after the five days of OCP monitoring above discussed. Although maintaining some similarities with the previously described pictures of Fig. 5.4, the naturally occurring corrosion during a longer conditioning time led, in most cases, to a more severe damage, if compared with the accelerated corrosion induced by potentiodynamic anodic polarizations.

The non-inhibited control case (Fig. 5.6a) showed the already described rough surface, but the spots of localized corrosion coalesced leading to a very deep attack; similar morphologies were also detected in the case of SMD for both the lower and the higher concentrations, reported in Fig.5.6(c) and 5.6(d), respectively.

When MBD was added to the solution, similarly to the case of the anodic polarization, large areas of the active surface resulted to be extremely well protected, even better than in the case of the anodic polarization. However, still some black deposits of corrosion products pointed out a non completed protection of the surface. In the case of TSP, as shown in Fig.5.6(e), at the end of the 5th conditioning day, the steel surface resulted to be homogeneously rough, because of the generalized attack, but not as damaged as the control case, thus pointing out a good protection offered by tri-sodium phosphate.

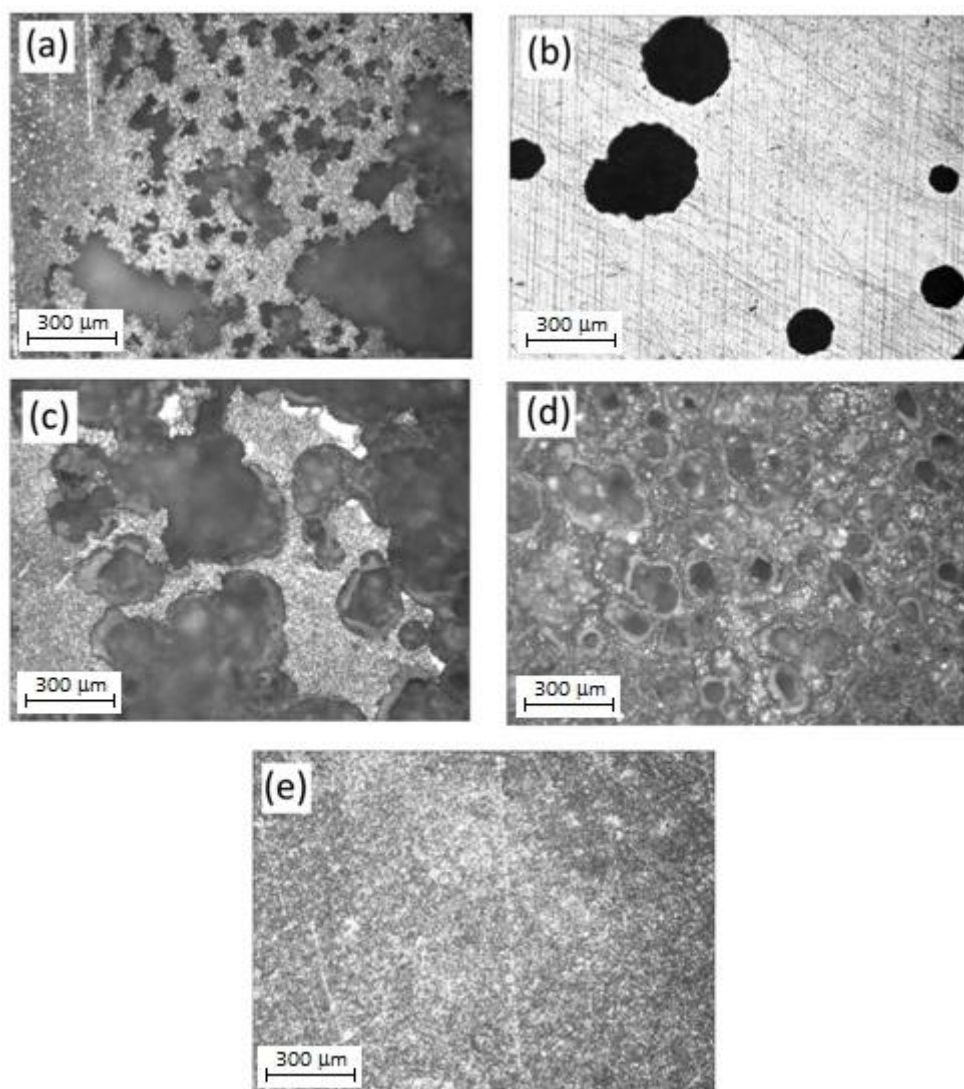


Fig. 5.6: Optical microscopy pictures of the steel surface after the 5 day OCP monitoring in 0.5% H_2SO_4 . Magnification 50X. (a) control case, (b) MBD 1mM, (c) SMD 1mM, (d) SMD 10mM, (e) TSP 1mM.

In order to conclude the preliminary screening of the selected corrosion inhibitors, steel samples prepared as in Chapter 4, Section 4.2.1 were conditioned for 10 days at 30°C in the diluted sulfuric acid solution in the presence of three inhibitors (MBD, SMD, TSP) at two different concentrations, and the weight loss was calculated at the end of the testing period (Fig. 5.7).

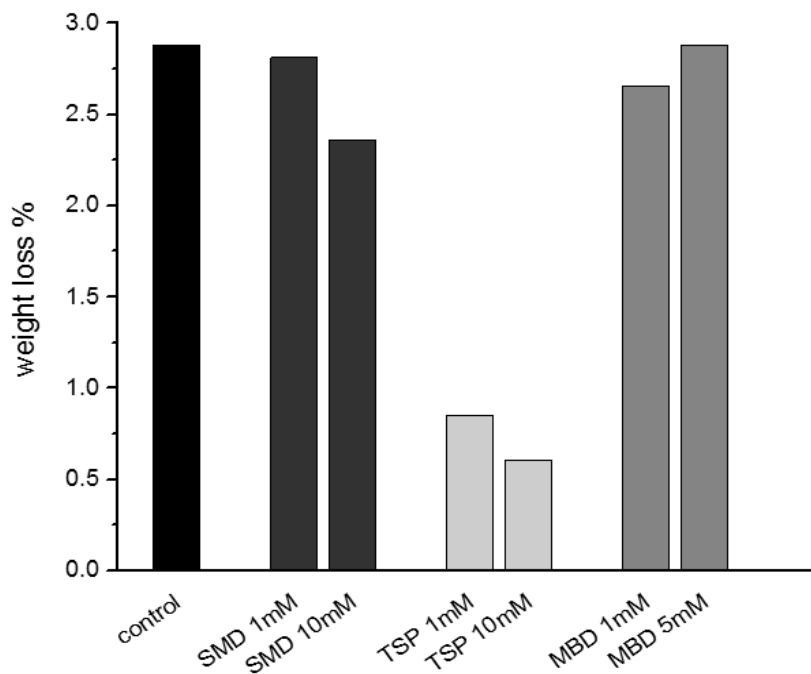


Fig. 5.7: Steel rebars weight loss, after 10 days of immersion in 0.5% H_2SO_4 . Effects of different inhibitors concentrations.

Coherently with what emerged from the potentiodynamic anodic polarizations reported in Fig. 5.3(a), the SMD effect resulted to be negligible at the lower concentration of 1mM, while a slight protection was detected by increasing the inhibitor concentration up to 10 mM. A significant decrease in the weight loss measurements were detected for tri-sodium phosphate. Such results are fully in agreement with the reduced cathodic current densities shown in Fig. 5.3(h) and with the homogeneous, generalized corrosion observed in Fig. 5.6(e). In the case of MBD, although the potentiodynamic anodic polarizations pointed out a significant decrease of the current densities, both the optical microscopy observations and the weight loss measurements seemed to indicate a certain deterioration of the steel samples. Motivation for such a behaviour could arise from the fact that every MBD molecule, being positively charged, bears a chloride ion as a counterion. The organic molecule, being adsorbed on the steel surface, protects it, while chlorides are well known for their corrosion stimulation. Notwithstanding the ambiguous effect of MBD, it was chosen to continue the experimentation with such organic molecule, because of its dye nature that would simplify the release monitoring from an inorganic host.

In conclusion, among the different inhibitors tested, methylene blue dye and tri-sodium phosphate showed the most promising results, and were selected for further experimentation aiming to develop a "smart" inhibitive system.

The smartness of the inhibitor deals with its ability to release the active compounds only when triggered by a significant pH decrease, such as that induced by the biogenic acidity. Thus, as described in Section 5.2.3, MBD was incorporated into two different inorganic reservoirs: a calcium carbonate based matrix, expected to be inactive from the corrosion point of view, and calcium phosphate based matrix, whose dissolution should deliver the phosphate ions, actively protecting the steel rebar from corrosion.

5.3.2. Characterisation of the hybrid inhibitive systems

Both the as synthesized hybrid compounds were characterized by means of XRD. Analyses were performed on both the MBD loaded and unloaded form of each compound. As the results showed that in either cases the presence of the organic molecule do not affect the crystalline structure, Fig.5.8 reports X-ray diffractogram of the unloaded forms only.

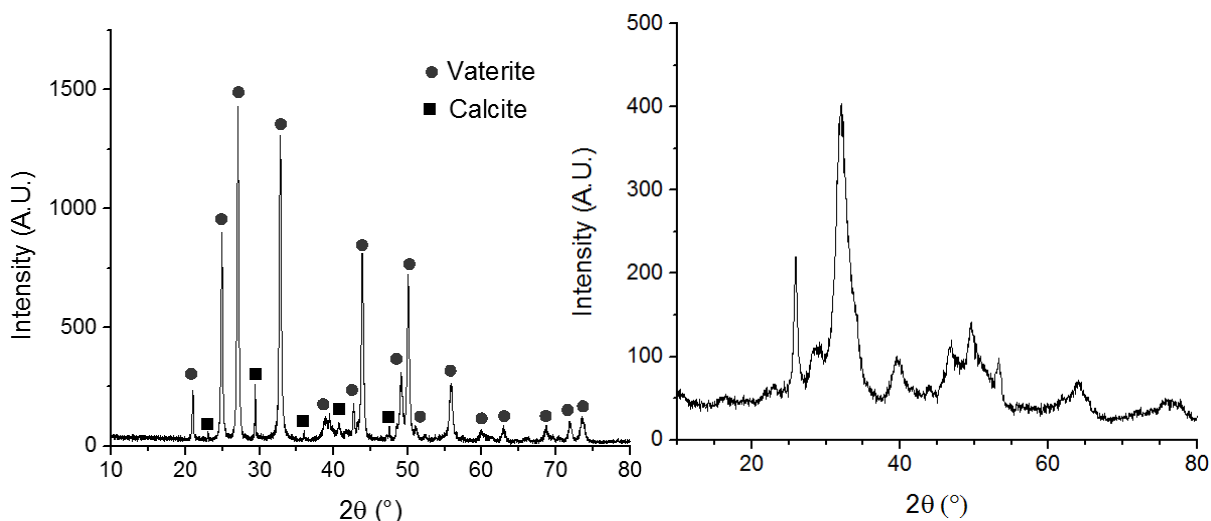
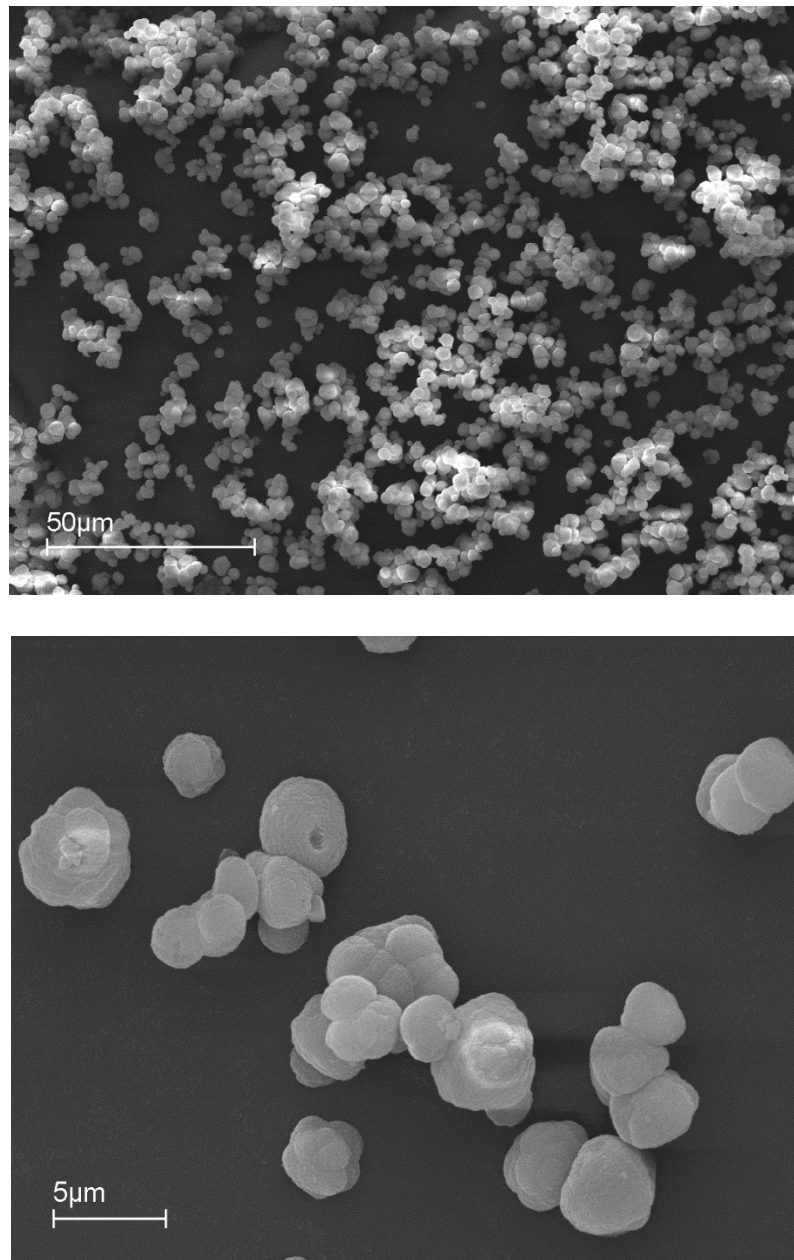


Fig. 5.8: X-ray diffractograms of the unloaded compounds, (a) Calcium carbonate based powder, (b) Calcium phosphate based powder.

The sharp and well defined peaks of Fig.5.8(a) indicated an highly crystalline structure, and according to the diffractogram library the main signals corresponded to the vaterite pattern. However, some less intense peaks were also detected and attributed to the calcite response. As above mentioned, among the calcium carbonate polymorphs, vaterite and aragonite are not thermodynamically stable; thus

it is not at all surprising that during the synthesis a small amount of calcite, that is the only stable form, was obtained.

SEM pictures of the Vaterite powder are shown in Fig. 5.9. From such images, it can be clearly noticed that the spherical shape of vaterite is absolutely predominant; however, as represented in Fig. 5.9(c), a few layered and rhombohedral calcite crystals can be found.



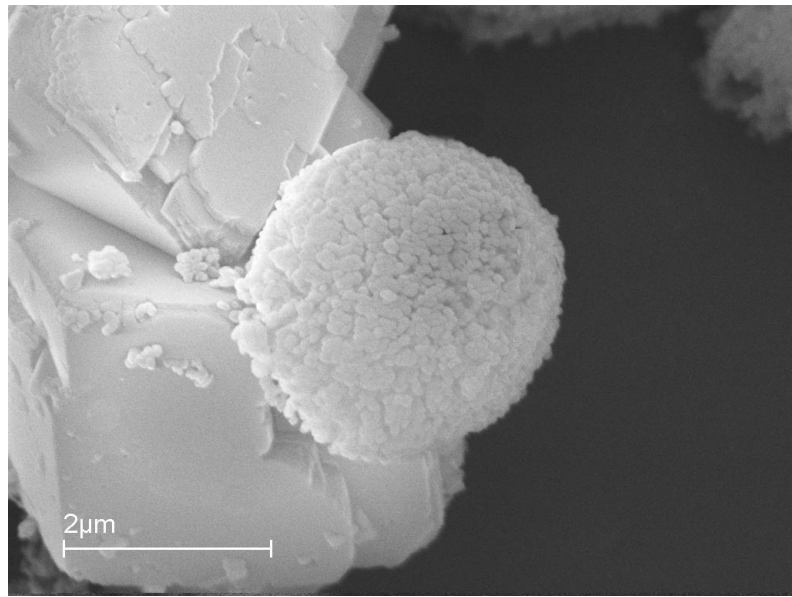
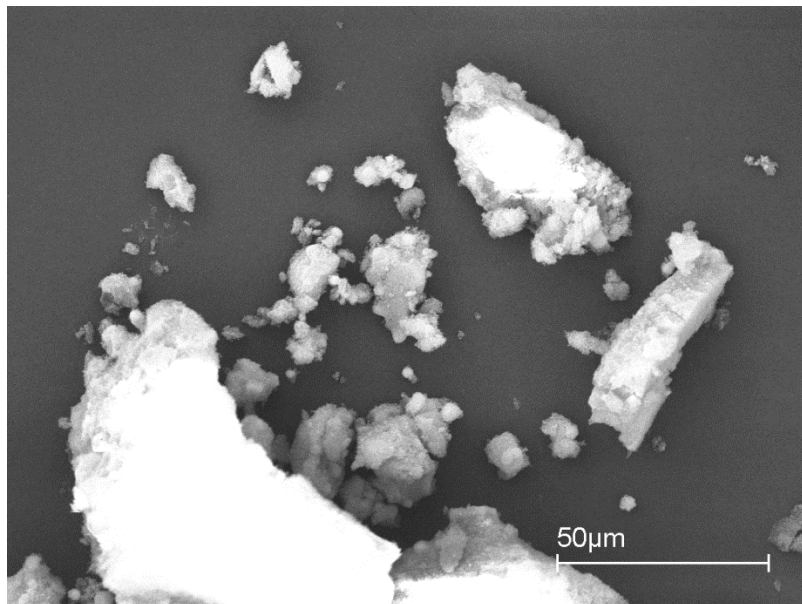


Fig. 5.9: SEM pictures of the unloaded Vaterite.

The X-ray diffractogram of the calcium phosphate based powder, shown in Fig. 5.8(b) was characterized by lower peak intensities and broader, less defined signals if compared to the vaterite ones; such features are commonly attributed to poorly crystalline structures. The signal identification pointed out the presence of hydroxylapatite and calcium hydrogen phosphate, whose XRD pattern are almost overlapped.

SEM pictures of the as synthesized hydroxylapatite, before mechanical grinding, are reported in Fig. 5.10. Differently from the homogeneous dimensions and spherical shape of vaterite, hydroxylapatite exhibited an highly irregular shape.



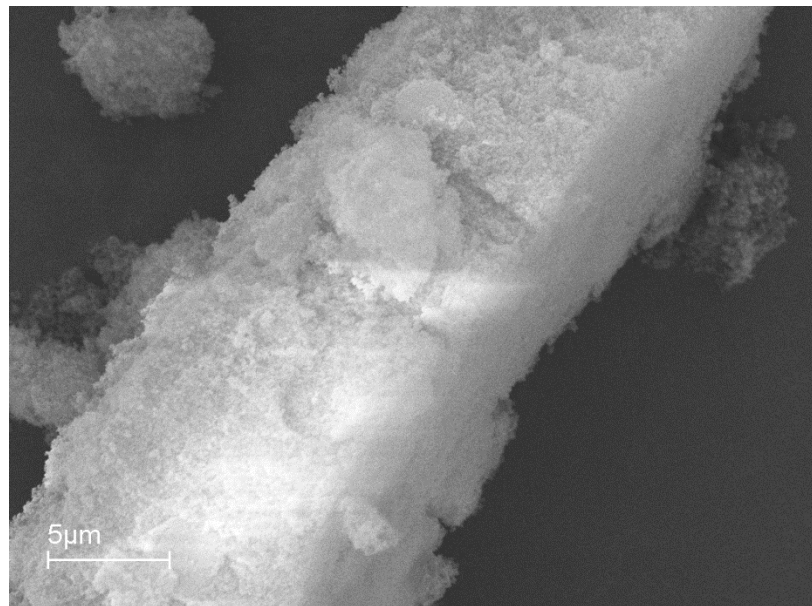


Fig. 5.10: SEM pictures of the as synthesized hydroxylapatite.

Porosity, although not being the only determining factor, definitely plays a key role in the loading capacity of a material; the BET surface area of the unloaded vaterite and hydroxylapatite are reported in table 5.2.

Table 5.2: Vaterite (VAT) and hydroxylapatite (HAP) BET surface area.

SAMPLE	BET surface area
Vaterite	$1.90 \pm 0.01 \text{ m}^2/\text{g}$
Hydroxylapatite	$84.3 \pm 0.6 \text{ m}^2/\text{g}$

The HAP surface area resulted to be significantly higher if compared to the VAT one. Because of the low surface area of the VAT powder, the pore size distribution determined by the nitrogen desorption isotherm cannot be considered as reliable, while the same elaboration for HAP data is reported in fig 5.11. Histograms representing the pore size distribution were centered around 12 nm, that is in the range of the mesoporous materials.

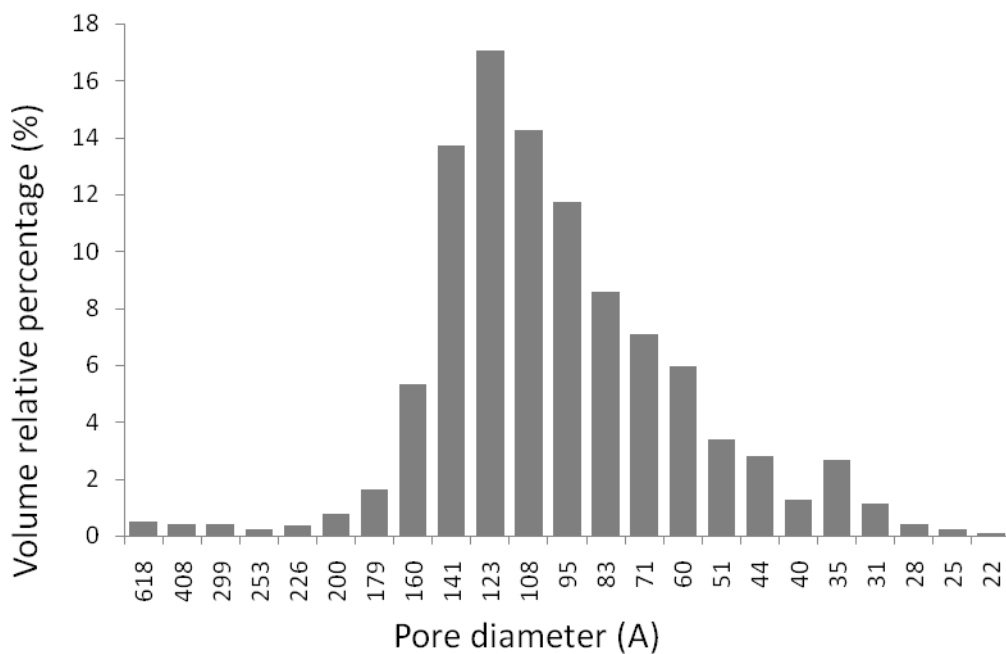


Fig. 5.11: Pore size distribution of the HAP powder.

The loading capacity of the two MBD-loaded hybrid systems were determined by means of spectrophotometric measurements of a strongly acidic solution, in which a precise amount of the inhibitor was completely dissolved. The results, reported in table 5.3, were in fully agreement with BET data, thus pointing out a significantly higher loading capacity for the more porous HAP with respect to the less porous VAT. Furthermore, a confirmation of the reliability of such results can be found in literature [18], where the same vaterite microbeads, but impregnated with salicylaldoxime instead of MBD resulted to have a loading capacity of 0.010 wt%.

Table 5.3: Loading capacity of the hybrid systems.

SAMPLE	Loading Capacity
Vaterite	0.014 wt%
Hydroxylapatite	6.95 wt%

The same procedure as for the determination of the loading capacity, but using solutions of different pH ranging from 12.6 to 1.3, allowed to determine the profile of the pH dependent release of methylene blue dye. Such data are reported in Fig.5.12

for the MBD-VAT hybrid system. In the same picture the equilibrium diagram of calcium carbonate in an aqueous solution calculated by means of MEDUSA software [27] is also plotted.

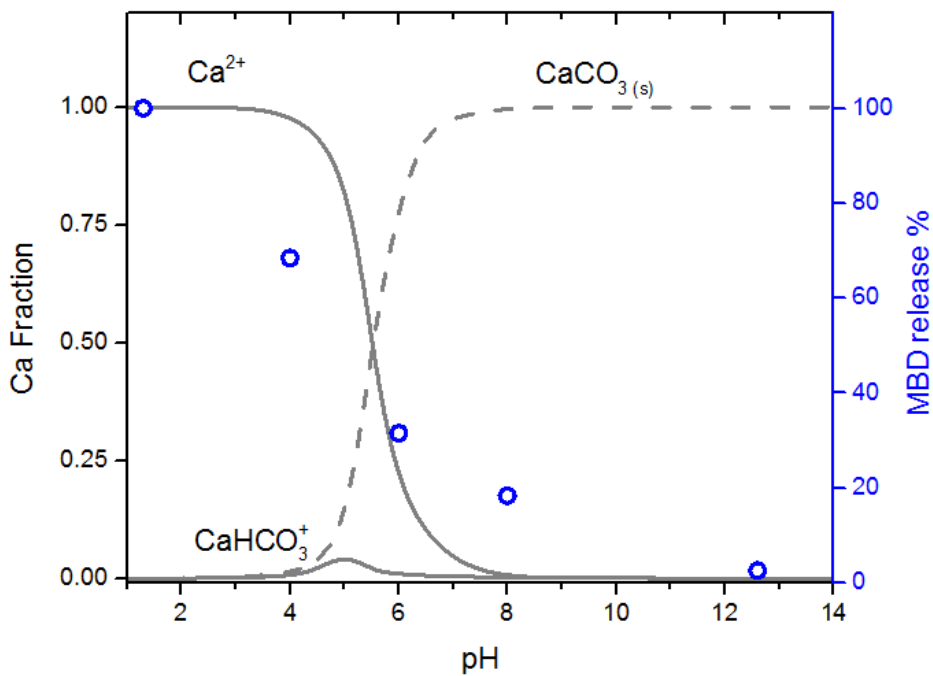


Fig. 5.12 Spectrophotometric determination of the pH dependent MBD release from the VAT hybrid. Equilibrium diagram of a calcium carbonate solution, dashed lines represent solid species, while continuous lines represent aqueous species.

The experimental data, related to the MBD release, outlined a sigmoidal shape extremely similar to that of Ca^{2+} ions resulting from the calcium carbonate dissolution, thus confirming that the latter was the main and the only responsible mechanism for the MBD delivery.

A similar plot, but related to the HAP based hybrid, is shown in figure 5.13; differently from the previous case the inhibitor release followed a double step mechanism with an initial liberation of a small amount of dye occurring around pH 10 and a second one taking place at pH 3.

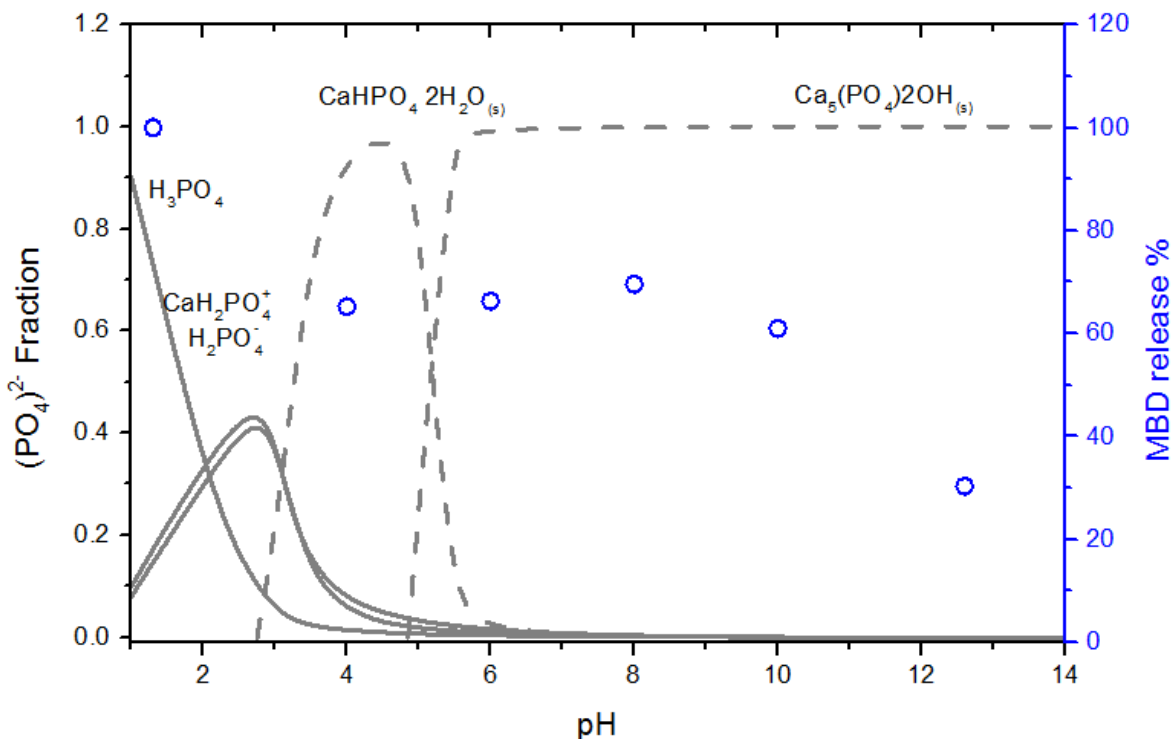


Fig. 5.13: Spectrophotometric determination of the pH dependent MBD release from the HAP hybrid, and equilibrium diagram of a calcium phosphate solution. Dashed lines represent solid species, while continuous lines represent aqueous species.

As can be clearly seen by the superimposition of the equilibrium diagram, the lower pH release is consistent with the complete dissolution of the two solid phases, both of them detected through the XRD analysis (Fig.5.8(b)). A reasonable explanation for the mechanism involved in the initial dye release occurring at the more alkaline pH was found by means of the PZC determination.

Results from the mass titration method are reported in Fig 5.14, and clearly showed a stabilization of the response, corresponding with the PZC, occurring at pH 8.95; such value resulted to be rather similar to that measured for a differently obtained HAP [28].

The point of zero charge is a concept relating to the phenomenon of adsorption, and it describes the condition when the electrical charge density on a surface is zero. As a general rule, when the pH is lower than the PZC value, the adsorbent surface is positively charged, conversely, above PZC the surface is negatively charged. In the present case, taking into consideration that the MBD molecule is positively charged, at pH more alkaline than 9 (above PZC) electrostatic attractive forces are developed between the organic molecule and the negatively charged HAP surface. As a consequence of acidification leading to a pH lower than 9 (below PZC), the HAP surface turned from negative to positive, thus transforming the attractive forces into repulsive ones and consequently causing the initial MBD release.

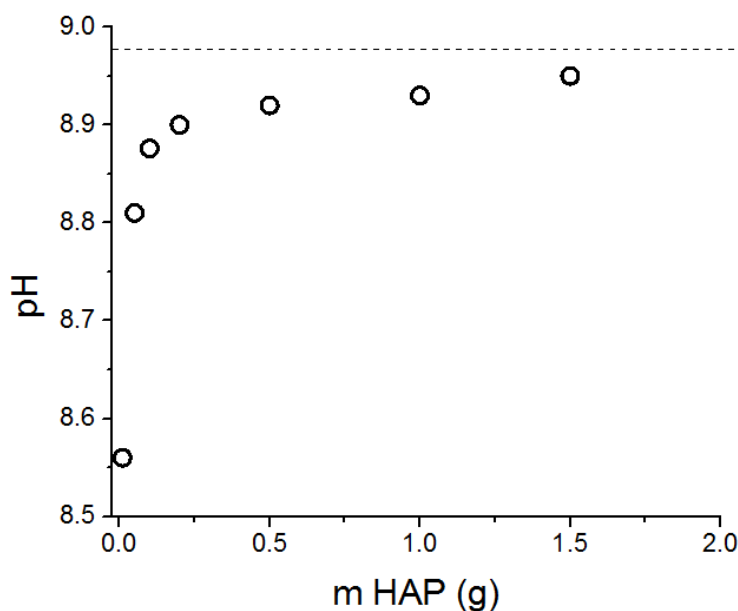


Fig. 5.14: Mass titration data of HAP in a 0.5 M KNO_3 solution.

In conclusion, two different inorganic hosting matrices, based on calcium carbonate (VAT) and calcium phosphate (HAP) were successfully synthesized and impregnated with methylene blue dye. The HAP, having an easier synthesis as it did not require any organic template, resulted also to have an higher porosity area and thus an higher storage capacity if compared with the vaterite microbeads. Furthermore, the dissolution of the MBD-HAP hybrid, leads to the release of both the organic molecule and phosphate ions, both of them having inhibitive properties, as clearly demonstrated in section 5.3.1 of the present chapter.

For such advantages, MBD-HAP was chosen for further experimentation aiming to assess the inhibitive properties of the hybrid system in model media.

5.3.3. Steel response in model medium in the presence of MBD-HAP

Acidic environment

As above mentioned, the main feature that unbalanced the preference towards HAP hybrid systems was the fact that together with the organic molecule also the inorganic hosting matrix resulted to have inhibitive properties, thus the final protection efficiency being affected by both the compounds.

Such thesis was confirmed by means of anodic and cathodic potentiodynamic polarizations by adding to the diluted sulfuric acid solution 1 mg/mL of either the impregnated MBD-HAP or the unloaded HAP (Fig. 5.15).

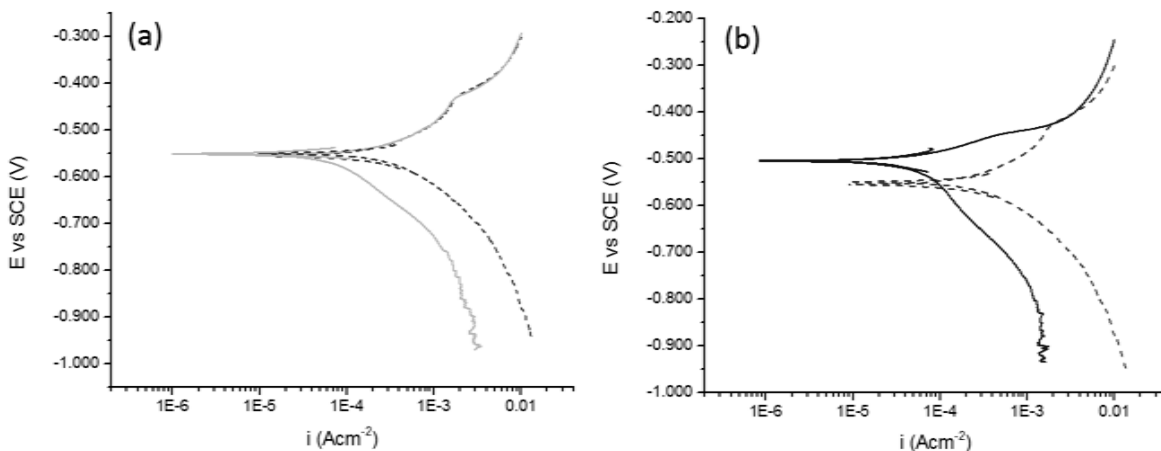


Fig. 5.15: Anodic and cathodic potentiodynamic polarization of mild carbon steel in a 0.5% diluted solution of sulfuric acid containing: (a) HAP 1 mg/mL, (b) MBD-HAP 1 mg/mL. The dashed lines are from the control case.

In the case of the unloaded HAP, shown in Fig. 5.15(a), coherently with the findings of Section 5.3.1 in the present chapter, the anodic curve perfectly overlapped that of the control case, thus pointing out that the hydroxyapatite dissolution did not affect the anodic process; while the cathodic curve showed a significant decrease in terms of current density. Conversely, the MBD loaded HAP hybrid system resulted to affect both the anodic and the cathodic processes, thus confirming the double effect due to the two different components.

In order to get more insight into the protection mechanism, and to know how the different components of the MBD-HAP hybrid singularly interact with the steel surface, a four day electrochemical monitoring campaign was performed by means of LPR and EIS on four different samples: the control case without any inhibitor (REF), the un loaded inorganic matrix 1 mg/mL (HAP), the impregnated hybrid 1 mg/mL (MBD-HAP) and also methylene blue dye alone (MBD) at the concentration of 0.07 mg/l. Such concentration was defined on the basis of the previously determined loading capacity of $\approx 7\%$, aiming to check which are the effects of the same amount of organic dye introduced in the other cases, but without the presence of the inorganic matrix.

Values of the polarization resistances, calculated from LPR measurements, are reported in figure 5.16. The two data sets, related to HAP and to the control case (REF) resulted to be very similar to each other, being both characterized by a continuous decrease in the R_p values that was attributed to the onset of a corrosion process. Such behavior pointed out that the inorganic hosting matrix alone, did not seem to guarantee an efficient protection.

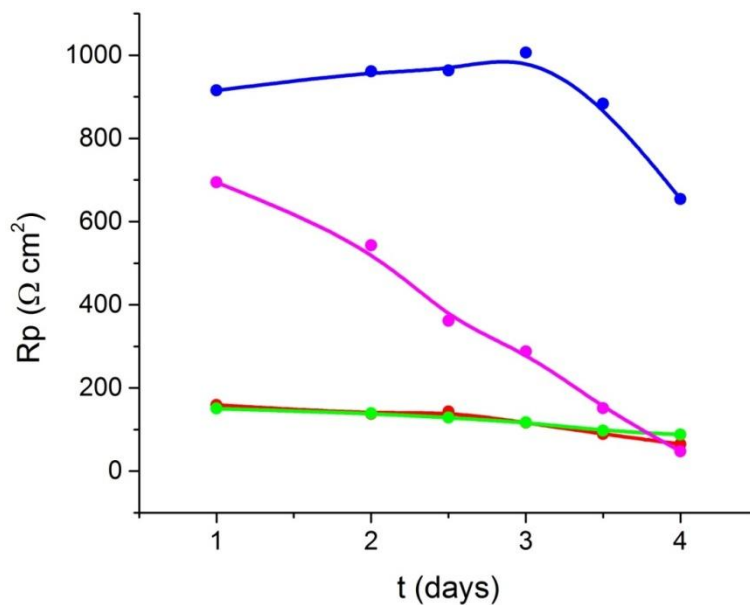


Fig. 5.16: Polarization resistances resulting from LPR monitoring of mild steel in 0.5% H_2SO_4 solution. ● REF, ● HAP 1 mg/mL, ● MBD-HAP 1 mg/mL, ● MBD 0.07mg/mL.

When MBD alone was added to the aggressive solution, the electrochemical response resulted to be characterized by an initial improvement of the steel performance, as indicated by higher polarization resistances. However, such values showed a fast decrease along the duration of the monitoring campaign and reached those of the HAP and the control case within the fourth day of monitoring. The decrease of the polarization resistance, being related to an increase of the corrosion current could be attributed to the already mentioned presence of chloride counterions, together with the MBD molecules. Such aggressive ions could be able to fast penetrate through the organic protective layer and thus inducing localized corrosion processes. Conversely, the MBD-loaded system exhibited higher R_p values, if compared to other cases and a certain stability in the response, at least for the first three days, after which the polarization resistance started to decrease although remaining more than 600 Ω higher than the control case. This latter case seems to suggest that the combination of MBD and HAP gives far better results than those of the two components singularly used.

Fig. 5.17 shows the representative Nyquist and Bode plots of mild steel in the diluted sulfuric acid solution. The Nyquist plot is characterized by a depressed semicircular shape, whose dimensions decrease with time. Such depressed shape is commonly reported in the literature for similar systems and is attributed to a frequency dispersion effect due to the roughness and inhomogeneity of the steel surface[12,29,30]. Together with the reducing dimensions of the depressed semicircular response in time (Nyquist plot, Fig.5.17a), a remarkable decrease of the impedance modulus was detected at the lower frequencies in the Bode plot (Fig. 5.17b); both these features pointing out the onset and propagation of a corrosion process.

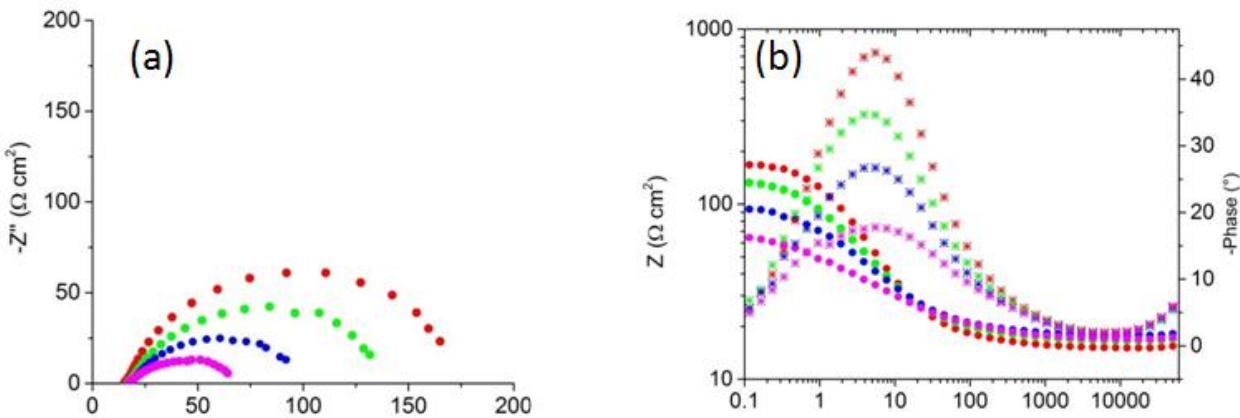


Fig.5.17: Nyquist and Bode plots of mild steel in 0.5% H_2SO_4 solution.
 ● day 1, ● day 2, ● day 3, ● day 4.

When the HAP powder was added to the sulfuric acid solution in a concentration of 1mg/mL, the pattern of the EIS response (Fig. 5.18(a,b)) did not substantially change with respect to the above described case. However, the slightly higher values of the real impedance in the Nyquist plot and of its modulus in the Bode plot confirmed the HAP beneficial effect. Such a slight improvement of corrosion resistance would not be sufficient to justify the use of HAP as a corrosion inhibitor. However, it is worth mentioning, that in the present approach, the primary role of HAP is to provide a pH sensitive reservoir, while, although relevant, the beneficial effects resulting from its dissolution, play a secondary role. Fig.5.18(c-d) shows the evolution of the EIS spectra as MBD is directly added to the acidic solution in a concentration of 0.07 mg/mL. In these latter plots, significant differences were detected with respect to the previous cases. Although keeping the semicircular shape and the decreasing values of $|Z|$ with time, a larger scatter was observed between the first and the last measurement; the former pointing out a certain protection of the surface, while the latter indicating an even worst behaviour if compared to the corroding control case of Fig. 5.17.

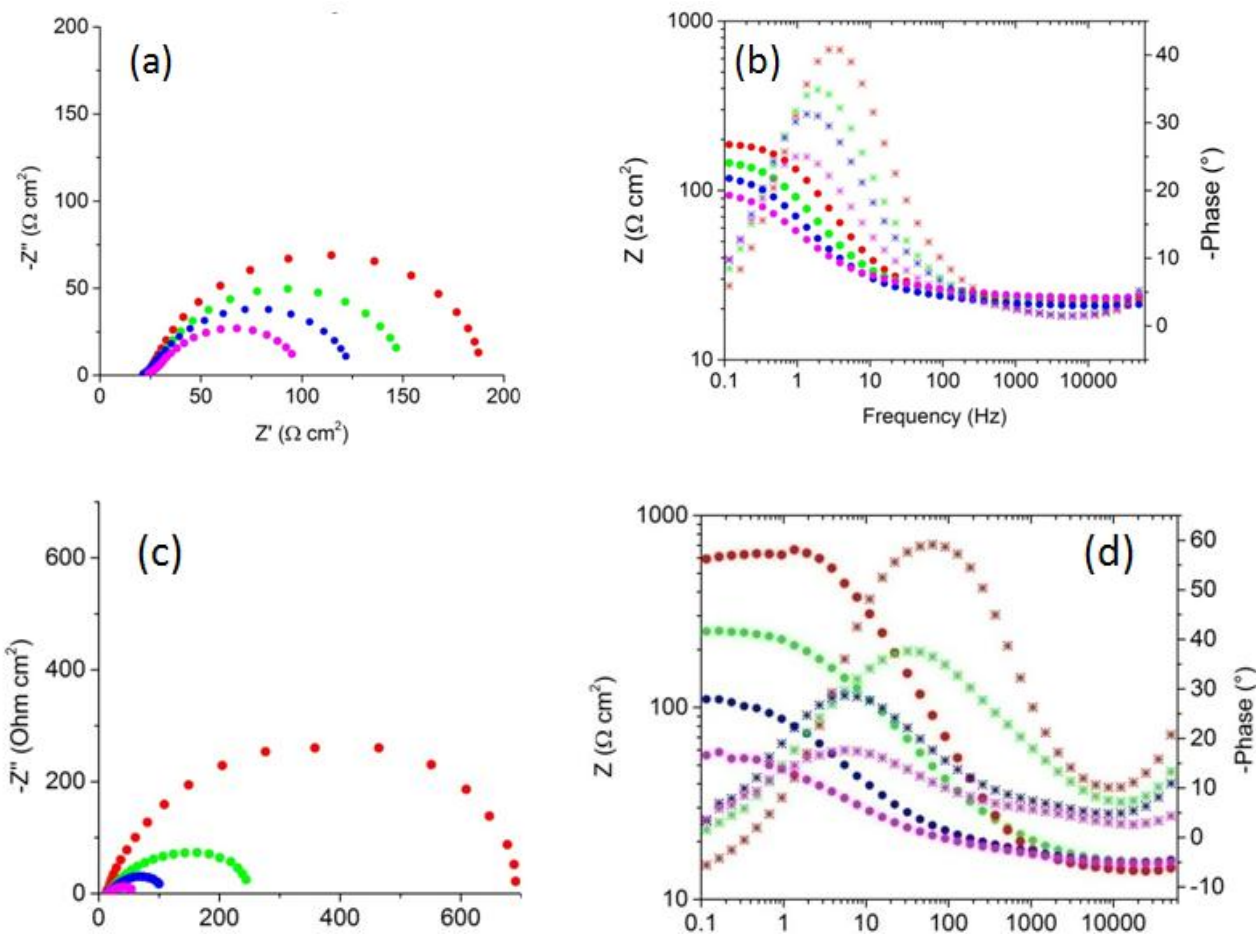


Fig. 5.18: Nyquist and Bode plots of mild steel in 0.5% H_2SO_4 solution: (a,b) HAP 1 g/L, (c,d) MBD 0.07 g/L. ● day 1, ● day 2, ● day 3, ● day 4.

The EIS response of the steel electrodes in model acidic solution, containing the MBD-HAP hybrid, are reported in Fig.5.19. Conversely to the above described trends, but coherently with LPR data, a rather stable response of the system was detected in the first three days, while in the fourth day a slight decrease of the impedance was recorded. However, values remained significantly higher, as compared to those in the previous cases. Such behaviour seems to indicate that the synergetic effect of MBD and HAP, together with the ability of HAP to provide a slow release of the organic dye (MBD), can provide a good protection of the steel.

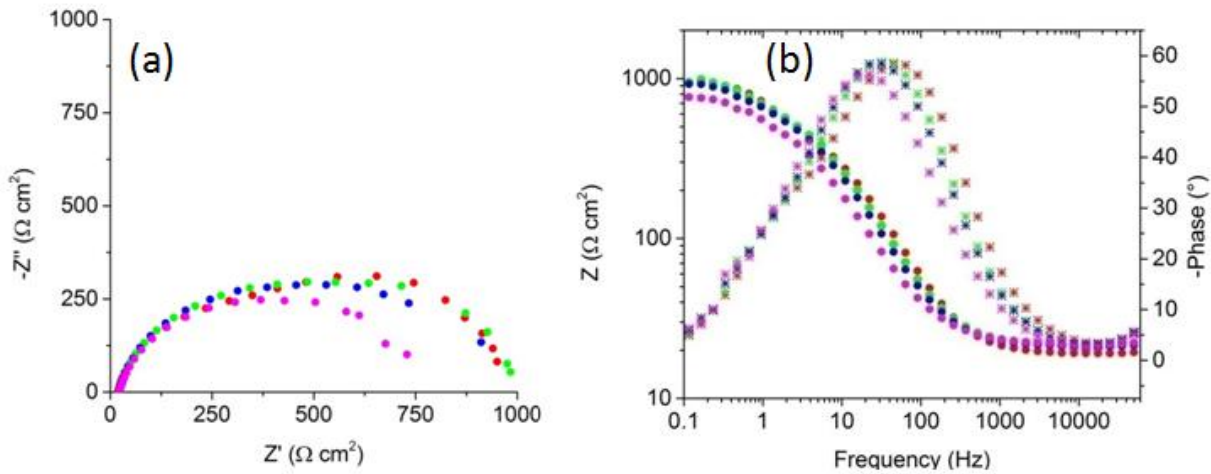


Fig. 5.19: Nyquist (a) and Bode (b) plots of mild steel in 0.5% H_2SO_4 solution containing the MBD-HAB hybrid 1 g/L. ● day 1, ● day 2, ● day 3, ● day 4.

In order to gain more insights into the protection mechanism and its efficiency, the above presented EIS data were fitted with the equivalent electric circuits shown in Fig.5.20. According to literature, most of the studies dealing with steel corrosion inhibition in sulfuric acid, simplifies the EIS data interpretation by using a single time constant circuit as that reported in Fig. 5.20(a) [12,30], eventually nesting a RL (resistance, inductance) circuit in order to more appropriately fit the lower frequencies portion of EIS spectra. [29,31]

When hydrochloric acid is used instead of sulfuric acid, a two time constant circuit, characterized by two nested RC circuit is commonly used for the fitting of experimental data [32-34]

A simple Randles equivalent circuit i.e. single time constant circuit (Fig. 5.20(a)) was used in the case of the uninhibited H_2SO_4 solution as well as in the HAP containing one, thus suggesting that the mild steel corrosion in such acidic environment was mainly controlled by a charge transfer process. The electrochemical response in presence of MBD, both alone and within the inorganic hosting matrix, resulted to be more complex, and required a two time constant equivalent circuit (Fig.5.20(b)) to be optimally fitted.

In the two circuits of fig. 5.20, R_s represents the electrolyte resistance, R_1 CPE₁ are related to the charge transfer resistance R_{ct} and the double layer pseudo capacitance CPE_{dl}, while the lower frequencies time constant R_2 CPE₂ describes processes related to MBD and MBD-HAP hybrid, i.e. adsorption of the organic molecule and alterations in the (corrosion) product layer on the steel surface. Constant phase elements (CPE) were used instead of pure capacitances as a generally accepted approach to account for surface heterogeneity and/or non-ideal capacitive response [12].

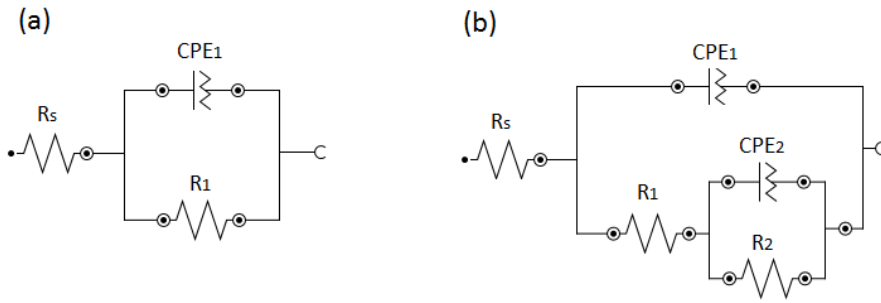


Fig. 5.20: Equivalent electric circuits used for the fitting of the experimental EIS data.

Fig.5.21 shows the evolution of the calculated best fit parameters. The solid lines represent the charge transfer resistance and the double layer pseudo-capacitance of the elements R_1 and CPE_1 , while dashed lines are related to the calculated values for the low frequencies time constant R_2 , CPE_2 , a color code differentiates the samples.

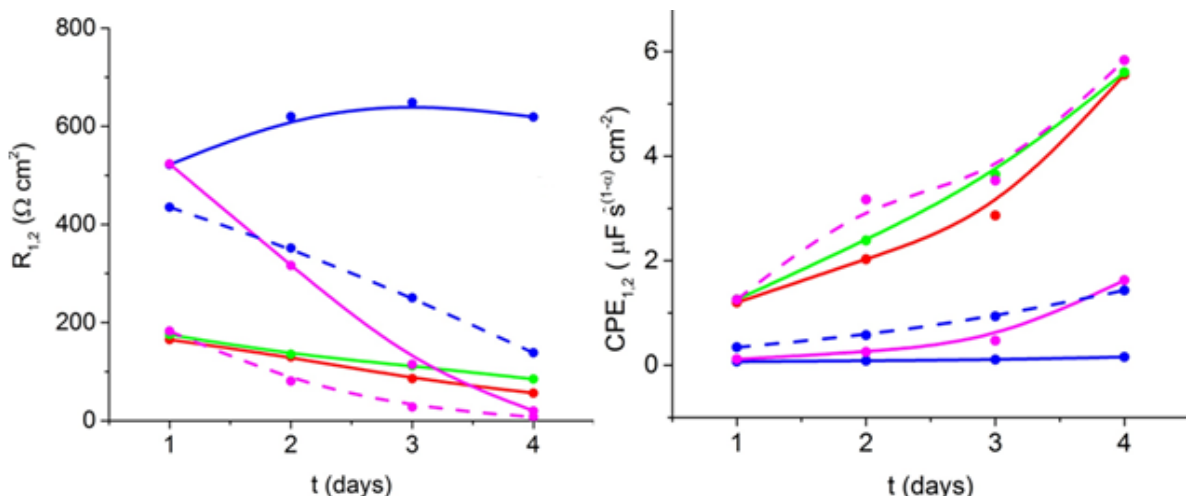


Fig. 5.21: Fitting of EIS spectra: (a) resistances, (b) pseudo capacitances. ● REF , ● HAP 1g/L , ● MBD 0.07 g/L, ● MBD-HAP 1 g/L (continuous line: R_1 , CPE_1 . dashed lines: R_2 , CPE_2).

In the case of the non-inhibited sample, as reflected by the trend of the Nyquist and Bode plots above discussed, a continuous decrease of the R_{ct} and a parallel increase of the CPE_{dl} were detected. Both these features can be attributed to the response of an active, corroding steel surface. The presence of HAP induced minor changes in values of the circuit components, leading to a slight increase of the R_{ct} , thus indicating a very small improvement in terms of corrosion resistance. The double layer pseudo-capacitance instead remained slightly higher than that of the control case, confirming that in such conditions the phosphate ions were not able to create an efficient protecting layer.

A significantly different behavior was obtained in the presence of the MBD alone. In such case, coherently with indications from the Nyquist and Bode plots, a large

difference was recorded between the first and the last measurement. The charge transfer resistance of the MBD containing experiment resulted to be almost three times higher than the one of the reference system on the first day, but decreased until reaching the values of the corroding sample on the fourth monitoring day. Conversely, the double layer pseudo-capacitance, although having a shift to higher values over time remained significantly lower than the control case.

The double layer capacitance is generally attributed to the local dielectric constant and/or the integrity of the adsorbed inhibitor layer on the metal surface [30]. The above presented time dependent increase could be consequently attributed to the deterioration of the protective organic layer, leading to the onset of steel dissolution reaction. The low frequencies time constant, representing the electrochemical response attributed to the adsorbed MBD layer (dashed lines in Fig. 5.21) was characterized by lower values of the resistance and higher values of the pseudo-capacitance if compared to R_{ct} and CPE_{dl} , but still maintaining the respectively decreasing and increasing trend previously described for the former. Such a response could be interpreted as due to the presence of chloride ions that penetrated through the organic layer, thus inducing localized corrosion processes. Furthermore, it is worth mentioning that such explanation would also fit with the drastic R_p decrease previously described.

In the case of the MBD loaded hybrid the high frequency time constant showed a stable behavior in terms of both charge transfer resistance and double layer pseudo-capacitance, being the former and the latter significantly higher and lower than the reference case, respectively. Such values could be attributed to an efficient protection offered by the synergic action deriving from the HAP dissolution and MBD release.

The low frequency time constant, showed a pattern similar to that above discussed for MBD alone. However, the values of resistance and pseudo-capacitance in this latter case, remained respectively higher and lower than the MBD alone case, thus pointing out that in the presence of the hybrid system the chloride effect is limited and the overall electrochemical response is that of a protected surface. Such synergic effect of MBD and HAP could be attributed to an initial role played by the hydroxylapatite leading to a more homogeneous surface, as shown in Section 5.1(Fig.5.3 (e)), thus granting a more ordered and effective packing of the organic molecules resulting in a more efficient protection.

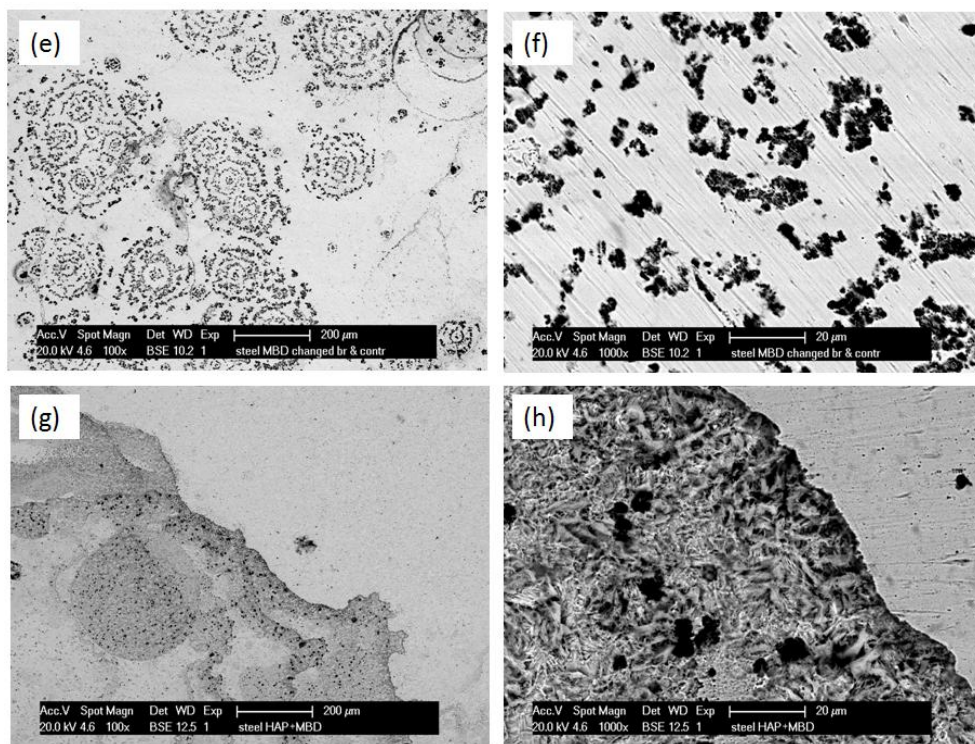
At the end of the conditioning period, the corrosion morphology was examined by means of a scanning electron microscopy; pictures of the steel surfaces at two different magnifications are reported in Fig. 5.22.

Similarly to the optical pictures previously described in Section 5.3.1, SEM micrographs for the control case (Fig. 5.22(a-b)) showed a rough surface typical of a generalized corrosion attack. When HAP was added to the solution a similar pattern

was obtained, but characterized by a significant increase in homogeneity (Fig.5.22(c-d)).

As expected, a completely different corrosion morphology was detected in the case of the MBD alone (Fig. 5.22(e-f)). In such case the adsorbed organic layer was able to protect the steel from the generalized corrosion induced by sulfuric acid, leaving a very clean surface where the polishing lines were still detectable. However, chlorides introduced into the solution together with MBD easily passed through the inhibitor barrier leading to an extensive localized corrosion .

Finally, in fully agreement with all the electrochemical measurements, the steel sample conditioned in the MBD-HAP acidic solution exhibited a generally smooth and protected surface. Nevertheless some defects of considerable dimensions were found, as clearly shown in Fig. 5.22(g-h), being the morphology, of these corroded areas, somewhat between the control and the HAP alone sample.



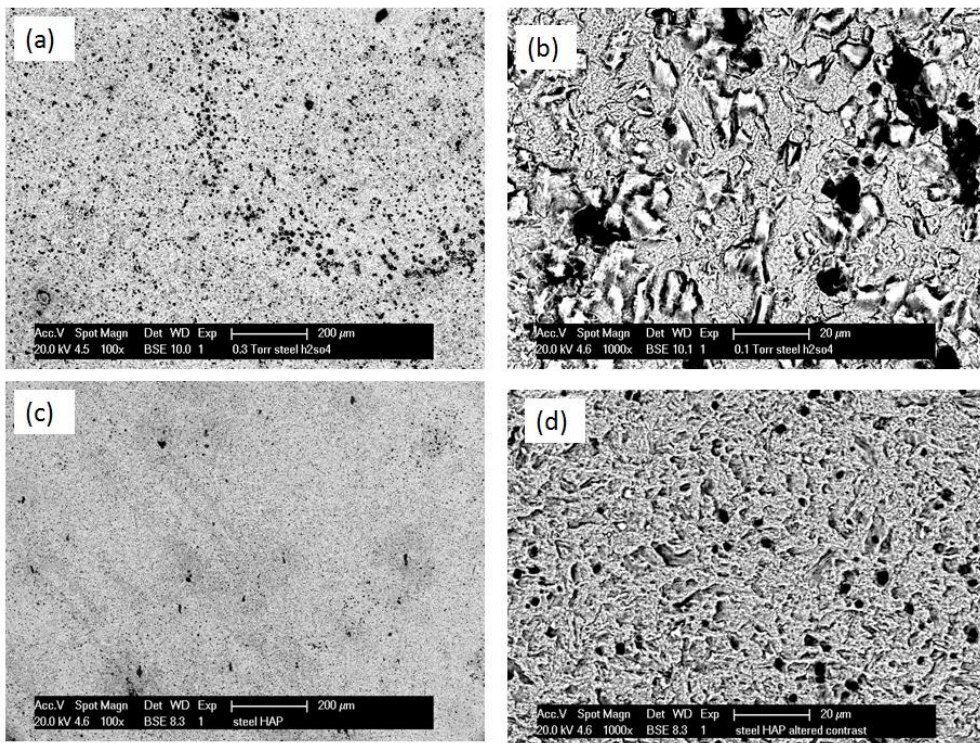


Fig. 5.22: SEM pictures of the steel surface after a four days conditioning in diluted sulfuric acid solution. (a-b) control. (c-d) HAP 1 mg/mL. (e-f) MBD 0.07 mg/mL. (g-h) MBD-HAP 1 mg/mL.

In conclusion, all the performed tests seem to indicate that beneficial effects are obtained by the combination of the anodic organic inhibitor with the cathodic inorganic one, resulting in an hybrid characterized by a mixed protective effect. Conversely to the literature findings [10-11], MBD alone does not result to be a valid inhibitor as it displaces from the less severe generalized corrosion to a more insidious localized attack. However, phosphate ions, released as a consequence of the inorganic matrix dissolution, significantly limited such a drawback.

Alkaline environment

Considering that the final objective of the present study is that of synthesizing a "smart" inhibitor for reinforced concrete structures, before activation, it is expected to remain exposed for long time to extremely alkaline environment due to the nature of concrete. Thus, it seemed important to test if the presence of such compounds can affect the steel passivation process.

At the highly alkaline pH of sound concrete the HAP should not dissolve and thus, although a small release of MBD superficially adsorbed is possible during the cement hydration, the bigger fraction is expected to remain entrapped into the HAP inorganic matrix. For such a reason, differently from test in acidic environment, only three cases will be considered:

- Saturated Ca(OH)₂ solution (pH 12.6) as control case

- HAP 1 mg/mL in sat Ca(OH)₂
- MBD-HAP 1 mg/mL in sat Ca(OH)₂

Fig.5.23 shows the polarization resistance values calculated from LPR measurements along the four days of the monitoring test.

All the samples exhibited an increasing trend of the values with time, indicating the growth of the oxide layer. Rp values for the control case resulted to have slightly higher values but differences with the other cases were not as big as to justify any kind of concern.

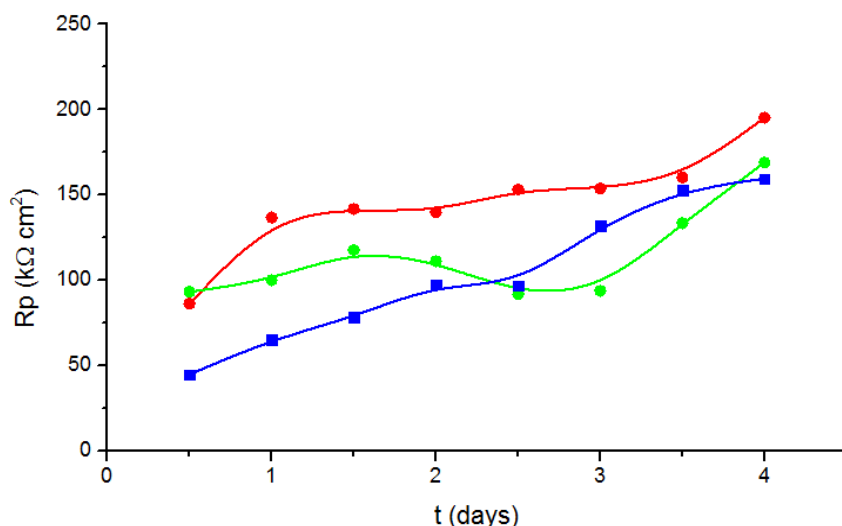


Fig. 5.23: Polarization resistances resulting from LPR monitoring of mild steel in saturated Ca(OH)₂ solution. ● REF, ● HAP 1 mg/mL, ■ MBD-HAP 1 mg/mL.

Nyquist and Bode plots resulting from the EIS monitoring are shown in Fig. 5.24. Also in this case there are just minor differences among the three cases. Similarly to EIS spectra already described in Chapter 3, Section 3.3.3, Nyquist plots were characterized by partial and depressed semicircles of increasing dimensions as time passed, indicating increasing resistances as a consequence of the oxide growth. Furthermore, as expected , in all cases the electrochemical responses tended to a stabilization over time. Nyquist plots for HAP and the MBD-HAP (Fig. 5.24(c,e)) resulted to have slightly smaller radius, if compared to the control case, thus indicating that the inhibitor presence implies a decrease in terms of resistances. From the point of view of the Bode plots, instead, no significant differences were detected among the three cases under investigation. As elsewhere detailed in the present thesis, impedance spectra of mild steel immersed in an alkaline environment are commonly fitted with a two time constants equivalent electric circuit as that shown in fig.5.20(b). The initial Rs accounts for the electrolyte resistance, the higher frequencies time constant (R1 - CPE1) is attributed to the charge transfer resistance and to the double layer pseudo-capacitance, while the low frequency time constant (R2 - CPE2) is attributed to redox reactions occurring within the oxide layer.

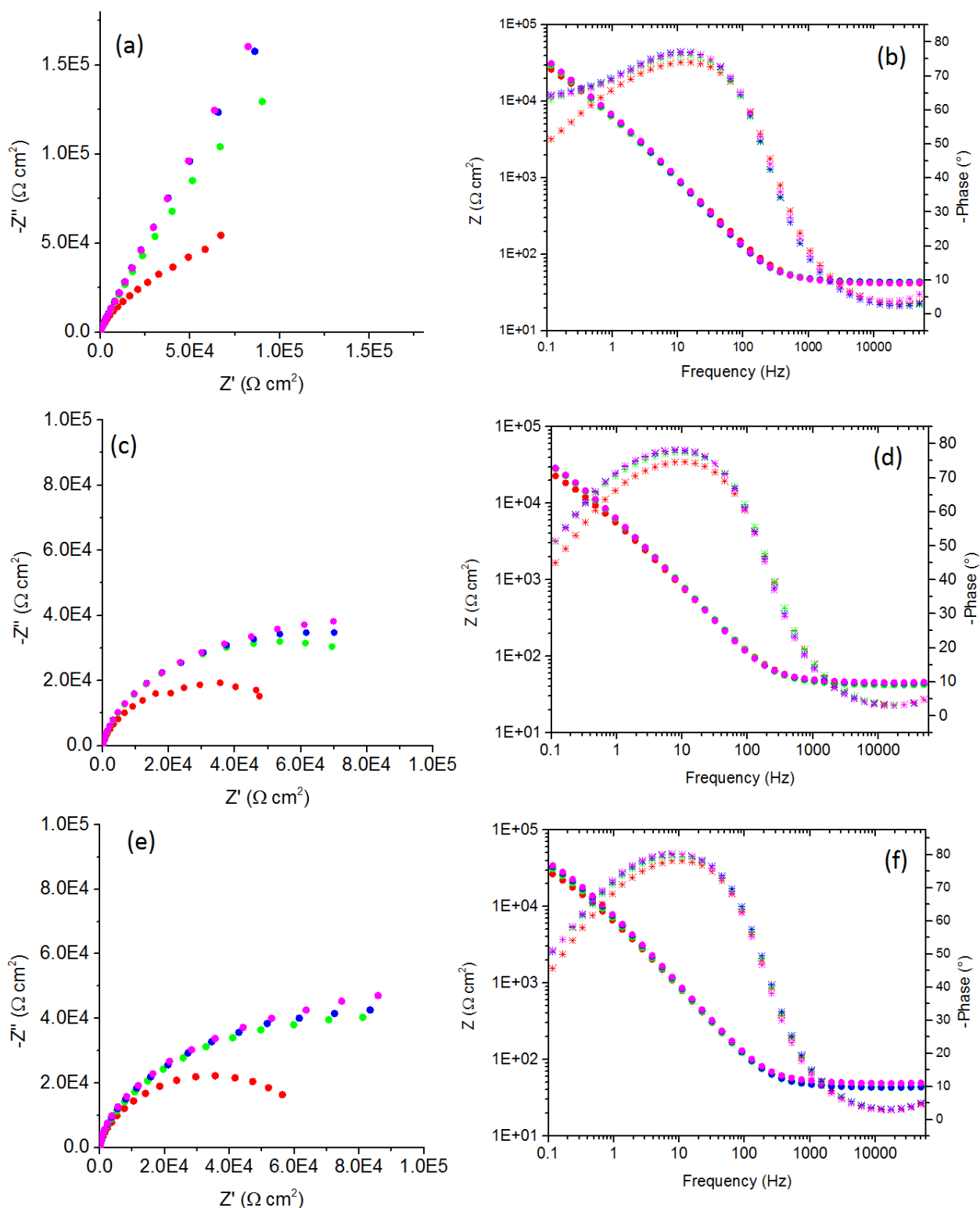


Fig.5.24: Nyquist and Bode plots of mild steel in saturated $\text{Ca}(\text{OH})_2$ solution.

(a-b) control case, (c-d) HAP 1 mg/mL, (e-f) MBD-HAP 1 mg/mL
 ● day 1, ● day 2, ● day 3, ● day 4.

Fitting of experimental data are reported in figure 5.25 and 5.26 showing resistances and pseudo-capacitances for the higher frequencies and for the lower frequencies time constants, respectively.

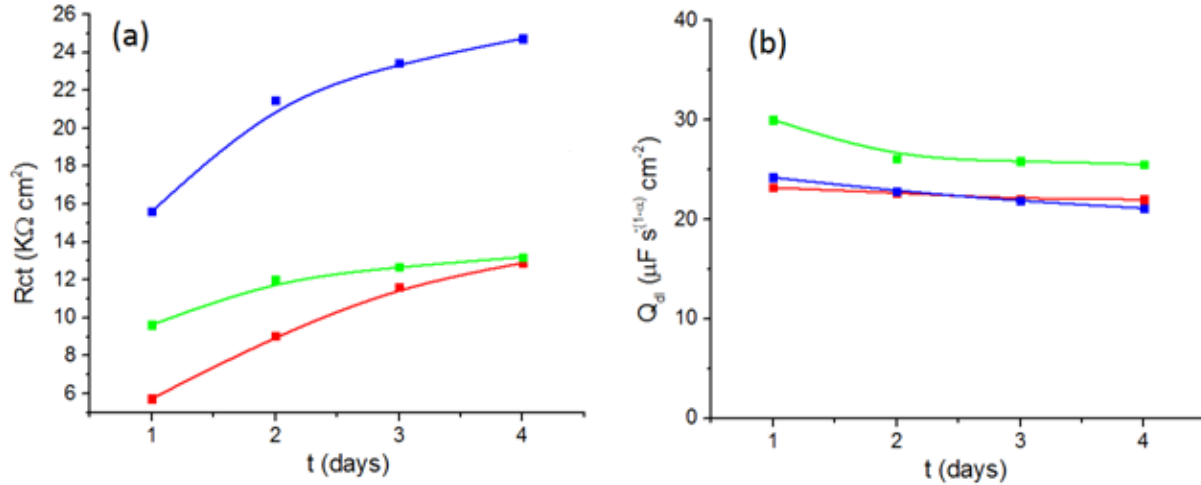


Fig. 5.25: Fitting of EIS spectra: (a) charge transfer resistance, (b) double layer pseudo capacitances. ● REF , ● HAP 1g/L , ● MBD-HAP 1 g/L.

All the charge transfer resistances (Fig. 5.25(a)) exhibited an increasing trend over time, the one related to the MBD-HAP case being higher with respect to the other two cases. Conversely, the double layer pseudo-capacitances resulted to be quite similar to each other, and their values of about $25 \mu\text{Fcm}^{-2}$ ($\alpha \approx 1$) suggested that the reason of these capacitances could be reasonably attributed to the double layer with the passive film. Furthermore, their slight decrease over time corresponded to the modification of passive film towards more organized and stable structure [35].

Similarly to the above described plots, also the pseudo-capacitances correlated with redox process of the oxide film were close to each other, while the related resistances, although having all an increasing trend, showed a significant scatter between the control case and the inhibited ones (Fig. 5.26).

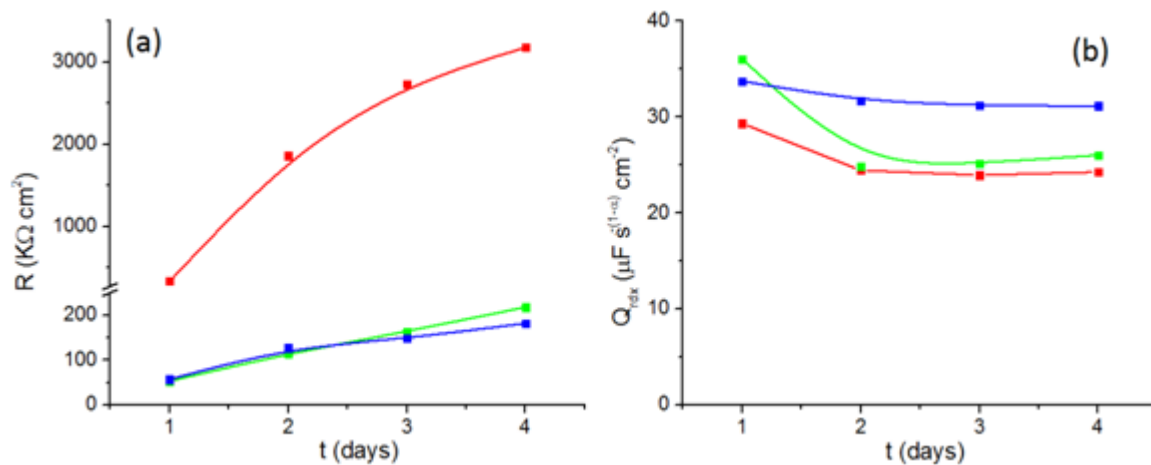


Fig. 5.25: Fitting of EIS spectra. Resistances and pseudocapacitances attributed to the lower frequencies time constant. ● REF, ● HAP 1g/L, ● MBD-HAP 1 g/L.

At the end of the conditioning period, coherently with the similarities of the electrochemical responses, the steel surfaces did not show any sign of deterioration or attack. However in order to get more insight into the possible effects that a small release of MBD could have on the steel passivation, a cyclovoltammetric experiment was performed as below detailed.

Ten voltammetric cycles were recorded expanding the scanned potential window until the limits of water stability; the control was just a saturated $\text{Ca}(\text{OH})_2$ solution, while in the other case MBD 0.03 mg/mL was added to the alkaline solution, thus simulating a release of half the loading capacity, possibly much higher than what expected in reality (Fig. 5.26).

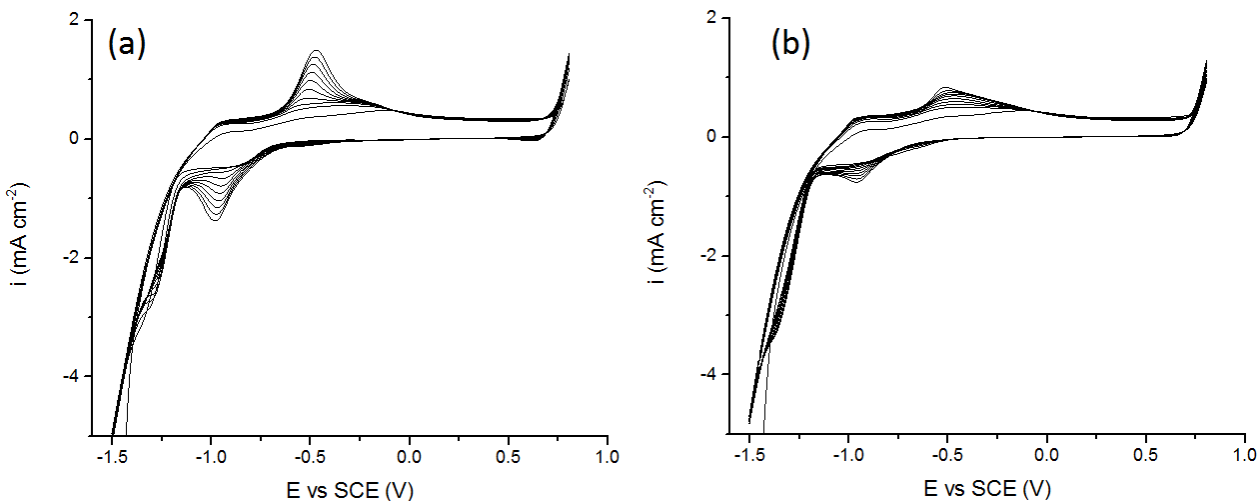


Fig. 5.26: Ten cycles voltammetries performed in sat. $\text{Ca}(\text{OH})_2$ solution at $v = 100 \text{ mV/s}$. (a) Control case, (b) MBD 0.03 mg/mL.

The cyclovoltammetric response of carbon steel in sat.Ca(OH)₂ solution was thoroughly discussed in Chapter 3. Presently, attentions were focused only on the two anodic peaks, the lower one at -0.9V vs. SCE attributed to Fe(II) formation and the higher one at -0.5 V vs. SCE attributed to magnetite formation. From the comparison of the two cyclovoltammograms of Fig.5.26, it can be clearly noticed that the main differences rely on the second peak, being characterized by significantly lower current densities when MBD was added to the solution; while no apparent differences were detected for the first peak.

For a further analysis of the voltammetric response, anodic charge accumulation of the two peaks was calculated through numerical integration of the experimental curves. Results are depicted in fig. 5.27.

The accumulation of the anodic charges gives a quantitative indication of the occurring reactions, the Fe(0) - Fe(II) reaction seemed not to be affected by the MBD presence; conversely, the magnetite formation, responsible of the passive layer, resulted to be slightly hindered by the organic molecule.

Such assumption was confirmed by lower currents detected in the cyclovoltammetries and by the higher R_p calculated from EIS measurements. In conclusion, although not having any harmful effect, it is probable that the small amount of MBD initially released by the hybrid as a consequence of the mixing in the aqueous environment is adsorbed of the freshly polished steel surface, thus delaying the formation of a stable oxide layer

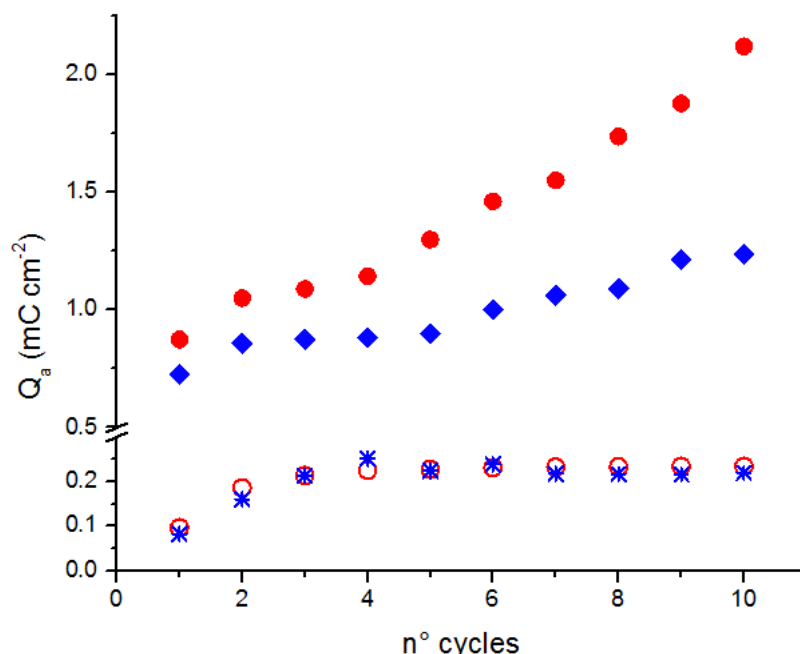


Fig. 5.27: Anodic charges calculated from integration of the voltammetric curves. (●, ♦) magnetite formation, (○, *) Fe(II) formation. Red symbols the control case, blu symbols MBD 0.03 mg/mL.

5.4 Conclusions

Aiming to develop an efficient smart inhibitor able to protect the steel rebars from corrosion induced by the acidification arising as a consequence of SOB, an initial screening of different inhibitors was performed in order to select the most promising ones.

Among all the tested inhibitors, trisodium sulfate was chosen because of its cathodic action and because of an already wide literature assessing its efficiency in RC structure protection. Furthermore MBD, although not resulting fully convincing because of the presence of chlorides as counterions, provided a good inhibition of the anodic process.

MBD was initially immobilized into a vaterite matrix, being its release fully due to the inorganic host dissolution occurring a pH lower than 6. However, because of the low porosity of vaterite, the storage capacity resulted to be extremely low.

A much more porous matrix was synthesized by reacting tri-sodium phosphate with a calcium salt, thus obtaining a highly porous, hydroxylapatite characterized by a higher loading capacity that could be easily impregnated with MBD.

In such way, together with the slow release of the organic molecule granted by the matrix dissolution, a further beneficial effect was obtained by phosphate ions liberated from the matrix itself.

Electrochemical tests performed in simulated acidic solutions pointed out a significant improvement of the corrosion resistance due to the synergic effect of the MBD-HAP system, while the components (MBD and HAP) do not provide a satisfactory protection if separately used.

Taking into consideration that such hybrid inhibitors should remain dispersed into the cementitious matrix and inactive for a long time, until a pH drop triggers the MBD release, a series of electrochemical tests were performed aiming to asses possible implications on the steel passivation. Results pointed out that a small release of the superficially adsorbed MBD was possible at early stage even at the more alkaline pH, and that could lead to a delay in the passive layer formation, being adsorbed on the steel surface. However, at the end of the test in the alkaline solution the steel surfaces were not affected by the inhibitor presence.

References

- [1] T.A. Soylev, M.G. Richardson, Corrosion inhibitions for steel in concrete: State of the art report, *Construction and Building Materials* 22 (2008) 609-622.
- [2] M. Diamanti, E. Perez Rosales, G. Raffaini, F. Ganazzoli, A. Brenna, M. Pedeferri, M. Ormellese, Molecular modeling and electrochemical evaluation of organic inhibitors in concrete, *Corrosion Science* (2015) 231-241.
- [3] C. Monticelli, A. Frignani, G. Trabanelli, A study on corrosion inhibitors for concrete application, *Cement and Concrete Research*, 30 (2000) 635-642.
- [4] M. Ormellese, L. Lazzari, S. Goidanich, G. Fuomagalli, A. Brenna, A study on organic substances as inhibitors for chloride induced corrosion in concrete, *Corrosion Science*, 51 (2009) 2959-2968.
- [5] G. Trabanelli, C. Monticelli, V. Grassi, A. Frignani, Electrochemical study on inhibitors of rebar corrosion in carbonated concrete, *Cement and Concrete research* 35 (2005) 1804-1813.
- [6] Y. Tang, G. Zhang, Y. Zuo, The inhibition effects of several inhibitors on reba in acidified concrete pore solution, *Construction and Building Materials* 28 (2012) 327-332.
- [7] M. Tommaselli, N. Mariano, S. Kuri, Effectiveness of corrosion inhibitors in saturates calcium hydroxide solutions acidified by acid rain components, *Construction and Building Materials* 23 (2009) 328-333.
- [8] D. Bastidas, M. Criado, V. La Iglesia, S. Fajardo, J.M. Bastidas, Comparative study of three sodium phosphate as corrosion inhibitors for steel reinforcements, *Cem. Concr. Comp.* 43 (2013) 31-38.
- [9] E.E. Oguzie, Y. Li, F.H. Wang, Effect of cysteine on the corrosion behaviour of low carbon steel in sulphuric acid, *Electrochimica Acta*, 2 (2007), 909-914.
- [10] E.E. Oguzie, G.N. Onuoha, A.I. Onuchukwu, Inhibitory mechanism of mild steel corrosion in 2 M sulphuric acid solution by methylene blue dye, *Mat. Chem. and Phys.* Vol. 89, 2-3 (2005), 305-311.
- [11] O Benali, L Larabi, S Merah, Y Harek, Influence of the Methylene Blue Dye (MBD) on the corrosion inhibition of mild steel in 0.5 M sulphuric acid, Part I: weight loss and electrochemical studies, *J. Mater. Environ. Sci.* 2 (2011) 39-48.
- [12] A. Doner, R. Solmaz, M. Ozcan, G. Cardas, Experimental and theoretical studies of thiazoles as corrosion inhibitors for mild steel in sulphuric acid solution, *Corr. Sci.* 53 (2011) 2902-2913.

- [13] M. Quraishi, J. Rawat, Inhibition of mild steel corrosion by some macrocyclic compounds in hot and concentrated hydrochloric acid, *Mater. Chem. Phys.* 73 (2002) 118-122.
- [14] M.A. Hegazy, H.M. Ahmed, A.S. El-Tabei, Investigation of the inhibitive effect of p-substituted 4-(N,N,N-dimethyldodecylammonium bromide) benzylidene - benzene-2-yl-amine on corrosion of carbon steel pipelines in acidic medium, *Corros. Sci.* 53 (2011) 671-678.
- [15] D. Snihirova, S. Lamaka, M. Taryba, A. Salak, S. Kallip, M. Zheludkevich, M. Ferreira, M. Montemor, Hydroxyapatite microparticles as feed back active reservoirs of corrosion inhibitors, *Applied Materials and Interfaces*, Vol.2 n° 11 (2010) 301-3022.
- [16] J. Hu, D.A. Koleva, P. Petrov, K. van Breugel, Polymeric vesicles for corrosion control in reinforced mortar: electrochemical behavior, steel surface analysis and bulk matrix properties, *Corrosion Science* 65 (2012) 414-430.
- [17] M. Montemor D. Snihirova, M. Taryba S. Lamaka, I. Kartsonakis, A. Balaskas, G. Kordas, J. Tedim, A. Kuznestova, M. Zheludkevich, M. Ferreira, Evaluation of self-healing ability in protective coating modified with combinations of layered double hydroxides and cerium molibdate nanocontainnes filled with corrosion inhibitors, *Electrochimica Acta* 60 (2012) 31-40.
- [18] D. Snihirova, S. Lamaka, M.F. Montemor, Smart protective ability of water based epoxy coating loaded with CaCO_3 microbeads impregnated with corrosion inhibitors applied on AA2024 substrates, *Electrochim. Acta*, 83 (2012) 439-447.
- [19] H. Tong, W. Ma, L. Wang, P. Wan, J. Hu, L. Cao; Control over crystal phase, shape, size and aggragation of calcium carbonate via a L-aspartic acid inducing process, *Biomaterials* 25 (2004) 3923-3929.
- [20] A. Popova , M. Christov, Evaluation of impedance measurements on mild steel corrosion in acid media in the presence of heterocyclic compounds, *Corr. Sci.* Vol. 48 10 (2006) 3208-3221.
- [21] M. A. Quraishi, M. A. Wajid Khan, M. Ajmal, S. Muralidharan, S. V. Iyer, Influence of substituted benzothiazoles on corrosion in acid solution, *J. App. Electrochem.*, Vol. 26 12 (1996), 1253-1258.
- [22] K. M. Ismail, Evaluation of cysteine as environmentally friendly corrosion inhibitor for copper in neutral and acidic chloride solutions, *Electrochimica Acta*, Vol. 52 28 (2007) 7811-7819.
- [23] C. Piccirillo, S. Perni, J. Gil-Thomas, P. Prokopovich ,M. Wilson, J. Pratten, I. P. Parkin; Antimicrobial activity of methylene blue and toluidine blue O covalently bound to a modified silicone polymer surface, *J.Mater.Chem.* Vol 19 (2009) 6167-617.

- [24] Kacem I, Laurent T, Blanchemain N, Neut C, Chai F, Haulon S, Hildebrand H, Martel B. Dyeing and antibacterial activation with methylene blue of a cyclodextrin modified polyester vascular graft, *J Biomed Mater Res A*, 102(9) (2014) 2942-2951.
- [25] I.M Zin, S.B. Lyon, V.I. Pokhmurskii; Corrosion control of galvanized steel using a phosphate/calcium ion inhibitor mixture, *Corr, Sci.* 45 (2003) 777-788.
- [26] Z. Szklarska-Smialowska, J. Mankowski, Centre Belge d'etude e de documentation des eaux 20 (1967) 474.
- [27] I. Puigdomenech, MEDUSA software, Royal Institute of technology, Stockholm, 1992.
- [28] D. Luna-Zaragoza, E. T. Romero-Guzmán, L. R. Reyes-Gutiérrez, Surface and Physicochemical Characterization of Phosphates Vivianite and Hydroxyapatite; *J. of Minerals & Materials Characterization & Engineering*, 8 (2009) 591-609.
- [29] K. Khaled, M. Amin, Corrosion monitoring of mild steel in sulfuric acid solutions in presence of some thiazole derivatives, *Corr. Sci.* 51 (2009) 1964-1975.
- [30] A. Farag, M. Hegazy, Synergistic inhibition effect of potassium iodide and noveshiff bases on X65 steel corrosion in 0.5 M H_2SO_4 , *Corr. Sci.* 74 (2013) 168-177.
- [31] X. Zheng, S. Zhang, W.Li, L. Yin, J. He, J.Wu, Investigation of 1-butyl-3-methyl-1H-benzimidazolium iodide as inhibitor for mild steel in sulfuric acid solution, *Corrosion Science* 80 (2014) 383-392.
- [32] M. Tourabi, K. Nohair, M. Traisnel, C. Jama, F. Bentiss; Electrochemical and XPS studies of the corrosion inhibition of carbon steel in hydrochloric acid pickling solutions by 3,5-bis(2-thienylmethyl)-4-amino-1,2,4-triazole, *Corrosion Science* 75 (2013) 123-133.
- [33] S.E. Nataraja, T.V. Venkatesha, K. Manjunatha, Boja Poojary, M.K. Pavithra, H.C. Tandon, Inhibition of the corrosion of steel in hydrochloric acid solution by some organic molecules containing the methylthiophenyl moiety, *Corrosion Science* 53 (2011) 2651-2659.
- [34] N.S. Ayati, S. Khandanel, M. Momeni, M.H. Moayed , A. Davoodi , M. Rahimizadeh; Inhibitive effect of synthesized 2-(3-pyridyl)-3,4-dihydro-4-quinazolinone as acorrosion inhibitor for mild steel in hydrochloric acid, *Materials Chemistry and Physics* 126 (2011) 873-879.
- [35] N. Etteyeb, L. Dhouibi, H. Takenouti, M.C. Alonso, E. Triki, Corrosion inhibition of carbon steel in alkaline chloride media by Na_3PO_4 , *Electrochimica Acta* 52 (2007) 7506-7512.

Chapter 6.

Preliminary tests of the "Smart" inhibitors in the cementitious matrix

Reinforced concrete is a composite material whose performance comes from the merging of concrete and steel properties. As a consequence, a key point in the development of solutions aiming to improve the performance or the durability of either the cementitious matrix or the steel reinforcing bars, is the assessment of eventual side effects on the other elements of the composite. The effects of MBD-HAP hybrid inhibitor on the properties of the cementitious matrix in terms of both hydration rate and strength development were carefully evaluated by means of isothermal calorimetry and standard compressive strength tests. Once excluded the onset of negative side effects, reinforced mortar samples containing different amount of the unloaded HAP and of the hybrid MBD-HAP were cast and exposed to a diluted sulfuric acid environment for about four months. However, such a conditioning period proved not to be long enough to induce the corrosion of the steel reinforcing bars.

6.1 Introduction

The previous chapter, dealing with the synthesis, characterization, and electrochemical testing in model media of hybrid "smart" inhibitors, pointed out promising features for the methylene blue/hydroxyapatite system (MBD-HAP), being characterized by high porosity, yielding to a high storage capacity and a pH triggered release of the organic molecules. Moreover, conversely to the majority of "smart" inhibitive systems, where reservoirs are just meant to protect the active compounds until their release, in the present case, the dissolution of the inorganic hosting matrix also plays a key role in the protection of the steel surface. The validation of the inhibitor efficiency in model media, although valuable indication of its performance, is however extremely far from a real situation, where the steel rebar are embedded into a cementitious matrix. Furthermore, it has to be considered that reinforced concrete is a composite material, and that what may have beneficial effects in terms of the steel protection could result, on the other hand, in detrimental effects on the cementitious matrix properties. It is often emphasized that chemical admixtures, can lead to collateral issues such as stiffness, variation of initial slump, large slump loss as well as modifications of the mechanical properties of the hardened cementitious matrix [1]. The evaluation of possible interactions between cement and chemical admixtures can be performed by focusing on the short term, that is, investigating how admixtures affect the cement hydration reaction, or alternatively measuring, in the long term, the mechanical properties evolution of the hardened paste. According to literature a common method for the investigation of the early stage of cement hydration is the thermal calorimetry [2-4], while the long term physical properties can be easily evaluated my means of the determination of compressive strength [5,6].

6.2 Experimental

6.2.1 Materials and samples

Mortar samples were produced in the shapes of cubes (40x40x40 mm) for standard compressive strength tests and of reinforced cylinders ($\phi = 32$ mm, $h = 100$ mm) for corrosion monitoring purposes. In both cases, casting was performed according to EN 196-1 norm, using standard sand, CEM I 42.5 R cement type and tap water; the water cement ratio was set to 0.5. Seven sets of samples were cast, each one constituted by 6 mortar cubes, and 5 reinforced mortar cylinders. Among the different series, one had no inhibitors; of the remaining six, three contained HAP and three contained MBD-HAP at concentrations of 0.02%, 0.1% and 0.5% expressed as percentages of dry cement. Reinforced mortar cylinders had a FeB500HKN carbon steel rebar embedded in the middle ($\phi = 6$ mm, $h = 100$ mm). Before casting, the rust deposits on the steel surface were carefully removed by brushing and its upper extremity was protected by means of a thermal shrinkable insulating sheath as to leave an exposed length of 70 mm (fig.6.1). Mortar samples

were demoulded after 24 hour from mixing, and cured for 28 days in a fog room at 25°C, 100% RH.

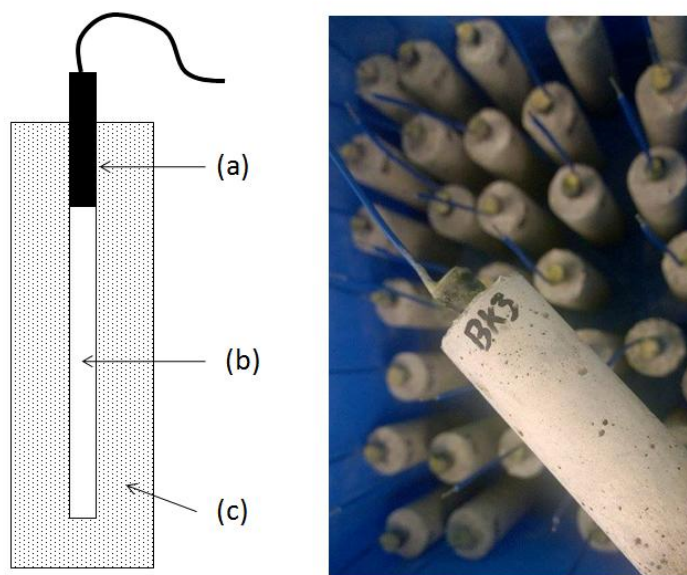


Fig. 6.1: Schematic and picture of reinforced mortar cylinders. (a) insulating sheath, (b) exposed length of the rebar, (c) mortar cover thickness.

Cement pastes were also produced for the calorimetric evaluation of the hydration rate; for such measurements CEM I 42.5R was mixed with tap water ($w/c = 0.5$) and HAP / MBD-HAP were added at the same concentrations as above, plus an higher concentration (3%). Aiming to check the effects of MBD alone, on the basis of the loading capacity ($\approx 7\%$, see Chapter 5, Section 5.3.2) the amount of the organic dye introduced with a 3% concentration of hybrid inhibitor was directly added to the cement paste.

6.2.2 Calorimetric measurements

Isothermal calorimetry was performed on two replicates using an eight channel micro-calorimeter (TEM Air 314) at 20°C. The mixing tools and the materials were stored at a constant temperature of 20°C for 24 hour before mixing. The entire mixing period was maintained within 60 ± 5 s. The cement paste was then carefully poured into calorimeter capsules and the weight of the cement paste in the ampoule was measured. The rate of hydration was measured as power (mW) and was normalized per gram of cement. Numerical integration of the resulting thermograms allowed to plot the heat evolution as a function of time.

6.2.3 Standard compressive strength tests

The standard compressive strength tests were performed on 40x40x40 mm mortar cubes at the ages of 1 day and 28 days, thus collecting values from the early to the late age of hydration. Every measurement was repeated on three replicates (fig.6.2).

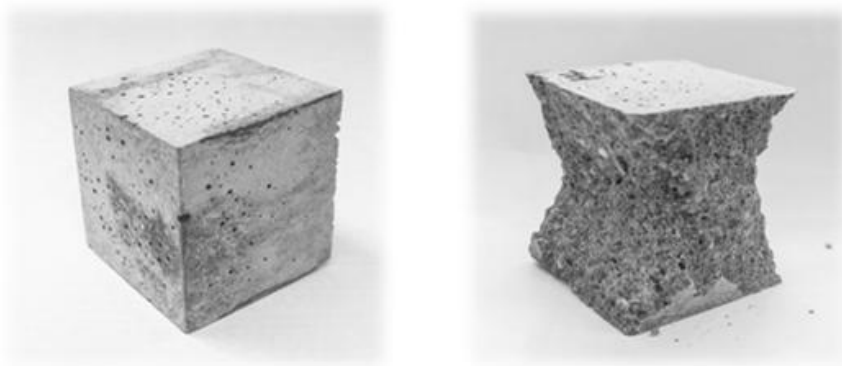


Fig. 6.2: Pictures of the mortar cubes, before and after the standard compressive tests.

6.2.4 Conditioning and OCP monitoring

After the 28 days of curing, reinforced mortar cylinders were removed from the fog room, left drying at room temperature for two days and then, partially immersed into the conditioning media. Of the five replicates per each sample type (no admixture, HAP(0.02%, 0.1% and 0.5%) and MBD-HAP(0.02%, 0.1% and 0.5%)) two samples were partially immersed into tap water and considered as control cases, while the remaining three were conditioned into a diluted 1% sulfuric acid solution. In order to maintain the aggressiveness of the acidic environment, the sulfuric acid solutions were weekly refreshed.

In the experimentation described in Chapter 4, reinforced mortar samples, previously carbonated, were conditioned in sulfide- containing and sulfuric acid solutions simulating bacteria metabolic products. The carbonation step aimed to simulate what really happens on the field, where bacteria colonize a concrete surface only when its alkalinity is partially neutralized by atmospheric CO₂. However, as highlighted in the conclusions of Chapter 4, the carbonation induced corrosion of the steel rebars, made the detection of aggressive effects related to the different conditioning media extremely difficult. For such a reason, in the present chapter, it was chosen to skip the carbonation stage, and to start the conditioning directly on sound samples.

Along the conditioning period, that lasted for about four months, the OCP of the steel rebars was regularly measured every two days.

6.2.5 ESEM observations

At the end of the conditioning period, reinforced mortar samples were removed from the solutions, impregnated with epoxy resin, in order to limit the damages resulting from the cutting procedure. Cross-sections were cut from the middle part of each specimen, then the surfaces of interest were grinded and polished up to the diamond paste of $0.25\text{ }\mu\text{m}$. Once polished, the surfaces were again covered with epoxy resin by means of vacuum impregnation, aiming to fill all the superficial porosity with the resin. The resin excess was finally removed by means of a new grinding and polishing procedure performed until the resin only remains into the mortar porosity (fig. 6.3)[7].

Scanning electron microscopy (ESEM Philips XL30) analysis was performed on three region of the samples: the edge that was in contact with the external surface, the bulk of the cement matrix and finally the steel/mortar interface.

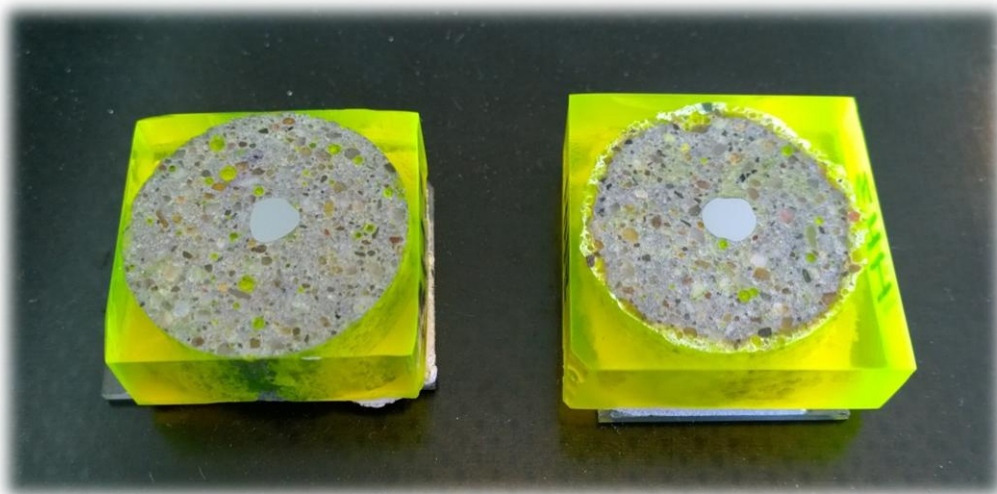


Fig. 6.3: Pictures of polished cross-section for ESEM examination. Left: sample conditioned in tap water. Right: sample conditioned in diluted H_2SO_4 .

6.3 Results and discussion

6.3.1 Effects on the cementitious matrix properties

According to literature [4,7], the exothermic reactions correlated to the cement hydration lead to a thermogram as that schematically depicted in fig. 6.4. Such figure clearly identifies five distinct stages that respectively correspond to:

- I. Initial hydration
- II. Induction period
- III. Acceleration and set

IV. Deceleration and hardening

V. Curing

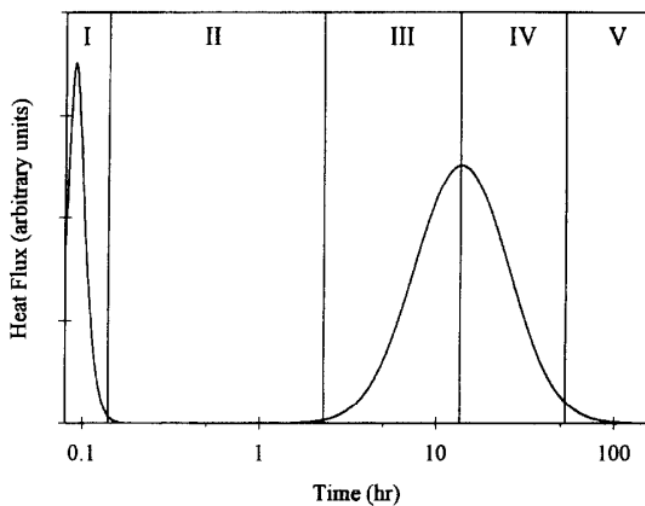


Fig. 6.4: Schematic of the heat evolution during the hydration process of Portland cement.

The first stage consists in the wetting of the surfaces of the highly hygroscopic cement grains, being characterized by a nucleation type growth of hydration products. Once the grains surfaces are covered with hydration products, the diffusion of reacting species is hindered, resulting into the decrease of the hydration rate characteristic of the induction period. The disruption of the hydrated protective layer because of the osmotic pressure and physico-chemical transformations of the hydrates leads to a new increase of the hydration rate and to the stiffening of the matrix. The depletion of the easily available unhydrated cement grains finally causes a decrease of the heat flux corresponding to a decrease of the hydration rate that however slowly continues for long times after the mixing of the different components.

Heat release and heat evolution of OPC cement pastes containing different amount of either the unloaded HAP or the loaded MBD-HAP were monitored over the first four days of hydration; results are reported in fig. 6.5. Among the different inhibitor concentrations, the cases of 0.02%, 0.1%, and 0.5% resulted to perfectly overlap the response of control case (no inhibitor), while only minor deviations were detected in the case of the higher concentration of 3%. However, what seemed a small delay of the hydration rate for both the higher concentrations of HAP and MBD-HAP did not result in any significant change in the heat evolution plots (fig. 6.5(b,d)).

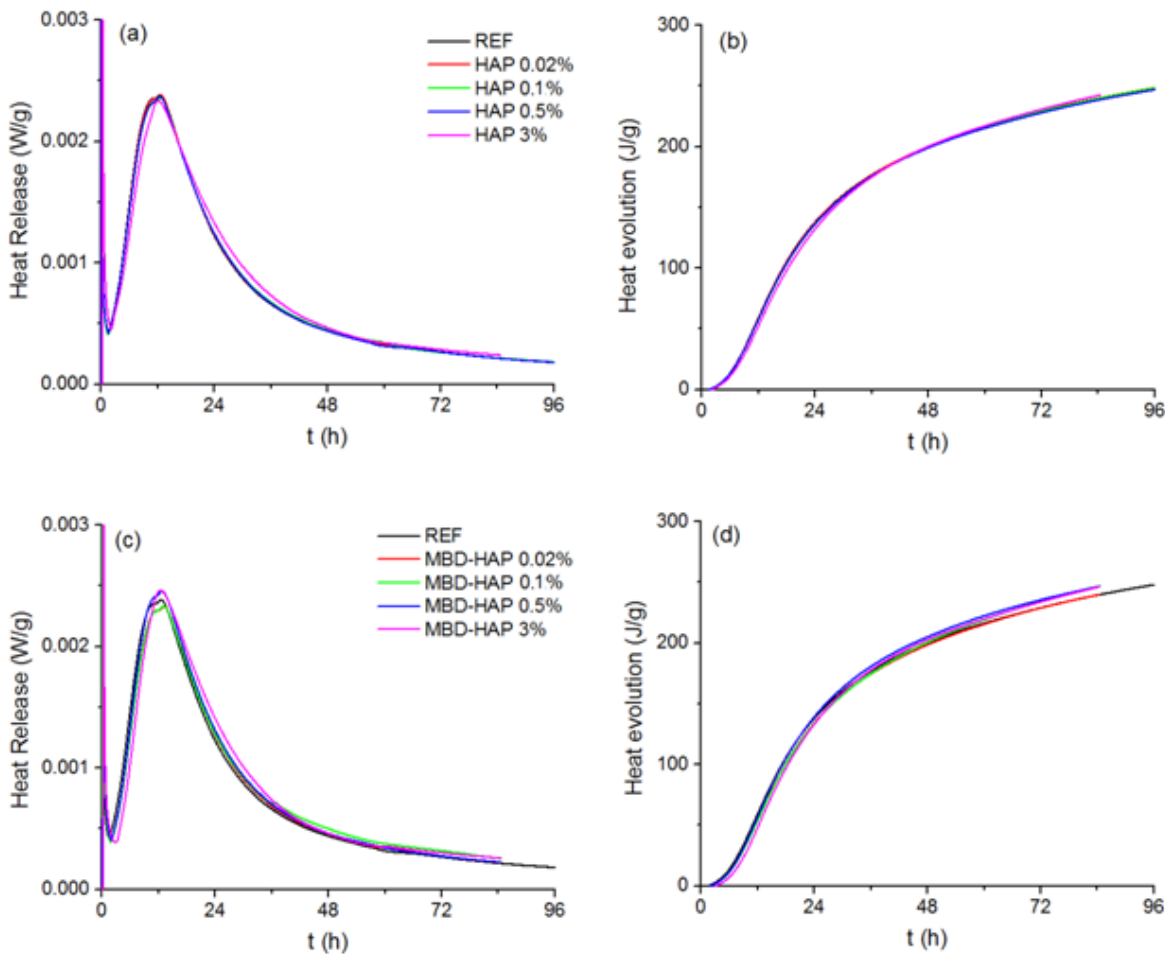


Fig. 6.5: Heat release and heat evolution plots of the hydration reaction of OPC cement paste containing different amount of HAP (a,b) and MBD-HAP (c,d).

Most of the chemical admixtures widely used in concrete for applications such as water reduction, set retardation or accelerator, fluidification or air entrainment are organic molecules that interacting with the hydrated or unhydrated surfaces of cement grains significantly affect the hydration reactions. In the present case, the organic molecules should be entrapped into the hydroxyapatite matrix, and at the very alkaline pH of sound concrete their release should be negligible. However, as demonstrated by the release tests of Chapter 5, Section 5.3.2, part of the organic molecules are superficially physisorbed, and such weak bounds could be easily broken during the initial hydration stage thus resulting in a small release of the organic inhibitor. The heat release and the evolution in a non realistic, extreme case of complete emptying of the 3% MBD-HAP admixture are shown in fig. 6.6

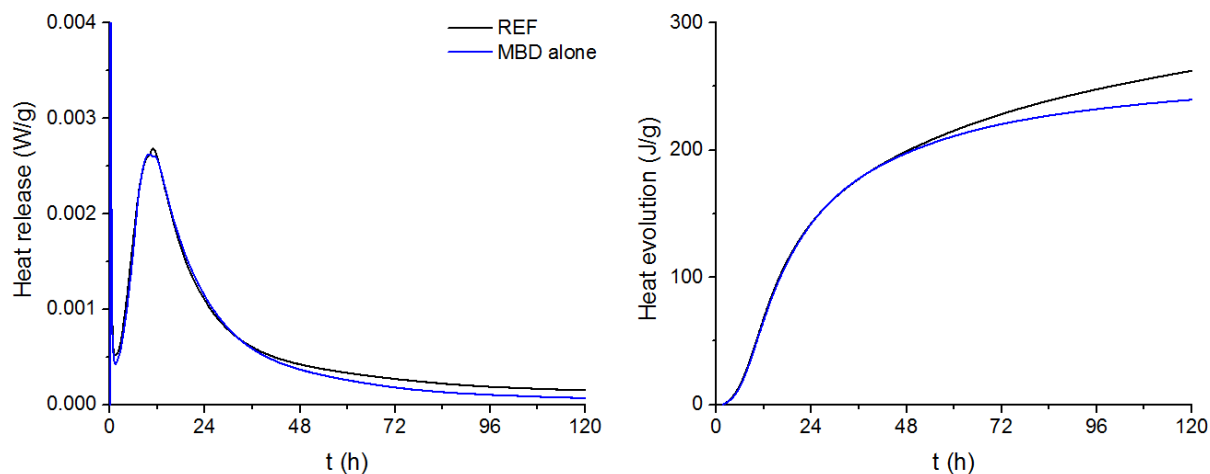


Fig. 6.6: Heat release and heat evolution plots of the hydration reaction of OPC cement paste containing MBD alone.

Both the plots of fig.6.6 showed that some differences occurred, starting at about two days from the mixing of the components. Actually a small decrease of the heat release during the last days of the monitoring period was reflected into a significant divergence in the heat evolution plot, thus confirming the occurrence of interactions between methylene blue dye molecules and hydrated products. However, as above stated, the complete release of methylene blue dye in an alkaline environment it is not likely to occur, so that within the considered range of concentrations, interactions between the hybrid inhibitor and cement hydrated products can be considered negligible.

In order to check if the HAP or MBD-HAP addition could affect the mechanical properties of the hardened cementitious matrix, standard compressive strength tests were performed on mortar cubes containing different amounts of the two inhibitors. Fig. 6.7 shows compressive strength measurements at the beginning and at the ending of the curing period, that is 24 hours and 28 days of ageing, respectively. By scrutiny of fig. 6.7, it can be clearly observed that neither the inorganic matrix alone, nor the organic/inorganic hybrid system induced any significant change in the mechanical properties of the mortar samples.

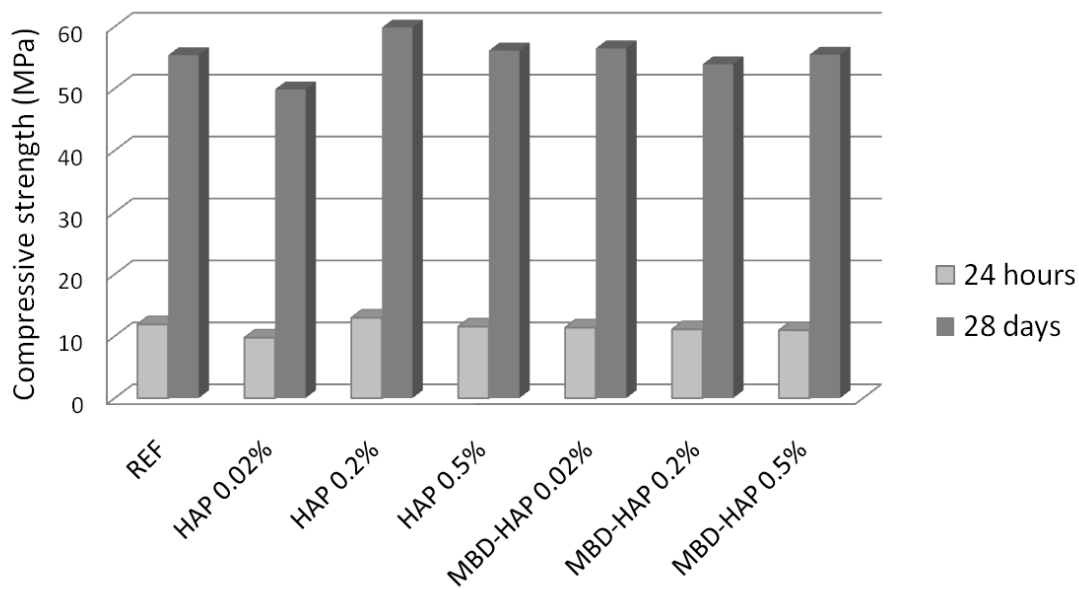


Fig. 6.7: Compressive strength of mortar cubes containing different amount of HAP and MBD-HAP, after 24 hours and 28 day of moist curing.

6.3.2 Effects on the steel rebars embedded in mortar

Once demonstrated that HAP and MBD-HAP addition did not induce any negative side effects on the mechanical properties of the resulting mortar, the attention was focused on their effects on the embedded steel rebar. In the previous Chapter, Section 5.3.3, after the evaluation of the inhibitors protective efficiency in acidic model media, some tests were also performed in alkaline solutions aiming to assess eventual effects of the hybrid inhibitors on the passive film formation. Such tests pointed out that, although MBD adsorption on the freshly polished steel surfaces could hinder the charge transfer mechanism, thus slightly affecting the oxide growth, its actual release from the HAP matrix in alkaline environment is so low, that effects on passivation can be considered negligible. Passing from the model media to steel rebars embedded into the reinforced mortar samples, OCP measurements (Fig. 6.8) performed during the 28 days of the curing period confirmed that no substantial differences were detected between the control case (dashed line) and the HAP, MBD-HAP containing samples (continuous lines)

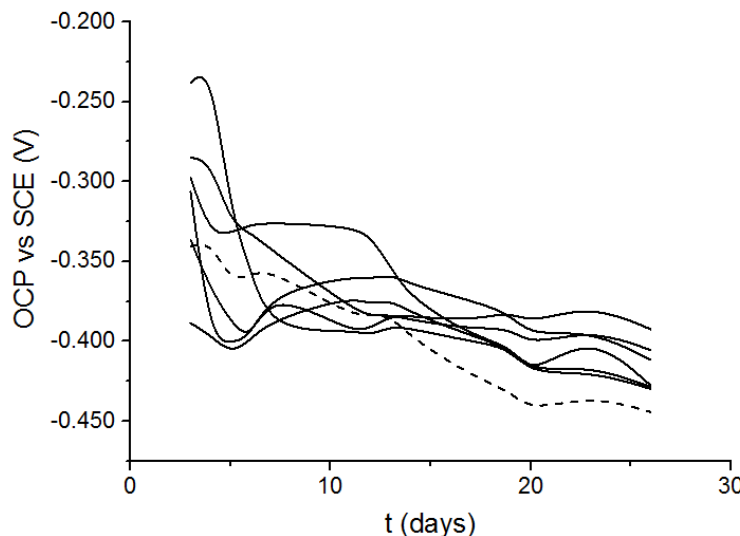


Fig. 6.8: OCP evolution steel rebars embedded in mortar along the 28 days of the curing period. (—) No inhibitors. (—) HAP and MBD-HAP at concentrations 0.02%, 0.1%, 0.5% with respect to the dry cement weight.

The OCP measurements depicted in fig. 6.8 did not show the typical responses of passivating systems such as those discussed in Chapter 3, Section 3.3.3 for steel in alkaline solutions. In the present case, a slightly decreasing trend was recorded over time and the measured values resulted to be significantly more negative than the above cited case of steel in model media. Both these features can however be attributed to the lack of oxygenation due to mortar saturation resulting from the curing environmental conditions (100% RH).

Once cured, the reinforced mortar samples were conditioned for about four months in a 1% H_2SO_4 solution, and in tap water as control cases; the evolution of the OCP measurements, averaged among the replicates, is reported in fig. 6.9.

By scrutiny of such OCP values, it is immediately confirmed that measurements performed during the curing period were heavily affected by the saturated condition of the mortar cover. Actually, according to the Standard ASTM C876 [9] these latter, being lower than -276 mV vs. SCE, would fall into the high corrosion risk region, but the same samples, after drying and partial immersion in tap water, exhibited OCP values typical of the passive state (dashed lines in fig 6.9).

For all the different types of samples, that is the plain ones (fig. 6.9a), and those containing different amounts of HAP (fig. 6.9b,d,f) and MBD-HAP (fig. 6.9c,e,g), the responses of the control cases conditioned in tap water resulted to be rather similar, being characterized by stable values of about -0.100 V vs. SCE. Similarities between the different cases confirmed that, as expected, in such conditions, MBD was still encapsulated into the HAP hosting matrix.

Conversely, samples conditioned in sulfuric acid exhibited higher initial corrosion potentials that regularly decreased over time.

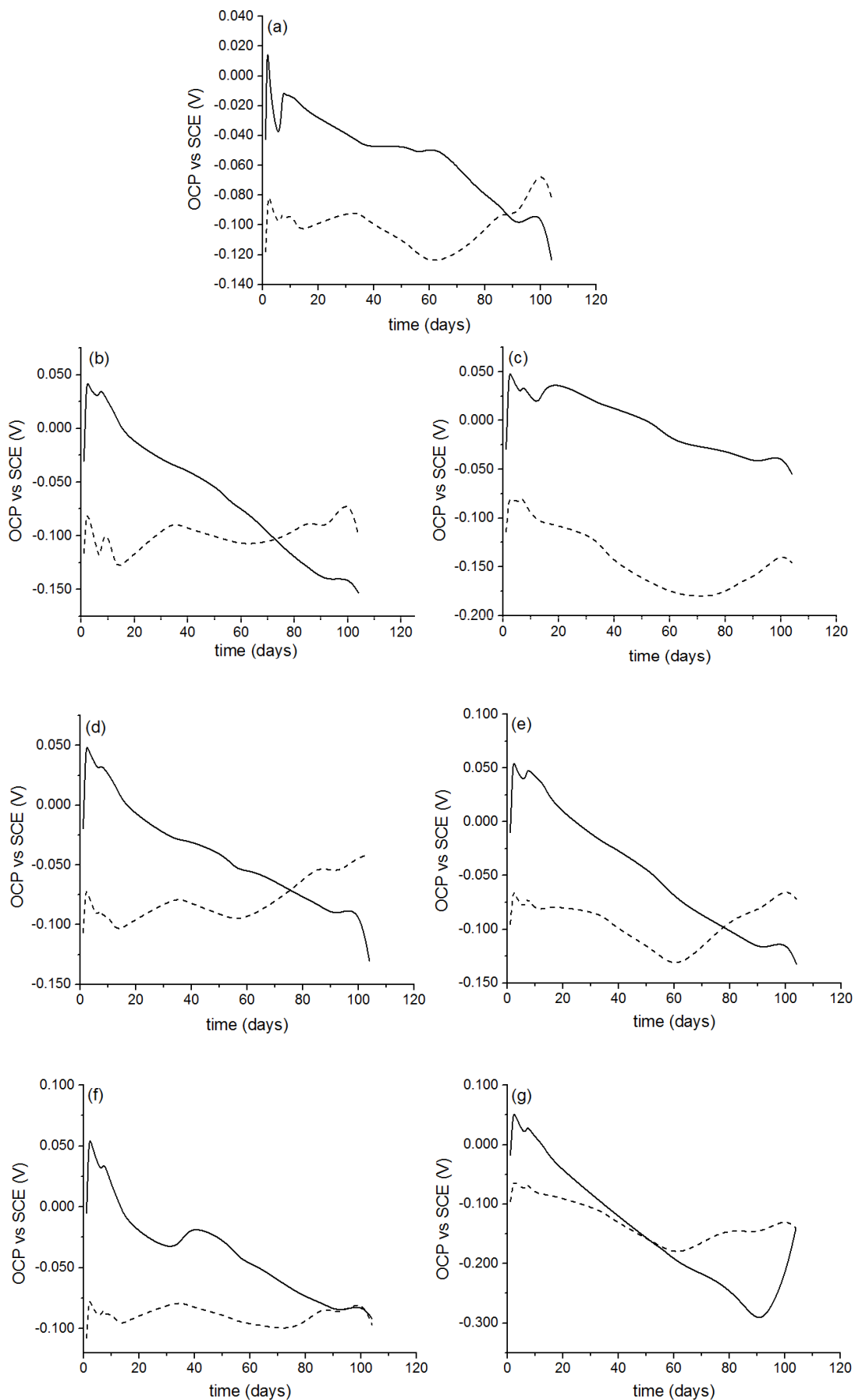


Fig. 6.9: OCP evolution steel rebars embedded in mortar along the conditioning period. (— — —) Control case partially immersed in tap water. (—) Reinforced mortar samples in 1% H₂SO₄. (a) plain mortar, (b) HAP 0.02%, (c) MBD-HAP 0.02%, (d) HAP 0.1%, (e) MBD-HAP 0.1%, (f) HAP 0.5%, (g) MBD-HAP 0.5%.

Except for the case of MBD-HAP at the lower concentration of 0.02% (fig. 6.9c) all the OCP values of the acidic conditioning crossed those of the relative control cases after about 80 days of immersion; a certain advance of such crossing was detected only in the case of MBD-HAP 0.5% that occurred instead at the 60th day. The decreasing trends of the OCP values in the cases of the acidic conditioning could indicate that, notwithstanding the presence of the protective barrier offered by the mortar cover, the external acidic environment can affect the steel rebar response. However, after 112 days, all the samples still exhibited OCP values characteristic of low/intermediate corrosion risk, and no effects were detected related to the presence of different amounts of HAP and MBD-HAP.

After such period, samples without any inhibitor taken from both the sulfuric acid solution and from tap water, were cut and their cross-sections sprayed with an alcoholic phenolphthalein solution (fig. 6.10). The violet tint of the bulk cementitious matrix detected in both cases confirmed that the neutralization process had affected only an extremely thin superficial layer. Actually on the left side of fig. 6.10 a whitish layer is clearly detectable.

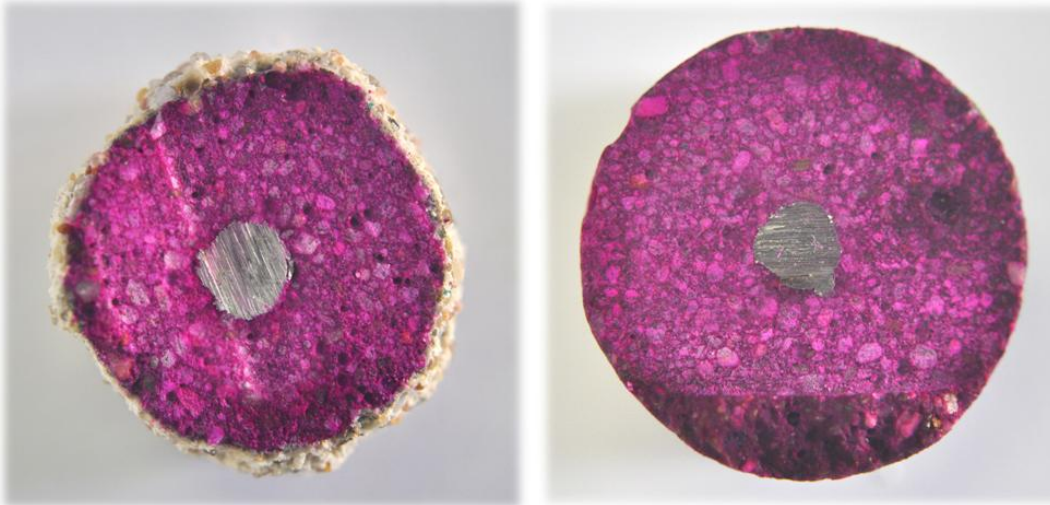


Fig. 6.10: Phenolphthalein test performed on the cross-section of two reinforced cylinders (not containing any inhibitor) after 112 conditioning days in: (left) 1% H₂SO₄, (right) tap water.

Further confirmation of the very limited penetration of the neutralization front was obtained by means of ESEM observations. Fig. 6.11 clearly shows the morphological changes between the external deteriorated area, having approximately a thickness of 1 mm, and the internal sound region. Higher magnification pictures, reported in figure

6.12, highlighted the differences between the compact microstructure of sound hydrated cement paste in the bulk area (left) and the loose, incoherent layer of the external surface.

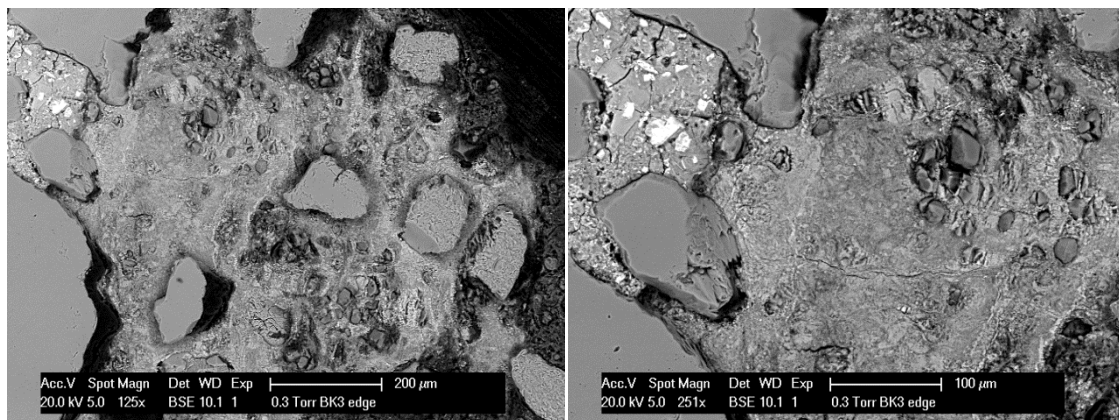


Fig. 6.11: ESEM pictures at two different magnification of the edge area of a cross-section cut from a reinforced mortar cylinder (no inhibitors) after 112 days of conditioning in 1% H_2SO_4 .

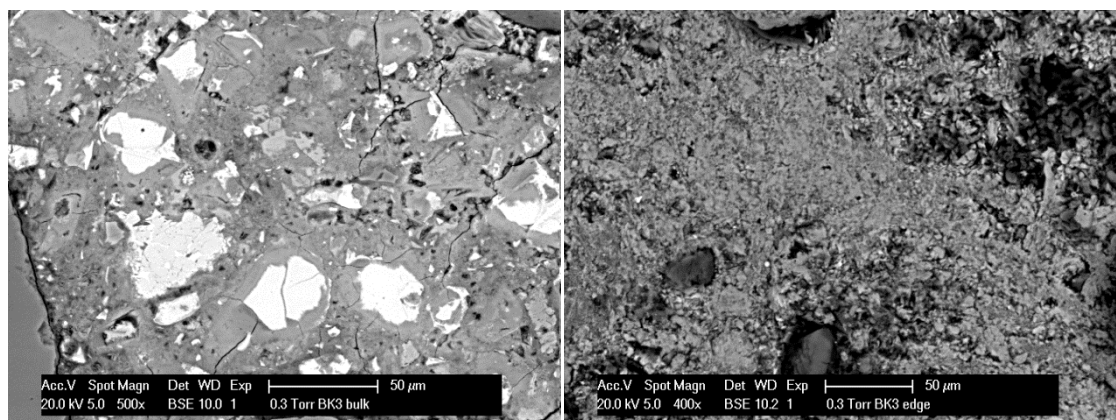


Fig. 6.12: ESEM pictures of a cross-section cut from a reinforced mortar cylinder (no inhibitors) after 112 days of conditioning in 1% H_2SO_4 . (left) bulk area, (right) edge.

EDX microanalysis, performed on both the edge and the bulk area of the samples are shown in fig. 6.17, and clearly indicated the presence of CaSO_4 resulting from the sulfuric acid attack of the cementitious matrix.

Coherently with the OCP measurements, indicating that the steel reinforcing bar was still in the passive state, no corrosion products were detected at the steel/mortar interface, as can be seen from the pictures reported in fig. 6.14.

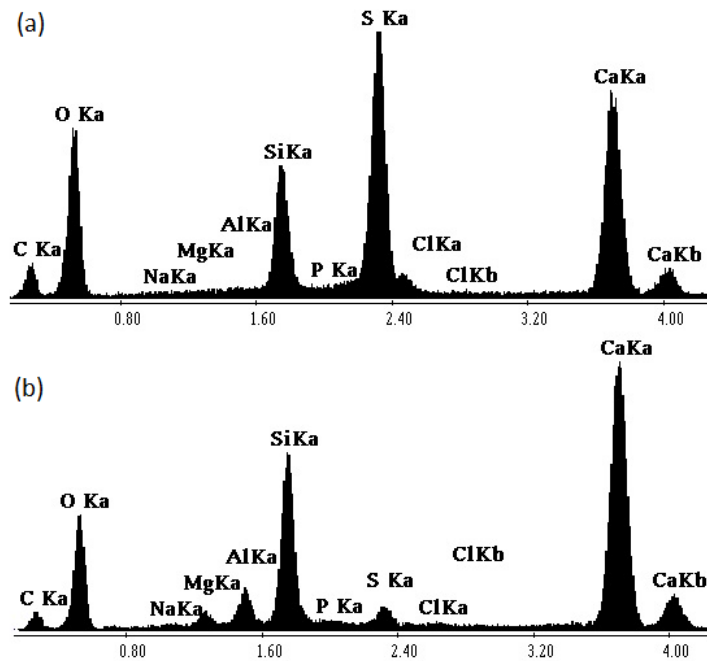


Fig. 6.13: EDX spectra captured on the cross section of a reinforced mortar sample conditioned in 1% H₂SO₄. (a) edge, (b) bulk.

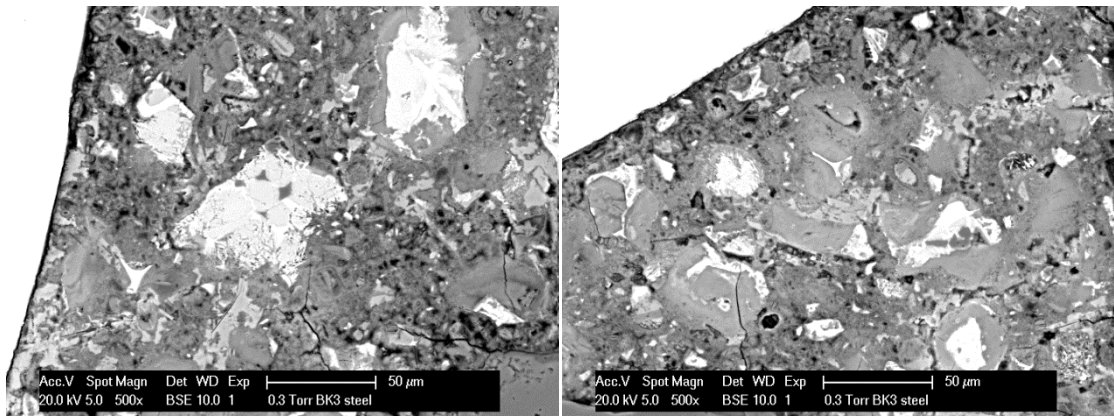


Fig. 6.14: ESEM pictures of a cross-section cut from a reinforced mortar cylinder (no inhibitors) after 112 days of conditioning in 1% H₂SO₄. Details of the steel/mortar interface.

As expected, ESEM observations of cross-sections cut from samples conditioned in tap water exhibited different morphologies especially for what concerns the external edge area. In the pictures reported in fig. 6.15, a thin superficial layer, that EDX analysis indicated as carbonated cement, was clearly detectable; its thickness is probably so low that it was not noticed with the phenolphthalein test of fig. 6.10.

No significant differences were instead detected between the acidic and the tap water conditioning in terms of bulk microstructures and steel/mortar interfaces, thus

confirming that during the four months of testing, the conditioning media only affected a thin superficial layer of the mortar cover thickness (fig 6.16).

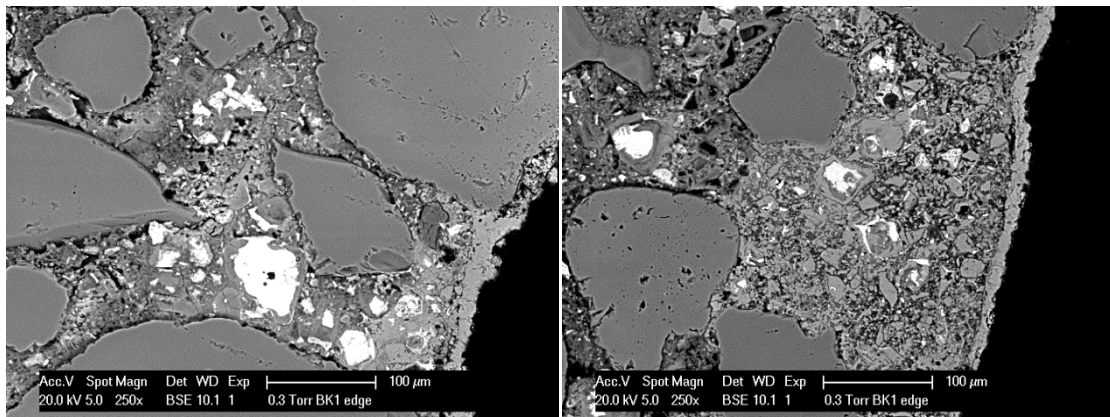


Fig. 6.15: ESEM pictures of a cross-section cut from a reinforced mortar cylinder (no inhibitors) after 112 days of conditioning in tap water. Details of the edge region.

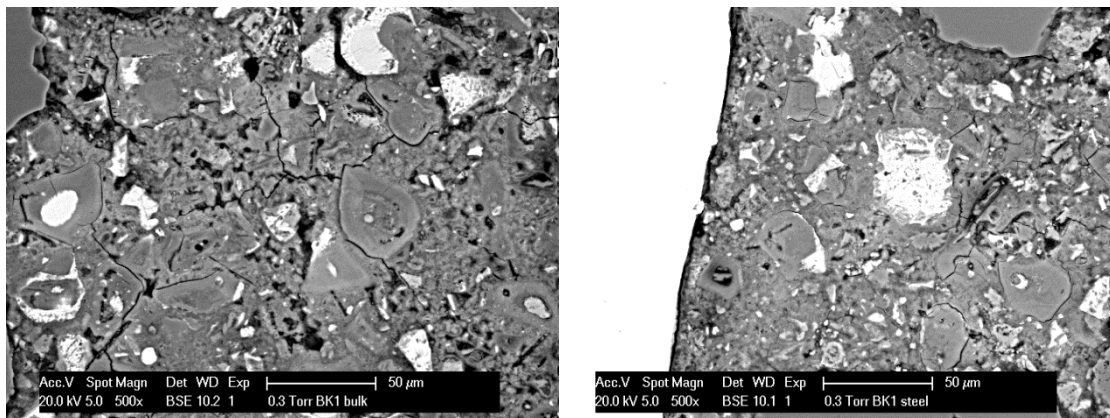


Fig. 6.16: ESEM pictures of a cross-section cut from a reinforced mortar cylinder (no inhibitors) after 112 days of conditioning in tap water. (left) bulk region, (right) steel/mortar interface.

6.4 Conclusion

The evaluation of possible interactions between the hybrid MBD-HAP inhibitor and cementitious matrix gave negative results, both in terms of calorimetric measurements of the hydration rate, and of mechanical properties measured by means of the standard compressive strength tests. Once demonstrated that the novel admixture does not negatively affect the properties of the cementitious matrix, reinforced mortar samples were realized aiming to investigate the MBD-HAP inhibitive efficiency in a system closer to a realistic simulation of what it is expected to happen on the field. Conversely to the reinforced mortar samples monitored in Chapter 4, in the present case the accelerated carbonation stage was skipped aiming

to better determine the transition from the passive state to the active one, as a function of the external conditioning environment. However, the non carbonated mortar cover proved to be a very efficient barrier against the acid attack, impeding the propagation of the neutralization front and maintained the embedded steel rebar in its initial passive state. Observations of the reinforced mortar samples cross-section after the 112 days of conditioning pointed out that the heavily deteriorated mortar thickness was only a very thin superficial layer, while the bulk of the cementitious matrix still maintained a sound microstructural morphology and a very alkaline pH, both these features playing major roles in the protection of the embedded steel reinforcing bars.

References

- [1] S. Hanehara, K. Yamada, Interaction between cement and chemical admixture from the point of cement hydration, absorption behaviour of the admixture and paste rheology, *Cement and Concrete Research* 29 (1999) 1159-1165.
- [2] P. Lawrence, M. Cyr, E. Ringot, Mineral admixtures in mortars - effect of inert materials on short-term hydration, *Cem. Concr. Res.*, Vol. 33, No. 12 (2003) 1939-1947.
- [3] J. Cheung, A. Jeknavorian, L. Roberts, D. Silva, Impact of admixtures on the hydration kinetics of Portland cement, *Cem. Concr. Res.*, Vol. 33, No. 41 (2011) 1298-1309.
- [4] C. Jolicoer, M.A. Simard, Chemical admixture-cement interactions:Phenomenology and Physico-chemical Concepts, *Cement and Concrete Composites*, 20 (1998) 87-101.
- [5] P. Lawrence, M. Cyr, E. Ringot, Efficiency of mineral admixtures in mortars: Quantification of the physical and chemical effects of fine, admixtures in relation with compressive strength, *Cement and Concrete Research*, Vol.36, No. 2 (2006) 264-277.
- [6] Don L. Ivey, Teddy J. Hirsch, Effects of chemical admixtures in concrete and mortar, research report (1967) 70-73.
- [7] G. Ye, J. Hu, K. van Breugel, P. Stroeven, Characterization of the development of microstructure and porosity of cement-based materials by numerical simulation and ESEM image analysis, *Mater. Struct.* 35 (2002) 603-613.
- [8] A.M. Neville, *Properties of Concrete*, 5th edition, Pearson, 2015.
- [9] ASTM C876 (1999) Standard test method for half cell potentials of uncoated reinforcing steel in concrete.

Chapter 7.

Conclusions and

Perspectives

7.1 Conclusions

The present text reports and discusses the more relevant results achieved during the course of my PhD research activity, that was mainly held in the "Corrosion Engineering and Applied Electrochemistry Laboratory" at Università degli Studi di Milano from November 2012 to October 2015.

The rationale behind the work was that of investigating the microbial induced reinforced concrete deterioration, especially focusing on the effects that abiotic solutions simulating bacteria metabolites have of the corrosion of the steel reinforcing bars. Once observed their aggressiveness, a specific "smart" corrosion inhibitor was developed and tested. The smartness consisted in the entrapment on an active compound into a porous matrix granting its release as a function of a pH triggered stimulus.

Investigations were started through the easier approach of initially testing the steel rebar directly immersed into model media, miming the concrete environment either in sound conditions and deteriorated by microbial activity. Once determined the most aggressive simulating conditions, a long term (500 days) corrosion monitoring was performed on reinforced mortar samples. Afterward, an hybrid organic/inorganic corrosion inhibitor was synthesized, characterized and tested for steel directly immersed in model media simulating the biogenic acidity. Finally, the effectiveness of the novel corrosion inhibitor was evaluated in cementitious systems.

Below, the main findings obtained in the present work are summarized:

1. *Cyclic voltammetry proved to be a valid tool for investigating the steel passivation in alkaline solutions.*

A saturated $\text{Ca}(\text{OH})_2$ solution (pH 12.6) is commonly used for the simulation of the alkaline environment of sound concrete. Such an high pH plays a key role in the corrosion protection of steel reinforcing bars allowing the growth of a protective passive layer on the steel surface. Cyclic voltammetry of a steel rebar in such solution allowed an easy detection of the double step, involving $\text{Fe}(\text{II})$ and $\text{Fe}(\text{III})$ transformations, leading to the formation of a protective oxide layer. By changing experimental parameters, such as the scanned potential windows or the preconditioning of the metallic surface, significant variations were detected, especially in the $\text{Fe}(\text{II}) / \text{Fe}(\text{III})$ transition, being such reaction the most relevant in the protective layer growing process.

2. At least three days of immersion of the steel in sat Ca(OH)₂ are required to obtain a mature and protective passive film.

The stabilization of the electrochemical response of the oxide film, being attributed to the growth of a passive layer that, in term of thickness, structure and protective performance, may be comparable to that forming naturally as steel is embedded in concrete, was monitored with time. Three days of immersion in a saturated Ca(OH)₂ solution turned out to be the minimum time required for a realistic simulation of a stable passive film.

3. Simulation of Sulfur Oxidizing Bacteria metabolic products led to an extensive generalized corrosion of the steel samples.

Diluted sulfuric acid solutions were used for the simulation of SOB metabolic products. Gravimetric tests and the electrochemical measurements pointed out the onset of a corrosion process, consisting in a fast dissolution of the protective oxide layer and a subsequent attack to the underneath steel surface. The attack morphology resulted to be of a generalized type.

4. Sulfides, simulating Sulfate Reducing Bacteria metabolic products, resulted to be able to interact with the steel surface, leading to localized corrosion.

Sulfides resulted to be a potentially aggressive species, their interactions with the steel surface being essentially dependent on the environment pH. At the more alkaline pH, the protective effect of the oxide layer prevails on the sulfide adsorption, but lowering the pH, the equilibrium was unbalanced toward the steel-sulfide interaction leading to a loose iron-sulfide film (mackinawite) and localized corrosion processes.

5. The electrochemical testing of reinforced mortar samples resulted to be much more complicated and time consuming than that of steel directly immersed in solutions

Cementitious materials are inherently heterogeneous because of the their composite nature, as a consequence, in order to get reliable electrochemical measurements multiple replicates are required. Furthermore the mortar cover thickness protected the steel by providing a physical barrier against all the aggressive species thus requiring very long conditioning times. The accelerated carbonation partially neutralized the cement alkalinity, leading to the rebar transition from the passive state to the active. Such transition probably played a preponderant role over the

effect the external conditioning environment, making the distinction of the effects of the latter rather difficult to detect.

6. The diluted sulfuric acid solution resulted to me more aggressive than the alkaline sulfide-containing one, in terms of corrosion of the mortar embedded rebar.

Notwithstanding the difficulties in the corrosion monitoring of carbonated, and water saturated reinforced mortar samples, the impedance spectra together with visual inspections performed on split samples at the end of the monitoring period, pointed out a major accumulation of corrosion products at the steel/mortar interface in the case of sulfuric acid conditioning. No significant differences were instead detected between the control case and the conditioning into the sulfide-containing solution.

7. Methylene blue dye and calcium phosphate were combined together in an hybrid inhibiting system (MBD-HAP).

Methylene blue dye and tri-sodium phosphate emerged from the testing of a series of different organic and inorganic compounds, as promising inhibitors of the sulfuric acid induced corrosion of carbon steel. The former, when adsorbed on the steel surface, was found to inhibit the anodic process, while the latter limited the cathodic reaction upon precipitation of a protective iron phosphate layer.

The organic dye was immobilized into a porous calcium phosphate matrix granting its storage until the dissolution of the latter occurring at about pH 3.

In such way together with the slow release of the organic molecule granted by the matrix dissolution, a further beneficial effect was obtained by phosphate ions freed from the matrix itself.

8. Both the components of the hybrid inhibitor played a synergic effect in the corrosion protection of a steel surface.

Electrochemical tests performed in simulated acidic solutions pointed out a significant improvement of the corrosion resistance due to the synergic effect of the MBD-HAP system, while the single components (MBD and HAP) did not provide a satisfactory protection if separately used. Such synergic effect could be attributed to a better adsorption of the organic molecules on the homogeneously attacked steel surface provided by the presence of phosphate ions.

9. The hybrid MBD-HAP inhibitor did not negatively affect the properties of the cementitious matrix.

The evaluation of possible side effects arising from interactions between the hybrid MBD-HAP inhibitor and cementitious matrix did not highlight any concerning issue. No effects were detected on the hydration rate, that was investigated by means of isothermal calorimetry as well as for the strength evolution, measured through standard compressive strength tests.

7.2 Perspectives

An intriguing feature of scientific research is that in most cases it consists in a never ending process. Very often, each result opens the way to several new question marks, or further analyses with different techniques could better confirm the already obtained results.

Therefore leads of suggested future research are clustered in topics as follows:

Corrosion monitoring of reinforced mortar samples

In the present work, steel testing in model media pointed out that at the pH of carbonated concrete, sulfides can interact with the steel promoting localized corrosion, however the electrochemical monitoring did not highlight any difference between the samples conditioning in the presence or in the absence of sulfides. Different results could be obtained by using gaseous H₂S instead of aqueous sulfide solutions.

Alternatively faster corrosion onset could be obtained by the investigation of the microbial induced corrosion (either with simulating solutions and with real bacteria) in cracked samples.

"Smart" corrosion inhibitors

The presented results are just preliminary data on a novel system, so that there exists a wide margins of optimization:

Alternative synthesis of the hydroxyapatite particles could be investigated aiming to increase porosity and storage capacity.

Methylene blue dye could be replaced with other organic inhibitors, thus overcoming the issues arising from the related chloride counterions.

New applications, other than concrete, could be investigated such as admixture to epoxy coating for steel protection etc.

